The Aptian evolution of the Galve sub-basin (Maestrat Basin; E Iberia)

Dissertation

zur Erlangung des Grades

Doktor der Naturwissenschaften

(Dr. rer. nat.)

an der

Fakultät für Biologie, Chemie und Geowissenschaften

an der Universität Bayreuth

vorgelegt von

Telm Bover-Arnal

geb. am 11. 09. 1979 in Barcelona

Erstgutachter: Prof. Dr. Klaus Bitzer

Zweitgutachter: Prof. Dr. Ulrich Heimhofer

Bayreuth, im Januar 2010

A Ramon Salas

Als meus pares

Die Untersuchungen zur vorliegenden Arbeit wurden von Mai 2006 bis Januar 2010 an der Universität Bayreuth unter der Leitung von Herrn Prof. Dr. Klaus Bitzer durchgeführt.

Vollständiger Abdruck der von der Fakultät für Biologie, Chemie und Geowissenschaften der Universität Bayreuth genehmigten Dissertation zur Erlangung des akademischen Grades eines Doktors der Naturwissenschaften (Dr. rer. nat.).

Promotionsgesuch eingereicht am:	11.01.2010
Tag des wissenschaftlichen Kolloquiums:	24.02.2010

Erster Gutachter:	Prof. Dr. K. Bitzer
Zweiter Gutachter:	Prof. Dr. U. Heimhofer / Ruhr-Universität Bochum
Vorsitzender:	Prof. Dr. B. Huwe
	Prof. Dr. F. Langenhorst
	Prof. Dr. L. Zöller

Summary

The epeiric mixed carbonate-siliciclastic sedimentary succession of Aptian stage (125-112 Ma) cropping out in the Galve sub-basin (western Maestrat Basin) in the eastern Iberian Chain (E Iberia) was analyzed by multiscale and multidisciplinary approaches. The integrated basin analysis presented in this thesis highlights the interplay between the solid Earth, oceans, atmosphere and life during this time interval, marked by higher CO_2 atmospheric concentrations than nowadays and, consequently, by extreme climatic warmth and higher global sea levels. The most noteworthy aspect of this sedimentary succession is that its analysis enables all major ocean-climate changes which occurred during this stage to be tracked, and it therefore constitutes an excellent means of measuring this time slice. The Aptian strata studied can be divided into four large-scale transgressive-regressive sequences, which were calibrated by geomagnetic polarity analysis and ammonoid and rudist biostratigraphic data. These sequences are consistent with the major transgressions and sea level falls recorded in other coeval Tethyan localities, indicating a significant eustatic control of the sedimentary succession, although synrift subsidence was the most important mechanism in providing accommodation. The main oceanographic and climate-driven Tethyan events detected were: 1) An Early Aptian transgressive phase accompanied by the widespread development of *Palorbitolina lenticularis* beds. 2) The $\delta^{13}C$ perturbations related to the OAE1a have been localized in the upper part of the *Deshayesites forbesi* biozone within a horizon of coral rubble deposits encrusted by *Lithocodium aggregatum* and *Bacinella irregularis*, coincident with the probable Early Aptian thermal maximum. These encrusted coral rubble levels with widespread presence of large-sized flattened *Palorbitolina lenticularis* are interpreted here as records of physical and chemical disturbances linked to the OAE1a. 3) A late Early Aptian long-term progressive cooling trend accompanied by a regressive context marked by the establishment of large carbonate platforms with typical Urgonian biotic associations dominated by rudist bivalves and corals. 4) The maximum of the aforementioned regressive phase, which exposed subaerially the carbonate platform formed during the late Early Aptian. As a result, a broad palaeokarst developed in its proximal setting, whilst forced regressive wedges were deposited basinwards. This late Early Aptian stratigraphic interval constitutes a text-book example of the application of the four-systems-tract sequence stratigraphic methodology to carbonate systems. 5) A late Early to Late Aptian long-

term regressive context, which gave rise to the establishment of littoral conditions during the Late Aptian. The installation of more proximal conditions in this area was coupled with significant terrigenous supplies, which were probably linked to regional tectonics and to a progressively changing climate from a semi-arid regime during the Early Aptian, to semi-humid conditions in the Middle-Late Aptian. Consequently, this study represents a well-documented example of the evolution of the Aptian epicontinental seas, and hence constitutes a valuable tool for calibrating analyses of other Aptian epeiric sedimentary successions.

Zusammenfassung

Die flachmarinen gemischten karbonatisch-klastischen Sedimentfolgen des Apts (125-112 Mio. J.) im Galve-Trog (westliches Maestrat-Becken in den Iberischen Ketten, Nordost-Spanien) wurden in einem multidisziplinaren Ansatz auf unterschiedlichen Skalenebenen untersucht. Die integrierte Beckenanalyse in dieser Arbeit beleuchtet das Wechselspiel zwischen Kontinentalbereichen, Ozean, Atmosphäre und biotischen Prozessen in einem Zeitabschnitt, der von erhöhten atmosphärischen CO_2 Konzentrationen, extrem warmen klimatischen Verhältnissen und einer Hochlage des Meeresspiegels gekennzeichnet ist. Der bemerkenswerteste Aspekt der Sedimentolge besteht darin, dass in ihr alle wichtigen den Ozean und das Klima betreffenden Veränderungen, die in diesem Zeitabschnitt erfolgten, abgebildet sind. Die Sedimentfolge stellt dadurch gewissermaßen ein ideales “Maßband” für dieses Zeitintervall dar. Die untersuchten Schichten des Apt können in vier großmaßstäbliche Transgressions-Regressions Sequenzen unterteilt werden, die mit Hilfe geomagnetischer Polaritäts-Analyse sowie Biostratigraphie anhand von Rudisten und Ammonoideen gegliedert werden konnte. Diese Sequenzen sind korrelierbar mit den Transgressionen und Meeresspiegelrückgängen, die aus anderen Bereichen der Tethys bekannt sind. Dies zeigt an, dass das Sedimentationsgeschehen im wesentlichen von eustatischen Meeresspiegelschwankungen geprägt wurde und die vorhandenen synrift-Absenkungstendenzen nur untergeordneten Einfluss bei der Konfiguration des Akkommodationsraums hatten. Folgende wesentliche ozeanographische und klimabezogene Ereignisse konnten nachgewiesen werden: 1) Eine frühe transgressive Phase im Apt, die begleitet wird von einem verbreiteten Auftreten von *Palorbitolina lenticularis* führenden Schichten. 2) Eine Änderung der C^{13} Isotopenverhältnisse, die an das OAE1a gebunden ist und die im oberen Bereich an die *Deshayesites forbesi* Biozone gebunden ist. In dieser Zone befindet sich eine Zone aus Korallenschutt, die durch Umkrustungen von *Lithocodium aggregatum* und *Bacinella irregularis* gekennzeichnet ist. Dieser Moment fällt zusammen mit dem vermuteten Auftreten des thermalen Maximums im frühen Apt. Der umkrustete Korallenschutt mit dem gehäuften Auftreten von gross-schaligen abgeflachten *Palorbitolina lenticularis* werden als Hinweis auf physiko-chemische Schwankungen in Verbindung mit dem OAE1a gedeutet. 3) Ein lang anhaltender Abkühlungstrend im späten Früh-Apt, der von einer Regression begleitet wird. Im Verlauf dieser Phase bilden sich ausgedehnte

Karbonatplatformen mit einer charakteristischen Urgon-Fazies, die von Rudisten und Korallen geprägt ist. 4) Das Maximum der regressiven Phase, in der die im späten Früh-Apt entstandenen Karbonatplatformen unter atmosphärischen Bedingungen freiliegen. In diesem Zeitabschnitt kommt es zur Bildung verbreiteter Paleo-Karst Strukturen, während sich zugleich die Sedimentation beckenwärts verlagert. Dieses Interval aus dem späten Früh-Apt stellt ein Lehrbuchbeispiel für eine sequenzstratigraphische Abfolge in Karbonatgesteinen mit vier "systems tracts" dar. 5) Ein vom späten Früh-Apt bis Spät-Apt dauernder regressiver Abschnitt, in dem sich littorale Bedingungen entwickeln. Die Etablierung proximaler Verhältnisse im Untersuchungsraum war begleitet von erheblichem siliziklastischem Sedimenteintrag, der vermutlich durch regionale Tektonik und zeitgleich ablaufende klimatische Veränderungen von einem semi-ariden Regime im frühen Apt zu semi-humiden Verhältnissen im mittleren bis späten Apt verursacht wird. Die vorliegende Untersuchung stellt ein gut dokumentiertes Beispiel für die Entwicklung des epikontinentalen Meeres im Apt dar und bietet ein Werkzeug zum Vergleich und zur Analyse anderer flachmariner Sedimentfolgen aus dem Apt.

Acknowledgements

Danke,
Klaus Bitzer, Richard Regner (when they built you Richy, they broke the mould), Sabine Thüns, Annika Bienert, Sandra Hollstein, Thorsten Parchent, Marika Kiefer, Ralf Saeugling, Matthias Rader, Lars Querndt, Johannes Reiß, Michael Selinger, Christiana Scharfenberg, Waltraud Fritsche, Tobias Schenk, Wiebke Menzel, Stefan Wedel, Rahel Volmer, Sebastian Willmes, Jochen Harttung, Felix Püplichhuisen, Christina Müller, Fabian Faller, Bernd Kremling, Felix Schlagintweit, Kristin Tirpitz, Ulrich Heimhofer, Adrian Immenhauser, Niels Rameil, Familie Rader, FSV Landau an der Isard, Maisel's Weisse, Krug-Bräu, Aktien, Hannes Löser, Familie Blumenstock, Rolf Schroeder, Simone Hösch, Christiane Bube und Gabriele Wittke.

Gràcies,
Ramon Salas, Josep Anton Moreno-Bedmar, Vinyet Baqués, Marià Franco, Sergi Raya, Maitessita Castillejo, Roger Clavera-Gispert, Oriol Mateu, Eulàlia Gili, Carles Martín-Closas, Jordi Illa, Marçal Rosell, Montserrat Franch, Toni Palau, Galdric Bover, Iu Bover, David García-Sellés, Juan Diego Martín-Martín, Oriol Solé, Irene Cantarero, Cristian Estop, Marc Aurell, Antoni Grauges, Lluís Cabrera i al Departament de Geoquímica, Petrologia i Prospecció Geològica de la Facultat de Geologia de la Universitat de Barcelona.

Gracias,
Jezabel Huemes, Séfora Figueroa, Sara Tomás, Ramón Mas, Miguel (de Villarroya de los Pinares), Carmen Pérez y familia Ibáñez Escorial.

Thanks,
Peter W. Skelton, Maurice E. Tucker, Octavian Catuneanu and the International Association of Sedimentologists.

Dank je wel,
Hemmo Abels en Frits Hilgen.

Table of contents

Summary i

Zusammenfassung iii

Acknowledgements v

Table of contents vi

CHAPTER 1 GENERAL INTRODUCTION 1

1.1 The Aptian 1

1.2 Objectives of the Thesis 4

1.3 Synopsis 4

1.4 List of manuscripts and specification of own contributions 9

1.5 References 11

CHAPTER 2 RESULTS 16

2.1 Sedimentary evolution of an Aptian syn-rift carbonate system (Maestrat Basin, E Spain): effects of accommodation and environmental change 16

2.1.1 Introduction 17

2.1.2 Study area and geological setting 19

2.1.3 Material and methods 22

2.1.4 Facies evolution and sequence stratigraphy 23

2.1.4.1 Sequence I 24

2.1.4.1.1 Eastern side 24

2.1.4.1.2 Western side 27

2.1.4.2 Sequence II 30

2.1.4.2.1 Eastern side 34

2.1.4.2.2 Western side 36

2.1.4.3 Sequence III 38
2.1.4.3.1 Eastern side 39
2.1.4.3.2 Western side 39
2.1.4.4 Sequence IV 41
2.1.4.4.1 Eastern side 41
2.1.4.4.2 Western side 42
2.1.5 Stable isotope (C, O) geochemistry **43**
2.1.5.1 Carbon-isotope data 43
2.1.5.2 Oxygen-isotope data 44
2.1.6 Quantitative subsidence analysis and accommodation **46**
2.1.7 Discussion **48**
2.1.7.1 Diagenetic alteration of stable isotope data 48
2.1.7.2 Carbon-isotope record 50
2.1.7.3 Oxygen-isotope record 51
2.1.7.4 The Aptian evolution of the Galve sub-basin: controlling factors 52
2.1.7.4.1 Eustatic sea level change 52
2.1.7.4.2 Subsidence and faulting 55
2.1.7.4.3 Environmental changes and facies succession 57
2.1.8 Conclusions **60**
2.1.9 Acknowledgements **62**
2.1.10 References **62**

2.2 Sequence stratigraphy and architecture of a late Early-Middle Aptian carbonate platform succession from the western Maestrat Basin (Iberian Chain) **75**
2.2.1 Introduction **76**
2.2.2 Geological setting of the study area **78**
2.2.3 Material and methods **81**
2.2.4 Facies Associations and distribution **82**
2.2.4.1 Facies Association I: slightly argillaceous-marly wackestone-packstone 82
2.2.4.2 Facies Association II: rudist and coral floatstone 85
2.2.4.3 Facies Association III: rudist and coral reworked floatstone-

rudstone 85
2.2.4.4 Facies Association IV: peloidal and bioclastic packstone-grainstone 86
2.2.4.5 Facies Association V: sandy limestone 86
2.2.4.6 Facies Association VI: oyster-rich calcarenite 87
2.2.4.7 Facies Association VII: corals embedded in marls 87
2.2.4.8 Facies Association VIII: marls with interbedded storm-induced turbidites 88
2.2.4.9 Facies Association IX: slightly cross-bedded calcarenite 88
2.2.4.10 Facies Association X: debris-flow deposits 89
2.2.5 Facies successions **89**
2.2.5.1 Parasequence A 91
2.2.5.2 Parasequence B 91
2.2.5.3 Parasequence C 92
2.2.5.4 Parasequence D 92
2.2.6 Sequence stratigraphic interpretation **93**
2.2.6.1 Highstand System Tract (Depositional Sequence A) 93
2.2.6.2 Forced Regressive Wedge Systems Tract (Depositional Sequence A) 98
2.2.6.3 Lowstand Prograding Wedge Systems Tract (Depositional Sequence B) 101
2.2.6.4 Transgressive System Tract (Depositional Sequence B) 104
2.2.6.5 Highstand System Tract (Depositional Sequence B) 108
2.2.7 Discussion **109**
2.2.8 Conclusions **114**
2.2.9 Acknowledgements **115**
2.2.10 References **116**

2.3 Lower Aptian coral rubble deposits from the western Maestrat Basin (Iberian Chain, Spain): records of chemical and physical disturbances **129**
2.3.1 Introduction **130**
2.3.2 Geographical and geological setting of the study area **132**
2.3.3 Data collection and methods **136**

2.3.4 Results **136**

2.3.4.1 Biotic composition 136

2.3.4.1.1 Corals 136

2.3.4.1.2 Microencrusters 137

2.3.4.1.3 Other micro and macrobiota 139

2.3.4.2 Bioerosional structures 141

2.3.4.3 Deposit fabric and sedimentary features 145

2.3.5 Discussion **147**

2.3.5.1 Origin, generation and deposition of coral rubble 147

2.3.5.2 Binding agents 153

2.3.5.3 Associated biotic community and bioerosion 155

2.3.5.4 Carbonate production, sedimentation rates and environmental factors 156

2.3.5.5 Regional and global significance of the Lithocodium-Bacinella event 158

2.3.6 Conclusions **160**

2.3.7 Acknowledgements **162**

2.3.8 References **162**

CHAPTER 3 GENERAL CONCLUSIONS 173

3.1 Conclusions 173

3.2 References 175

List of figures 200

List of tables 207

Appendix List of other publications 208

CHAPTER 1

GENERAL INTRODUCTION

1.1 The Aptian

The Aptian is one of the most fascinating stages in the history of the Earth: ”superplume” volcanic episodes in the Pacific Ocean; elevated levels of atmospheric CO_2; strong climatic changes; oceanic anoxic events; significant eustatic fluctuations; platform crises and turnover of biota. In essence, this was the stage at which severe natural processes challenged the lush widespread carbonate platforms spread throughout the Tethyan realm (e.g., Weissert and Lini, 1991; Erba, 1994; Weissert et al., 1998; Menegatti et al., 1998; Larson and Erba, 1999; Hochuli et al., 1999; Pittet et al., 2002; Wissler et al., 2003; Skelton, 2003a; Weissert and Erba, 2004; Föllmi et al., 2006; Dumitrescu et al., 2006; Burla et al., 2008; Bover-Arnal et al., 2009, under review, submitted for publication).

As current absolute dating methods indicate, the Aptian Stage, which is located within the Cretaceous period, ranged from between 125 and 112 million years (Ma) (Ogg and Ogg, 2006). This time interval, which was conditioned by extreme climatic warmth and consequently, higher global sea levels than nowadays, has classically been regarded as an excellent example of the Earth in greenhouse climatic mode (e.g., Larson and Erba, 1999).

Owing to the widely held belief that the increased levels of atmospheric CO_2 during recent decades - due to human activities such as the combustion of fossil fuels and deforestation - are having a deleterious effect upon the Earth’s weather and climate, the study of such an eventful time slice under intensified greenhouse conditions contributes to improving our understanding of the interplay between the solid Earth, oceans, atmosphere and life within a non anthropogenic-impacted greenhouse state geologic case study.

This thesis, then, is first and foremost intended as a portrayal of the Earth system during the Aptian, viewed from the Iberian carbonate systems developed during that time in the northern Tethyan margin, which may serve not only to increase

understanding of the Aptian world and its carbonate systems but also to provide some indication of what can be expected from the Earth's climate in the foreseeable future.

In order to address this central theme, the Aptian sedimentary succession cropping out in the Galve sub-basin (western Maestrat Basin; E Iberia) (Fig. 1.1) was thoroughly analyzed using multiscale and multidisciplinary approaches involving extensive fieldwork and laboratory analyses. The Galve sub-basin was chosen as the study area since it provides a superbly exposed, expanded (more than 800 m-thick; Bover-Arnal et al., under review), relatively complete and continuous Aptian sedimentary succession, which can be followed for 20 km, from proximal platform areas to basinal settings, with only minor tectonic overprint.

The integrated basin analysis presented here provides a detailed description and an overall interpretation from both regional and global perspectives of Aptian sedimentary evolution in the Galve sub-basin, focusing fundamentally on issues of sedimentary accommodation, seismic-scale geometries, facies heterogeneities and environmental change (see Chapter 2.1). In addition, two specific Aptian topics of key significance not only for those dealing with Aptian and Cretaceous sedimentary successions, but also for those engaged in global environmental change (see chapters 2.2 and 2.3) are addressed exhaustively.

In this regard, one of the most enigmatic and poorly studied events that occurred within this time window is a mid Aptian sea-level drop of probable glacio-eustatic magnitude, which, according to recent compilations (e.g., Bover-Arnal et al., 2009), could have had a widespread occurrence along the margin of the Tethys. With reference to Aptian glacio-eustasy, this issue is controversial in light of the conflicting evidence available and the widespread idea of greenhouse conditions during the Cretaceous period (see Price, 1999; Immenhauser, 2005). Given the importance of providing an ancient example of a cold snap within a greenhouse world in order to shed light on present day global warming, this global-scale fall in sea level is extensively investigated in the Galve sub-basin in Chapter 2.2.

Furthermore, in Chapter 2.3, the sedimentary expression of the early Aptian oceanic anoxic event (OAE1a) in the Galve sub-basin is analyzed in detail. This event, which was characterized by the global deposition of organic carbon-rich black shales in deep water settings (e.g., Menegatti et al., 1998), is widely assumed to be a consequence of high CO_2 atmospheric concentrations related to the emplacement of large igneous provinces in the Pacific Ocean, such as the Ontong Java and the Manihiki plateau

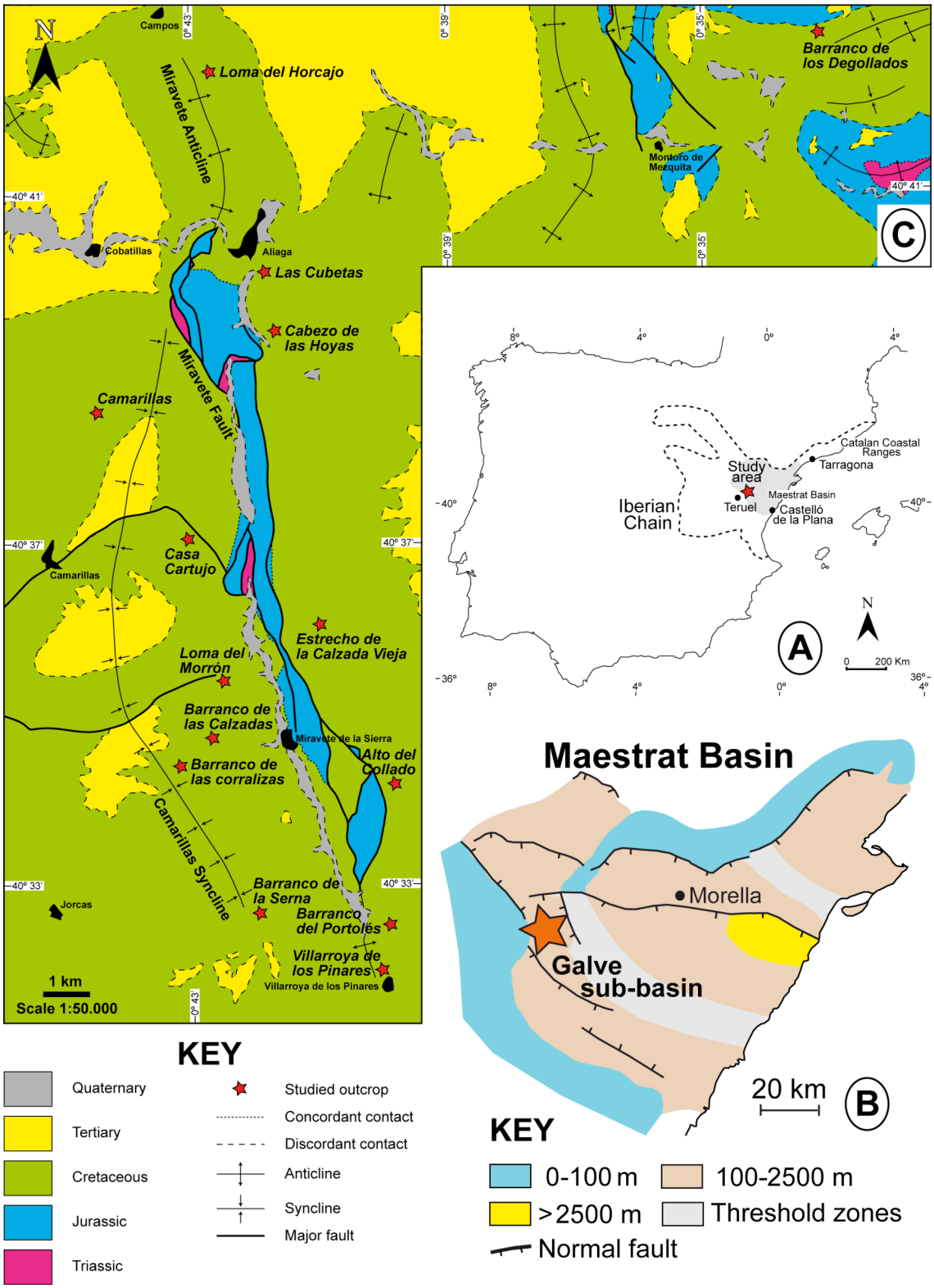

Figure 1.1. Location and geological map of the study area. A) Geographical location of the study area in the western Maestrat Basin (eastern Iberian Chain; E Iberia). B) Map of the Maestrat Basin with the location of the Galve sub-basin, which is marked by a red star, in its western marginal part. Modified from Salas et al. (2001). C) Geological setting and location of the studied outcrops in the Galve sub-basin. Modified after Canérot et al. (1979) and Gautier (1980).

(Larson and Erba, 1999), and the increased spreading rates at mid oceanic ridges (Larson, 1991). Therefore, the study of the OAE1a coeval strata in the Galve sub-basin provides an excellent opportunity to track all these environmental perturbations and determine their effects on the biotic communities established during this time interval in the Tethyan epicontinental seas.

1.2 Objectives of the thesis

The aim of this study was to provide a high-resolution characterization of the Aptian Stage in the Galve sub-basin by means of a multiscale and multidisciplinary analysis of its sedimentary succession. In order to achieve a realistic depiction of this time slice, displaying the interplay between the solid Earth, oceans, atmosphere and life, it was necessary to identify the different global and regional controlling factors and their effects on the composition and nature of the sedimentary record.

To this end, a primary objective was to establish a conceptual model that integrated the facies, sequence stratigraphy, carbon and oxygen isotopes, and quantitative subsidence analysis of the Aptian sedimentary succession cropping out in the western Maestrat Basin, seeking: a) to discriminate the effects of eustasy and tectonism controlling accommodation and their impact on the evolution of this mixed carbonate-siliciclastic system; b) to trace climatic and environmental changes and their effects on the carbonate-producing biota and sedimentation; c) to contextualize these platform carbonates in order to establish parallelisms and differences with other Aptian carbonate systems which flourished along the margin of the Tethys; d) to provide an apropriate means of measuring this time slice for calibrating the analysis of other coeval epeiric sedimentary records; e) above all, to improve our understanding of the Aptian Stage and its carbonate systems.

1.3 Synopsis

The Aptian synrift epeiric sedimentary succession of the Galve sub-basin can be subdivided into five formations (Morella, Xert, Forcall, Villarroya de los Pinares and Benassal) and four large-scale transgressive-regressive (T-R) sequences, which were calibrated by means of geomagnetic polarity analysis and ammonoid and rudist biostratigraphic data. The T-R sequences interpreted are fairly correlatable with the Aptian global sequences of Ogg and Ogg (2006), indicating a significant eustatic

imprint on sedimentation, although synrift subsidence was the most important mechanism in controlling accommodation. In this respect, the sedimentary record studied was largely conditioned by the activity of the Miravete master normal transfer fault, which compartmentalized the sub-basin into a hanging-wall western side (central Galve sub-basin) and a foot-wall eastern side (eastern Galve sub-basin). This fault conditioned the architecture of the facies and thickness between the two sides throughout the Aptian (Simón et al., 1998).

The transgressive systems tract (TST) of Sequence I starts with fluviatile deposits of basal Aptian age (Salas et al., 2005), which overlie the Barremian marine deposits of the Artoles Formation. These continental deposits belong to the Morella Formation. The latter formation is only recorded in the central part of the Galve sub-basin. During the earliest Aptian, the Miravete fault acted as a trap for these continental deposits and retained them in the hanging-wall western side. Above these continental deposits the sedimentary succession becomes progressively more marine in character, giving rise to the marine deposits of the Xert Formation. On the eastern side of the Miravete fault, the basal part of the Xert Formation constitutes the base of Sequence I. The transgressive deposits of the Xert Formation are distinguished by wave- and tidally-influenced mixed carbonate-siliciclastic deposits, which evolve basinwards and upwards in the succession to beds with abundant large-sized flattened *Palorbitolina lenticularis*.

The regressive systems tract (RST) of Sequence I is characterized by the development of carbonate platforms with small rudist bivalves, corals and green algae at both sides of the Miravete fault. These regressive deposits correspond to the upper part of the Xert Formation. The marine deposits of the Xert Formation laid down on both sides of the Miravete fault along a homoclinal-type of ramp. Sequence I is bounded below by a transgressive ravinement surface (TRS) on the eastern side of the Miravete fault and by a subaerial unconformity (SU) on the western side. The top of Sequence I is marked by a maximum regressive surface (MRS) on both sides of the Miravete fault.

Widespread deposition of marls with interbedded limestones containing abundant large-sized discoidal *Palorbitolina lenticularis* constitutes the Forcall Formation and characterizes the TST of Sequence II. This transgressive phase corresponds to the acme of the Early Aptian long-term transgression recorded along the margin of the Tethys, which was accompanied by a bloom of *Palorbitolina lenticularis* displaying large discoidal morphologies (Embry, 2005). This broad transgression was linked to a global warming event triggered by exceptional volcanic episodes in the

Pacific Ocean and increased spreading rates at mid ocean ridges (Larson, 1991; Larson and Erba, 1999). The intensified greenhouse conditions induced by such exceptional igneous events would have led to the Early Aptian oceanic anoxic event (OAE1a) (Weissert et al., 1998; Weissert and Erba, 2004).

In the Galve sub-basin, the carbon-isotope negative spike that marks the onset of the OAE1a (according to Li et al., 2008; Méhay et al., 2009; Tejada et al., 2009; Millán et al., 2009) was identified at the upper part of the *Deshayesites forbesi* ammonite biozone, within a horizon formed by sand- to cobble-sized coral rubble rigidly bound by *Lithocodium aggregatum* and *Bacinella irregularis*. This encrusted horizon, which is coeval with the probable Early Aptian thermal maximum, is interpreted here as a record of chemical and physical disturbances related to the OAE1a. Consequently, it would have formed as a result of severe storms, elevated seawater temperatures and ocean acidification induced by the aforementioned high atmospheric concentrations of CO_2. These physico-chemical disturbances would have had a highly recurrent catastrophic impact on the coral communities developing in the Galve sub-basin, resulting in sub-basin-wide coral rubble piles. The presence of a hard substratum, the slow sedimentation rates registered at that time and the increased nutrient and alkalinity fluxes due to intensified rainfall triggered by the aforementioned intensified conditions, would have favored the binding of these deposits by *Lithocodium-Bacinella* crusts, and the widespread occurrence of large-sized flattened *Palorbitolina lenticularis* and bioeroders. Moreover, feedback mechanisms of these high atmospheric concentrations of CO_2, such as burial of carbon inventories, would have induced a cooling tendency throughout the OAE1a time interval. This cooling trend is supported by the OAE1a coeval positive excursion displayed by the oxygen-isotope curve measured along Lower Aptian strata in the Galve sub-basin.

Furthermore, during most of the Early Aptian, the Galve sub-basin registered the highest rate of rapid synrift subsidence for the Aptian, which was associated with significant extension by normal faulting. Therefore, earthquake-induced physical disturbances might also have been responsible, at least in part, for the formation and reworking of the aforementioned coral rubble carpets.

The maximum flooding surface (MFS) of Sequence II is interpreted to be at the base of the encrusted coral rubble levels. Hence, these resedimented deposits constitute the onset of the RST of Sequence II. On the eastern side of the Miravete fault, above the levels bearing *Lithocodium-Bacinella* crusts, a distally steepened ramp containing rudist

bivalves and corals developed (Villarroya de los Pinares Formation). On the western side of the Miravete fault, and due to the differential subsidence caused by the activity of the Miravete fault, the early RST of Sequence II corresponds to an alternation of marls and limestones with abundant large-sized flattened *Palorbitolina lenticularis* and ammonites, which belong to the Forcall Formation. However, during the late RST of Sequence II (late Early Aptian) and due to the slowing down of sea level rise to a near standstill, a flat-topped non-rimmed carbonate platform with rudists and corals flourished on this hanging-wall side (Villarroya de los Pinares Formation). On both sides of the Miravete fault, the evolution from a homoclinal-type of ramp during Sequence I to a distally steepened ramp on the eastern side and to a flat-topped non-rimmed depositional profile on the western side during the RST of Sequence II was the result of synrift normal faulting.

The platform to basin transitional area of the carbonate platform which developed during the late Early Aptian on the western side of the Miravete fault shows all the attributes of a "four-systems-tract" depositional sequence (*sensu* Hunt and Tucker, 1992). Therefore, an alternative sequence stratigraphic interpretation is provided. In this platform margin, five differentiated systems tracts within two distinct depositional sequences can be recognized: the Highstand Systems Tract (HST and Forced Regressive Wedge Systems Tract (FRWST) of Depositional Sequence A; and the Lowstand Prograding Wedge Systems Tract (LPWST), Transgressive Systems Tract (TST) and Highstand Systems Tract (HST) of Depositional Sequence B. The HST of Depositional Sequence A is distinguished by a large carbonate platform with rudist bivalves and corals stacked in a prograding pattern. The FRWST corresponds to a detached cross-bedded calcarenite situated at the toe of the former highstand slope, in a basinal position. The LPWST of Depositional Sequence B is constituted by a small carbonate platform with rudists and corals, which downlaps over the detached forced regressive calcarenite and onlaps landwards. With the TST, the lowstand prograding platform started to backstep and evolved to marly sedimentation after drowning. The establishment of new carbonate platforms of corals and large rudist bivalves and nerineid gastropods characterizes the HST of Depositional Sequence B.

These systems tracts were possible to characterize on account of the identification of the different surfaces with sequence stratigraphic significance that bound them. In this regard, a basal surface of forced regression, a correlative conformity, a transgressive surface exhibiting a hardground, a maximum flooding

surface and a subaerial unconformity with broad palaeokarst development, which constitutes the boundary between Sequence II and III at the western side of the Miravete fault, are all well-documented and mappable throughout the stratigraphic interval constituting this platform margin.

The forced regression of relative sea level occurred at the uppermost Early Aptian that resulted in the depostion of calcarenitic wedges basinwards had a glacio-eustatic magnitude and is interpreted as having global significance. Hence, this lowering sea level could be linked to the cooling tendency proposed in the literature for the late Early Aptian (Hochuli et al., 1999; Steuber et al., 2005). This long-term cooling trend would have started with the global burial of organic carbon during the OAE1a.

On the eastern side of the Miravete fault, no signs of subaerial exposure were identified at the top of Sequence II. Therefore, the limit between Sequence II (Early Aptian) and Sequence III (Middle Aptian) corresponds to a MRS, which separates regressive platform carbonates with rudists and corals from the transgressive marls and limestones with orbitolinids of the Benassal Formation. Locally, this boundary correponds to a TRS, which is overlain by hydrodynamic deposits interpreted as the transgressive lag of Sequence III.

The establishment of carbonate platforms with rudists and corals distinguishes the RST of Sequence III on the western side of the Miravete fault. On the eastern side of the Miravete fault, this RST is characterized by the widespread development of beds with abundant orbitolinids. However, in the proximal setting of this latter side, limestones with bivalves and corals alternating with siliciclastic-influenced deposits exhibiting hydrodynamic structures occur. The top of this sequence is marked by a MRS on both sides of the Miravete fault.

The TST of Sequence IV corresponds to bluish marls with calcareous nodules and marly limestones with nodular bedding containing *Mesorbitolina parva*. The RST is characterized by the establishment of littoral conditions and enhanced siliciclastic supplies. The installation of more proximal conditions in this area during the Late Aptian is the result of the late Early to Late Aptian long-term regressive context. The presence of widespread siliciclastic deposits is probably linked to regional tectonics and to a progressively changing climate from a semi-arid regime during the Early Aptian, to a semi-humid mode in the Middle-Late Aptian (Ruffell & Worden, 2000).

The top of Sequence IV is marked by a regional unconformity, which passes basinwards to a MRS that separates the mixed carbonate-silicilastic deposits of the RST of Sequence IV (Benassal Formation) from the Albian coal-bearing Escucha Formation.

Given these results, the Aptian sedimentary evolution of the Galve sub-basin described here faithfully reflects all the major ocean-climate perturbations which occurred during this stage. Thus, this sedimentary record may be of relevance as a reference for the study of other time-equivalent epeiric stratigraphic intervals.

1.4 List of manuscripts and specification of own contributions

In this cumulative dissertation, three manuscripts are included (chapters 2.1, 2.2 and 2.3). The first one is under review in Geologica Acta, the second one is published in Sedimentary Geology and the last one is submitted for publication to Palaios.
The authors listed on the different studies contributed approximately as follows:

Chapter 2.1

Authors: Bover-Arnal, T., Moreno-Bedmar, J.A., Salas, R., Skelton, P.W., Bitzer, K. and Gili, E.

Title: Sedimentary evolution of an Aptian syn-rift carbonate system (Maestrat Basin, E Spain): effects of accommodation and environmental change

Status: under review

Journal: Geologica Acta

Contributions

Bover-Arnal, T.	75% (idea, data collection, data analysis, discussion of the results, manuscript preparation)
Moreno-Bedmar, J.A.	5% (data collection, discussion of the results)
Salas, R.	5% (data analysis, discussion of the results)
Skelton, P.W.	5% (data analysis, discussion of the results)
Bitzer, K.	5% (discussion of the results)

Gili, E.	5% (discussion of the results)

Chapter 2.2

Authors: Bover-Arnal, T., Salas, R., Moreno-Bedmar, J.A. and Bitzer, K.

Title: Sequence stratigraphy and architecture of a late Early-Middle Aptian carbonate platform succession from the western Maestrat Basin (Iberian Chain)

Status: published

Journal: Sedimentary Geology

Contributions

Bover-Arnal, T.	80% (idea, data collection, data analysis, discussion of the results, manuscript preparation)
Salas, R.	10% (data analysis, discussion of the results)
Moreno-Bedmar, J.A.	5% (discussion of the results)
Bitzer, K.	5% (discussion of the results)

Chapter 2.3

Authors: Bover-Arnal, T., Salas, R., Martín-Closas, C., Schlagintweit, F. and Moreno-Bedmar, J.A.

Title: Lower Aptian coral rubble deposits from the western Maestrat Basin (Iberian Chain, Spain): records of chemical and physical disturbances

Status: submitted for publication

Journal: Palaios

Contributions

Bover-Arnal, T.	80% (idea, data collection, data analysis, discussion of the results, manuscript preparation)

Salas, R.	5% (data analysis, discussion of the results)
Martín-Closas, C.	5% (discussion of the results)
Schlagintweit, F.	5% (discussion of the results)
Moreno-Bedmar, J.A.	5% (data collection, discussion of the results)

1.5 References

Bover-Arnal, T., Salas, R., Moreno-Bedmar, J.A. and Bitzer, K. (2009). Sequence stratigraphy and architecture of a late Early-Middle Aptian carbonate platform succession from the western Maestrat Basin (Iberian Chain, Spain). Sedimentary Geology, 219, 280-301.

Bover-Arnal, T., Moreno-Bedmar, J.A., Salas, R., Skelton, P.W., Bitzer, K. and Gili, E. (under review). Sedimentary evolution of an Aptian syn-rift carbonate system (Maestrat Basin, E Spain): effects of accommodation and environmental change. Geologica Acta.

Bover-Arnal, T., Salas, R., Martín-Closas, C., Schlagintweit, F. and Moreno-Bedmar, J.A. (submitted for publication). Lower Aptian coral rubble deposits from the western Maestrat Basin (Iberian Chain, Spain): records of chemical and physical disturbances. Palaios.

Burla, S., Heimhofer, U., Hochuli, P.A., Weissert, H. and Skelton, P. (2008). Changes in sedimentary patterns of coastal and deep-sea successions from the North Atlantic (Portugal) linked to Early Cretaceous environmental change. Palaeogeography, Palaeoclimatology, Palaeoecology, 257, 38-57.

Canérot, J., Crespo, A. and Navarro, D. (1979). Montalbán, hoja nº 518. Mapa Geológico de España 1:50.000. 2ª Serie. 1ª Edición. Servicio de Publicaciones, Ministerio de Industria y Energía, Madrid, 31 pp.

Dumitrescu, M., Brassell, S.C., Schouten, S., Hopmans, E.C. and Sinninghe Damsté, J.S. (2006). Instability in tropical Pacific sea-surface temperatures during the early Aptian. Geology, 34, 833-836.

Embry, J.C. (2005). Paléoécologie et architecture stratigraphique en haute résolution des platesformes carbonatées du Barrémien-Aptien de la Néo-Téthys (Espagne, Suisse, Provence, Vercors) – impact respectif des différents facteurs de contrôle. Doctoral thesis. Museum National d'Histoire Naturelle – Institut Français du Petrole, Paris, 299 pp.

Erba, E. (1994). Nannofossils and superplumes: The early Aptian "nannofossil crisis". Paleoceanography, 9, 483-501.

Föllmi, K.B., Godet, A., Bodin, S. and Linder, P. (2006). Interactions between environmental change and shallow water carbonate buildup along the northern Tethyan margin and their impact on the Early Cretaceous carbon isotope record. Paleoceanography, 21, PA4211, doi:10.1029/2006PA001313.

Gautier, F. (1980). Villarluengo, hoja nº 543. Mapa Geológico de España 1:50.000. 2ª Serie. 1ª Edición. Servicio de Publicaciones, Ministerio de Industria y Energía, Madrid, 45 pp.

Hochuli, P.A., Menegatti, A.P., Weissert, H., Riva, A., Erba, E. and Premoli Silva, I. (1999). Episodes of high productivity and cooling in the early Aptian Alpine Tethys. Geology, 27, 657-660.

Immenhauser, A. (2005). High-rate sea-level change during the Mesozoic: New approaches to an old problem. Sedimentary Geology, 175, 277-296.

Larson, R.L. (1991). Geological consequences of superplumes. Geology, 19, 963-966.

Larson, R.L. and Erba, E. (1999). Onset of the mid-Cretaceous greenhouse in the Barremian-Aptian: Igneous events and the biological, sedimentary, and geochemical responses. Paleoceanography, 14, 663-678.

Li, Y-X., Bralower, T.J., Montañez, I.P., Osleger, D.A., Arthur, M.A., Bice, D.M., Herbert, T.D., Erba, E. and Premoli Silva, I. (2008). Toward an orbital chronology for the early Aptian Oceanic Anoxic Event (OAE1a, ~120 Ma). Earth and Planetary Science Letters, 271, 88-100.

Méhay, S., Keller, C.E., Bernasconi, S.M., Weissert, H., Erba, E., Botín, C. and Hochuli, P.A. (2009). A volcanic CO_2 pulse triggered the Cretaceous Oceanic Anoxic Event 1a and a biocalcification crisis. Geology, 37, 819-822.

Menegatti, A.P., Weissert, H., Brown, R.S., Tyson, R.V., Farrimond, P., Strasser, A. and Caron, M. (1998). High-resolution $\delta^{13}C$ stratigraphy through the early Aptian "Livello Selli" of the Alpine Tethys. Paleoceanography, 13, 530-545.

Millán, M.I., Weissert, H.J., Fernández-Mendiola, P.A. and García-Mondéjar, J. (2009). Impact of Early Aptian carbon cycle perturbations on evolution of a marine shelf system in the Basque-Cantabrian Basin (Aralar, N Spain). Earth and Planetary Science Letters, 287, 392-401.

Ogg, J.G. and Ogg, G. (2006). Updated by James G. Ogg (Purdue University) and Gabi Ogg to: GEOLOGIC TIME SCALE 2004 (Gradstein, F.M., Ogg, J.G., Smith, A.G. et al.; Cambridge University Press).

Pittet, B., Van Buchem, F.S.P., Hillgärtner, H., Razin, P., Grötsch, J. and Droste, H. (2002). Ecological succession, palaeoenvironmental change, and depositional sequences of Barremian-Aptian shallow-water carbonates in northern Oman. Sedimentology, 49, 555-581.

Price, G.D. (1999). The evidence and implications of polar ice during the Mesozoic. Earth-Science Reviews, 48, 183-210.

Ruffell, A. and Worden, R. (2000). Palaeoclimate analysis using spectral gamma-ray data from the Aptian (Cretaceous) of southern England and southern France. Palaeogeography, Palaeoclimatology, Palaeoecology, 155, 265-283.

Salas, R., Guimerà, J., Martín-Closas, C., Meléndez, A. and Alonso, A. (2001). Evolution of the Mesozoic Central Iberian Rift System and its Cainozoic inversion (Iberian Chain). In: Ziegler, P.A., Cavazza, W., Roberston, A.H.F. and Crasquin-Soleau, S. (eds.). Peri-Tethys Memoir 6: Peri-Tethyan Rift/Wrench Basins and Passive Margins. Mémoires du Muséum National d'Histoire Naturelle, Paris, 186, 145-186.

Salas, R., Martín-Closas, C., Delclòs, X., Guimerà, J., Caja, M.A. and Mas, R. (2005). Factores principales de control de la sedimentación y los cambios bióticos durante el tránsito Jurásico-Cretácico en la Cadena Ibérica. Geogaceta, 38, 15-18.

Simón, J.L., Liesa, C.L. and Soria, A.R. (1998). Un sistema de fallas normales sinsedimentarias en las unidades de facies Urgon de Aliaga. Geogaceta, 24, 291-294.

Skelton, P.W. (2003). The Cretaceous World. Cambridge, ed. Cambridge University Press, 360 pp.

Steuber, T., Rauch, M., Masse, J.-P., Graaf, J. and Malkoc, M. (2005). Low-latitude seasonality of Cretaceous temperatures in warm and cold episodes. Nature, 437, 1341-1344.

Tejada, M.L.G., Suzuki, K., Kuroda, J., Coccioni, R., Mahoney, J.J., Ohkouchi, N., Sakamoto, T. and Tatsumi, Y. (2009). Ontong Java Plateau eruption as a trigger for the early Aptian oceanic anoxic event. Geology, 37, 855-858.

Weissert, H. and Lini, A. (1991). Ice Age Interludes During the Time of Cretaceous Greenhouse Climate? In: Müller, D.W., McKenzie, J.A. and Weissert, H. (eds.). Controversies in Modern Geology: Evolution of Geological Theories in Sedimentology, Earth History and Tectonics. Academic Press, London, 173-191.

Weissert, H., Lini, A., Föllmi, K.B. and Kuhn, O. (1998). Correlation of Early Cretaceous carbon isotope stratigraphy and platform drowning events: a possible link? Palaeogeography, Palaeoclimatology, Palaeoecology, 137, 189-203.

Weissert, H. and Erba, E. (2004). Volcanism, CO2 and palaeoclimate: a Late Jurassic-Early Cretaceous carbon and oxygen isotope record. Journal of the Geological Society, London, 161, 1-8.

Wissler, L., Funk, H. and Weissert, H. (2003). Response of Early Cretaceous carbonate platforms to changes in atmospheric carbon dioxide levels. Palaeogeography, Palaeoclimatology, Palaeoecology, 200, 187-205.

CHAPTER 2

RESULTS

2.1 Sedimentary evolution of an Aptian syn-rift carbonate system (Maestrat Basin, E Spain): effects of accommodation and environmental change

Telm Bover-Arnal[1*], Josep A. Moreno-Bedmar[2], Ramon Salas[2], Peter W. Skelton[3], Klaus Bitzer[1] and Eulàlia Gili[4]

[1]Abteilung Geologie, Fakultät für Biologie, Chemie und Geowissenschaften, Universität Bayreuth, Universitätsstr, 30, 95440, Bayreuth, Germany
[2]Departament de Geoquímica, Petrologia i Prospecció Geològica, Facultat de Geologia, Universitat de Barcelona, Martí i Franqués s/n, 08028, Barcelona, Spain
[3]Department of Earth and Environmental Sciences, The Open University, Milton Keynes MK7 6AA, UK
[4]Departament de Geologia, Facultat de Ciències, Universitat Autònoma de Barcelona, Edifici Cs, 08193, Bellaterra (Cerdanyola del Vallès), Spain

*corresponding author
E-mail address: Telm.Bover@uni-bayreuth.de

Under review in Geologica Acta

Abstract: We report an integrated study of an expanded and relatively complete syn-rift continental to epeiric marine succession of Aptian age, cropping out in the western Maestrat Basin (eastern Iberian Chain). Four transgressive-regressive sequences are recognized throughout this mixed carbonate-siliciclastic succession, with excellent age control provided by ammonite biostratigraphic data. The transgressive systems tracts

consist mainly of alternations of marls and limestones rich in orbitolinids. The regressive systems tracts are essentially characterized by wave- and tidally influenced siliciclastic and carbonate deposits, and by the development of carbonate platforms with rudists, corals, orbitolinids and green algae. Carbon and oxygen isotope curves were established in order to identify the global $\delta^{13}C$ perturbations related to the OAE1a. These perturbations commence with a horizon of coral rubble encrusted by *Lithocodium aggregatum* and *Bacinella irregularis* with widespread large-sized discoidal *Palorbitolina lenticularis*. Associated $\delta^{18}O$ values indicate high-frequency cooling-warming climatic cycles. The fault-controlled rapid syn-rift subsidence recorded during this stage was the most important factor in producing accommodation. However, the major transgressions, sea level falls and biotic changes recorded in the eastern Iberian Chain are in agreement with those registered in other contemporaneous basins of the Tethys. Thus, the resulting sedimentary succession faithfully reflects the major oceanographic and climatically-driven global changes that characterized this stage albeit within a context established by regional tectonics. Hence, this well-documented record of the evolution of an Aptian epicontinental sea provides a useful comparative case study for the analysis of other Aptian epeiric sedimentary successions.

Keywords: Carbonate system, Sequence stratigraphy, OAE1a, Aptian, Iberian Chain

2.1.1 Introduction

Many authors have characterized the Aptian as an eventful time with strong climatic changes ranging from greenhouse to sub-glacial conditions, a "superplume" volcanic episode in the Pacific Ocean, an oceanic anoxic event, significant eustatic variations, a platform crisis and turnover of marine biota (e.g., Weissert and Lini, 1991; Erba, 1994; Weissert et al., 1998; Menegatti et al., 1998; Larson and Erba, 1999; Hochuli et al., 1999; Pittet et al., 2002; Wissler et al., 2003; Skelton, 2003a; Weissert and Erba, 2004; Föllmi et al., 2006; Dumitrescu et al., 2006; Burla et al., 2008). In the Neo-Tethyan realm, large carbonate platforms dominated by rudists, corals, orbitolinids and green algae developed during this time (e.g., Malchus et al., 1996; Vilas et al., 1995; Rosales, 1999; Vennin and Aurell, 2001; Pittet et al., 2002; Hillgärtner et al., 2003; Millán et al., 2007; Bover-Arnal et al., 2008, 2009; Tomás et al., 2008). Platform carbonate producing biota are variously controlled by light, temperature, hydrodynamic conditions,

basin-floor topography, seawater chemistry (O_2, CO_2, Mg, Ca, nutrients and salinity) and, over longer time intervals, eustasy (e.g., Hallock and Schlager, 1986; Pomar and Kendall, 2007). Hence, their observed ecological responses to changing external factors can be interpreted in terms of all these tectonically and climatically-driven events in the sedimentary record.

The Maestrat Basin (E Iberian Chain, Spain), especially the Galve sub-basin (western Maestrat Basin), offers an exceptional opportunity to study the interaction of these factors in a continuous and well-exposed continental to epicontinental marine succession that encompasses the entire Aptian Stage, with excellent time control based on ammonite biostratigraphy. To this end, the present work establishes a conceptual model that integrates the facies, sequence stratigraphy, carbon and oxygen isotopes, and quantitative subsidence analysis of the sedimentary succession.

Vennin and Aurell (2001) and Embry (2005) were the first to extensively document the sedimentary evolution of the Aptian succession in the Galve sub-basin. Vennin and Aurell (2001) performed facies and sequence stratigraphic analyses in the eastern part of the sub-basin. Embry (2005) revisited these sections and studied them in further detail, carrying out C- and O-isotope analyses and discussing palaeoenvironmental aspects of the platform carbonates. With this background, the present paper aims to further analyze and illustrate the sedimentary evolution of the Galve sub-basin. The inclusion of the central part of the sub-basin in the present study, together with the original data presented here, provide a more detailed and complete sub-basin-wide view of the Aptian Stage in this western margin of the Maestrat Basin. Moreover, alternative sequence stratigraphic and depositional models, different interpretations of the $\delta^{13}C$ and $\delta^{18}O$ curves, and extensive discussion of the tectonic and environmental factors controlling sedimentary evolution offer a revised global perspective. Recently, Bover-Arnal et al. (2009) carried out facies analysis and applied a four systems tract-based sequence stratigraphic method (see Hunt and Tucker, 1992) to the interpretation of late Early-Middle Aptian strata that were generated in the carbonate platform margin located in the central Galve sub-basin. The current paper, by contrast, analyzes the whole of the Aptian sedimentary succession throughout the Galve sub-basin in terms of transgressive-regressive (T-R) sequences (see Catuneanu et al., 2009).

The goals of the present study are: (a) to show the relationship between tectonism, eustasy and evolution of this mixed carbonate-siliciclastic system; (b) to investigate how these sensitive marine environments were affected by ocean-climate system perturbations;

(c) to contextualize the carbonate succession stratigraphically in order to establish similarities and differences with other Aptian carbonate systems developed along the Tethyan margins; and (d) to provide an outstanding record of this stage that could serve to calibrate the analysis of other Aptian sedimentary successions. Furthermore, the implications concerning the roles of tectonics and eustasy in controlling accommodation, sequence stratigraphy, environmental change, carbonate platform evolution and carbon- and oxygen-isotope geochemistry are also of potential value for other non-Aptian studies.

2.1.2 Study area and geological setting

During Late Jurassic (Late Oxfordian) to Early Cretaceous (Middle Albian) times, the Iberian plate underwent extension due to the opening of the Central and North Atlantic domains. Rifting led to the formation of several intraplate basins in Iberia such as the Maestrat Basin. Later, as a result of the collision between the Iberian and European plates during the Alpine orogeny (Late Eocene to Early Miocene), the Iberian basins underwent tectonic inversion to form the Iberian Chain (Salas et al., 2001). The study area is located in the eastern Iberian Chain (E Spain) (Fig. 2.1.1A), between the villages of Campos, Camarillas and Villarroya de los Pinares, and the investigated succession crops out along two main Tertiary folds: the Camarillas syncline, striking NNE-SSW in the north and NNW-SSE in the south, and the Miravete anticline to the East of the latter, striking NNW-SSE (Fig. 2.1.1B). The area corresponds to the western margin of the Maestrat Basin known as the Galve sub-basin (Salas and Guimerà, 1996). Continental and marine carbonate and siliciclastic terrigenous sedimentation occurred in a context of differential subsidence with several half-graben structures related to synsedimentary ENE-WSW normal listric faulting. The latter were confined by steep NNW-SSE normal transfer faults (Fig. 2.1.1B) (Simón et al., 1998; Soria, 1997; Vennin and Aurell, 2001; Liesa et al., 2006). The Miravete fault was a NNW-SSE Mesozoic normal transfer fault that partitioned the study area into a western, hanging-wall side, and an eastern, foot-wall side (Fig. 2.1.1B). This fault controlled facies architecture and thickness differences between the two sides (Simón et al., 1998).

The Aptian succession in the Galve sub-basin is up to 810 m thick, spans 13 Ma (the absolute age interval for the Aptian according to Ogg and Ogg, 2006), and is composed of five lithostratigraphic units with the rank of formations (Canérot et al., 1982). This stratigraphic record can be divided into four large-scale T-R sequences, the

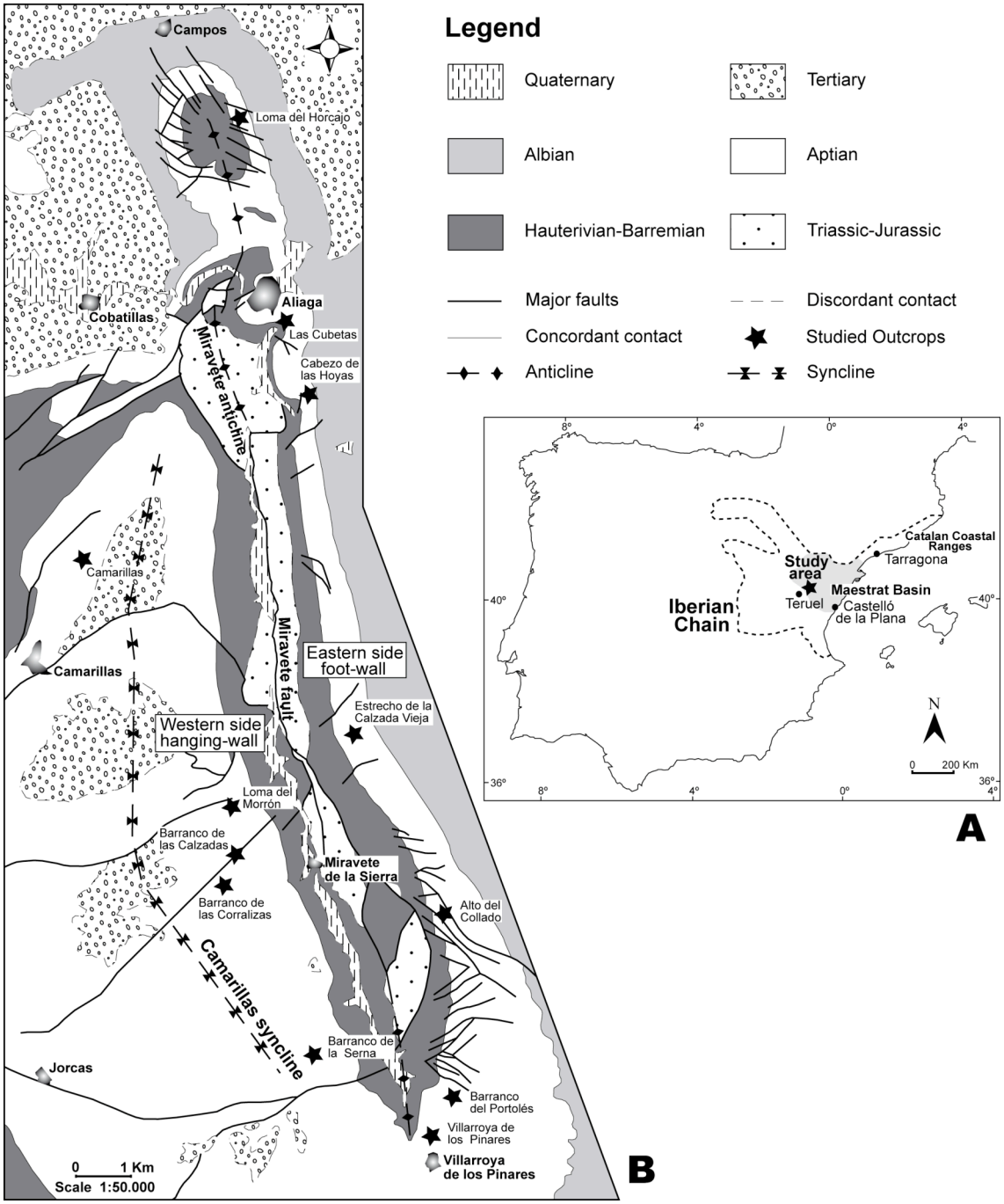

Figure 2.1.1. A) Geographical location of the study area in the eastern Iberian Chain (E-Spain). B) Geological setting and location of the studied outcrops. Modified after Canérot et al. (1979) and Gautier (1980).

ages of which were calibrated with ammonite biostratigraphic data from the Galve sub-basin provided by Weisser (1959) and Moreno-Bedmar et al. (2009, accepted), geomagnetic polarity (Salas et al., 2005) and rudist biostratigraphy. The analyzed succession overlies a regional subaerial unconformity that separates Barremian marine mixed carbonate-siliciclastic sediments of the Artoles Formation (below; Salas, 1987),

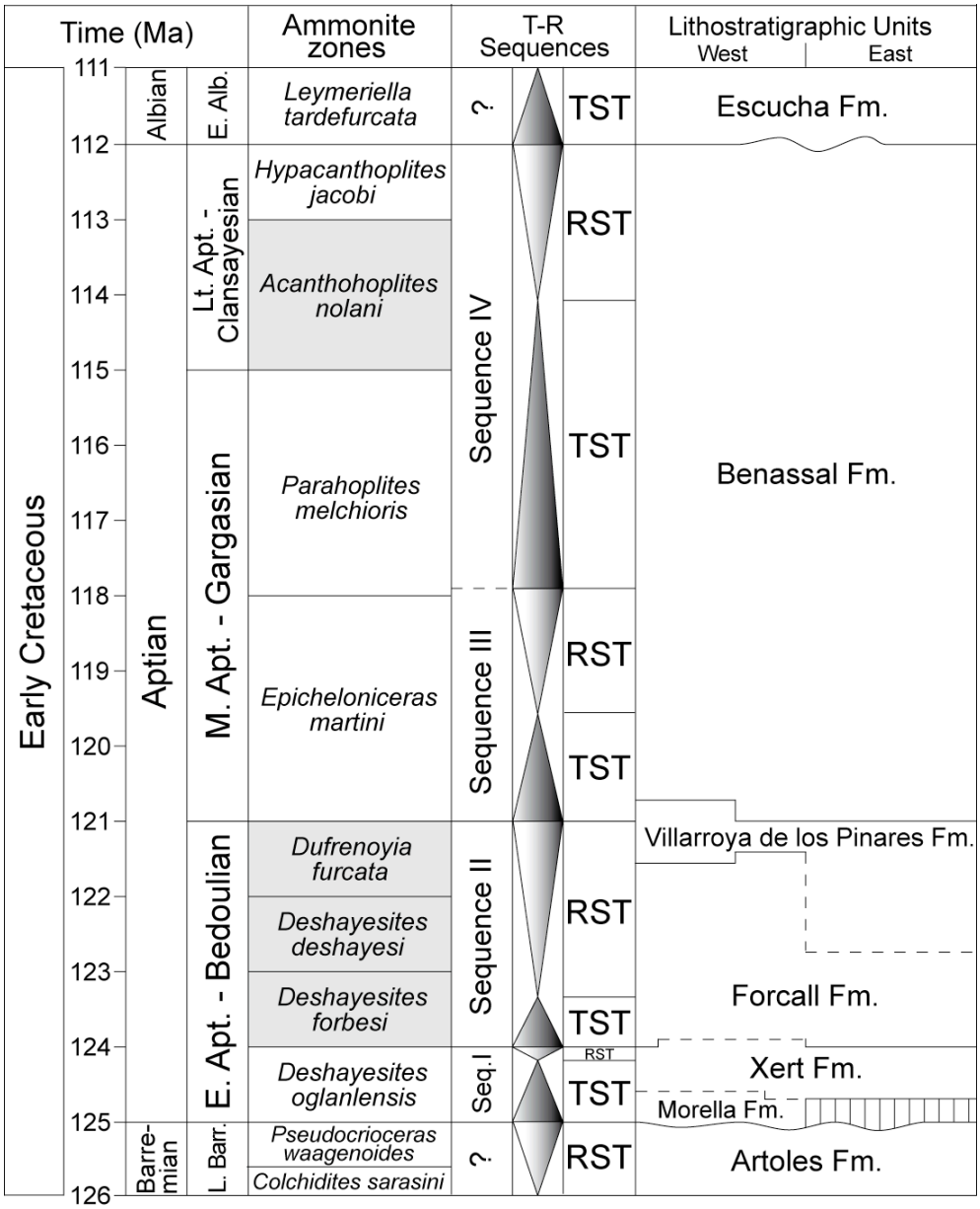

Figure 2.1.2. Stratigraphic framework and age relationships for the Aptian in the Galve sub-basin. Identified ammonite biozones are indicated in grey (Weisser, 1959; Moreno-Bedmar et al., 2009, accepted). Discontinuous lines indicate lack of absolute dating. Absolute ages are from Ogg and Ogg (2006). Modified from Bover-Arnal et al. (2009).

from fluviatile deposits of the Morella Formation or terrigenous marine sediments of the lower part of the Xert Formation (above; Fig. 2.1.2). The continental sediments of the Morella Formation are of earliest Aptian age (Salas et al., 2005) and become progressively more marine in character upwards in the succession. The four T-R sequences interpreted in this study comprise the last-mentioned formation, and the Xert, Forcall, Villarroya de los Pinares and Benassal formations (Fig. 2.1.2). With the

exception of the continental siliciclastic-rich earliest Aptian deposits, these sequences were produced in epeiric marine environments characterized by classical Tethyan Urgonian facies associations dominated by rudists, corals, green algae, orbitolinids and other benthic foraminifera. The top of the studied succession is marked by another regional unconformity (Fig. 2.1.2), which passes basinwards to a maximum regressive surface, and separates the transitional wave- and tidal-influenced sediments of the upper part of the Benassal Formation (below), from the carbon-rich deltaic deposits of the Escucha Formation (above). The base of this last-mentioned formation is of earliest Albian age (Moreno-Bedmar et al., 2008; Villanueva-Amadoz et al., 2008).

2.1.3 Material and methods

Twelve well-exposed stratigraphic sections were measured along the Miravete anticline and Camarillas syncline. Five of them were logged on the east side of the Miravete fault (foot-wall), in Loma del Horcajo, Las Cubetas, Cabezo de las Hoyas, Estrecho de la Calzada Vieja and Alto del Collado. On the west side (hanging-wall), the remaining seven sections were logged in Camarillas, Loma del Morrón, Barranco de las Calzadas, Barranco de las Corralizas, Barranco de la Serna, Barranco del Portolés and Villarroya de los Pinares (Fig. 2.1.1B). A detailed sedimentological analysis was performed for each section. Microfacies were described from 166 thin sections of samples collected during field work.

The difficulty of recognizing lithostratigraphic surfaces with sequence stratigraphic significance *sensu* Van Wagoner et al. (1988) or Hunt and Tucker (1992) in most of the Aptian sedimentary succession studied here, has led us to adopt the approach of identifying T-R sequences (see Catuneanu et al., 2009). In exposed epicontinental carbonate sedimentary successions, the distinguishing physical characteristics of the three or four systems tract-based depositional sequences (Van Wagoner et al., 1988; Hunt and Tucker, 1992) are often masked or not preserved because of poor exposure conditions, variable rates of sediment production and accumulation, erosion or superimposition of surfaces. By contrast, the characterization of T-R sequences is mainly based on the recognition of surfaces that mark large-scale changes in trend from deepening- to shallowing-upwards, or *vice versa*. These surfaces are subaerial unconformities, transgressive ravinement surfaces, maximum regressive surfaces and maximum flooding surfaces (see Catuneanu et al., 2009). Aerial

photographs and panoramic photomosaics of the outcrops were utilized for mapping, sequence stratigraphic analysis and correlation of sequences along the study area.

The geochemical analysis of $\delta^{13}C$ and $\delta^{18}O$ was measured on 66 bulk rock samples of limestones, marly limestones and marls, using standard analytical techniques. Samples were taken about every 2 m in the Barranco de las Calzadas and were analyzed, using for each analysis 60-70 μg for limestones and 100-1000 μg for marls and marly limestones. Carbonate powder from limestones was extracted with a microdrill in order to avoid large skeletal components, corals, microencrusters and diagenetic calcite veins. The samples were treated with H_3PO_4 (100%) at 70 ºC and the evolved CO_2 was analyzed with a Thermo Finnigan MAT-252 stable isotope ratio mass spectrometer in the *Unitat de Medi Ambient - Serveis Cientificotècnics de la Universitat de Barcelona* laboratory. The isotope results are expressed in ‰ relative to the VPDB standard, and their precision was ± 0.03 for $\delta^{13}C$ and ± 0.06 for $\delta^{18}O$.

In order to explain the accommodation changes, quantitative subsidence analysis was carried out on five selected representative stratigraphic columns using standard back-stripping methods (Sclater and Christie, 1980; Watts, 1981; Bond and Kominz, 1984). Variables used in these techniques concerned lithology, absolute age (based on Ogg and Ogg, 2006) and palaeobathymetry values that were estimated from fossil assemblages and hydrodynamic structures. Density values for each type of lithology and porosity/depth relationships (c factors) were used to calculate decompaction (Sclater and Christie, 1980; Schmoker and Halley, 1982). No eustatic corrections were performed. The total subsidence (decompacted) was calculated for each selected stratigraphic section. The total accommodation was obtained from the total subsidence corrected with estimated palaeo-water depth values (Vilas et al., 2003).

2.1.4 Facies evolution and sequence stratigraphy

The Aptian sedimentary evolution and sequence stratigraphical framework of the Galve sub-basin is here presented in detail for the twelve studied outcrops. Ten facies assemblages ranging from continental to basinal were defined from lithology, texture, skeletal and non-skeletal components, sedimentary structures and the stratigraphic context. Each facies assemblage reflects a specific depositional environment based on inferred bathymetry and hydrodynamic conditions. The facies assemblages are described and classified in Table 2.1.1, and illustrated in Figs. 2.1.3,

2.1.4A-D and 2.1.4F. Moreover, four large-scale T-R sequences were interpreted based on the observed facies succession and the recognition of ten main surfaces with sequence stratigraphical implications. Together the sequences span the entire duration of the Aptian, about 13 Myr (according to the Aptian absolute ages from Ogg and Ogg, 2006). A chart displaying the distribution of the facies assemblages and sequence stratigraphy analysis for the five sections from the eastern side of the Miravete fault is shown in Fig. 2.1.5. The chart for the remaining seven sections on the western side is displayed in Fig. 2.1.6. A sequence stratigraphic interpretation of the exposure on the eastern side Las Cubetas section and the western side Villarroya de los Pinares section is shown in Fig. 2.1.7.

2.1.4.1 Sequence I

Sediments deposited during this sequence, which spans approximately 1 Ma (according to the Aptian absolute ages of Ogg and Ogg, 2006), mainly constitute the Morella and Xert formations (Fig. 2.1.2). The age of these deposits has been determined based on a geomagnetic polarity analysis carried out along the Morella Formation (Salas et al., 2005), which provided the identification of the magnetic anomaly M0r, and the recognition of the *Deshayesites forbesi* biozone at the lower part of Sequence II (Moreno-Bedmar et al., 2009, accepted). Accordingly, these sediments could be correlatable with the *Deshayesites oglanlensis* biozone. Sequence I reaches a maximum thickness of up to 193 m in the Barranco de las Calzadas section, and thins to 38 m in the Cabezo de las Hoyas section.

2.1.4.1.1 Eastern side

The basal boundary of Sequence I is represented by a transgressive ravinement surface that separates the Barremian mixed carbonate-siliciclastic marine deposits (below) from the Aptian shallow-water carbonate and siliciclastic marine sediments of the Xert Formation (above). The transgressive systems tract (TST) of this sequence is distinguished by an initial wedge of high energy deposits stacked in a retrogradational pattern that thickens landwards. From the Cabezo de las Hoyas section to the south (basinwards), these high energy lithofacies grade into marls and limestones dominated by large-sized discoidal *Palorbitolina lenticularis*, which agglutinated quartz grains.

During the early transgressive phase, the eastern side tectonics probably positioned the Alto del Collado section area as a wave-influenced threshold zone. This

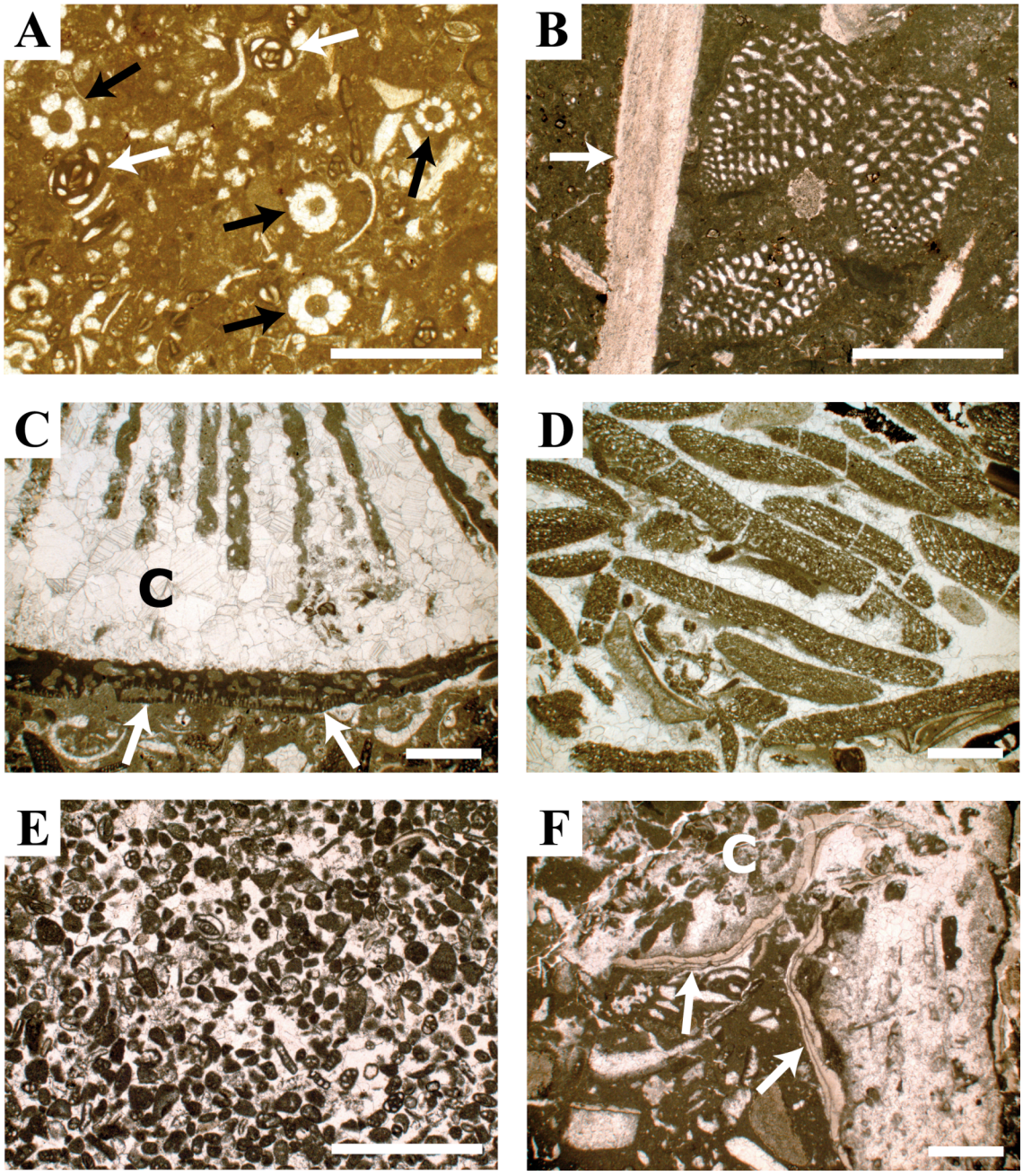

Figure 2.1.3. Photomicrographs of representative microfacies of the different general depositional settings. Scale bars = 1 mm. A) Wackestone of miliolids (white arrows) and fragments of dasycladaceans (black arrows) (Facies Assemblage 4; Table 2.1.1). Xert Formation, Alto del Collado section. B) Floatstone of Chondrodonta with Orbitolinopsis praesimplex. The white arrow points to a fragment of Chondrodonta (Facies Assemblage 4; Table 2.1.1). Xert Formation, Las Cubetas section. C) Lithocodium aggregatum (white arrows) bioeroded by clionid sponges, encrusting coral debris (black C) (Facies Assemblage 9; Table 2.1.1). Forcall Formation, Estrecho de la Calzada Vieja section. D) Grainstone of large-sized discoidal Palorbitolina lenticularis agglutinating quartz particles in the tests (Facies Assemblage 7; Table 2.1.1). Villarroya de los Pinares Formation, Las Cubetas section. E) Peloidal-foraminiferal (mostly miliolids) grainstone (Facies Assemblage 3; Table 2.1.1). Villarroya de los Pinares Formation, Barranco de las Calzadas section. F) Debris-flow facies of coral fragments (white C) and other unidentified bioclasts encrusted by peyssonneliaceans (white arrows) (Facies Assemblage 10; Table 2.1.1). Villarroya de los Pinares Formation, Barranco de las Calzadas section.

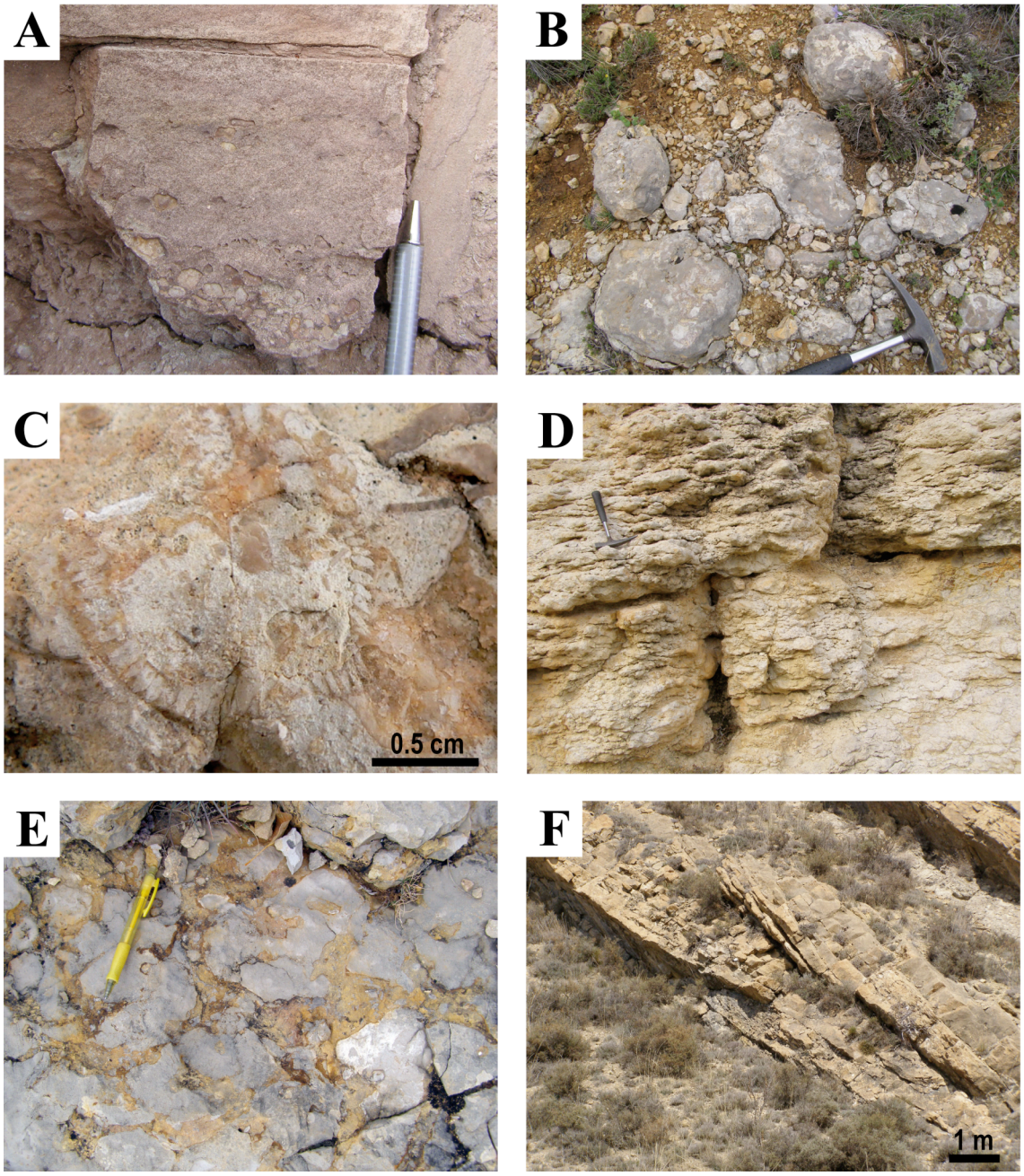

Figure 2.1.4. Outcrop photographs of representative facies of the general depositional settings. A) Detail of a coarse-grained siliciclastic lag at the erosive base of a channelized sandstone (Facies Assemblage 1; Table 2.1.1). Morella Formation, Barranco de las Calzadas section. B) Dome-shaped corals embedded in marls (Facies Assemblage 6; Table 2.1.1). Villarroya de los Pinares Formation, Barranco de las Calzadas section. C) Detail of a Caprina parvula section (Facies Assemblage 4; Table 2.1.1). Villarroya de los Pinares Formation, Barranco de las Calzadas section. D) Outcrop-scale image of debris-flow deposits (Facies Assemblage 10; Table 2.1.1). Note the nodular aspect of these resedimented lithofacies. Villarroya de los Pinares Formation, Barranco de las Calzadas section. E) Detail of the boundary surface between Sequence II and Sequence III exhibiting palaeokarst development. Villarroya de los Pinares Formation, Camarillas section. F) Detail of a herringbone cross-stratification (Facies Assemblage 2; Table 2.1.1). Benassal Formation, Barranco del Portolés section.

circumstance isolated the area from direct detrital influx, favouring the deposition of peloidal-bioclastic grainstones containing skeletal fragments and benthic foraminifera such as miliolids, *Choffatella decipiens* and small-sized conical orbitolinids. The Alto del Collado palaeohigh evolved within the late TST to limestones rich in *Palorbitolina lenticularis*. In addition, episodes of sedimentation below fair-weather wave base during the TST are indicated by the intercalation of floatstones with miliolids, dasycladaceans (Fig. 2.1.3A), small requieniid rudists and *Chondrodonta* in the Cabezo de las Hoyas and Alto del Collado sections. According to Vennin and Aurell (2001) and due to the lack of bulging of sedimentary bodies or step-like geometries, the eastern side depositional profile corresponded to a homoclinal-type of ramp (Fig. 2.1.5).

The transition between the TST and the regressive systems tract (RST) is marked by a facies change between the transgressive siliciclastic and orbitolinid-rich deposits, and the regressive carbonate lithologies dominated by dasycladaceans, miliolids, *Choffatella decipiens*, *Palorbitolina* sp., *Orbitolinopsis praesimplex* (Fig. 2.1.3B), unidentified benthic foraminifera, *Chondrodonta* and other molluscs. Interbedded sandy limestones and peloidal-bioclastic grainstones displaying cross-bedding and plane-parallel stratification also occur. These latter are mostly present along the middle-lower ramp, and signify the basinwards progradation during regression of the energetic facies trend formed in the upper ramp during the previous transgression (Fig. 2.1.5).

2.1.4.1.2 Western side

The lower boundary of the sequence corresponds to a subaerial unconformity, which separates Barremian carbonate and siliciclastic marine sediments (below) from the basal Aptian non-marine deposits of the Morella Formation (above). The Morella Formation consists of fluviatile sediments made up of red clay and channelized sandstones (Fig. 2.1.4A), occasionally reworked by tidal currents, which become progressively more marine in character upwards in the succession. This formation is only recorded on the western side of the Miravete fault (Fig. 2.1.6). During the earliest Aptian, the Miravete fault apparently acted as a trap for these continental deposits, and retained them in the hanging-wall block. The Morella Formation changes laterally to the marine siliciclastic-influenced sediments of the Xert Formation. The TST exhibits

FACIES ASSEMBLAGE	DESCRIPTION	MAIN CONSTITUENTS	OTHER COMMON ELEMENTS	SEDIMENTARY FEATURES	DEPOSITIONAL ENVIRONMENT
1	Sandstones and red clay	Quartz, mica and feldspar	Dinosaur remains and fragments of wood	Low angle cross-bedding or plane-parallel stratification, and occasionally, massive or nodular bedding; tidal bundles (occasionally); crevasse splay structures (occasionally); basal lag deposits; root bioturbation (occasionally); erosive bases	Fluvial with tidal influence, low- to high-energy conditions. Supratidal to intertidal.
2	Ferruginous ooid grainstones, sandstones, sandy limestones and tan clay	Quartz, ooids and peloids	Mica, feldspar, oncoids, glauconite (occasionally), orbitolinids, miliolids, other foraminifera, oysters, unidentified bivalves, brachiopods (rarely) and fragments of gastropods, other molluscs, serpulids, bryozoans, echinoids, dasycladaceans and red algae	Low angle cross-bedding, plane-parallel or massive stratification, and occasionally, nodular bedding or herringbone stratification; unidentified burrows; *Lithophaga* borings (occasionally); hardgrounds; erosive bases	Marine shallow-water, low- to high-energy conditions. Intertidal to subtidal.
3	Sandstones, sandy limestones, ooid-peloid grainstones and bioclastic calcarenites	Quartz, mica, feldspar, ooids, peloids, miliolids, other foraminifera, and fragments of gastropods, echinoids and bivalves	Orbitolinids, oncoids, glauconite (occasionally), and fragments of corals, *Chondrodonta*, unidentified oysters, rudists, other molluscs, serpulids, bryozoans, red algae and dasycladaceans	Low angle cross-bedding, plane-parallel or massive stratification, and occasionally, herringbone stratification; tidal bundles (occasionally); tidal channels (occasionally); tidal bars (occasionally); unidentified burrows; hardgrounds; erosive bases	Marine shallow-water, moderate- to high-energy conditions. Intertidal to subtidal.
4	Mudstones and rudist-dominated wackestone to floatstone	Requieniid and elevator rudists, branching corals and miliolids	Sheet-like, platy and irregular massive corals, gastropods, *Chondrodonta*, other oysters, unidentified bivalves, echinoids, orbitolinids, sessile foraminifera, other foraminifera, bryozoans, dasycladaceans, red algae, codiaceans and peloids (occasionally)	Massive or nodular bedding; *Lithophaga* borings; unidentified burrows (occasionally); hardgrounds (occasionally)	Below fair-weather wave base to below storm wave base, low-energy conditions. Subtidal.
5	Limestones bearing scattered massive corals	Irregular massive corals	Sheet-like, platy and domal corals, coral debris, orbitolinids, sessile foraminifera, other foraminifera, encrusting red algae, gastropods, bryozoans, echinoids, rudists, unidentified bivalves, *Lithocodium aggregatum*, *Bacinella irregularis* and peloids	Massive or nodular bedding; *Lithophaga* borings	Below fair-weather wave base to below storm wave base, low-energy conditions. Subtidal.

6	Dome-shaped corals embedded in marls	Domal corals	Sheet-like, branching and irregular massive corals, *Chondrodonta*, other oysters, elevator rudists, unidentified bivalves, gastropods, echinoids, brachiopods and hydrozoans	*Lithophaga* borings; unidentified burrows (occasionally)	Below storm wave base, low-energy conditions. Subtidal.
7	Orbitolinid-dominated wackestone to grainstone	Orbitolinids	Peloids, sessile foraminifera, other foraminifera, oysters, unidentified bivalves, echinoids, gastropods, serpulids, bryozoans, belemnites, fish teeth, and fragments of undiagnosed molluscs, corals and dasycladaceans	Massive or nodular bedding, and occasionally, plane-parallel stratification; unidentified burrows and occasionally, *Thalassinoides*; hardgrounds (occasionally); erosive bases (occasionally)	Below fair-weather wave base to hemipelagic, low- to moderate-energy conditions. Subtidal.
8	Marls with interbedded storm-induced turbidites, marly limestones and mudstone to packstone limestones	Orbitolinids	Ammonites, nautiloids, oysters, unidentified bivalves, gastropods, echinoids, solitary corals, brachiopods, sessile foraminifera and occasionally, peloids, dasycladaceans, fish teeth, decapods, pyritized fragments and quartz	Massive or nodular bedding, and occasionally, plane-parallel stratification; *Thalassinoides* and other unidentified burrows; hardgrounds (occasionally); erosive bases (occasionally)	Hemipelagic, low- to moderate-energy, conditions. Subtidal.
9	Coral rubble encrusted by microorganisms	*Lithocodium aggregatum*, *Bacinella irregularis*, coral debris and orbitolinids	Encrusting red algae, sessile foraminifera, brachiopods, serpulids, briozoans, sponges, echinoids, corals, oysters, caprinid rudists and solitary corals	Nodular bedding	Below fair-weather wave base to hemipelagic, low- to moderate-energy conditions. Subtidal.
10	Rudist-dominated wackestone to rudstone debris flows	Requieniid and elevator rudists, miliolids and fragments of corals and rudists	Peloids, orbitolinids, other foraminifera, *Lithocodium aggregatum*, *Bacinella irregularis*, and fragments of gastropods, bryozoans, *Chondrodonta*, other oysters, unidentified bivalves, other molluscs, echinoids, encrusting red algae, dasycladaceans and codiaceans	Massive or nodular bedding; unidentified burrows; slump scars (occasionally); erosive bases	Below fair-weather wave base to hemipelagic, low- to moderate-energy conditions. Subtidal.

Table 2.1.1. Facies classification and interpretation of depositional environment.

greater thicknesses and reflects deeper environments than in the east side. The siliciclastic wedge is made of fining-upwards tidal channel and bar deposits displaying erosive bases, tidal bundles, cross-bedding and herringbone cross-stratification. Bioturbation is commonly present, as well as oysters, unidentified bivalves and the infaunal echinoid *Heteraster oblongus*. Basinwards, these deposits are interbedded with marls rich in mica. The intertidal lithofacies evolve upwards and laterally to marls and limestones with abundant large-sized discoidal *Palorbitolina lenticularis*, which agglutinated minute quartz grains. At the distal Barranco del Portolés and Villarroya de los Pinares sections, especially in their uppermost TST, these orbitolinid-rich carbonates alternate with oolitic-bioclastic packstones to grainstones containing miliolids, *Choffatella decipiens*, other unidentified foraminifera and skeletal fragments (Fig. 2.1.6).

The maximum flooding surface is marked by a facies turnover from transgressive *Palorbitolina*-dominated beds to regressive wackestone to floatstone limestones containing *Chondrodonta*, small requieniid rudists, other molluscs, miliolids, *Choffatella decipiens*, *Palorbitolina praecursor*, *Orbitolinopsis* sp., *Rectodictyoconus giganteus* and other benthic foraminifera. Locally, bioturbated horizons occur. The lateral continuity of beds that thicken in a southerly direction together with the absence of bulges or step-like geometries indicate that the depositional profile during the RST was a homoclinal carbonate ramp, as inferred on the eastern side for the same time interval (Fig. 2.1.6).

2.1.4.2 Sequence II

Sequence II is equivalent to the Forcall and the main part of the Villarroya de los Pinares formations (Fig. 2.1.2). On the western side, the top of the Xert Formation also belongs to the basal transgressive deposits of this sequence, which spans approximately 3 Ma (according to the absolute ages for the Aptian of Ogg and Ogg, 2006), and reaches its maximum thickness of up to 237 m in the Barranco de las Calzadas section. At the Alto del Collado section the sequence thins to 141 m. The recognition of the ammonite species *Deshayesites kiliani* at the lower part of this sequence permits us to constrain its base to the *Deshayesites forbesi* biozone. The lower boundary of the sequence is formed by a sharp contact, which corresponds to a maximum regressive surface, though no

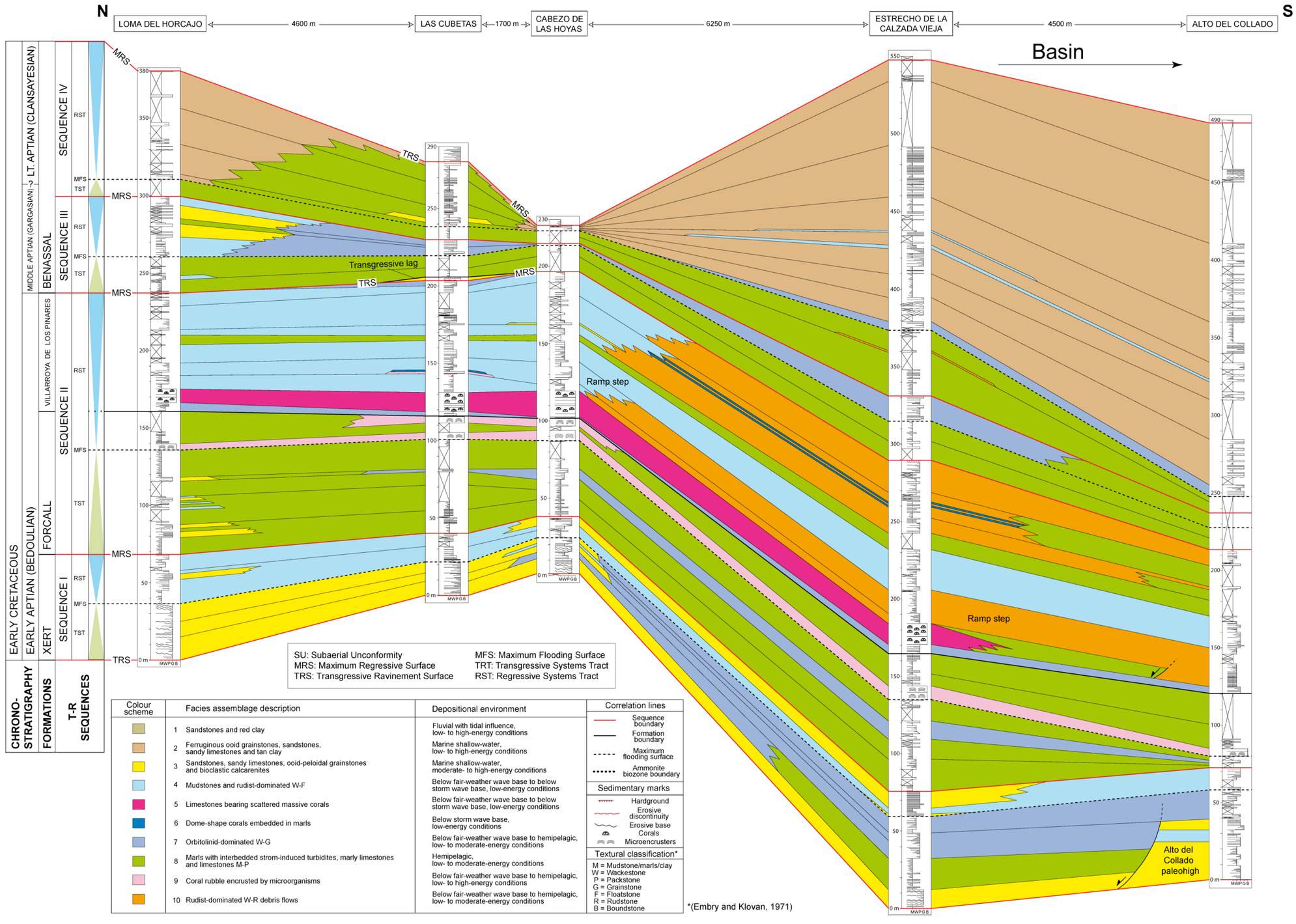

Figure 2.1.5. Eastern side sequence correlation scheme and distribution of the facies assemblages.

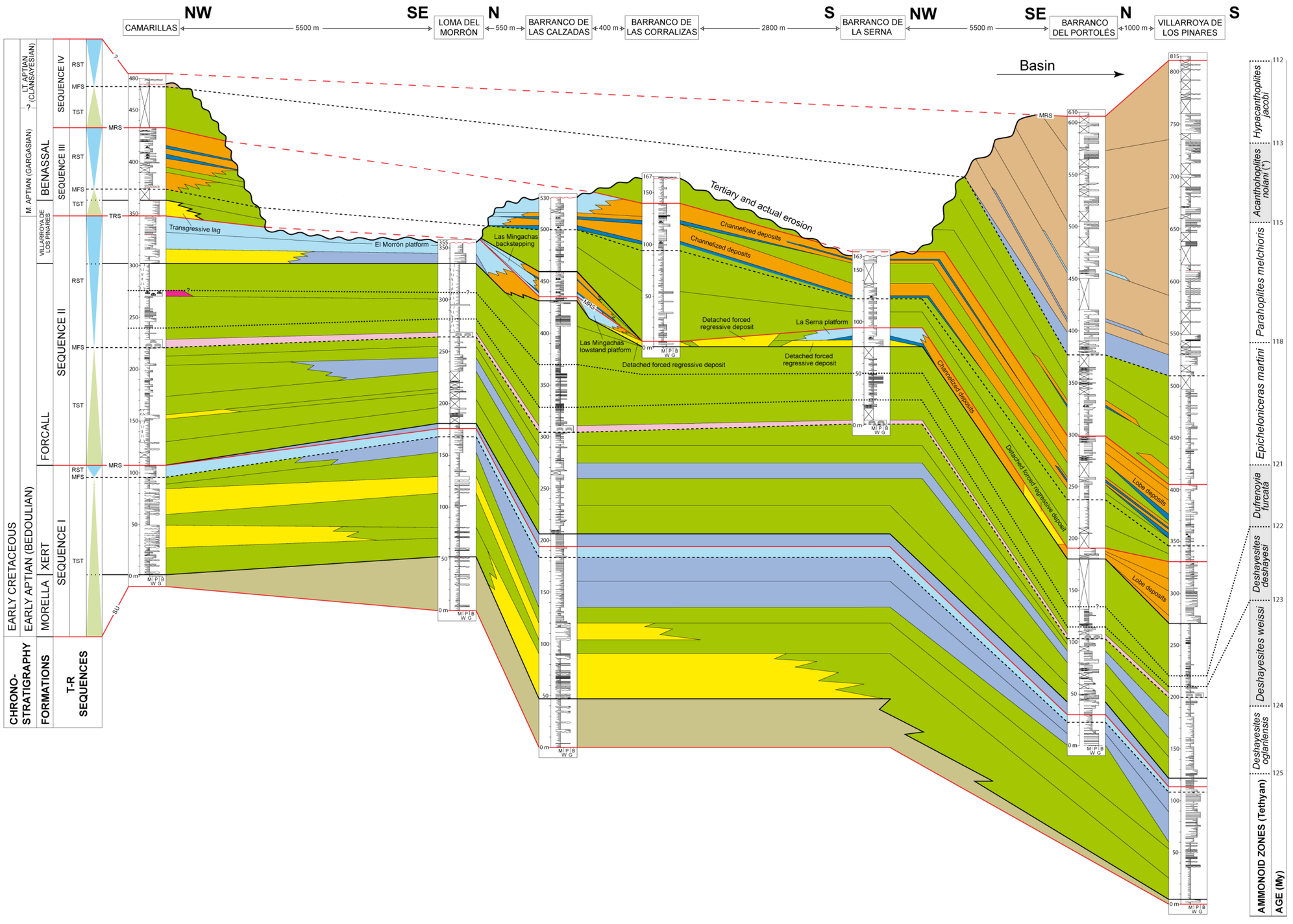

Figure 2.1.6. Western side sequence correlation scheme and distribution of the facies assemblages. Identified ammonite biozones are indicated in grey. See Fig. 2.1.5 for legend.

signs of subaerial exposure or erosion were identified. This sequence boundary is marked by a drastic facies change, which separates the carbonate lithologies with small requieniid rudists, miliolids and *Chondrodonta* of the uppermost part of the Xert Formation (below) from the transgressive green marls of the Forcall Formation (above). On the western side, these basal transgressive deposits correspond to orbitolinid-dominated beds, which constitute the top of the Xert Formation. With the early TST, the incipient carbonate platforms established during the regressive phase of Sequence I were drowned and evolved into a succession of interbedded green marls, marly limestones, silty limestones and limestones displaying frequent nodular bedding and burrow bioturbation. Its faunal content suggests deeper water conditions and is characterized by the bivalves *Panopea* sp., *Trigonia* sp. and *Neithea* sp., other molluscs, the echinoid *Heteraster oblongus*, terebratulid brachiopods, *Palorbitolina lenticularis*, *Praeorbitolina cormyi*, *Palorbitolina* sp., *Choffatella decipiens* and other undiagnosed foraminifera. The orbitolinids present large-sized discoidal morphologies and agglutinated quartz grains. At the proximal sections of Camarillas and Loma del Horcajo it is common to find intercalations of sandy limestones, peloidal grainstones displaying plane-parallel stratification and layers with abundant green algae and molluscs, denoting shallower environments (Figs. 2.1.5 and 2.1.6).

An orbitolinid-dominated stratigraphic interval, composed of nodular bioturbated limestones showing a more carbonate-rich lithology, interrupts these marly-dominated deposits. The episode is continuous and correlatable along the sub-basin except in the Loma del Horcajo and Camarillas sections, where it was not identified, probably due to their proximal setting. Above this, another flooding pulse occurs, with recovery of the marly condition of elsewhere in the succession. At the western side, this deepening is made more evident by the occurrence of a few levels with *Heminautilus saxbii* and ammonites belonging to the *Roloboceras hambrovi* horizon (Moreno-Bedmar et al., 2009). The late TST is characterized by several layers containing abundant orbitolinids at the base of coral rubble deposits, up to 5 m thick, which are completely encrusted by *Lithocodium aggregatum* (Fig. 2.1.3C), *Bacinella irregularis* and sessile foraminifera. Abundant *Palorbitolina lenticularis* displaying large discoidal morphologies and agglutinating quartz particles, echinoids, solitary corals, the rudists *Caprina douvillei* and *Horiopleura dumortieri* are also found inside the *Lithocodium*/*Bacinella*-coral rubble horizon. The maximum flooding surface is

interpreted to underlie the coral rubble deposits, which therefore constitute the earliest RST (Figs. 2.1.5 and 2.1.6).

2.1.4.2.1 Eastern side

The early RST begins with several microorganism-encrusted coral rubble layers, which change laterally southwards and upwards in the succession to interbedded marls and limestones with abundant large-sized discoidal *Palorbitolina lenticularis* with agglutinated quartz particles. At the Alto del Collado section, a specimen of *Deshayesites deshayesi* was recognized, establishing the presence of the *Deshayesites deshayesi* biozone above the *Lithocodium*-coral rubble horizon. Above the latter, widespread *Palorbitolina lenticularis* beds mark the beginning of the Villarroya de los Pinares Formation and are followed by limestones with sparsely distributed irregular massive corals. The coral-bearing limestones, which reach up to 15 m thick in the Cabezo de las Hoyas section, form a continuous level from the Loma del Horcajo section to the Estrecho de la Calzada Vieja section, and pinch out into marls after this last-mentioned section. Fragments of molluscs, abundant *Palorbitolina lenticularis*, *Praeorbitolina cormyi*, other unidentified foraminifera, and *Lithocodium aggregatum*, *Bacinella irregularis* and sessile foraminifera encrusting the corals, are also important components of the facies. However, the abundance of microencrusters is not as significant as for the preceding coral rubble episodes. Above this, the RST exhibits a progradational pattern of sedimentary bodies grouped in metre-thick small-scale sequences. This part of the succession is distinguished by the development of abundant carbonate producers such as *Toucasia carinata*, *Polyconites* new species (Skelton et al., in press) grouped in bouquets, small specimens of an unidentified monopleurid, *Chondrodonta*, other molluscs, corals, miliolids, *Orbitolinopsis simplex*, *Orbitolinopsis praesimplex* and other unidentified foraminifera. Burrow bioturbation and hardgrounds with encrusting oysters are also common (Fig. 2.1.5).

The depositional profile during this regressive stage corresponded to a distally steepened ramp with most carbonate production situated in the upper ramp. Where syn-sedimentary normal faulting caused major steepening of the ramp approximately south of the Cabezo de las Hoyas section (Fig. 2.1.8), the latter lithofacies pass basinwards to debris-flow deposits. Marls with embedded dome-shaped corals displaying *Lithophaga* borings are intercalated between these resedimented lithofacies. In addition, a syn-

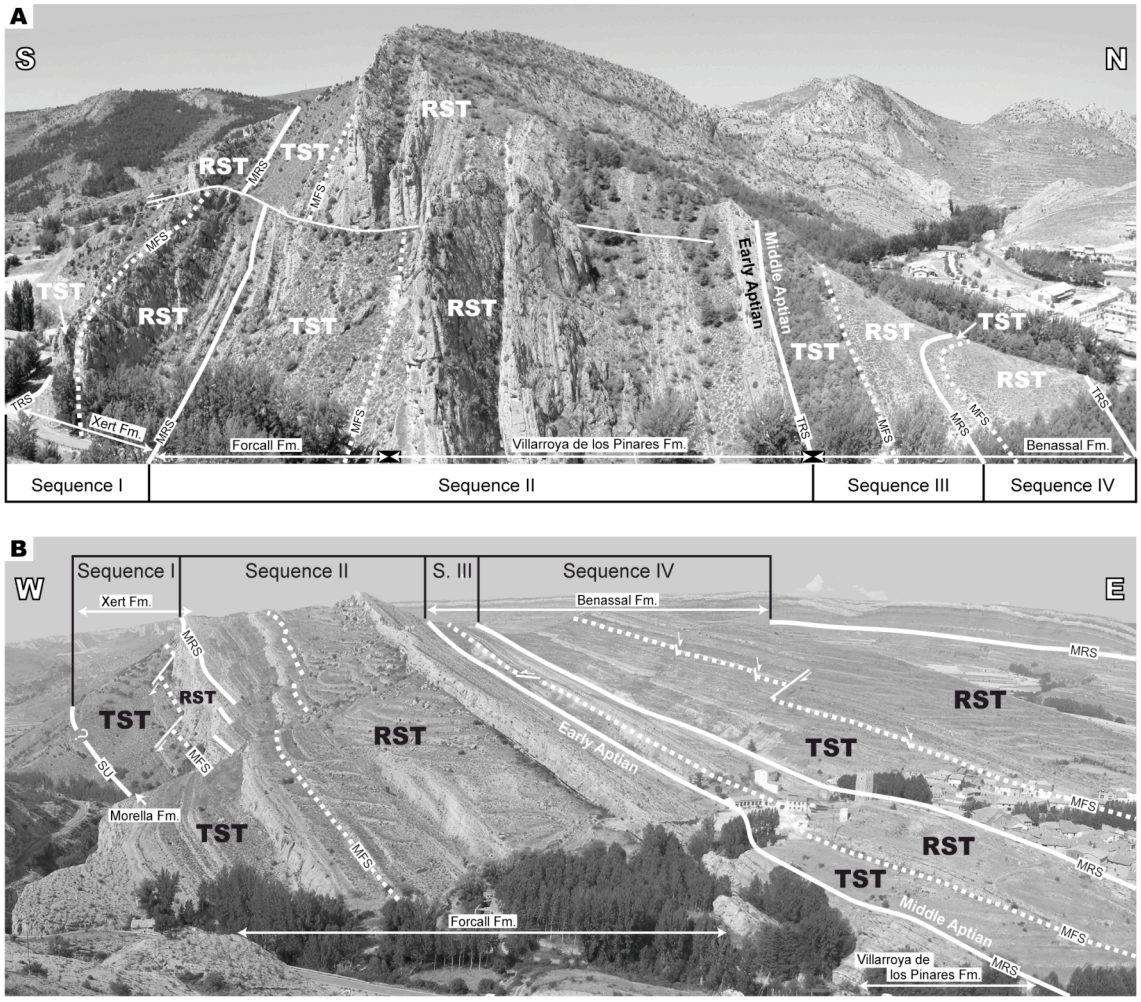

Figure 2.1.7. Sequence stratigraphic interpretation of the Aptian sedimentary succession in the Las Cubetas section (eastern side of the Miravete fault) (A) and the Villarroya de los Pinares section (western side of the Miravete fault) (B). See Fig. 2.1.5 for legend.

sedimentary fault located southwards of the Estrecho de la Calzada Vieja caused a second steepening of the ramp as deduced by the bulging and step-like geometries of the beds (Fig. 2.1.8). Distal ramp facies were recognized in the Alto del Collado section, which correspond to eight high-order cycles composed of centimetric mudstones overlain by decimetric floatstones containing fragments of *Chondrodonta*, rudists and delicate branching corals. The mudstones are interpreted to reflect parautochthonous sedimentation, while the floatstones, in which all skeletal components are fragmented, correspond to debris-flow episodes. In the Las Cubetas section, a facies representing a short episode of platform crisis has been found intercalated between limestones dominated by miliolids, corals, rudists and other molluscs. This episode is distinguished by two units of rock-forming *Palorbitolina lenticularis* and a 1.5 metre-thick level of coral rubble encrusted by *Lithocodium aggregatum*, *Bacinella irregularis* and sessile

foraminifera. The presence of coral rubble and orbitolinid beds displaying packstone to grainstone textures indicates reworking. The orbitolinids exhibit large flat morphologies with abundant quartz aggregation (Fig. 2.1.3D) (Fig. 2.1.5).

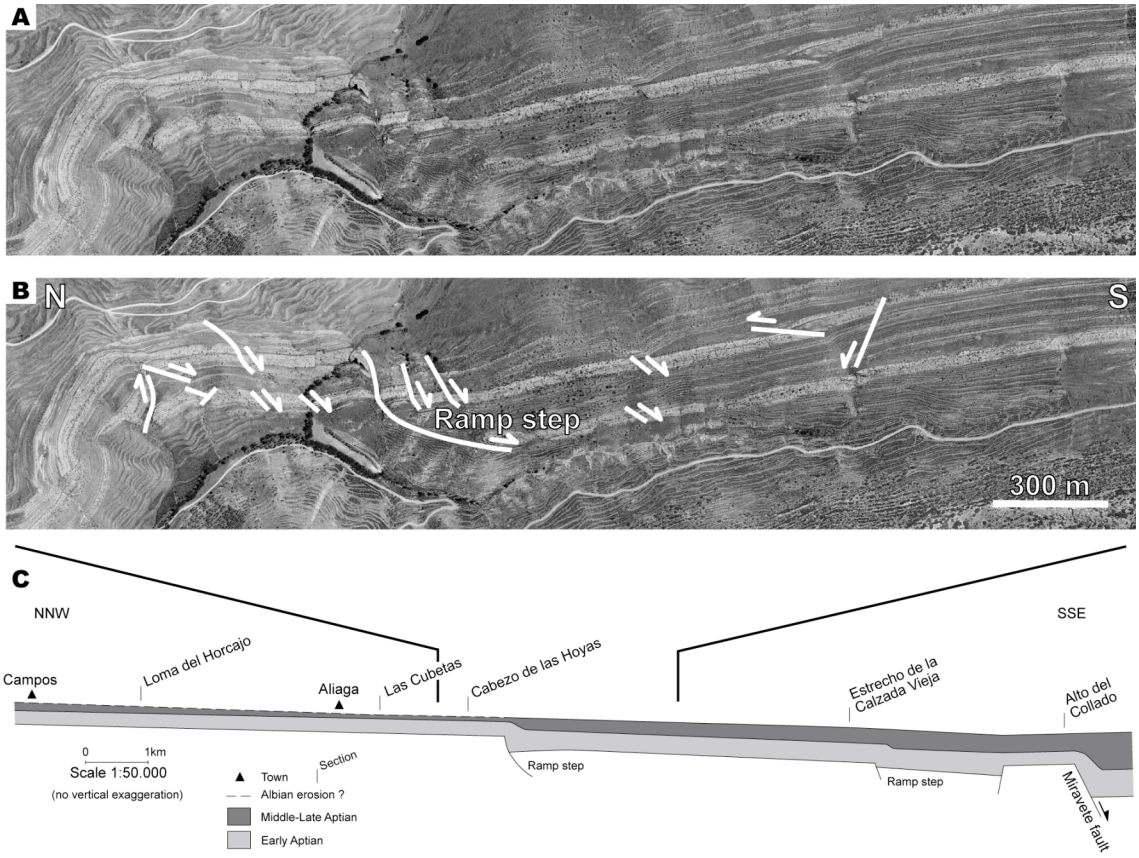

Figure 2.1.8. A) Aerial photograph of the area surrounding the Cabezo de las Hoyas section (see Fig. 2.1.1B for location), which belongs to the eastern side of the Miravete fault. B) Interpreted aerial photograph with the situation of the major ramp step located southwards of the Cabezo de las Hoyas section. C) Schematic cross-section of the eastern side distally steepened ramp of Sequence II showing the situation of the two steps located nearby to the south of the Cabezo de las Hoyas section and southwards of the Estrecho de la Calzada Vieja section. The depositional profile was reconstructed from the aerial photo. See Fig. 2.1.1B for situation.

2.1.4.2.2 Western side

Above the encrusted coral rubble deposits, the RST reveals the bathymetric differences between the eastern side (foot-wall) and the western side (hanging-wall) of the Miravete fault. The sedimentary record exhibits larger thicknesses and is built-up of small-scale sequences (in the sense of Strasser et al., 1999) each with a centimetre- to metre-thick marly transgressive term, and a centimetre- to decimetre-thick regressive term, comprising marly limestones, sandy/silty limestones and/or limestones displaying

nodular bedding. *Thalassinoides* and other burrow bioturbation are common, especially at the bases of the regressive layers and local levels with storm-induced turbidites (see Bover-Arnal et al., 2009). The faunal content also reflects a deeper environment than in the eastern part of the sub-basin, and is characterized by ammonites (see Fig. 2.1.10 for species), terebratulid and rhynchonellid brachiopods, solitary corals, the orbitolinids *Palorbitolina lenticularis* and *Praeorbitolina gr. cormyi-wienandsi*, which commonly agglutinated quartz particles and exhibit large-sized discoidal morphologies. Also present are the nautiloids *Eucymatoceras plicatum* and *Cymatoceras neckerianum*, the bivalves *Trigonia* sp., *Plicatula placunea*, *Panopea* sp. and *Neithea* sp., other unidentified molluscs, the echinoid *Toxaster collegnoi* and the decapod *Mecochirus magnus*. Pyritized fragments also occur. A 5-metre level of centimetre-sized coral colonies is present in the proximal section of Camarillas. The ammonite record, which is abundant and complete, especially in the Barranco de las Calzadas section (see Fig. 2.1.10; Moreno-Bedmar et al., 2009, accepted) provided two timelines for the Bedoulian (Early Aptian): the *Deshayesites forbesi* biozone-*Deshayesites deshayesi* biozone boundary, and the *Deshayesites deshayesi* biozone-*Dufrenoyia furcata* biozone boundary (Fig. 2.1.6).

Above this, the regressive succession corresponds to the lower part of the Villarroya de los Pinares Formation, and is distinguished by below-wave base accumulation of carbonate-producing biota dominated by the rudists *Toucasia carinata* and *Polyconites* new species (Skelton et al., in press), with rarer *Monopleura* sp., *Caprina parvula* (Fig. 2.1.4C) and *Offneria* sp. Also present are *Chondrodonta*, nerineid gastropods, other undiagnosed molluscs, corals, *Orbitolinopsis simplex*, miliolids, other benthic foraminifera and green algae. Intercalation of plane-parallel stratified oolitic-peloidal grainstones with abundant miliolids and other unidentified benthic foraminifera also occur (Fig. 2.1.3E), indicating short higher energy episodes. The sedimentary bodies are stacked in a prograding pattern constituting metre-thick small-scale sequences. In the Camarillas and the Barranco de la Serna sections, this late RST starts with fine-grained sandy limestones and calcarenites displaying cross-bedding and plane-parallel stratification. The depositional profile corresponds to a flat-topped non-rimmed carbonate platform (see Bover-Arnal et al., 2009), which is continuous from the Camarillas section to the Loma del Morrón section, where the platform margin is situated. Basinwards, these platform facies change laterally into debris-flow deposits (Fig. 2.1.3F), which are locally channelized, and marls with embedded dome-shaped corals (Fig. 2.1.4B), representing the slope environments. Irregular massive, sheet-

like and branching corals, and *Polyconites* grouped in bouquets are also present in this depositional setting (Fig. 2.1.6).

In the Barranco de la Serna section, the carbonate platform established during this time interval shows detached development due to its palaeosituation in an upthrown part of a half-graben structure related to the ENE-WSW normal listric faulting (Fig. 2.1.1B). This isolated platform is characterized by the presence of large delicate branching corals, *Toucasia carinata* and caprinid rudists, including *Caprina parvula* and *Pachytraga* sp. Southeastwards, it passes laterally to slope lithofacies. In the Barranco del Portolés and Villarroya de los Pinares sections, the late regressive phase corresponds to basinal debris-flow deposits accumulated in lobes. In the Barranco de las Calzadas section, the sediments that mark the top of the RST of Sequence II constitute a lowstand prograding wedge in the sense of Hunt and Tucker (1992). This lowstand wedge corresponds to a small prograding flat-topped non-rimmed carbonate platform situated in the area of Las Mingachas (see Bover-Arnal et al., 2009). Towards the basin, this lowstand carbonate platform changes laterally into slope lithofacies of debris-flows deposits (Fig. 2.1.4D) and marls with embedded dome-shaped, irregular massive and branching corals, which downlap over a detached forced regressive calcarenite situated in a basinal position. Basinwards, the maximum fall in sea level at the top of the RST is marked by several discontinuous cross-bedded and plane-parallel stratified calcarenites embedded in marls, which contain oysters, *Orbitolinopsis simplex*, *Palorbitolina lenticularis*, unidentified benthic foraminifera and fragments of molluscs, echinoids and decapods. These calcarenites constitute detached forced regressive deposits (Fig. 2.1.6).

2.1.4.3 Sequence III

Sequence III contains basically the lower part of the Benassal Formation (Fig. 2.1.2). In the Camarillas, Barranco de las Calzadas and Las Cubetas sections, Sequence III is also equivalent to the uppermost part of the Villarroya de los Pinares Formation. This sequence is interpreted to span approximately 3.1 Ma (according to the absolute Aptian ages of Ogg and Ogg, 2006), and has a maximum thickness of 135 m in the Barranco de las Corralizas section. In the Cabezo de las Hoyas section, this sequence thins to 20 m. Its base is early Middle Aptian in age, inferred from rudist biostratigraphy. The boundary between the sequences II and III appears to correspond to

the limit between the Early (Bedoulian) and the Middle Aptian (Gargasian), where the rudist family Caprinidae disappears from all sections known so far (Skelton, 2003a).

2.1.4.3.1 Eastern side

In the Las Cubetas section an erosive surface has been identified at the top of the regressive deposits of Sequence II. This surface is interpreted as the sequence boundary between Sequence II and III and corresponds to a transgressive ravinement surface (Fig. 2.1.5). The unconformity is overlain by oolitic-peloidal grainstones with fragments of dasycladaceans and echinoids, which are interpreted to represent the transgressive lag of the TST of Sequence III. A hardground with encrusting oysters and borings marks the top of these hydrodynamic deposits. In the other sections studied on the eastern side of the Miravete fault, no signs of subaerial exposure or erosion have been identified above the prograding regressive deposits of Sequence II. Hence, the lower boundary of Sequence III is interpreted to be a maximum regressive surface. The TST of this sequence is characterized by marls with calcareous nodules. Upwards in the succession the presence of nodular limestones with large flat orbitolinids becomes dominant. The maximum flooding surface separates these marly facies from widespread limestones dominated by *Mesorbitolina parva* and *Mesorbitolina* gr. *lotzei-parva* that correspond to the RST and reflect a shallowing-upwards trend. Interbedded marls with calcareous nodules and peloidal-bioclastic grainstones are present, as well as highly bioturbated levels. In the Loma del Horcajo section, this orbitolinid horizon changes landwards to an alternation of limestones with rudists, coral fragments, nerineid gastropods, orbitolinids and miliolids, and sandstones and sandy limestones with cross-bedding and plane-parallel stratification, indicating a shallower and proximal setting with episodes of detrital influx (Fig. 2.1.5).

2.1.4.3.2 Western side

The basal boundary of the sequence records a relative sea level fall with subaerial exposure and erosion of the previous carbonate platform established during the late Early Aptian between the Camarillas and Loma del Morrón sections (Fig. 2.1.6). This discontinuity corresponds to a transgressive ravinement surface (Fig. 2.1.9) with palaeokarst features (Fig. 2.1.4E). Southwards of the Camarillas section, this sequence boundary is eroded, but it is interpreted as having continued until the Barranco

de las Calzadas section, where it has also been identified. After this last-mentioned section and towards the basin, the transgressive ravinement surface changes to a maximum regressive surface. In the Camarillas section, the TST begins with a cross-bedded and plane-parallel stratified orange calcarenite containing oysters, foraminifera and fragments of echinoids and unidentified molluscs. This calcarenite is stacked in a retrograding pattern and represents the transgressive lag that onlaps the sequence boundary (Fig. 2.1.9). The base of this deposit is erosive and presents mud pebbles with minute imbricated quartz particles. A little way to the south of the Barranco de las Calzadas section, the onset of the TST is marked by a maximum regressive surface that corresponds to a hardground with a ferruginous crust and borings. This transgressive surface is situated above the lowstand prograding wedge established during the RST of Sequence II. Over the hardground, the lowstand prograding carbonate platform of Las Mingachas starts to backstep northwards (see Bover-Arnal et al., 2009), forcing the establishment of the typical slope facies association in this area. These lithofacies are distinguished by the settlement of domal, irregular massive and branching coral colonies embedded in marls, cut across by channelized debris-flow deposits. Above this and towards the basin, the transgressive phase changes laterally to bluish marly deposits with interbedded calcareous nodules and nodular limestones containing *Mesorbitolina parva*, decapods, the nautiloid *Eucymatoceras plicatum*, echinoids, *Panopea* sp., *Trochonerita gigas*, *Tylostoma* sp. and other molluscs. Highly bioturbated levels are common. In the Barranco de las Corralizas section, there are interbedded sandy limestones displaying plane-parallel stratification (Fig. 2.1.6).

The maximum flooding surface marks a drastic facies change from marly sedimentation to below-wave base carbonate-platform production that characterizes the RST. However, this regressive stage mainly reflects sedimentation in slope environments. The slope lithofacies are characterized by small patch-reefs with domal, irregular massive and branching corals embedded in marls, *Polyconites* new species (Skelton et al., in press) grouped in bouquets, gastropods, oysters and other unidentified molluscs. Channelized debris-flow deposits of platform sediments with *Toucasia carinata* and nerineid gastropods cut across these marly deposits. In the Barranco del Portolés and Villarroya de los Pinares sections the debris-flow deposits are accumulated in lobes interbedded with marly levels containing calcareous nodules. Bioturbated levels are present throughout the regressive tract (Fig. 2.1.6).

2.1.4.4 Sequence IV

Sequence IV corresponds to the upper part of the Benassal Formation. It is interpreted to span approximately 5.9 Ma (according to the Aptian absolute ages from Ogg and Ogg, 2006), and comprises the upper part of the Middle Aptian (Gargasian) and the entire Late Aptian (Clansayesian) (Fig. 2.1.2). The age of the base of the sequence has not been exactly determined due to the absence of age-diagnostic fauna. Nevertheless, Weisser (1959) recognized an ammonoid specimen of *Acanthohoplites bergeroni*, which according to Bogdanova and Tovbina (1994) is attributable to the *Diadochoceras nodoscostatum* subzone (*Acanthohoplites nolani* biozone), in the basal regressive stage of this sequence. Moreover, Moreno-Bedmar et al. (2008) collected ammonite specimens from the *Leymeriella tardefurcata* biozone (basal Albian) in the lower part of the Escucha Formation, which overlies the Benassal Formation, in the Salzadella sub-basin nearby to the East. Villanueva-Amadoz et al. (2008) also determined an Early-Middle Albian age for the Escucha Formation using palynomorphs. The limit between the Benassal and Escucha formations is also equivalent to the upper boundary of Sequence IV. The upper limit of this sequence may thus be constrained effectively to the boundary between the Aptian and the Albian. The sequence has a maximum thickness of 410 m in the Villarroya de los Pinares section, and thins to 18 m in the Cabezo de las Hoyas section. The boundary between sequences III and IV corresponds to a maximum regressive surface, which has been recognized on both sides of the Miravete fault. This boundary is characterized by a drastic facies change from limestones deposited below wave influence, containing rudists, corals and orbitolinids, to marly sedimentation. At Las Cubetas this lower sequence boundary consists of a well-developed hardground. The upper sequence boundary is constituted by a regional unconformity, which passes basinwards to a maximum regressive surface, overlain by the white sandstones and coal deposits of the Escucha Formation.

2.1.4.4.1 Eastern side

The TST is represented by an alternation of marls with calcareous nodules and marly limestones containing *Mesorbitolina parva*, echinoids and molluscs. Occasionally, resedimented deposits of rudists and coral fragments with floatstone to rudstone texture occur. The maximum flooding surface marks a drastic change in the facies trend, from deepening to shallowing-upwards. The base of the RST is constituted

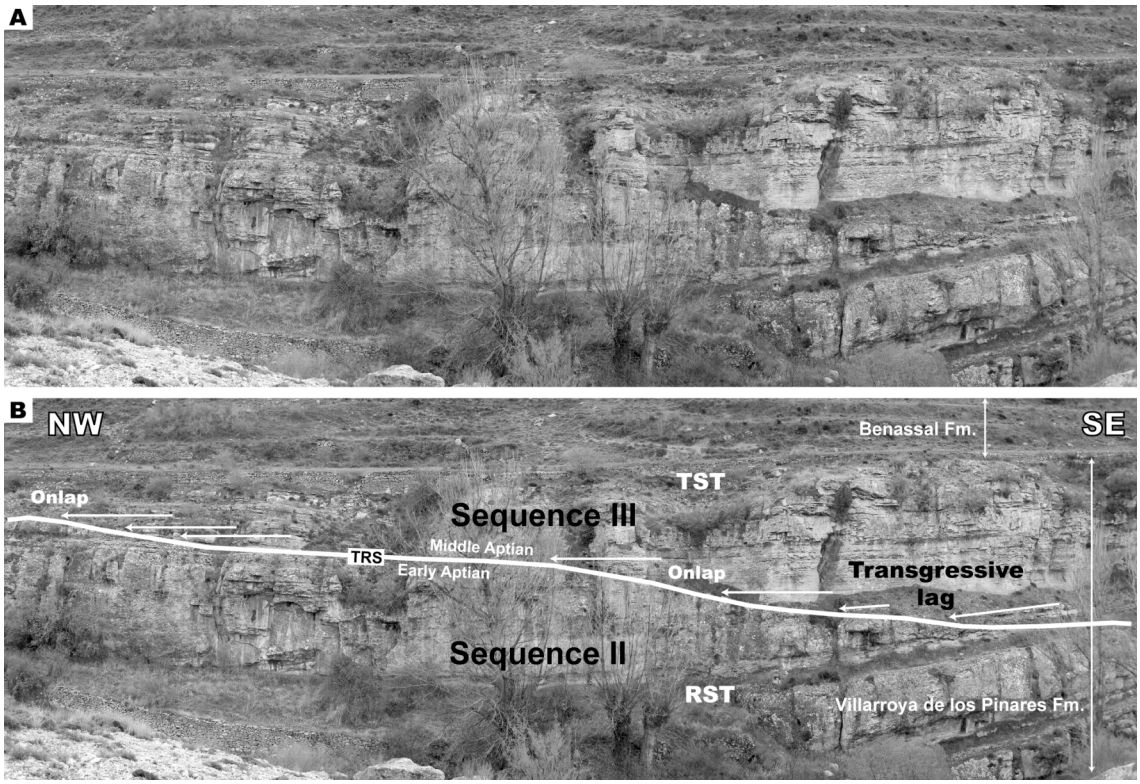

Figure 2.1.9. A) Outcrop-scale view of the boundary between Sequence II (Early Aptian) and Sequence III (Middle Aptian) located southwards of the Camarillas section (western side of the Miravete fault). B) Photograph interpretation of the boundary between Sequence II (Early Aptian) and Sequence III (Middle Aptian) located southwards of the Camarillas section (western side of the Miravete fault). See Fig. 2.1.5 for legend.

by highly bioturbated orbitolinid beds with molluscs and echinoids. The presence of hardgrounds with encrusting oysters is common. Above this, an alternation of tan clay, oolitic-peloidal packstone to grainstone limestones, sandy limestones and sandstones with erosive bases, cross-bedding and plane-parallel stratification become dominant. Intercalation of two small layers with *Eoradiolites* sp., *Toucasia* sp. and small delicate branching corals has been observed in the distal parts of both eastern and western sides, indicating the establishment of two incipient carbonate platforms, which were soon suppressed, however, by the high current activity and detrital influx that prevailed during the regressive phase of Sequence IV (Fig. 2.1.5).

2.1.4.4.2 Western side

The TST is distinguished by bluish marls with calcareous nodules and marly limestones with nodular bedding, containing *Mesorbitolina parva*, oysters, unidentified bivalves, echinoids and gastropods. Intercalation of bioclastic-peloidal packstone to

grainstone limestones with plane-parallel stratification, orbitolinid beds and sandy limestones indicate intermittent higher energy conditions or reworking. Pervasively bioturbated levels are common. Debris-flow deposits with floatstone to rudstone texture, containing rudists, orbitolinids, oysters and fragments of delicate branching corals are also present. Below these resedimented lithofacies dome-shaped and irregular massive corals are frequently found embedded in marls, which may represent slope environments. The maximum flooding surface is marked by an abrupt facies change, from a deepening to a shallowing-upwards trend. The RST begins with resedimented packstone to grainstone limestones of *Mesorbitolina parva* with erosive bases in the Barranco del Portolés and Villarroya de los Pinares sections. Above these orbitolinid beds, the establishment of littoral conditions is reflected by red oolitic-bioclastic grainstones with glauconite, sandy limestones, sandstones and tan clay. The beds feature erosive bases, cross-bedding, plane-parallel, herringbone stratification (Fig. 2.1.4F) and are occasionally channelized. Bioturbated levels, and hardgrounds with encrusting oysters and *Lithophaga* occur. The presence of mica is noticeable in the late regressive phase. Oysters, unidentified bivalves, echinoids, gastropods and rarely, brachiopods, dominate the faunal content (Fig. 2.1.6).

2.1.5 Stable isotope (C, O) geochemistry

Carbonate carbon and oxygen isotope analysis has been carried out with samples from the Barranco de las Calzadas section, throughout the upper part of the Forcall Formation where the boundaries between the *Deshayesites forbesi*, *Deshayesites deshayesi* and *Dufrenoyia furcata* ammonite biozones have been exactly determined (Moreno-Bedmar et al., 2009, accepted). Hence, this section offers an excellent opportunity to link the characteristic $\delta^{13}C$ perturbations related to the OAE 1a with high-quality ammonite biostratigraphic data. The C and O isotopic data measured are reported and graphically presented in Fig. 2.1.10.

2.1.5.1 Carbon-isotope data

The carbon-isotope values obtained range between -1.41‰ and 5‰. The resulting $\delta^{13}C_{carb}$ curve has been divided into eight segments (C1-C8; Fig. 2.1.10) in order to simplify its analysis and discussion following Menegatti et al. (1998), Bellanca et al. (2002), and de Gea et al. (2003). The lowest part of the C-isotope curve begins in

the *Roloboceras hambrovi* horizon (*Deshayesites forbesi* biozone) with a slightly negative excursion from 1.02‰ to -0.30‰ (C1), followed by a positive trend to 0.72‰ (C2). Straight afterwards, the $\delta^{13}C_{carb}$ values reach an absolute minimum of -1.41‰ in a sharp negative excursion (C3), with a subsequent well-developed positive shift to 0.72‰ (C4). After this step-like positive excursion, an interval marked by similar C_{carb}-isotopic values ranging between 2.66‰ to 2.83‰ (C5) begins. Then, the curve shows another steep positive shift to 3.85‰ (C6), followed by a large gentle positive trend with many minor reversals that begins before the top of the *Deshayesites forbesi* biozone and passes through the entire *Deshayesites deshayesi* biozone into the base of the *Dufrenoyia furcata* biozone, where it reaches an absolute maximum of 5‰ (C7). Subsequently, the $\delta^{13}C_{carb}$ values drop again along the top of the Forcall Formation, where a relative minimum of 2.85‰ is reached (C8).

2.1.5.2 Oxygen-isotope data

The resulting oxygen-isotope values vary between -7.11‰ and -3.09‰. Despite much fluctuation, seven relative trends indicating cooling-warming tendencies can be interpreted in the isotope curve obtained (O1 to O7; Fig. 2.1.10). The $\delta^{18}O$ curve begins inside the *Deshayesites forbesi* biozone with a minor positive excursion that may reflect a cooling tendency (O1). This initial positive shift is equivalent to the segment C1. The subsequent trend corresponds to an irregular negative evolution of the oxygen-isotope data that reaches the absolute minimum value of the curve (O2), which could denote a progressive warming episode. This negative trend can be correlated with the segment C2 and the lower part of the segment C3. The third interpreted trend draws a positive shift of the $\delta^{18}O$ values suggesting a cooling event (O3), which is correlatable with the upper part of the segment C3, the segments C4, C5 and the lower part of segment C6. Straight afterwards, the $\delta^{18}O$ curve describes another negative trend indicating a possible warming interval (O4), which comprises the top of the *Deshayesites forbesi* biozone and the base of the *Deshayesites deshayesi* biozone, and it is equivalent with the lower part of the segment C7. Then, the curve displays a long positive shift that reaches the top of the *Deshayesites deshayesi* biozone, which may denote a cooler climate (O5), followed by a warming event marked by the subsequent negative excursion that coincides with the lower part of the *Dufrenoyia furcata* biozone (O6). After this shift towards negative values, the $\delta^{18}O$ curve shows a positive tendency that

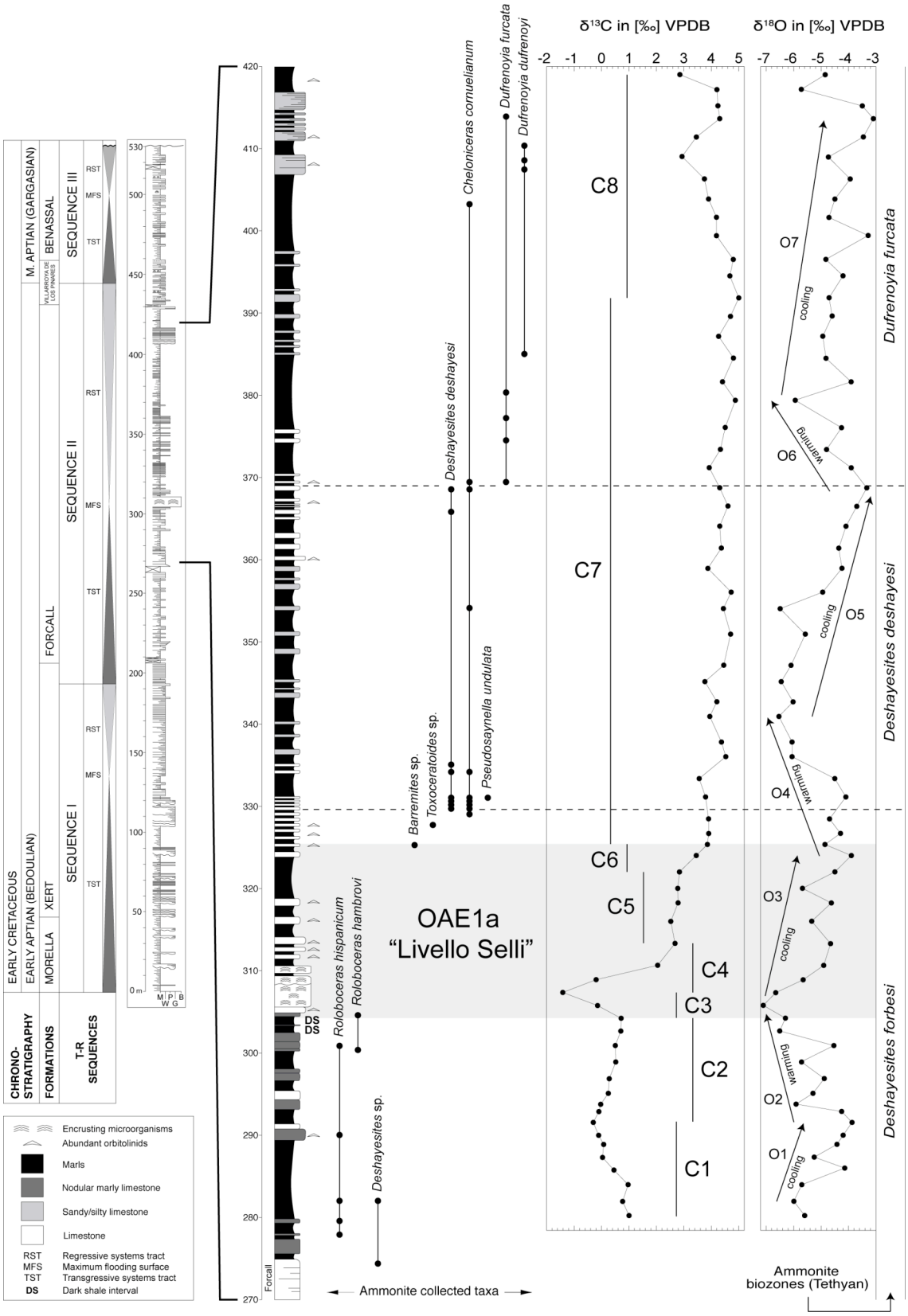

Figure 2.1.10. Detailed section log from Barranco de las Calzadas, featuring carbon- and oxygen-isotope curves, the situation of the OAE1a interval (indicated in grey), and the collected ammonite taxa. Segments C1-C8 and O1-O7 indicate $\delta^{13}C$ and $\delta^{18}O$ trends, respectively. Refer to text for detailed discussion.

could reflect another cooling time interval (O7), which reaches the absolute maximum O-isotope value inside the lower part of the *Dufrenoyia furcata* biozone. This last shift towards positive $\delta^{18}O$ values is correlatable with the upper part of the segment C7 and the segment C8.

2.1.6 Quantitative subsidence analysis and accommodation

In the Galve sub-basin, Aptian carbonate and siliciclastic sedimentation was tectonically controlled by the activity of the Miravete transfer fault and five main tilted blocks, which experienced syn-rift differential subsidence and compartmentalised both sides of the sub-basin (Fig. 2.1.11, left). In the following, the total sediment accommodation for each block is calculated, taking into account total subsidence (with decompaction) and estimated palaeo-water depths (see Material and Methods for details). For this purpose five representative stratigraphic columns, each one belonging to a different block, were selected (Fig. 2.1.11, left). Despite small magnitude differences, the five calculated total subsidence curves mainly display the same general pattern (Fig. 2.1.11, right). The western side curves of Camarillas, Barranco de las Calzadas and Villarroya de los Pinares show higher subsidence rates than those of the eastern side, at Las Cubetas and the Estrecho de la Calzada Vieja. These differences can be attributed to the activity of the Miravete master normal transfer fault, which generated a western side hanging-wall and an eastern side foot-wall. In addition, the magnitude of total subsidence also increases towards the basin. On the eastern side, the distal Estrecho de la Calzada Vieja section displays a higher subsidence rate than the proximal Las Cubetas section. Likewise on the western side, the basinal Villarroya de los Pinares section shows a higher magnitude of total subsidence than the more proximal Camarillas and Barranco de las Calzadas sections. However, all five curves display two major differentiated stages of rapid/slow total subsidence (Fig. 2.1.11, right).

The first stage (R/S1) is characterized by an initial episode of rapid subsidence, associated with significant extension and normal faulting throughout Sequence I and the TST and early RST of Sequence II (125 to approximately 122.8 Ma). Thus, an array of normal faults affecting the last-mentioned depositional sequences (Xert and Forcall formations) can be observed in the area surrounding Villarroya de los Pinares (Fig. 2.1.12). This initial phase reflects the highest subsidence rate for the Aptian in the Galve

sub-basin, and is followed by a period of decelerating subsidence that includes the late RST of Sequence II, Sequence III and the TST of Sequence IV (approximately 122.8 to approximately 114.2 Ma). The second stage (R2) is marked by a resumption of accelerated subsidence, which comprises the RST of Sequence IV (approximately 114.2-112 Ma). High subsidence rates in the distal curves of Villarroya de los Pinares and the Estrecho de la Calzada Vieja characterize this second rapid subsidence interval (R2), while the proximal curve of Las Cubetas shows minor acceleration of subsidence. In the Villarroya de los Pinares section, normal faulting linked to this interval of rapid subsidence can be observed affecting the lower part of the RST of Sequence IV (Benassal Formation) (Fig. 2.1.7B).

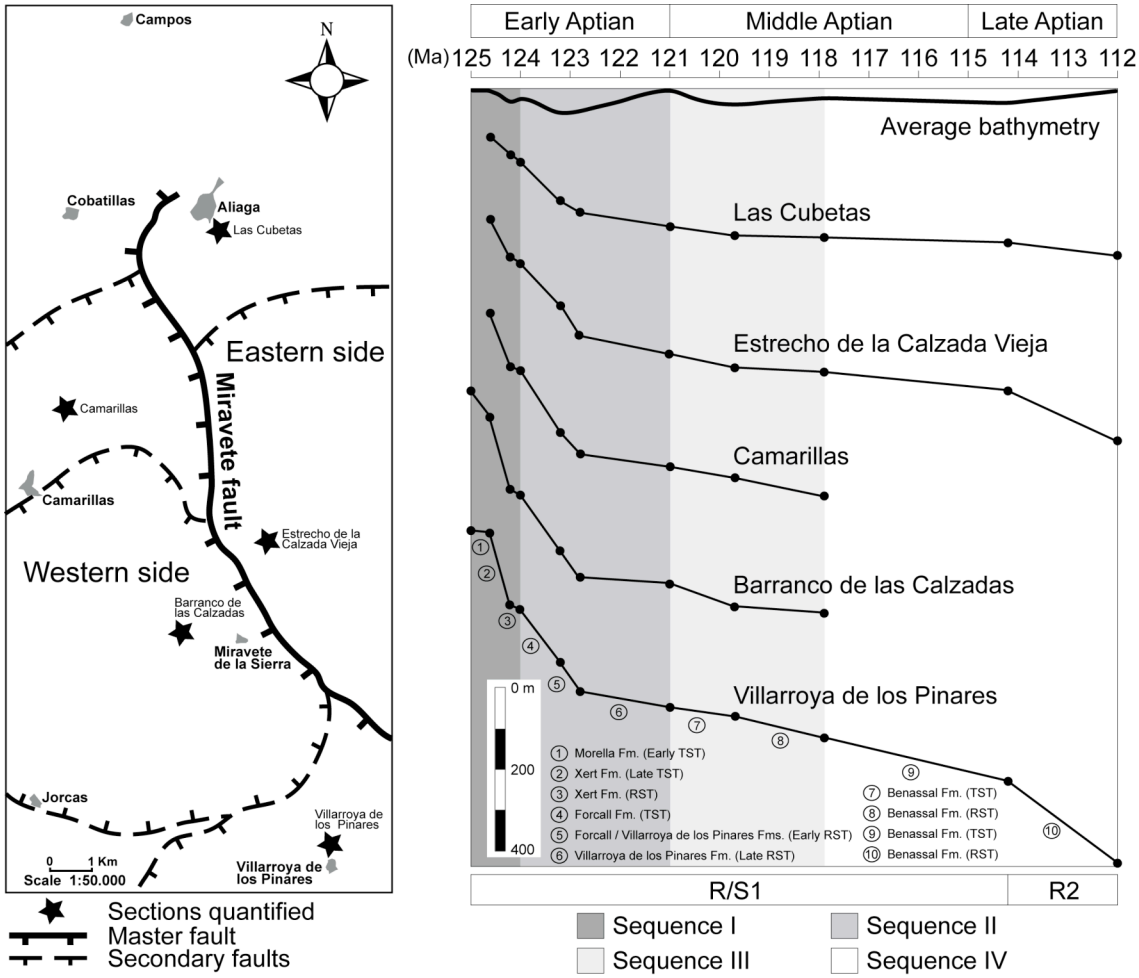

Figure 2.1.11. Left figure: Schematic tectonic map of the Galve sub-basin showing the situation of the different sections used in the quantitative subsidence analysis. Right figure: Decompacted total subsidence curves corrected for palaeobathymetries representing total accommodation. The average bathymetry curve is also indicated. Absolute ages are from Ogg and Ogg (2006). R/S: Stage of rapid/slow total subsidence. R: Stage of rapid total subsidence.

The rapid phases of total subsidence correspond to periods of fault activity and reactivation of tilting of blocks (syn-rift subsidence), producing gains of accommodation. The slower episodes of total subsidence in this area indicate local periods of thermal re-equilibration of the crust, heated during fracture phases (see McKenzie, 1978; Salas et al., 2001), so giving rise to losses of accommodation.

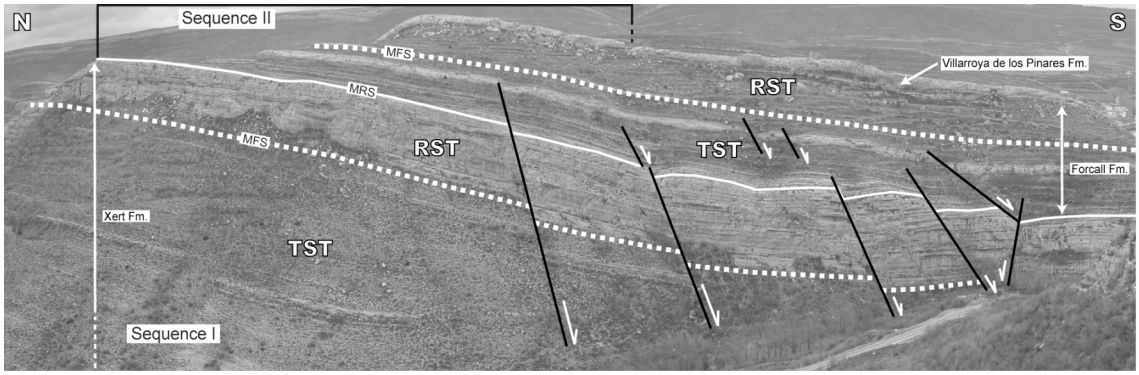

Figure 2.1.12 Photograph of the lower part of the Villarroya de los Pinares section showing an array of synsedimentary normal faults affecting Sequence I and the TST of Sequence II (Xert and Forcall formations). See Fig. 2.1.5 for legend.

2.1.7 Discussion

2.1.7.1 Diagenetic alteration of stable isotope data

The carbon- and oxygen-isotope data display more negative values than those from other time equivalent-isotope records in the Mid-Pacific Mountains (Jenkyns, 1995), Oman (Vahrenkamp, 1996), Italy and Switzerland (Menegatti et al., 1998), France (Moullade et al., 1998), Greece (Grötsch et al., 1998), Sicily (Bellanca et al., 2002), Spain (de Gea et al., 2003), Switzerland (Wissler et al., 2003) and Portugal (Burla et al., 2008). This discrepancy is consistent with the observation that $\delta^{13}C$ and $\delta^{18}O$ in platform limestones commonly show depleted values compared with those from pelagic environments (see Vahrenkamp, 1996; Grötsch et al., 1998; Immenhauser et al., 2001; Immenhauser et al., 2005; Sattler et al., 2005; Burla et al., 2008). Different authors have explained several mechanisms that can contribute to this fact such as subaerial exposure, euxinic conditions, fresh-water runoff or diagenetic alteration during burial (Scholle and Arthur, 1980; Allan and Matthews, 1982; Marshall, 1992; Patterson and Walter 1994; Menegatti et al., 1998; Sattler et al., 2005).

Generally, low $\delta^{13}C$ and $\delta^{18}O$ compositions of limestones are associated with diagenetic changes, with increased meteoric influence (Allan and Matthews, 1982; Patterson and Walter, 1994). Due to the epeiric nature of the Barranco de las Calzadas succession such diagenetic effects may have been superimposed on the original isotopic signal. Nevertheless, the $\delta^{13}C$ signal is considered not to be strongly affected by such processes in contrast to what happens with the $\delta^{18}O$ signal (see Scholle and Arthur, 1980; Immenhauser et al., 2001). Therefore, and despite the slight negative shift of the C-isotope values, it is commonly admitted that $\delta^{13}C$ records frequently preserve original patterns (Scholle and Arthur, 1980; Menegatti et al., 1998; Burla et al., 2008). Besides, in the Barranco de las Calzadas section, subaerial exposure surfaces have not been observed, and thin sections show no significant diagenetic features. The absence of a strong diagenetic overprint is also demonstrated by the low covariance ($R^2 = 0.0789$) between the $\delta^{13}C$ and $\delta^{18}O$ values (Fig. 2.1.13) (see Menegatti et al., 1998; Grötsch et al., 1998; Burla et al., 2008). Therefore, and due to the similarity between the Barranco

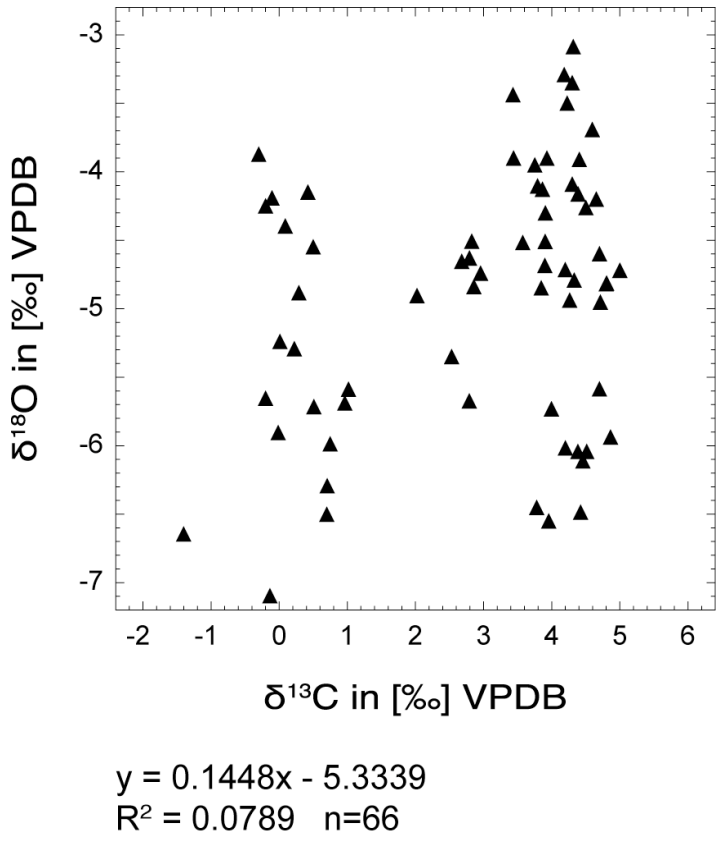

Figure 2.1.13. Cross-plot of $\delta^{13}C$ and $\delta^{18}O$ results. The low covariance between $\delta^{13}C$ and $\delta^{18}O$ ($R^2 = 0.0789$) indicates lack of significant diagenetic overprint.

de las Calzadas isotopic patterns and other Early Aptian examples reported, e.g., Vahrenkamp (1996), Menegatti et al. (1998), Bellanca et al. (2002), de Gea et al. (2003), the resulting $\delta^{13}C$ curve is interpreted to reflect global trend fluctuations.

2.1.7.2 Carbon-isotope record

The C_{carb}-isotopic record of the Barranco de las Calzadas section is subdivided into eight stratigraphic segments (C1-C8; Fig. 2.1.10), which are interpreted to reflect globally recognizable patterns (Menegatti et al., 1998; Bellanca et al., 2002; de Gea et al., 2003). Menegatti et al. (1998) defined the Early Aptian oceanic anoxic event (OAE1a; "Livello Selli") chemostratigraphically as the interval comprising the segments C4, C5 and C6 (Fig. 2.1.10). Nevertheless, in this paper the OAE1a time span will be interpreted to include the negative spike of segment C3, as well, as established in other recent studies (Fig. 2.1.10; see Li et al., 2008; Méhay et al., 2009; Tejada et al., 2009; Millán et al., 2009). This event is globally correlatable and can be identified in many other $\delta^{13}C$ curves (e.g., Vahrenkamp, 1996; Menegatti et al., 1998; Moullade et al., 1998; Bellanca et al., 2002; de Gea et al., 2003; Sattler et al., 2005). The ammonites collected in the Barranco de las Calzadas section permit us to attribute the Early Aptian oceanic anoxic event to the *Roloboceras hambrovi* horizon (upper part of the *Deshayesites forbesi* biozone; Fig. 2.1.10; see Moreno-Bedmar et al., 2009, accepted for details).

The C- and O-isotopic analysis carried out by Embry (2005) in the Estrecho de la Calzada Vieja section (eastern side of the Miravete fault) displays two similar positive $\delta^{13}C_{carb}$ excursions (C2 and C4) at the same stratigraphic levels as observed in the Barranco de las Calzadas section (western side of the Miravete fault) but with more positive values. Despite evident diagenetic effects, the two negative-positive spikes (C1-C2 and C3-C4; Fig. 2.1.10) of the $\delta^{13}C$ evolution are interpreted to be of global significance, and could be equivalent with the ones observed in La Bédoule section (France; Moullade et al., 1998) and the Mt. Kanala section (Greece; Grötsch et al., 1998). In both cases, the onset of the OAE1a has been ascribed to the second positive shift (C4; Fig. 2.1.10). By contrast, Embry (2005) attributed the onset of the OAE1a to the first positive C-isotope excursion (C2 of this study; Fig. 2.1.10). However, and as mentioned earlier, in this study the inception of the OAE1a was placed at the negative $\delta^{13}C$ spike of C3 (see Fig. 2.1.10) following Li et al. (2008), Méhay et al. (2009),

Tejada et al. (2009) and Millán et al. (2009). Although the term oceanic anoxic event is used throughout this work, the presence of diverse and abundant biota throughout the OAE1a time span, suggests oxygenated conditions rather than anoxia, in this area at least.

2.1.7.3 Oxygen-isotope record

On account of the susceptibility to diagenetic alteration of oxygen isotopes during burial conditions (Scholle and Arthur, 1980; Patterson and Walter, 1994; Menegatti et al., 1998), the $\delta^{18}O$ results are unreliable and display no regular patterns like those observed for the carbon isotopic values. For this reason, the resulting oxygen-isotope data should be treated with caution. However, the low covariance obtained between the $\delta^{13}C$ and $\delta^{18}O$ values (Fig. 2.1.13) and the absence of homogeneous $\delta^{18}O$ values or marked persistent saw-tooth-shaped excursions (Fig. 2.1.10), may be indicative of only weak diagenetic overprint (see Menegatti et al., 1998; Grötsch et al., 1998; Sattler et al., 2005; Burla et al., 2008). The marly nature of the succession probably diminished fluid circulation, and therefore excluded the possibility of stronger diagenetic effects. Hence, the oxygen-isotope results exhibit a gentle-scattered sinusoidal-shaped curve build-up of seven relative trends (O1 to O7; Fig. 2.1.10), which could preserve original high-frequency climatically-driven tendencies.

In this respect, the interpreted segments O2 and O3 (Fig. 2.1.10) have been also reported by Menegatti et al., (1998), Hochuli et al., (1999), Bellanca et al., (2002), de Gea et al., (2003) and Ando et al., (2008). The segment O2, which may reflect a warming episode, could be linked to high light carbon concentrations introduced into the ocean-atmosphere system by marine volcanism (Méhay et al., 2009) and/or to massive (isotopically light) methane-release from clathrates (Jenkyns and Wilson, 1999; Jahren et al., 2005; Beerling et al., 2002), peaking in C3 due to greenhouse warming, while segment O3 would reflect a cooling episode resulting from the burial of organic carbon during OAE1a (Fig. 2.1.10). Furthermore, the $\delta^{18}O$ curve interval comprising the segments O3 to O7 seems to describe a scattered positive trend through the top of the *Deshayesites forbesi* biozone, the *Deshayesites deshayesi* biozone and the lower part of the *Dufrenoyia furcata* biozone, which may also indicate a slow but progressive cooling period, though with a temporary reversal in O4 and O6 (Fig. 2.1.10). This shift to a cooler global climate during the late early Aptian has been also reported by Hochuli

et al. (1999), in a combined palynological and organic geochemical study in the Cismon section (Italian Alps), Steuber et al. (2005), in a $\delta^{13}C$ and $\delta^{18}O$ study of shells of rudist bivalves from different Tethyan localities, and Ando et al. (2008), in the central Pacific Ocean.

2.1.7.4 The Aptian evolution of the Galve sub-basin: controlling factors

The sedimentary evolution of the Galve sub-basin during the Aptian was the result of a complex interaction between different local, regional and global factors that controlled the type and rate of sediment production/supply, the available accommodation and how it was filled. These variables mainly concerned extensional faulting linked to the opening of the Atlantic Ocean (Salas et al., 2001), oceanic volcanic/tectonic activity (Larson and Erba, 1999), eustatic variations in sea level, fluctuations in climate and associated environmental consequences. Below, the factors controlling the evolution of the Galve sub-basin are identified and their effect on the composition and nature of the sedimentary record are discussed.

2.1.7.4.1 Eustatic sea level change

The durations of the interpreted sequences range from 1 Ma to approximately 5.9 Ma. These estimates are based on available biostratigraphic data and polarity reversals of the geomagnetic field. No substantial sedimentary gaps were identified. However, the boundary between sequences III and IV, which lies in the Middle Aptian time interval, lacks precise age attribution. The fact that sequences I, II, and the upper boundary of Sequence IV seem to correlate rather well with the Aptian global sequences of Ogg and Ogg (2006) (Fig. 2.1.14), indicates at least a partial eustatic imprint on Aptian sedimentation in the Galve sub-basin. For the Middle Aptian substage, no significant increase in rift activity has been obtained from the quantitative subsidence analysis (Figs. 2.1.11 and 2.1.14). Hence, the boundary between the sequences III and IV was probably also a response, at least in part, to eustasy. Consequently, the boundary has been interpreted to be equivalent with that between the Ap4 and Ap5 global sequences of Ogg and Ogg (2006). This interpretation leads to an estimated duration of 3.1 Ma for Sequence III and 5.9 Ma for Sequence IV.

The exact stratigraphic position of the maximum flooding surface in Sequence II is also problematical. Due to the absence of a well-defined correlatable surface marking

a large-scale change from a deepening- to a shallowing-up trend, this surface has been placed at the base of the horizon of coral rubble encrusted by *Lithocodium aggregatum* and *Bacinella irregularis*. The latter horizon coincides with the minimum $\delta^{18}O$ values reached at the termination of segment O2 (Figs. 2.1.5, 2.1.6 and 2.1.10). The top of this negative $\delta^{18}O$ shift is thought to mark a thermal maximum and consequently a likely culmination of continental ice melting leading to a global highstand of relative sea level. However, the occurrence in some parts of the western side of two levels of laminated dark shales below the orbitolinid bed that underlies the encrusted coral rubble horizon may be indicative of dysoxic conditions due to the absence of bioturbation and the presence of preserved organic matter (see Fig. 2.1.10). These dark shale episodes probably correspond to the deeper facies recognized throughout Sequence II. Nevertheless, these characteristic intervals were not observed in the eastern side, thus invalidating them as correlatable maximum flooding surface within the sub-basin. Besides, these dark shale levels might only reflect local dysoxic conditions, and not necessarily the expression of the maximum flooding deposit of Sequence II. Whatever the exact position of the maximum flooding surface of Sequence II, both possibilities are situated within the *Roloboceras hambrovi* horizon (upper part of the *Deshayesites forbesi* biozone) a little below the position shown for it in the Aptian global sequence Ap3 of Ogg and Ogg (2006), which lies at the limit between the *Deshayesites forbesi* and *Deshayesites deshayesi* biozones (Fig. 2.1.14).

If this interpretation is correct, these results imply global eustatic sea level changes within a time frame of a few My or less during the Aptian. In this regard, many authors (e.g., Immenhauser, 2005; Gréselle and Pittet, 2005) have suggested glacio-eustasy as the most feasible single known mechanism that could best explain such rapid and significant sea level oscillations. Also Peropadre et al. (2008), in an alternative interpretation of the Aptian sedimentary succession studied here, arrived at the same conclusion. And indeed, over the last couple of decades, several studies have put forward the possibility of the existence of short cooling episodes during the Aptian, which could have favoured the transient presence of small- to moderate-sized ice sheets situated in high altitudes and/or high latitudes (Frakes and Francis, 1988; Weissert and Lini, 1991; Stoll and Schrag, 1996; Price, 1999; Immenhauser, 2005; Gréselle and Pittet, 2005; see also Skelton, 2003b, pp. 172-3). The occurrence of cooling events during this stage is likewise indicated by the oxygen-isotope record presented in this paper. Geochemical analyses reported by Hochuli et al. (1996), Dumitrescu et al.

(2006), Ando et al. (2008), report similar patterns. Moreover, glacio-eustasy could also explain why many of these relative sea level changes recognized in the Galve sub-basin have been also identified in other coeval Tethyan basins (Fig. 2.1.14).

The most remarkable case of significant relative sea level fluctuations is the fall that gave rise to the RST of Sequence II, which resulted in subaerial exposure around latest Early Aptian time at the western hanging-wall side of the Miravete fault (Bover-Arnal et al., 2009). This drop in sea level is interpreted to have been partially eustatic in origin, as no signs of tectonic uplift have been identified in the study area. Furthermore, despite small differences in age, it has been also recognized in the Russian Platform (Sahagian et al., 1996), southern Croatia (Husinec and Jelaska, 2006), the United Arab Emirates (Yose et al., 2006), Oman (Hillgärtner et al., 2003; Gréselle and Pittet, 2005; Rameil et al., under review) and probably, along the margin of the Tethys (Ogg and Ogg, 2006). In Oman, as in the western side of the Miravete fault in the Galve sub-basin, the maximum fall in sea level gave rise to forced regressive deposits (Bover-Arnal et al., 2009). Nevertheless, in the Galve sub-basin, conclusive signs of subaerial exposure around the latest Early Aptian in the eastern foot-wall side of the Miravete fault were not recognized. Vennin and Aurell (2001) identified forced regressive deposits and evidence of subaerial processes of late Early Aptian age in this part of the sub-basin, but our field data do not support such an interpretation. Further work needs to be done in this respect. On the other hand, and in line with the foregoing, during the late Early Aptian, the Galve sub-basin apparently experienced decelerating subsidence that, together with an increase of carbonate production and accumulation rates, could also have favoured the shallowing of relative sea level (Fig. 2.1.11). For this time interval, the slow rate of total subsidence is supported by the diminution of the accommodation during the late RST of Sequence II (Villarroya de los Pinares Formation). Thus, the small-scale high-frequency sequences or simple sequences (*sensu* Strasser et al., 1999; Vail et al., 1991), which are frequently interpreted to be formed by high-frequency Milankovitch-driven climate changes (e.g., Vail et al., 1991), become thinner towards the top of the RST. This fact has been also observed in the central and oriental sub-basins of the Maestrat Basin.

Notwithstanding the unknown absolute age of the boundary between sequences III and IV, and the small phase-lags of age, when compared with the Aptian global chronostratigraphic sequences of Ogg and Ogg (2006), of the upper boundary of Sequence IV and of the maximum flooding surface of Sequence II, eustasy is apparently

one of the main controls on the Aptian sedimentary evolution of the Galve sub-basin (Fig. 2.1.14).

2.1.7.4.2 Subsidence and faulting

In addition to the influence of eustasy, subsidence also played an important role in creating accommodation throughout the Aptian. Subsidence analysis shows that the fault-controlled rapid syn-rift subsidence registered during Sequence I, the TST and the early RST of Sequence II and the RST of Sequence IV, was the primary factor producing accommodation (Fig. 2.1.11). The climax of rifting for the Aptian occurred during Sequence I (Morella and Xert formations with important siliciclastic supplies) and the TST and early RST of Sequence II (Forcall Formation) in which up to 430 m of mixed carbonate-siliciclastic deposits were deposited in approximately 2.2 Ma (the absolute age is based in Ogg and Ogg, 2006) (Figs. 2.1.11, 2.1.12 and 2.1.14). Hence, it is evident that the Aptian sedimentary record of the Galve sub-basin was controlled by both tectonics and eustasy. Despite the high rates of syn-rift subsidence recorded during the Early and the Late Aptian, tectonic activity failed to mask the global eustatic trends. During the Early Aptian, the high rate of syn-rift subsidence probably acted as an amplifier of the widely recognized long-term transgressive context recorded around the Tethys (Föllmi et al., 1994; Sahagian et al., 1996; Weissert et al., 1998; Wissler et al., 2003; Husinec and Jelaska, 2006). On the other hand, the rapid subsidence interval registered towards the basin during the RST of Sequence IV (latest Late Aptian substage) was apparently counterbalanced by enhanced supply and accumulation of terrigenous material that presumably matched the subsidence, permitting the regression recorded around the boundary between the Aptian and the Albian as also seen in other parts of the Tethyan realm (Sahagian et al., 1996; Gréselle and Pittet, 2005; Husinec and Jelaska, 2006).

The four T-R sequences recognized in this study present significant thickness differences between the different sections logged (Figs. 2.1.5 and 2.1.6). This fact reveals that local differential subsidence within the sub-basin also influenced the distribution of sediment and facies assemblages during the Aptian in this western margin of the Maestrat Basin (Fig. 2.1.11). The most striking tectonic feature, the Miravete fault (Fig. 2.1.1B), gave rise in its eastern foot-wall side to mostly thinner sequences with facies assemblages reflecting shallower water conditions than on the

western hanging-wall side (Figs. 2.1.5 and 2.1.6). The effects of differential subsidence can also be noted within the eastern side foot-wall where the sequences identified in Las Cubetas, Cabezo de las Hoyas and Alto del Collado sections are thinner than the same sequences recognized in the Loma del Horcajo and Estrecho de la Calzada Vieja sections (Fig. 2.1.5). Nevertheless, the RST of Sequence IV in the proximal Loma del Horcajo, Las Cubetas and Cabezo de las Hoyas sections is significantly thinner than in the distal Estrecho de la Calzada Vieja and Alto del Collado sections; this difference seems not to be related to syn-sedimentary normal faulting, but may be linked to erosive processes either previous to, or linked with deposition of the Albian coal-bearing Escucha Formation (Fig. 2.1.5 and 2.1.8). However, this unconformity was recognized only in the Las Cubetas section, where a transgressive ravinement surface was identified. Within the western hanging-wall side of the Miravete fault, the increase in thickness of Sequence I in the Loma del Morrón and Barranco de las Calzadas with respect to the Camarillas section can also be interpreted in terms of differential subsidence. The thickness reduction of this sequence and Sequence II in the distal

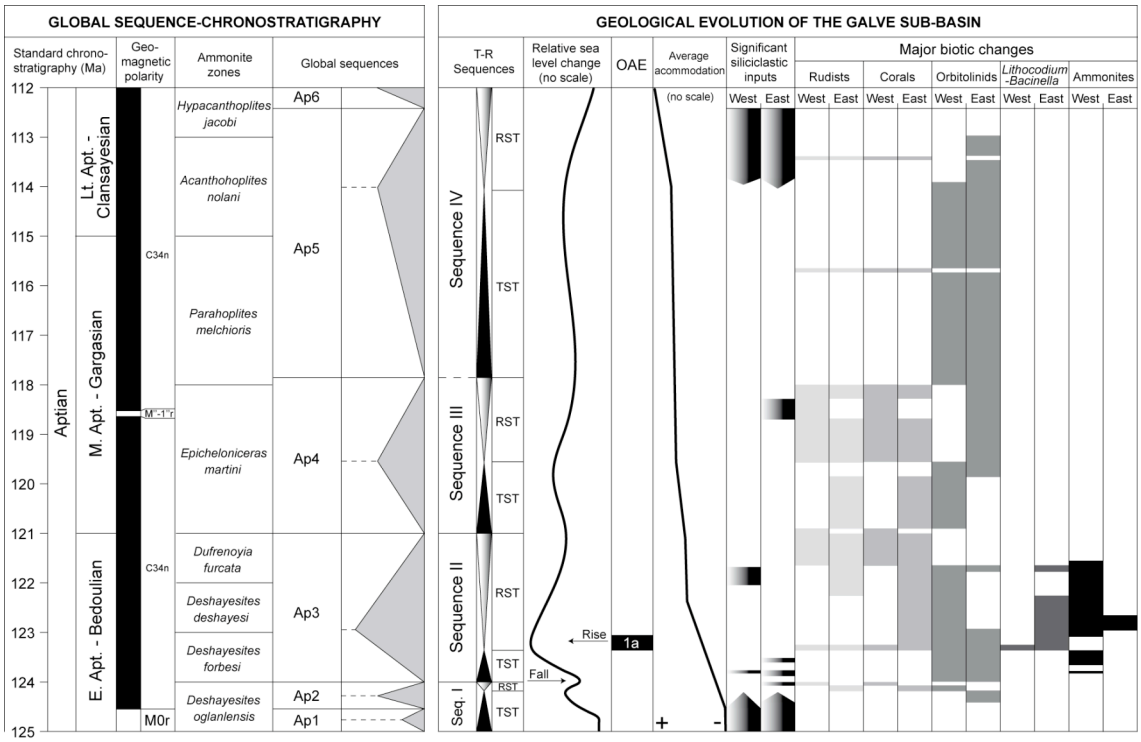

Figure 2.1.14. Comparison chart between the Aptian sequence chronostratigraphy according to Ogg and Ogg (2006), and the Aptian evolution of the Galve sub-basin, with the large-scale T-R sequences, stacking patterns, relative sea level curve, situation of the OAE1a, average accommodation, terrigenous inputs and biotic changes.

Barranco del Portolés and Villarroya de los Pinares in comparison with the more proximal sections may be related to basinal starvation (Fig. 2.1.6).

2.1.7.4.3 Environmental changes and facies succession

It has been shown that the mixed carbonate-siliciclastic Aptian sedimentary succession of the Galve sub-basin was substantially controlled by variations in accommodation linked to relative fluctuations of sea level, of both eustatic and tectonic origin. Carbonate producers, moreover, are also very sensitive to changes of other environmental factors, which mainly control the type of carbonate-producing biota and the amount of carbonate produced. The Aptian has been commonly interpreted as a time interval of strong climatic and oceanographic changes (Weissert and Lini, 1991; Larson and Erba, 1999; Hochuli et al., 1999; Pittet et al., 2002; Wissler et al., 2003; Skelton, 2003b; Weissert and Erba, 2004, among others). These ocean-climate system disturbances must also be considered in order to explain the observed facies succession and the biotic changes recorded throughout the Aptian Stage in the western Maestrat Basin.

In the area studied, the Aptian sedimentary evolution starts with fluvial lowstand deposits with tidal influence (Morella Formation), which become progressively more marine in character upwards in the succession, merging laterally into the Xert Formation. Both formations are marked by important fluxes and accumulation of siliciclastics (Figs. 2.1.5, 2.1.6 and 2.1.14). This significant supply of siliciclastic sediments could have been caused by the high-rate of extensional tectonic activity recorded for this time in the Galve sub-basin (Fig. 2.1.11), and the associated erosion in the uplifted areas. These terrigenous inputs possibly brought excess nutrients to the sea, inducing a low rate of carbonate production (see Hallock and Schlager, 1986), and favouring the widespread development of facies dominated by large-sized discoidal orbitolinids, mainly by *Palorbitolina lenticularis*, in the Xert Formation (Figs. 2.1.5, 2.1.6 and 2.1.14) (Vilas et al., 1995; Pittet et al., 2002; Embry, 2005). The diminution of siliciclastic fluxes during the RST of Sequence I may have caused changes in the trophic conditions, lowering the nutrient concentration in the basin and favouring the establishment of incipient carbonate ramps characterized by green algae, miliolids, small requieniid rudists and *Chondrodonta* (Figs. 2.1.5 and 2.1.6).

Another episode of widespread development of orbitolinids occurred during the TST of Sequence II. This systems tract represents the acme of the overall transgressive context recorded during the Early Aptian throughout the Tethys (Föllmi et al., 1994; Sahagian et al., 1996; Wissler et al., 2003; Husinec and Jelaska, 2006). Further, as discussed already, this sea level rise was amplified in the Galve sub-basin by local rapid syn-rift subsidence (Figs. 2.1.11 and 2.1.14). The magnitude of this transgressive phase was larger than that recorded in Sequence I, and together with intensified greenhouse conditions and consequently, an acceleration of the hydrological cycle, probably triggered by major volcanic events in the Pacific Ocean, might have provoked another episode of significant nutrient influx into the basin (Weissert et al. 1998; Larson and Erba, 1999). This event caused the drowning of the incipient carbonate platforms with small requieniid rudists, *Chondrodonta*, miliolids and green algae established during the regressive phase of Sequence I (upper part of the Xert Formation), and the widespread development of large-sized discoidal *Palorbitolina lenticularis* beds throughout the Forcall Formation. The latter transgression moved the littoral belt further landwards and, with it, the source of siliciclastic supply. However, silt-sized siliciclastic particles still arrived in the basin. The widespread development of orbitolinids during the Early Aptian in the Galve sub-basin has already been discussed by Embry (2005), who linked it with the overall occurrence of orbitolinid beds around the Tethyan realm during the Early Aptian broad transgression (Vilas et al., 1995; Pittet et al., 2002; Burla et al., 2008).

The marly deposits interbedded with marly limestones and limestones rich in orbitolinids that characterize the TST of Sequence II (Forcall Formation) are interrupted by amalgamated episodes of coral rubble encrusted by *Lithocodium aggregatum* and *Bacinella irregularis*. The base of this encrusted coral rubble horizon is distinguished by the presence of resedimented *Palorbitolina lenticularis* with large flat morphologies in rock-forming abundance. These characteristic deposits are synchronous with the widely recognized $\delta^{13}C$ negative spike that marks the onset of OAE1a and the lower part of the succeeding positive carbon-isotope excursion, as well as with the warming-cooling trends (O2 and O3) associated with these events (Fig. 2.1.10). The fact that these lithofacies dominated by *Lithocodium-Bacinella* include significant terrigenous inputs, evidence of strong bioerosion and large-sized discoidal *Palorbitolina lenticularis* suggests that they were developed under nutrient-rich conditions (Hallock and Schlager, 1986; Vilas et al., 1995; Pittet et al., 2002). The base of these encrusted

coral debris deposits also coincides with the minimum $\delta^{18}O$ value reached throughout the Barranco de las Calzadas section (Fig. 2.1.10). This absolute minimum value of the oxygen-isotope curve might have been linked to intensified greenhouse conditions and thus to the maximum flooding surface of Sequence II, due to the minimum presence of continental ice, as well as to increased humidity, weathering and erosion resulting in enhanced land-ocean nutrient fluxes. In Oman, Immenhauser et al. (2005) already noted the possible relation between the problematical *Lithocodium-Bacinella* association and the OAE1a, as well as a probable linkage of these facies with high trophic levels (see also Rameil et al., in press). Furthermore, several authors have also related the OAE1a and episodes of transgression within the Early Aptian with elevated nutrient levels in the sea (Föllmi et al., 1994; Erba, 1994; Weissert et al., 1998; Weissert and Erba, 2004). In addition, elevated seawater temperatures and changes in ocean water chemistry such as acidification triggered by the aforementioned global warming event that may have led to the OAE1a could also have played a part in favouring the generation of coral rubble and the widespread development of *Lithocodium-Bacinella* facies (see also Hillgärtner et al., 2003; Immenhauser et al., 2005; Rameil et al., in press).

On the other hand, just after the inception of the OAE1a, a long progressive cooling period began (Fig. 2.1.10), also recognized in other regions of the Tethys (Hochuli et al., 1999; Bellanca et al., 2002; Steuber et al., 2005; Ando et al., 2008, among others), and a long-term regressive phase that ended around the boundary between the Aptian and the Albian occurred (Fig. 2.1.14). This long-term regressive phase, spanning the late Early Aptian, and the Middle and Late Aptian substages, has been also described around the Neo-Tethys (e.g., Husinec and Jelaska, 2006). On the eastern side of the Miravete fault (foot-wall block), above the level of the carbon-isotope perturbations corresponding to the OAE1a and associated with the aforementioned progressive regression of relative sea level, a large carbonate platform with corals and rudists developed during the *Deshayesites deshayesi* and *Dufrenoyia furcata* biozones, giving rise to the RST of Sequence II (Villarroya de los Pinares Formation) (Fig. 2.1.5). On the western side (hanging-wall block), the sedimentary succession, which consists of green marls with interbedded limestones, marly limestones and silty limestones with abundant orbitolinids and ammonites, indicates that bathymetry was probably too significant to permit the establishment of carbonate platforms. However, during the upper part of the *Dufrenoyia furcata* biozone (late Early Aptian), and linked with the subsequent lowering of sea level, a large carbonate

platform dominated by *Toucasia carinata*, *Polyconites* new species (Skelton et al., in press) and corals (Villarroya de los Pinares Formation) developed in the proximal setting of this side (Fig. 2.1.6).

All these carbonate systems drowned with the TST of Sequence III, mainly evolving to marly sediments with calcareous nodules and orbitolinids (Benassal Formation). During the following RST carbonate production was able to recover in both sides of the Miravete fault. However, during this regressive episode inputs and accumulation of siliciclastic materials occurred in proximal areas of the eastern side of the Miravete fault during an interval of decelerating subsidence (Figs. 2.1.11 and 2.1.14). These siliciclastic events on the eastern side of the Miravete fault, which are interpreted to have been linked with enhanced weathering on the continents caused by a long-term rise in humidity that prevailed from the Middle to Late Aptian (Ruffell and Worden, 2000), might have shut down the carbonate factories and provoked the development of orbitolinid-rich deposits at certain times. The subsequent transgression (TST of Sequence IV) moved the siliciclastic belt landwards and caused the definitive drowning of these Middle Aptian carbonate platforms.

The major siliciclastic influx for the Aptian in the Galve sub-basin generated the RST of Sequence IV (Figs. 2.1.5, 2.1.6 and 2.1.14). This event favoured once again the development of orbitolinid beds, in the basal part of this regressive phase, followed by the establishment of littoral conditions rich in terrigenous sediments. For the RST of Sequence IV, only two small incipient carbonate platforms of corals and rudists were recognized on both sides of the Miravete fault. These carbonate factories were rapidly shut down by the high current energy conditions and input of siliciclastics that characterized the latest Aptian. This major terrigenous episode close to the boundary between the Aptian and the Albian occurred during the acme of the regression that began in the late Early Aptian. This siliciclastic event was probably triggered by resumption of the rapid syn-rift subsidence (Figs. 2.1.11 and 2.1.14), coupled with an intensified humid climate (Ruffell and Worden, 2000), which could have significantly increased chemical weathering on continents and runoff during the latest Aptian.

2.1.8 Conclusions

The Aptian stratigraphic record of the western Maestrat Basin is an instructive example of a terrigenous-influenced carbonate system controlled by both regional tectonic

factors and global ocean-climate changes. This sedimentary record can be subdivided into four T-R sequences reflecting long-term relative sea level variations: (i) Sequence I (lowermost Aptian); (ii) Sequence II (Lower Aptian); (iii) Sequence III (Middle Aptian); and (iv) Sequence IV (Middle-Upper Aptian). The transgressive systems tracts of these sequences are dominated by alternations of marls and limestones rich in orbitolinids, while the regressive systems tracts essentially consist of wave- and tidally influenced siliciclastic and carbonate deposits, and by the development of carbonate platforms with rudist bivalves, corals, orbitolinids and green algae. Three types of carbonate platforms were identified: (i) homoclinal ramp (lowermost Aptian of the eastern and western sides of the Miravete fault); (ii) distally steepened ramp (Lower Aptian of the eastern side of the Miravete fault); and (iii) flat-topped non-rimmed shelf (Lower Aptian of the western side of the Miravete fault).

Throughout the evolution of this sedimentary system, syn-rift subsidence was the most important provider of accommodation, though it failed to mask global eustatic trends. Accordingly, the T-R sequences and relative sea level changes interpreted for the Aptian of the Galve sub-basin are consistent with the global sequences and inferred rises and falls of relative sea level recorded in other coeval Tethyan basins, as well as with the major environmental changes discussed in the literature for this time slice. The Aptian sedimentary succession of the western Maestrat Basin thus reflects the following components.

(i) a transgression of Early Aptian age accompanied by the widespread development of *Palorbitolina lenticularis* beds associated with the probable intensified greenhouse conditions and enhanced terrigenous influxes that may have led to the OAE1a. Carbon-isotope analysis shows that the negative $\delta^{13}C$ spike that marks the onset of the OAE1a lies in the *Deshayesites forbesi* ammonite biozone and is coincident with a horizon of coral rubble encrusted by *Lithocodium aggregatum* and *Bacinella irregularis*, and abundant large-sized discoidal *Palorbitolina lenticularis*. The $\delta^{18}O$ curve seems to reflect high-frequency climatically-driven cyclicity and displays a warming trend that ends around the inception of the OAE1a. This is followed by a subsequent long-term progressive cooling episode throughout the late Early Aptian, which was accompanied by regression characterized by the establishment of a large carbonate platform with typical Urgonian biotic associations dominated by rudist bivalves and corals.

(ii) a latest Early Aptian forced regression of relative sea level that ended in subaerial exposure of the carbonate platform that had developed during the late Early Aptian, and in the basinward deposition of forced regressive wedges.

(iii) a late Early to Late Aptian long-term regressive phase, which gave rise to the installation of littoral conditions during the Late Aptian with enhanced terrigenous supply, which were probably related to regional tectonics and to a climate progressively changing from a semi-arid regime during the Early Aptian, to a semi-humid mode in the Middle-Late Aptian.

A close interaction between global environmental factors including eustatic trends, regional tectonics and sedimentary and biological succession can thus be observed in the Aptian rocks of the western Maestrat Basin. Consequently, due to the expanded and relatively complete nature of the sedimentary succession reported here, the present study constitutes an outstanding record of changing Aptian conditions of considerable potential value for the analysis, comparison, calibration and better understanding of other time-equivalent epicontinental sedimentary records.

2.1.9 Acknowledgements

We are grateful to Marc Aurell, Ramón Mas, Niels Rameil and the editor Lluís Cabrera who critically read the manuscript and offered useful suggestions. Rolf Schroeder is sincerely thanked for determining the orbitolinid species. We also thank Miquel Company for his valuable comments on the ammonite biostratigraphy. Roger Clavera-Gispert and Richard Regner are acknowledged for their helpful contributions during the writing of this study. Luis Pomar and Peter van der Beek read a first version of the manuscript. Financial support for the research was provided by the project Bi 1074/1-2 of the Deutsche Forschungsgemeinschaft, by the I+D+i research projects: CGL2005-07445-CO3-01, CGL2008-04916 and CGL2006-02153, by the Consolider-Ingenio 2010 programme, under CSD 2006-0004 “Topo-Iberia”, by the Grup Consolidat de Recerca “Geologia Sedimentària” (2005SGR-00890 and 2009SGR-1451), and by the Departament d’Universitats, Recerca i Societat de la Informació de la Generalitat de Catalunya i del Fons Social Europeu.

2.1.10 References

Allan, J.R. and Matthews, R.K. (1982). Isotope signatures associated with early meteoric diagenesis. Sedimentology, 29, 797-817.

Ando, A., Kaiho, K., Kawahata, H. and Kakegawa, T. (2008). Timing and magnitude of early Aptian extreme warming: Unraveling primary $\delta^{18}O$ variation in indurated pelagic carbonates at Deep Sea Drilling Project Site 463, central Pacific Ocean. Palaeogeography, Palaeoclimatology, Palaeoecology, 260, 463-476.

Bellanca, A., Erba, E., Neri, R., Premoli Silva, I., Sprovieri, M., Tremolada, F. and Verga, D. (2002). Palaeoceanographic significance of the Tethyan 'Livello Selli" (Early Aptian) from the Hybla Formation, northwestern Sicily: biostratigraphy and high-resolution chemostratigraphic records. Palaeogeography, Palaeoclimatology, Palaeoecology, 185, 175-196.

Bogdanova, T.N. and Tovbina, S.Z. (1994). On development of the Aptian Ammonite zonal standard for the Mediterranean region. Géologie Alpine, Mémoire Hors Serie, 20, 51-59.

Bond, G.C. and Kominz, M.A. (1984). Construction of tectonic subsidence curves for the early Paleozoic miogeocline, southern Canadian Rocky Mountains: Implications for subsidence mechanisms, age of break-up, and crustal thinning. Geological Society of America Bulletin, 95, 155-173.

Bover-Arnal, T., Moreno-Bedmar, J.A., Salas, R. and Bitzer, K. (2008). Facies architecture of the late Early-Middle Aptian carbonate platform in the western Maestrat basin (Eastern Iberian Chain). Geo-Temas, 10, 115-118.

Bover-Arnal, T., Salas, R., Moreno-Bedmar, J.A. and Bitzer, K. (2009). Sequence stratigraphy and architecture of a late Early-Middle Aptian carbonate platform succession from the western Maestrat Basin (Iberian Chain, Spain). Sedimentary Geology, 219, 280-301.

Burla, S., Heimhofer, U., Hochuli, P.A., Weissert, H. and Skelton, P. (2008). Changes in sedimentary patterns of coastal and deep-sea successions from the North Atlantic

(Portugal) linked to Early Cretaceous environmental change. Palaeogeography, Palaeoclimatology, Palaeoecology, 257, 38-57.

Canérot, J., Crespo, A. and Navarro, D. (1979). Montalbán, hoja nº 518. Mapa Geológico de España 1:50.000. 2ª Serie. 1ª Edición. Servicio de Publicaciones, Ministerio de Industria y Energía, Madrid, 31 pp.

Canérot, J., Cugny, P., Pardo, G., Salas, R. and Villena, J. (1982). Ibérica Central-Maestrazgo. In: García, A. (ed.). El Cretácico de España. Universidad Complutense de Madrid, 273-344.

Catuneanu, O., Abreu, V., Bhattacharya, J.P., Blum, M.D., Dalrymple, R.W., Eriksson, P.G., Fielding, C.R., Fisher, W.L., Galloway, W.E., Gibling, M.R., Giles, K.A., Holbrook, J.M., Jordan, R., Kendall, C.G.St.C., Macurda, B., Martinsen, O.J., Miall, A.D., Neal, J.E., Nummedal, D., Pomar, L., Posamentier, H.W., Pratt, B.R., Sarg, J.F., Shanley, K.W., Steel, R.J., Strasser, A., Tucker, M.E. and Winker, C. (2009). Towards the standardization of sequence stratigraphy. Earth-Science Reviews, 92, 1-33.

de Gea, G.A., Castro, J.M., Aguado, R., Ruiz-Ortiz, P.A. and Company, M. (2003). Lower Aptian carbon isotope stratigraphy from a distal carbonate shelf setting: the Cau section, Prebetic zone, SE Spain. Palaeogeography, Palaeoclimatology, Palaeoecology, 200, 207-219.

Dumitrescu, M., Brassell, S.C., Schouten, S., Hopmans, E.C. and Sinninghe Damsté, J.S. (2006). Instability in tropical Pacific sea-surface temperatures during the early Aptian. Geology, 34, 833-836.

Embry, A.F. and Klovan, J.E. (1971). A Late Devonian reef tract on northeastern Banks Island, N.W.T. Bulletin of Canadian Petroleum Geology, 19, 730-781.

Embry, J.C. (2005). Paléoécologie et architecture stratigraphique en haute résolution des platesformes carbonatées du Barrémien-Aptien de la Néo-Téthys (Espagne, Suisse, Provence, Vercors) – impact respectif des différents facteurs de contrôle.

Doctoral thesis. Museum National d'Histoire Naturelle – Institut Français du Petrole, Paris, 299 pp.

Erba, E. (1994). Nannofossils and superplumes: The early Aptian "nannofossil crisis". Paleoceanography, 9, 483-501.

Föllmi, K.B., Weissert, H., Bisping, M. and Funk, H. (1994). Phosphogenesis, carbon-isotope stratigraphy, and carbonate-platform evolution along the Lower Cretaceous northern Tethyan margin. Geological Society of America Bulletin, 106, 729-746.

Föllmi, K.B., Godet, A., Bodin, S. and Linder, P. (2006). Interactions between environmental change and shallow water carbonate buildup along the northern Tethyan margin and their impact on the Early Cretaceous carbon isotope record. Paleoceanography, 21, PA4211, doi:10.1029/2006PA001313.

Frakes, L.A. and Francis, J.E. (1988). A guide to Phanerozoic cold polar climates from high-latitude ice-rafting in the Cretaceous. Nature, 333, 547-549.

Gautier, F. (1980). Villarluengo, hoja nº 543. Mapa Geológico de España 1:50.000. 2ª Serie. 1ª Edición. Servicio de Publicaciones, Ministerio de Industria y Energía, Madrid, 45 pp.

Gréselle, B. and Pittet, B. (2005). Fringing carbonate platforms at the Arabian Plate margin in northern Oman during the Late Aptian-Middle Albian: Evidence for high-amplitude sea-level changes. Sedimentary Geology, 175, 367-390.

Grötsch, J., Billing, I. and Vahrenkamp, V. (1998). Carbon-isotope stratigraphy in shallow-water carbonates: implications for Cretaceous black-shale deposition. Sedimentology, 45, 623-634.

Hallock, P. and Schlager, W. (1986). Nutrient excess and the demise of coral reefs and carbonate platforms. Palaios, 1, 389-398.

Hillgärtner, H., Van Buchem, F.S.P., Gaumet, F., Razin, P., Pittet, B., Grötsch, J. and Droste, H. (2003). The Barremian-Aptian evolution of the eastern Arabian carbonate platform margin (northern Oman). Journal of Sedimentary Research, 73, 756-773.

Hochuli, P.A., Menegatti, A.P., Weissert, H., Riva, A., Erba, E. and Premoli Silva, I. (1999). Episodes of high productivity and cooling in the early Aptian Alpine Tethys. Geology, 27, 657-660.

Hunt, D. and Tucker, M.E. (1992). Stranded parasequences and the forced regressive wedge systems tract: deposition during base-level fall. Sedimentary Geology, 81, 1-9.

Husinec, A. and Jelaska, V. (2006). Relative sea-level changes recorded on an isolated carbonate platform: Tithonian to Cenomanian succession, Southern Croatia. Journal of Sedimentary Research, 76, 1120-1136.

Immenhauser, A., Van der Kooij, B., Van Vliet, A., Schlager, W. and Scott, R.W. (2001). An ocean-facing Aptian-Albian carbonate margin, Oman. Sedimentology, 48, 1187-1207.

Immenhauser, A. (2005). High-rate sea-level change during the Mesozoic: New approaches to an old problem. Sedimentary Geology, 175, 277-296.

Immenhauser, A., Hillgärtner, H. and Van Bentum, E. (2005). Microbial-foraminiferal episodes in the Early Aptian of the southern Tethyan margin: ecological significance and possible relation to oceanic anoxic event 1a. Sedimentology, 52, 77-99.

Jenkyns, H.C. (1995). Carbon-isotope stratigraphy and paleoceanographic significance of the Lower Cretaceous shallow-water carbonates of Resolution Guyot, Mid-Pacific Mountains. In: Winterer, E.L., Sager, W.W., Firth, J.V. and Sinton, J.M. (eds.). Proceedings of the Ocean Drilling Program, Scientific Results, 143, 99-104.

Jenkyns, H.C. and Wilson, P.A. (1999). Stratigraphy, paleoceanography, and evolution of Cretaceous Pacific guyots: relics from a greenhouse Earth. American Journal of Science, 299, 341-392.

Larson, R.L. and Erba, E. (1999). Onset of the mid-Cretaceous greenhouse in the Barremian-Aptian: Igneous events and the biological, sedimentary, and geochemical responses. Paleoceanography, 14, 663-678.

Li, Y-X., Bralower, T.J., Montañez, I.P., Osleger, D.A., Arthur, M.A., Bice, D.M., Herbert, T.D., Erba, E. and Premoli Silva, I. (2008). Toward an orbital chronology for the early Aptian Oceanic Anoxic Event (OAE1a, ~120 Ma). Earth and Planetary Science Letters, 271, 88-100.

Liesa, C.L., Soria, A.R., Meléndez, N. and Meléndez, A. (2006). Extensional fault control on the sedimentation patterns in a continental rift basin: El Castellar Formation, Galve sub-basin, Spain. Journal of the Geological Society, London, 163, 487-498.

Malchus, N., Pons, J.M. and Salas, R. (1996). Rudist distribution in the lower Aptian shallow platform of la Mola de Xert, Eastern Iberian Range, NE Spain. Revista Mexicana de Ciencias Geológicas, 12, 224-235.

Marshall, J.D. (1992). Climatic and oceanographic isotopic signals from the carbonate rock record and their preservation. Geologic Magazine, 129, 143-160.

McKenzie, D. (1978). Some remarks on the development of sedimentary basins. Earth and Planetary Science Letters, 40, 25-32.

Méhay, S., Keller, C.E., Bernasconi, S.M., Weissert, H., Erba, E., Botín, C. and Hochuli, P.A. (2009). A volcanic CO_2 pulse triggered the Cretaceous Oceanic Anoxic Event 1a and a biocalcification crisis. Geology, 37, 819-822.

Menegatti, A.P., Weissert, H., Brown, R.S., Tyson, R.V., Farrimond, P., Strasser, A. and Caron, M. (1998). High-resolution $\delta^{13}C$ stratigraphy through the early Aptian "Livello Selli" of the Alpine Tethys. Paleoceanography, 13, 530-545.

Millán, M.I., Fernández-Mendiola, P.A. and García-Mondéjar, J. (2007). Pulsos de inundación marina en la terminación de una plataforma carbonatada (Aptiense inferior de Aralar, Cuenca Vasco-Cantábrica). Geogaceta, 41, 127-130.

Millán, M.I., Weissert, H.J., Fernández-Mendiola, P.A. and García-Mondéjar, J. (2009). Impact of Early Aptian carbon cycle perturbations on evolution of a marine shelf system in the Basque-Cantabrian Basin (Aralar, N Spain). Earth and Planetary Science Letters, 287, 392-401.

Moullade, M., Kuhnt, W., Bergen, J.A., Masse, J.P. and Tronchetti, G. (1998). Correlation of biostratigraphic and stable isotope events in the Aptian historical stratotype of La Bédoule (Southeast France). Comptes-Rendus de l'Académie des Sciences, Paris, (II), 327, 693-698.

Moreno-Bedmar, J.A., Bulot, L., Latil, J.L., Martínez, R., Ferrer, O., Bover-Arnal, T. and Salas, R. (2008). Precisiones sobre la edad de la base de la Fm. Escucha, mediante ammonoideos, en la subcuenca de la Salzedella, Cuenca del Maestrat (E Cordillera Ibérica). Geo-Temas, 10, 1269-1272.

Moreno-Bedmar, J.A., Company, M., Bover-Arnal, T., Salas, R., Delanoy, G., Martínez, R. and Grauges, A. (2009). Biostratigraphic characterization by means of ammonoids of the lower Aptian Oceanic Anoxic Event (OAE1a) in the eastern Iberian Chain (Maestrat Basin, eastern Spain). Cretaceous Research, 30, 864-872.

Moreno-Bedmar, J.A., Company, M., Bover-Arnal, T., Salas, R., Delanoy, G., Maurrasse, F.J., Grauges, A. and Martínez, R. (accepted). Lower Aptian ammonite biostratigraphy in the Maestrat Basin (Eastern Iberian Chain, Spain). Geologica Acta.

Ogg, J.G. and Ogg, G. (2006). Updated by James G. Ogg (Purdue University) and Gabi Ogg to: GEOLOGIC TIME SCALE 2004 (Gradstein, F.M., Ogg, J.G., Smith, A.G. et al.; Cambridge University Press).

Patterson, W.P. and Walter, L.M. (1994). Depletion of ^{13}C in seawater ΣCO_2 on modern carbonate platforms: Significance for the carbon isotopic record of carbonates. Geology, 22, 885-888.

Peropadre, C., Meléndez, N. and Liesa, C.L. (2008). Variaciones del nivel del mar registradas como valles incisos en la Formación Villarroya de los Pinares en la subcuenca de Galve (Teruel, Cordillera Ibérica). Geo-Temas, 10, 167-170.

Pittet, B., Van Buchem, F.S.P., Hillgärtner, H., Razin, P., Grötsch, J. and Droste, H. (2002). Ecological succession, palaeoenvironmental change, and depositional sequences of Barremian-Aptian shallow-water carbonates in northern Oman. Sedimentology, 49, 555-581.

Pomar, L. and Kendall, C.G.St.C. (2007). Architecture of carbonate platforms: A response to hydrodynamics and evolving ecology. In: Lukasik, J., Simo, A. (eds.). Controls on Carbonate Platform and Reef Development. SEPM Special Publication, 89, 187-216.

Price, G.D. (1999). The evidence and implications of polar ice during the Mesozoic. Earth-Science Reviews, 48, 183-210.

Rameil, N., Immenhauser, A., Csoma, A.É. and Warrlich, G. (under review). Surfaces with a long history: The Aptian top Shu'aiba Formation unconformity, Sultanate of Oman. Sedimentology.

Rameil, N., Immenhauser, A., Warrlich, G., Hillgärtner, H. and Droste, H.J. (in press). Morphological patterns of Aptian *Lithocodium-Bacinella* geobodies–relation to environment and scale. Sedimentology.

Rosales, I. (1999). Controls on carbonate-platform evolution on active fault blocks: the Lower Cretaceous Castro Urdiales platform (Aptian-Albian, northern Spain). Journal of Sedimentary Research, 69, 447-465.

Ruffell, A. and Worden, R. (2000). Palaeoclimate analysis using spectral gamma-ray data from the Aptian (Cretaceous) of southern England and southern France. Palaeogeography, Palaeoclimatology, Palaeoecology, 155, 265-283.

Sahagian, D., Pinous, O., Olferiev, A. and Zakharov, V. (1996). Eustatic curve for the Middle Jurassic-Cretaceous based on Russian Platform and Siberian stratigraphy: zonal resolution. AAPG Bulletin, 80, 1433-1458.

Salas, R. (1987). El Malm i el Cretaci inferior entre el Massís de Garraf i la Serra d'Espadà. Analisi de Conca. Doctoral thesis. Universitat de Barcelona, 345 pp.

Salas, R. and Guimerà, J. (1996). Rasgos estructurales principales de la cuenca cretácica inferior del Maestrazgo (Cordillera Ibérica oriental). Geogaceta, 20, 1704-1706.

Salas, R., Guimerà, J., Mas, R., Martín-Closas, C., Meléndez, A. and Alonso, A. (2001). Evolution of the Mesozoic Central Iberian Rift System and its Cainozoic inversion (Iberian Chain). In: Ziegler, P.A., Cavazza, W., Roberston, A.H.F. and Crasquin-Soleau, S. (eds.). Peri-Tethys Memoir 6: Peri-Tethyan Rift/Wrench Basins and Passive Margins. Mémoires du Muséum National d'Histoire Naturelle, Paris, 186, 145-186.

Salas, R., Martín-Closas, C., Delclòs, X., Guimerà, J., Caja, M.A. and Mas, R. (2005). Factores principales de control de la sedimentación y los cambios bióticos durante el tránsito Jurásico-Cretácico en la Cadena Ibérica. Geogaceta, 38, 15-18.

Sattler, U., Immenhauser, A., Hillgärtner, H. and Esteban, M. (2005). Characterization, lateral variability and lateral extent of discontinuity surfaces on a Carbonate Platform (Barremian to Lower Aptian, Oman). Sedimentology, 52, 339-361.

Schmoker, J.W. and Halley, R.B. (1982). Carbonate porosity versus depth: a predictable relation for south Florida. AAPG Bulletin, 66, 2561-2570.

Scholle, P.A. and Arthur, M.A. (1980). Carbone isotope fluctuations in Cretaceous pelagic limestones: potential stratigraphic and petroleum exploration tool. AAPG Bulletin, 64, 67-87.

Sclater, J.G. and Christie, P.A.F. (1980). Continental stretching: an explanation of the post-mid-Cretaceous subsidence of the central North Sea Basin. Journal of Geophysical Research, 85, 3711-3739.

Simón, J.L., Liesa, C.L. and Soria, A.R. (1998). Un sistema de fallas normales sinsedimentarias en las unidades de facies Urgon de Aliaga. Geogaceta, 24, 291-294.

Skelton, P.W. (2003a). Rudist evolution and extinction - a north African perspective. In: Gili, E., Negra, M., Skelton, P.W. (eds.). North African Cretaceous Carbonate Platform Systems. NATO Science Series IV: Earth and Environmental Sciences, Kluwer Academic Publishers, 28, 215-227.

Skelton, P.W. (2003b). The Cretaceous World. Cambridge, ed. Cambridge University Press, 360 pp.

Skelton, P.W., Gili, E., Bover-Arnal, T., Salas, R. and Moreno-Bedmar, J.A. (in press). A new species of *Polyconites* from the Lower Aptian of Iberia and the early evolution of polyconitid rudists. Turkish Journal of Earth Sciences.

Soria, A.R. (1997). La sedimentación en las cuencas marginales del surco Ibérico durante el Cretácico inferior y su control estructural. Doctoral thesis. Universidad de Zaragoza, 363 pp.

Steuber, T., Rauch, M., Masse, J.-P., Graaf, J. and Malkoc, M. (2005). Low-latitude seasonality of Cretaceous temperatures in warm and cold episodes. Nature, 437, 1341-1344.

Stoll, H.M. and Schrag, D.P. (1996). Evidence for glacial control of rapid sea level changes in the Early Cretaceous. Science, 272, 1771-1774.

Strasser, A., Pittet, B., Hillgärtner, H. and Pasquier, J-B. (1999). Depositional sequences in shallow carbonate-dominated sedimentary systems: concepts for a high-resolution analysis. Sedimentary Geology, 128, 201-221.

Tejada, M.L.G., Suzuki, K., Kuroda, J., Coccioni, R., Mahoney, J.J., Ohkouchi, N., Sakamoto, T. and Tatsumi, Y. (2009). Ontong Java Plateau eruption as a trigger for the early Aptian oceanic anoxic event. Geology, 37, 855-858.

Tomás, S., Löser, H. and Salas, R. (2008). Low-light and nutrient-rich coral assemblages in an Upper Aptian carbonate platform of the southern Maestrat Basin (Iberian Chain, eastern Spain). Cretaceous Research, 29, 509-534.

Vahrenkamp, V.C. (1996). Carbon isotope stratigraphy of the upper Kharaib and Shuaiba Formations: implications for the Early Cretaceous evolution of the Arabian Gulf region. AAPG Bulletin, 80, 647-662.

Van Wagoner, J.C., Posamentier, H.W., Mitchum, R.M., Vail, P.R., Sarg, J.F., Loutit, T.S. and Hardenbol, J. (1988). An overview of the fundamentals of sequence stratigraphy and key definitions. In: Wilgus, C.K., Hastings, B.S., Kendall, C.G.St.C., Posamentier, H.W., Ross, C.A. and Van Wagoner, J.C. (eds.). Sea level changes: an integrated approach. SEPM, Special Publication, 42, 39-45.

Vail, P.R., Audemard, F., Bowman, S.A., Eisner, P.N. and Perez-Cruz, C., (1991). The Stratigraphic Signatures of Tectonics, Eustasy and Sedimentology – an Overview. In: Einsele, G., Ricken, W. and Seilacher, A. (eds.). Cycles and Events in Stratigraphy. Springer-Verlag Berlin Heidelberg 1991, 617-659.

Vennin, E. and Aurell, M. (2001). Stratigraphie séquentielle de l'Aptien du sous-bassin de Galvé (Province de Teruel, NE de l'Espagne). Bulletin de la Société Géologique de France, 172, 397-410.

Vilas, L., Masse, J.P. and Arias, C. (1995). *Orbitolina* episodes in carbonate platform evolution: the early Aptian model from SE Spain. Palaeogeography, Palaeoclimatology, Palaeoecology, 119, 35-45.

Vilas, L., Martín-Chivelet, J. and Arias, C. (2003). Integration of subsidence and sequence stratigraphic analyses in the Cretaceous carbonate platforms of the Prebetic (Jumilla-Yecla Region), Spain. Palaeogeography, Palaeoclimatology, Palaeoecology, 200, 107-129.

Villanueva-Amadoz, U., Pons, D., Diez, J.B., Sender, L.M. and Ferrer, J. (2008). Registro de granos de polen de angiospermas durante el Albiense-Cenomaniense en el NE de España. In: Ruiz-Omeñaca, J.I., Piñuela, L. and García-Ramos, J.C. (eds.). Libro de resúmenes. XXIV Jornadas de la Sociedad Española de Paleontología, Museo del Jurásico de Asturias (MUJA), Colunga, 15-18 de octubre de 2008, 219-220.

Watts, A.B. (1981). The U.S. Atlantic continental margin: subsidence history, crustal structure and thermal evolution. In: Bally, A.W., Watts, A.B., Grow, J.A., Manspeizer, W., Bernoulli, D., Schreiber, C. and Hunt, J.M. (eds.). Geology of passive continental margins: history, structure and sedimentologic record (with special emphasis on the Atlantic margin). AAPG, Education Course Note Series, 19, Ch. 2, 24pp.

Weisser, D. (1959). Acerca de la estratigrafía del Urgo-Aptense en las cadenas Celtibéricas de España. Notas y comunicaciones del Instituto Geológico y Minero de España, 55, 17-32.

Weissert, H. and Lini, A. (1991). Ice age interludes during the time of Cretaceous greenhouse climate? In: Müller, D.W., McKenzie, J.A. and Weissert, H. (eds.).

Controversies in Modern Geology: Evolution of Geological Theories in Sedimentology, Earth History and Tectonics. Academic Press, 173-191.

Weissert, H., Lini, A., Föllmi, K.B. and Kuhn, O. (1998). Correlation of Early Cretaceous carbon isotope stratigraphy and platform drowning events: a possible link? Palaeogeography, Palaeoclimatology, Palaeoecology, 137, 189-203.

Weissert, H. and Erba, E. (2004). Volcanism, CO2 and palaeoclimate: a Late Jurassic-Early Cretaceous carbon and oxygen isotope record. Journal of the Geological Society, London, 161, 1-8.

Wissler, L., Funk, H. and Weissert, H. (2003). Response of Early Cretaceous carbonate platforms to changes in atmospheric carbon dioxide levels. Palaeogeography, Palaeoclimatology, Palaeoecology, 200, 187-205.

Yose, L.A., Ruf, A.S., Strohmenger, C.J., Schuelke, J.S., Gombos, A., Al-Hosani, I., Al-Maskary, S., Bloch, G., Al-Mehairi, Y. and Johnson, I.G. (2006). Three-dimensional characterization of a heterogeneous carbonate reservoir, Lower Cretaceous, Abu Dhabi (United Arab Emirates). In: Harris, P.M. and Weber, L.J. (eds.). Giant hydrocarbon reservoirs of the world: From rocks to reservoir characterization and modeling. AAPG Memoir 88/SEPM, Special Publication, 173-212.

2.2 Sequence stratigraphy and architecture of a late Early-Middle Aptian carbonate platform succession from the western Maestrat Basin (Iberian Chain)

Telm Bover-Arnal[1*], Ramon Salas[2], Josep A. Moreno-Bedmar[2] and Klaus Bitzer[1]

[1]Abteilung Geologie, Fakultät für Biologie, Chemie und Geowissenschaften, Universität Bayreuth, Universitätsstr, 30, 95440, Bayreuth, Germany
[2]Departament de Geoquímica, Petrologia i Prospecció Geològica, Facultat de Geologia, Universitat de Barcelona, Martí i Franqués s/n, 08028, Barcelona, Spain

*corresponding author
E-mail address: Telm.Bover@uni-bayreuth.de

Published in Sedimentary Geology, July 2009, 219, 280-301

Abstract: The attributes of a 'four-systems-tract' sequence are at times difficult to identify in outcrop-scale carbonate successions. Poor exposure conditions, variable rates of sediment production, erosion and/or superposition of surfaces that are intrinsic to the nature of carbonate systems frequently conceal or remove its physical features. The late Early-Middle Aptian platform carbonates of the western Maestrat Basin (Iberian Chain, Spain) display facies heterogeneity enabling platform, platform-margin and slope geometries to be identified, and provide a case study that shows all the characteristics of a quintessential four systems tract-based sequence. Five differentiated systems tracts belonging to two distinct depositional sequences can be recognized: the Highstand Systems Tract (HST) and Forced Regressive Wedge Systems Tract (FRWST) of Depositional Sequence A; and the Lowstand Prograding Wedge Systems Tract (LPWST), Transgressive Systems Tract (TST) and subsequent return to a highstand stage of sea-level (HST) of Depositional Sequence B. An extensive carbonate platform of rudists and corals stacked in a prograding pattern marks the first HST. The FRWST is constituted by a detached, slightly cross-bedded calcarenite situated at the toe of the slope in a basinal position. The LPWST is characterized by a small carbonate platform of rudists and corals downlapping over the FRWST and onlapping landwards. The TST

exhibits platform backstepping and marly sedimentation. Resumed carbonate production in shelf and slope settings characterizes the second HST. A basal surface of forced regression, a subaerial unconformity, a correlative conformity, a transgressive surface and a maximum flooding surface bound these systems tracts, and are well documented and widely mappable across the platform-to-basin transition area analyzed. Moreover, the sedimentary succession studied is made up of four types of parasequence that constitute stratigraphic units deposited within a higher-frequency sea-level cyclicity. Ten lithofacies associations form these basic accretional units. Each facies assemblage can be ascribed to an inferred depositional environment in terms of bathymetry, hydrodynamic conditions and trophic level. The architecture of the carbonate platform systems reflects a flat-topped non-rimmed depositional profile. Furthermore, these carbonate shelves are interpreted as having been formed in low hydrodynamic conditions. The long-term relative fall in sea-level occurred during the uppermost Early Aptian, which subaerially exposed the carbonate platform established during the first HST and resulted in the deposition of the FRWST, is interpreted as one of global significance. Moreover, a possible relationship between this widespread sea-level drop and glacio-eustasy seems plausible, and could be linked to the cooling event proposed in the literature for the late Early Aptian. Because of the important implications in sequence stratigraphy of this study, the sedimentary succession analyzed herein could serve as an analogue for the application of the four-systems-tract sequence stratigraphic methodology to carbonate systems.

Keywords: Sequence stratigraphy, Carbonate platforms, Sea-level changes, Aptian, Iberian Chain, Spain

2.2.1 Introduction

During the Aptian stage, the Tethyan realm underwent one of the most widespread developments of carbonate platforms in the history of the Earth (e.g., Masse et al. 1993; Vilas et al. 1993; Hunt and Tucker 1993a; Funk et al. 1993; Grötsch 1996; Rosales 1999; Skelton 2003a; Hillgärtner et al. 2003; Millán et al. 2007). The Maestrat Basin, which was located in tropical latitudes along the eastern margin of the Iberian plate, was no exception (Vennin and Aurell 2001; Salas et al. 2005; Tomás 2007; Tomás et al. 2007; Bover-Arnal et al. 2008a).

The main protagonists of these carbonate environments were rudist bivalves, corals and orbitolinids (e.g., Malchus et al. 1996; Vilas et al. 1995; Masse et al. 1998; Skelton and Masse 2000; Pittet et al. 2002; Tomás et al. 2008). The aforementioned carbonate-producing communities were probably highly sensitive to physico-chemical changes in the ocean-atmosphere system (e.g., Weissert et al. 1998; Pittet et al. 2002; Wissler et al. 2003; Burla et al. 2008). Therefore, the climatically- and tectonically-driven perturbations that occurred throughout Aptian time conditioned these carbonate factories and resulted in the growth and demise of carbonate settings (e.g., Föllmi et al. 1994; Weissert et al. 1998; Pittet et al. 2002; Hillgärtner et al. 2003; Wissler et al. 2003; Weissert and Erba 2004; Föllmi et al. 2006; Burla et al. 2008; Skelton et al. 2008a).

One of the most important parameters controlling carbonate-producing organisms and, consequently, carbonate platforms, is the relative fluctuations in sea-level (e.g., Kendall and Schlager 1981; Strasser et al. 1999; Pittet et al. 2000; Bádenas et al. 2004; Aurell and Bádenas 2004; Rameil 2005; Thrana and Talbot 2006; Pomar and Kendall 2007; Bover-Arnal et al. 2008b). Relative variations in sea-level are due to tectonic activity and eustasy, and they play a major part in determining the available accommodation space that can be filled, as well as the growth potential of light-dependent carbonate-producers (Sarg 1988; Pomar 2001). Although it is widely demonstrated that nutrients, temperature, salinity, CO_2, hydrodynamics and other physico-chemical variables also play a significant role in controlling the evolution of carbonate platforms (e.g., Hallock and Schlager 1986; Föllmi et al. 1994; Weissert et al. 1998; Pomar 2001; Pittet et al. 2002; Hillgärtner et al. 2003; Mutti and Hallock 2003; Pomar and Kendall 2007), the present study will focus on the effects of relative changes in sea-level.

To this end, a high-resolution characterization of a late Early-Middle Aptian carbonate platform succession from the western Maestrat Basin (E Iberian Chain, Spain) was undertaken. This study involved a sedimentological and geometrical analysis of the lithofacies succession, the recognition of variations in stratal stacking patterns and sequence stratigraphy.

Many Cretaceous centered studies dealing with similar subjects have been published in the last decade (Lehmann et al. 1998; Rosales 1999; Booler and Tucker 2002; Drzewiecki and Simo 2000; Borgomano 2000; Pittet et al. 2002; Kerans 2002; Bernaus et al. 2003; Hillgärtner et al. 2003; Bauer et al. 2003; Gréselle and Pittet 2005; Pomar et al. 2005; Husinec and Jelaska 2006; Gil et al. 2006; Zagrarni et al. 2008).

However, what makes this work noteworthy is the exceptional preservation and exposure of the platform-to-basin transition investigated given that it constitutes a high quality case study, which provides evidence that the four systems tracts of Hunt and Tucker (1992), and the surfaces that separate them, can be well documented not only on seismic lines but also in outcrops.

Carbonate platform margins constitute the best setting to study and estimate relative fluctuations in sea-level (Pomar et al. 2005; Gréselle and Pittet 2005). This privileged location, with the exception of rimmed margins, normally does not have significant stratigraphic gaps, which are common in more proximal parts of the carbonate platforms, nor undergo sediment starvation, which characterizes basinal environments (Pomar et al. 2005). Moreover, well-exposed transitional settings between platform and basin offer an excellent opportunity to observe the complete architecture of the lithofacies, and thus, the possibility to identify the different building blocks (*sensu* Van Wagoner et al. 1988) that form the sedimentary succession.

This paper seeks to a) investigate the response of a late Early-Middle Aptian carbonate system from the northern Tethyan margin to a forced regression and subsequent rise in relative sea-level; b) show all features at outcrop-scale of a four-systems-tract type of sequence; c) identify the different basic accretional units that build up this carbonate succession; d) put these platform carbonates in a global context in order to establish parallelisms and differences with coeval carbonate systems from other Tethyan localities; e) hypothesize about the mechanism that could have triggered the aforementioned relative sea-level fall, and to f) improve our understanding of the Aptian carbonate systems.

In essence, the model proposed herein constitutes an excellent example of how relative sea-level fluctuations of diverse order control facies and architecture of carbonate platforms, and of how sequence stratigraphy can be an effective tool to analyze them. Furthermore, the detailed analysis of lithofacies, parasequences and architecture, in addition to the Tethyan-wide treatment provided in the discussion could constitute a valuable case study not only for those engaged in sequence stratigraphy but also for those working on carbonate platforms and Aptian sedimentary successions.

2.2.2 Geological setting of the study area

The late Early-Middle Aptian carbonate platform succession lies in the eastern part of the Iberian Chain (Spain). These sedimentary units crop out along the Camarillas syncline, between the towns of Miravete de la Sierra, Camarillas, Jorcas and Villarroya de los Pinares (Teruel province) (Fig. 2.2.1).

Throughout the Late Jurassic-Early Cretaceous time interval, a rifting event linked to the spreading Atlantic Ocean and to the opening of the Bay of Biscay, divided the northeastern Iberian plate into four strongly subsident basins: the Cameros, Columbrets, South Iberian and Maestrat (Salas et al. 2001; Salas et al. 2005). The area analyzed here was situated in the Galve sub-basin (Salas and Guimerà 1996), which corresponded to a western peripheral part of the Maestrat Basin in the eastern Iberian Chain (Fig. 2.2.1). During the Aptian stage, up to 810 m of continental and epicontinental marine, mixed carbonate-siliciclastic sediments were deposited in the sub-basin (Bover-Arnal et al. under review). Subsequently, as a result of the convergence between the Iberian and European plates during the Late Cretaceous-Miocene period, the Iberian basins were tectonically inverted, giving rise to the Iberian Chain in the Paleogene (Salas and Casas 1993; Salas et al. 2001).

In the central part of the Galve sub-basin, where the study area is located (Fig. 2.2.1), the Aptian sedimentary succession can be divided into five formations: Morella, Xert, Forcall, Villarroya de los Pinares and Benassal (Canérot et al. 1982; Salas et al. 2001; Bover-Arnal et al. under review). The outcrops analyzed span the late Early-Middle Aptian time slice, and comprise the marly sediments of the top of the Forcall Formation, the platform carbonates of the Villarroya de los Pinares Formation and the marly deposits and carbonate rocks of the lower part of the Benassal Formation. The age of this succession is based on ammonite and rudist biostratigraphy (Moreno and Bover 2007; Bover-Arnal et al. under review) (Fig. 2.2.2).

The Aptian sedimentary record of the Galve sub-basin can also be divided into four long-term transgressive-regressive (T-R) sequences (Bover-Arnal et al. under review). The sediments studied constitute the uppermost part of T-R Sequence II and the whole of T-R Sequence III (Fig. 2.2.2).

Three well-preserved carbonate platform successions were analyzed to the northwest of Miravete de la Sierra and northeast of Camarillas (Fig. 2.2.1). The area studied in Camarillas is interpreted as the proximal part of the carbonate platform established during the late Early Aptian in the central part of the Galve sub-basin (Villarroya de los Pinares Formation). The outcrops located close to Miravete de la

Sierra (El Morrón and Las Mingachas, see Fig. 2.2.1) correspond to the more distal part and to the more marginal setting of the aforementioned carbonate platform, respectively. The lack of tectonic overprint and vegetation in the three sections offers an excellent opportunity to carry out a sedimentological, geometrical, architectural, stacking pattern and sequence stratigraphic based analysis.

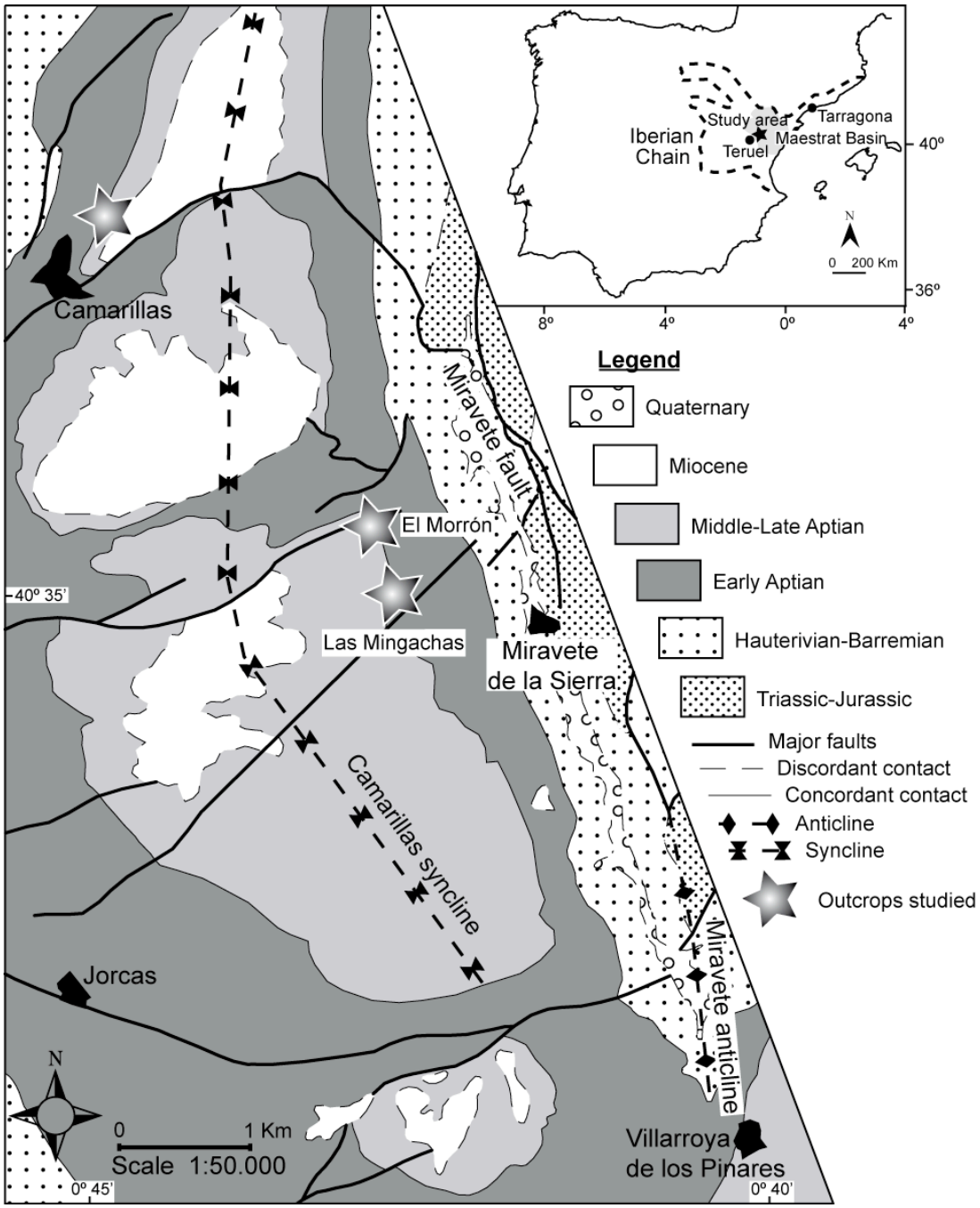

Figure 2.2.1. Geological map of the central Galve sub-basin with its location inside the Iberian Peninsula. The areas studied are marked with a star. Modified after Gautier (1980).

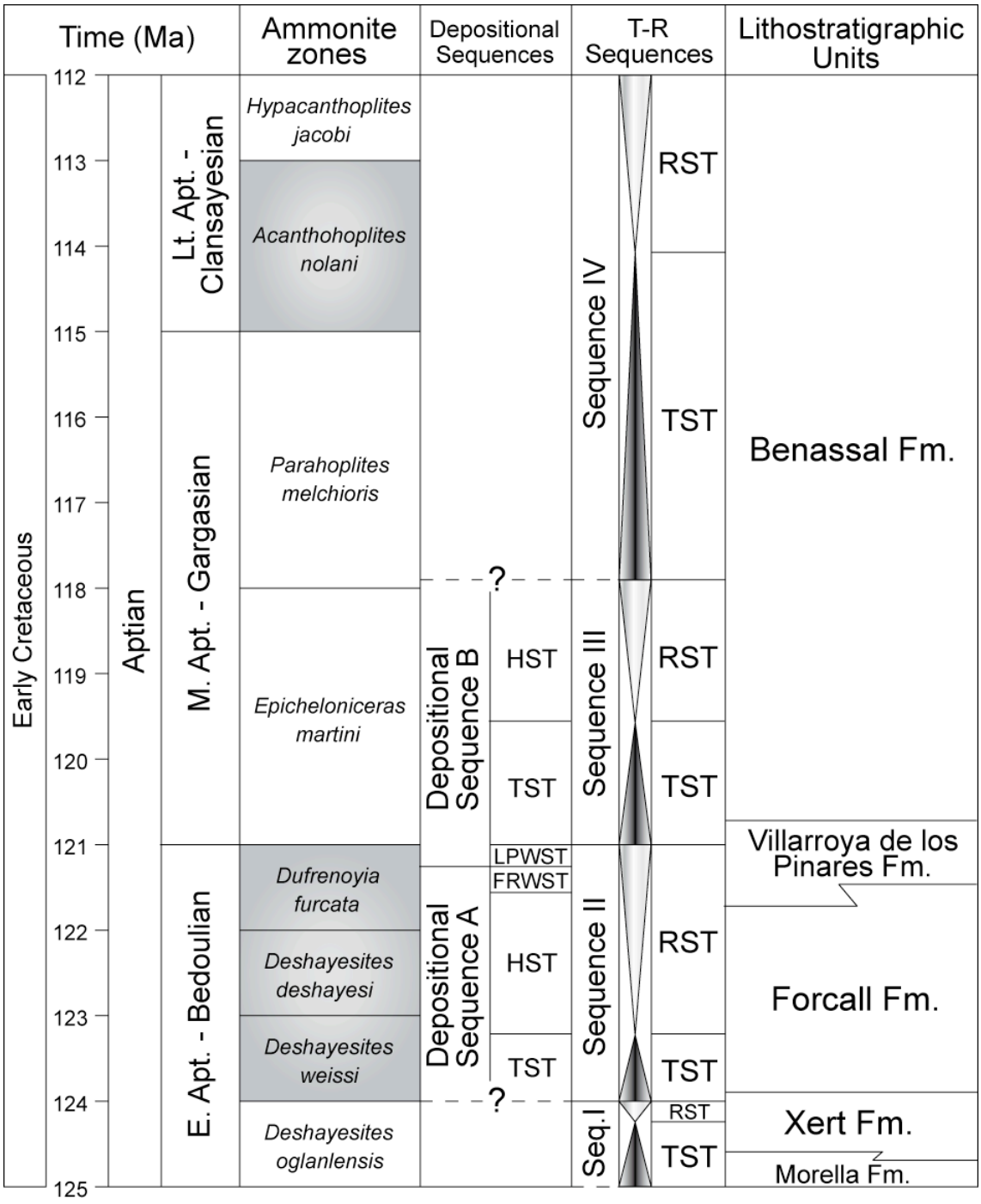

Figure 2.2.2. Aptian lithostratigraphy of the central part of the Galve sub-basin. The ammonite biozones identified are dashed in grey (Moreno and Bover 2007; Bover-Arnal et al. under review). Absolute ages are based on Ogg and Ogg (2006).

2.2.3 Material and methods

Four sedimentary logs were measured, and the facies variations, subaerial unconformities and, maximum flooding, transgressive and other key sedimentary surfaces were mapped on panoramic photomosaics of the outcrops. A Laser Scanner ILRIS 3D Optech Inc. equipped with a differential GPS Top Con with a receiver GB

1000 and an antenna PG-A1 was used to measure distances, heights and angles within the carbonate strata.

Microfacies analysis was carried out on 82 thin sections. Rock textures follow the classification of Embry and Klovan (1971). The terminology used in the sequence stratigraphic analysis is taken from the works of Hunt and Tucker (1992, 1993b, 1995), Catuneanu (2006) and Catuneanu et al. (2009).

2.2.4 Facies Associations and distribution

Ten major lithofacies associations were determined on the basis of lithology, texture, sediment constituents and sedimentary features. These lithofacies assemblages reflect different bathymetric, hydrodynamic and trophic conditions. The recognition of facies heterogeneity and shelf, shelf-margin and slope geometries across the carbonate platform succession permitted to ascribe each facies group to a particular sedimentary setting: platform, slope or basin. The descriptions and interpretations of the lithofacies associations are the following:

2.2.4.1 Facies Association I: slightly argillaceous-marly wackestone-packstone

This facies association consists of a few centimeter-thick, light grey, slightly argillaceous-marly limestones with wackestone-packstone texture (Fig. 2.2.3a). It exhibits nodular bedding, and at times, occurs interbedded with thin argillaceous-marly levels up to 5-cm-thick. The most characteristic components of this lithofacies are medium- to large-sized discoidal orbitolines (diameter up to 5 mm). Other benthic foraminifera and skeletal fragments of echinoderms, oysters, undiagnosed bivalves and gastropods are also common. Silt- to fine-sand sized quartz grains are commonly present.

This facies association was recognized in platform and slope settings. The presence of argillaceous-marly sediments could be indicative of low hydrodynamic conditions. The input of terrigenous material may have resulted in nutrient-rich episodes, which could have favoured the widespread development of discoidal orbitolinids (Pittet et al. 2002), possibly linked to relatively small-scale transgressive pulses (Vilas et al. 1995).

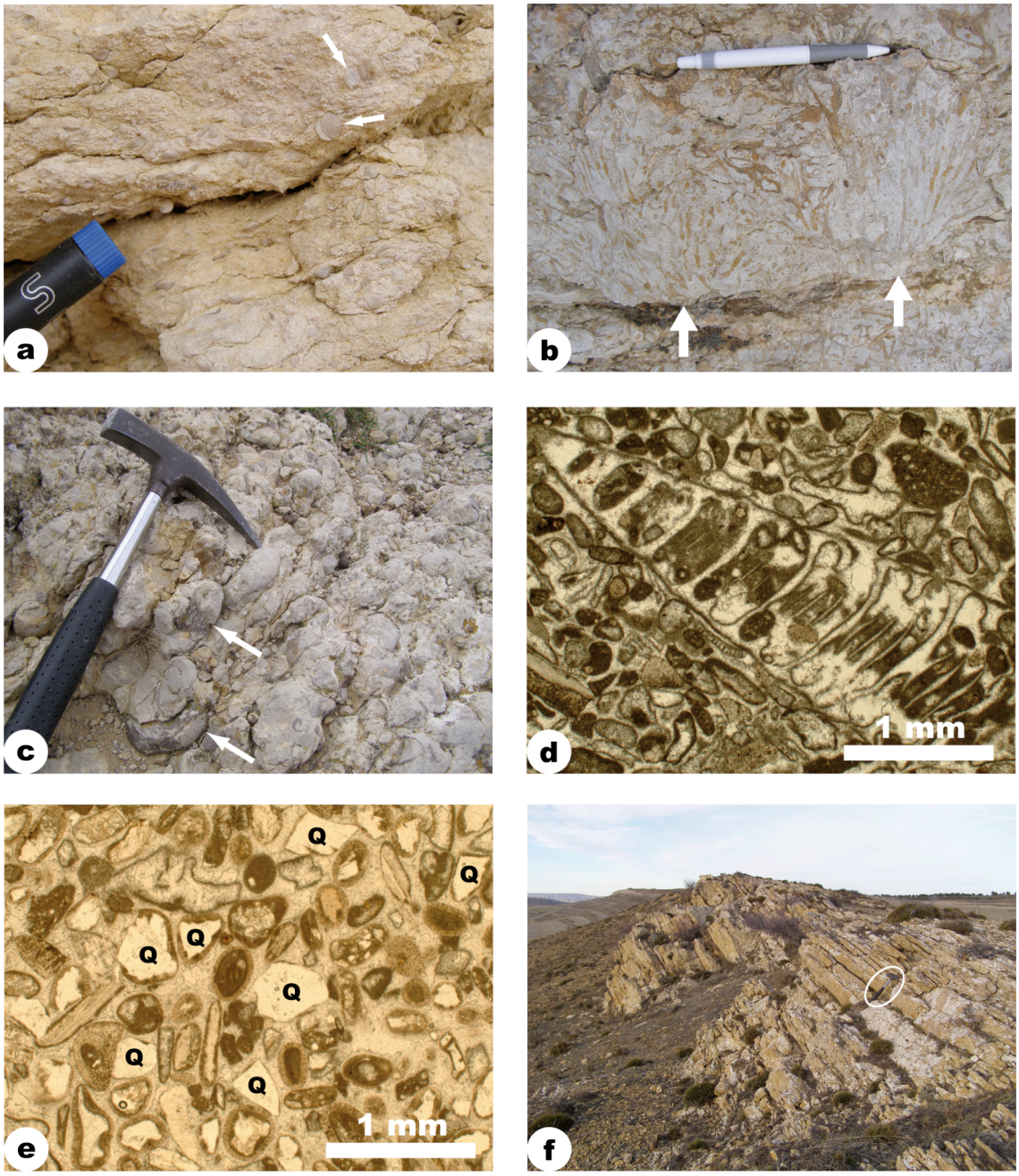

Figure 2.2.3. Sedimentary facies: a) Argillaceous-marly wackestone rich in orbitolines. White arrows point to specimens of Orbitolina. Facies Association I. Las Mingachas (see Fig. 2.2.7 for exact location). b) Floatstone of rudists and corals. Note the massive aspect of the lithofacies. White arrows point to delicate branching corals in growth position. Facies Association II. Las Mingachas (see Fig. 2.2.7 for exact location). c) Rudist and coral reworked floatstone-rudstone. Note the nodular aspect of the lithofacies. White arrows point to specimens of Toucasia carinata. Facies Association III. Camarillas. d) Photomicrograph of peloidal and bioclastic packstone-grainstone microfacies. Note the presence of a small nerineid gastropod at the centre of the image. Facies Association IV. El Morrón. e) Photomicrograph of sandy limestones microfacies. Note the presence of quartz (Q) particles and ooids. Facies Association V. Camarillas. f) Plane-parallel stratified calcarenite rich in oysters. Hammer encircled for scale. Facies Association VI. Camarillas.

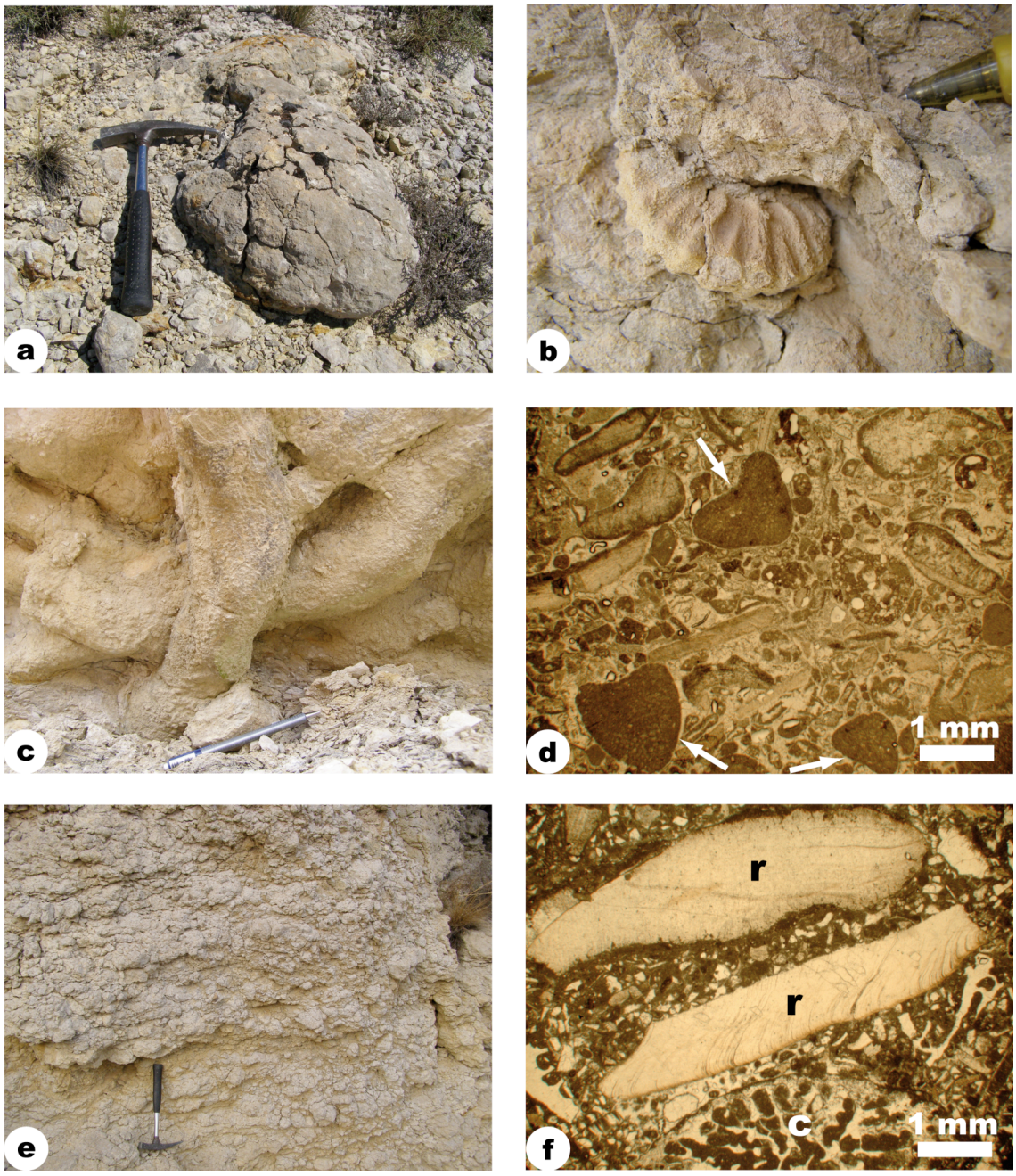

Figure 2.2.4. Sedimentary facies (see Fig. 2.2.7 for exact location): a) Flattened dome-shaped coral colony embedded in marls. Facies Association VII. Las Mingachas. b) Dufrenoyia dufrenoyi ammonite specimen. Facies Association VIII. Las Mingachas. c) Large Thalassinoides bioturbation at the base of a storm-induced turbidite. Note the marly sediments at the lower part of the photograph. Facies Association VIII. Las Mingachas. d) Photomicrograph of the slightly cross-bedded calcarenite wedge microfacies. White arrows point to specimens of Orbitolinopsis simplex. Facies Association IX. Las Mingachas. e) Outcrop photograph of the debris-flow deposits. Note the nodular and chaotic aspect of the lithofacies. Facies Association X. Las Mingachas. f) Photomicrograph of debris-flow microfacies. Note the presence of rudist (r) and coral (c) fragments. Facies Association X. Las Mingachas.

2.2.4.2 Facies Association II: rudist and coral floatstone

Decimeter- to meter-thick (up to 6 m) light grey floatstone limestones dominated by rudists and corals in life position characterize this facies association. The floatstones exhibit massive and tabular bedding. Locally, hardgrounds surmounting the beds and burrow bioturbation are present. The rudist species identified are *Toucasia carinata*, *Polyconites hadriani* (Skelton et al. 2008b; in press), *Monopleura* sp., *Caprina parvula* and *Offneria* sp. The polyconitid rudists are usually grouped in bouquets. The corals display sheet-like, platy, tabular, branching (Fig. 2.2.3b), domal and irregular massive morphologies. *Lithophaga* borings on corals are frequent. Other common constituents of this lithofacies are *Chondrodonta*, oysters, unidentified bivalves, nerineid gastropods, other undiagnosed gastropods, *Orbitolinopsis simplex*, miliolids, other benthic foraminifera, green algae, echinoderms and microencrusters such as sessile foraminifera, *Lithocodium aggregatum*, *Bacinella irregularis* and Peyssonneliaceans encrusting shell debris. Saddle dolomite within coral and rudist skeletal components is common.

Given the large amount of lime mud present and the type of carbonate factory identified, the good fossil preservation and common occurrence in life position suggest that this facies association represents low-energy and muddy platform and platform-margin environments with probable nutrient fluxes as deduced from the strong bioerosion observed on corals (Hallock and Schlager 1986) and from the broad occurrence of suspension-feeder fauna.

2.2.4.3 Facies Association III: rudist and coral reworked floatstone-rudstone

This facies association is characterized by light grey, nodular floatstone-rudstone limestones mainly constituted by fragmented skeletal remains (Fig. 2.2.3c). The beds exhibit decimeter- to meter-scale thicknesses (up to 3 m) and display a chaotic structure. The presence of argillaceous-marly drapes within these deposits is conspicuous. The skeletal fragments are generally angular and correspond to the biotic community described in Facies Association II. However, wholly preserved rudists and other molluscs are also commonly found in this facies association.

This lithofacies represents the reworked deposits of Facies Association II and is interpreted as reflecting moderate hydrodynamic conditions in wave-agitated areas of

the platform. Nevertheless, these reworked sediments could also be related to storm-induced currents.

2.2.4.4 Facies Association IV: peloidal and bioclastic packstone-grainstone

This facies association is formed by light grey packstone-grainstone tabular beds (up to 0.8-m-thick) with plane-parallel and massive stratification. The bases often display erosive surfaces. The limestones with packstone texture are poorly sorted and are largely made up of peloids (diameter up to 0.2 mm), miliolids, other benthic foraminifera and poorly rounded bioclasts of diverse size (up to 4 mm). The bioclasts are mainly skeletal fragments of rudists, echinoderms, corals, green algae, gastropods and other molluscs. The largest bioclasts are commonly bioeroded. The presence of coated grains with a micrite envelope is also worth noting. The limestones with a grainstone fabric are rather well sorted and contain peloids (diameter up to 0.2 mm), orbitolines, miliolids, other benthic foraminifera and poorly rounded bioclasts (size up to 1 mm) of echinoderms, green algae, corals and molluscs. Larger bioeroded skeletal fragments and small entire gastropods are locally present (size up to 3 mm) (Fig. 2.2.3d).

The texture of this lithofacies and the occurrence of plane-parallel stratification suggest that this facies assemblage was deposited in a high-energy environment. The grainstones may reflect an above fair-weather wave-base environment, whereas the packstone textures could represent a slightly deeper-water setting, close to fair-weather wave base.

2.2.4.5 Facies Association V: sandy limestone

Decimeter- to meter-thick (up to 6 m), light grey to ochre, fairly well sorted sandy limestones exhibiting cross-bedding and plane-parallel stratification represent this group of lithofacies (Fig. 2.2.3e). Locally, the beds of this facies association display erosive and irregular bases. These terrigenous-influenced deposits have a grainstone texture and are composed of angular to sub-rounded, very fine- to medium-grained, quartz particles, well rounded ooids of diameter 0.2-0.3 mm with detrital, peloidal and bioclast cores, peloids (diameter up to 0.3 mm), orbitolines, other benthic foraminifera, and sub-angular- to sub-rounded-shaped fragments of echinoderms and molluscs.

The sedimentary structures as well as the rock texture and the components observed suggest that this facies assemblage was formed in high-energy, siliciclastic-influenced shoal environments in a proximal platform setting.

2.2.4.6 Facies Association VI: oyster-rich calcarenite

The facies consists of a cross-bedded and plane-parallel stratified orange calcarenite (up to 15-m-thick), rich in oysters (Fig. 2.2.3f). This deposit is stacked in a retrograding pattern, and shows a lower part characterized by a well-sorted grainstone fabric, whereas the upper part is dominated by a poorly- to moderately-sorted packstone-grainstone fabric. The base of this lithofacies is erosive and exhibits clay drapes and mud pebbles, which contain preferentially imbricated silt-sized quartz grains. The main components of the facies are peloids, benthic foraminifera, and fragments of undiagnostic oysters, other unidentifiable molluscs and echinoderms. The bioclasts exhibit sub-rounded to rounded edges. Silt- to fine sand-sized quartz grains are also present. The top of the calcarenite is capped by a hardground displaying borings and ferruginous stains.

The rock texture and the presence of cross-bedding and plane-parallel stratification suggest that this facies association represents a high-energy, shallow platform environment, above or close to fair-weather wave base. The retrograding stacking pattern may reflect a transgressive context.

2.2.4.7 Facies Association VII: corals embedded in marls

This assemblage is characterized by small patch-reefs and isolated coral colonies embedded in marls. The corals occur in growth position, showing excellent preservation, with domal (Fig. 2.2.4a), irregular massive and branching morphologies. The size of coral colonies ranges from centimeters to meters (up to 2.3-m-width). Coral rubble and dislodged colonies were not observed. *Lithophaga* borings on corals are abundant. The presence of *Polyconites hadriani* (Skelton et al. 2008b; in press) grouped in bouquets, *Chondrodonta*, oysters, nerineid gastropods, unidentified molluscs, brachiopods, echinoderms, *Dufrenoyia dufrenoyi* and hydrozoans is also typical of this facies association.

This group of lithofacies is characteristic of marly slope environments. The presence of marls with well-preserved sparsely distributed isolated coral colonies,

which locally form small patch-reefs, may reflect low hydrodynamic settings, probably, below storm wave-base. Moreover, the occurrence of strong bioerosion on corals and suspension-feeder fauna could be indicative of nutrient-rich conditions.

2.2.4.8 Facies Association VIII: marls with interbedded storm-induced turbidites

This facies association basically consists of green marls with interbedded storm-induced deposits and mudstone to wackestone limestones. The marls contain abundant *Palorbitolina lenticularis* and *Praeorbitolina cormyi*, *Dufrenoyia dufrenoyi* (Fig. 2.2.4b), undiagnostic oysters, other bivalves, gastropods, unidentified molluscs, brachiopods, echinoderms and pyritized skeletal fragments. Calcareous nodules and bioturbation are also common. The turbidites are characterized by yellowish centimeter- to meter-thick calcarenitic layers with massive stratification and erosive and smooth bases. Locally, the bases of these storm-induced deposits exhibit large *Thalassinoides* burrows (Fig. 2.2.4c). The mudstone to wackestone limestones display centimeter- to decimeter-thick massive and nodular stratified yellowish and greyish beds with smooth bases and common bioturbation. The main constituents of the storm-related sediments and the limestones with mudstone and wackestone fabric are silt- to medium sand-sized quartz grains, peloids, orbitolines, other benthic foraminifera, ammonites, and fragments of echinoderms, oysters, rudists and other unidentified molluscs.

The facies assemblage is interpreted as being deposited in relatively deep basinal environments as suggested by the dominant marl, the interbedded storm-induced deposits, and the faunal content. The storm-induced nature of the turbidites is deduced from the presence of abundant silt- to medium sand-sized quartz, which is interpreted as having been transported from proximal settings to basinal environments by storm-induced turbidity currents.

2.2.4.9 Facies Association IX: slightly cross-bedded calcarenite

This facies mainly corresponds to a yellowish, slightly planar cross-bedded centimeter- to meter-thick (up to 4 m) calcarenite wedge. The lower part of this wedge presents a tabular stratified calcarenitic layer overlain by a highly bioturbated calcarenitic unit exhibiting nodular bedding. The bases of these deposits have sharp surfaces that exhibit abundant *Planolites* bioturbation and locally, *Thalassinoides*

burrows. The lithofacies displays a poorly to moderately sorted packstone-grainstone texture. The main components are peloids, serpulids, *Orbitolinopsis simplex* (Fig. 2.2.4d), other benthic foraminifera, *Dufrenoyia furcata* and sub-rounded to rounded fragments of rudists, oysters, other bivalves, gastropods, unidentified molluscs, echinoderms, corals and green algae.

Owing to the basinal position of this calcarenitic wedge, the presence of entire preserved ammonite specimens and the sedimentary structures observed, the facies association is interpreted as allochthonous debris reworked by bottom currents at the toe-of-slope.

2.2.4.10 Facies Association X: debris-flow deposits

This facies consists of centimeter- to meter-thick, light grey, nodular-bedded chaotic floatstones and rudstones of rudist and coral fragments (Fig. 2.2.4e). Massive stratified beds are rarely present. This facies assemblage commonly displays channelized bodies and erosive surfaces. Locally, slump scars, hardgrounds and unidentified bioturbation occur. The most important constituents of these lithofacies are the same as those described in facies associations II and IV. The fragmented bioclasts mainly show angular edges. The floatstone-rudstone fabric is very poorly sorted (Fig. 2.2.4f).

This type of facies is interpreted as debris-flow deposits of facies associations II and IV. The resedimented lithofacies formed under low- to moderate-energy conditions in slope and basinal environments. These deposits occur across slopes, filling in channels or accumulated in lobes at the toe of the slopes.

2.2.5 Facies successions

At outcrop scale, the platform stratal arrangement and distribution of the lithofacies assemblages described above basically form deepening-shallowing small-scale (up to few meters thick) symmetrical cycles. These elementary cycles, which are interpreted as having developed in response to high-frequency, low-amplitude relative sea-level fluctuations, correspond to parasequences (*sensu* Spencer and Tucker 2007). The repetition of these basic accretional units builds up the major part of the sedimentary succession studied. Four types of parasequence can be recognized across the carbonate platform system analyzed (Fig. 2.2.5):

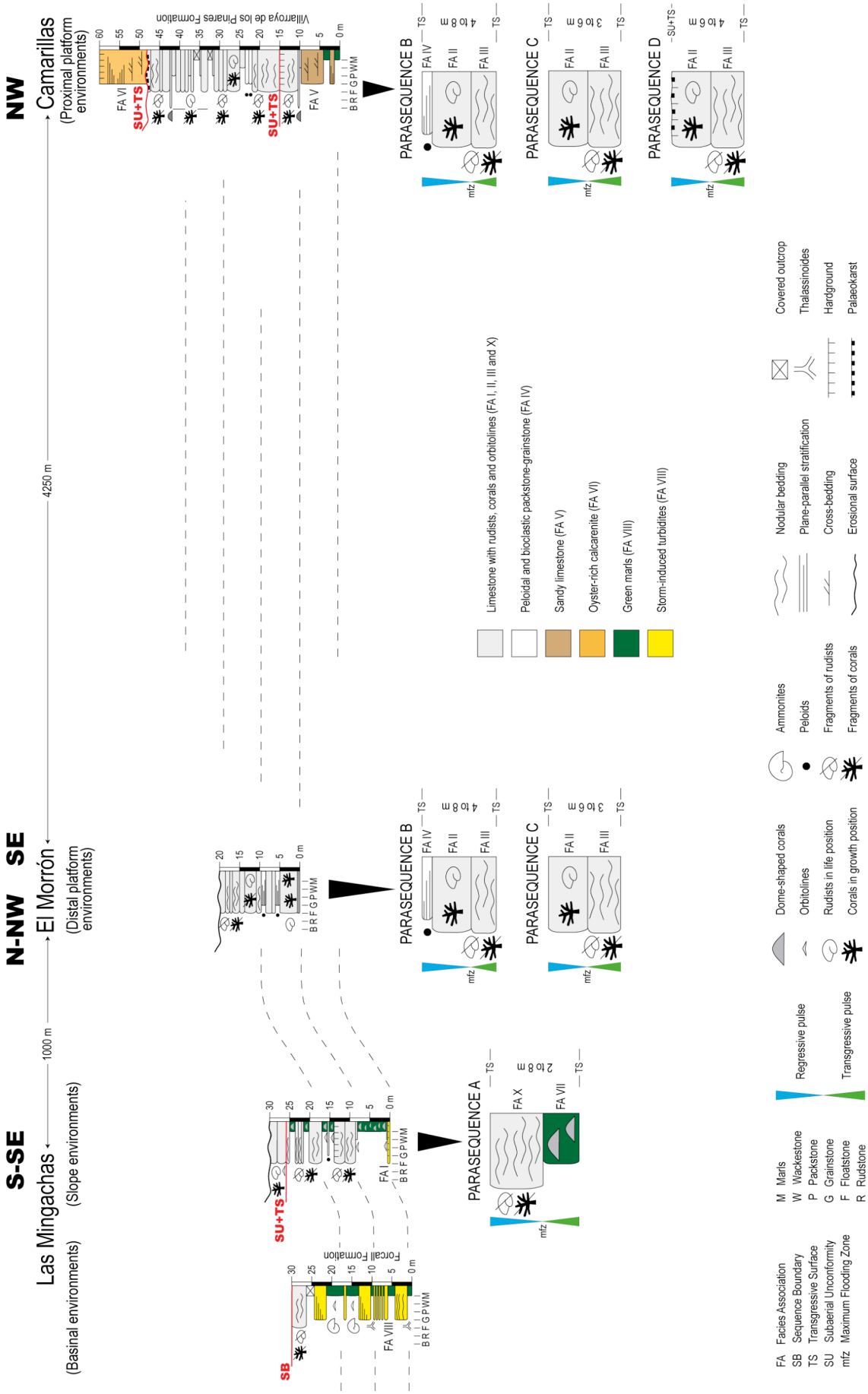
S-SE
N-NW SE
NW
Las Mingachas
(Basinal environments)
1000 m
(Slope environments)
El Morrón
(Distal platform environments)
4250 m
Camarillas
(Proximal platform environments)
Villarroya de los Pinares Formation
Forcall Formation
FA VI
FA V
FA VIII
FA I
SU+TS
SB
PARASEQUENCE A
PARASEQUENCE B
PARASEQUENCE C
PARASEQUENCE D
FA X
FA VII
FA IV
FA II
FA III
2 to 8 m
4 to 8 m
3 to 6 m
TS
mfz
Limestone with rudists, corals and orbitolines (FA I, II, III and X)
Peloidal and bioclastic packstone-grainstone (FA IV)
Sandy limestone (FA V)
Oyster-rich calcarenite (FA VI)
Green marls (FA VIII)
Storm-induced turbidites (FA VIII)
Nodular bedding
Plane-parallel stratification
Cross-bedding
Erosional surface
Covered outcrop
Thalassinoides
Hardground
Palaeokarst
Ammonites
Peloids
Fragments of rudists
Fragments of corals
Dome-shaped corals
Orbitolines
Rudists in life position
Corals in growth position
Regressive pulse
Transgressive pulse
FA Facies Association
SB Sequence Boundary
TS Transgressive Surface
SU Subaerial Unconformity
mfz Maximum Flooding Zone
M Marls
W Wackestone
P Packstone
G Grainstone
F Floatstone
R Rudstone
B Boundstone

◀ *Figure 2.2.5. Simplified scheme of the late Early Aptian platform-to-basin cross-section studied with the measured section logs (see Fig. 2.2.1 for location) and the idealized elementary sequences (parasequences) identified within each setting.*

2.2.5.1 Parasequence A

This parasequence is 2- to 8-m-thick and is bounded by smooth transgressive surfaces. Locally, these surfaces are marked by a hardground. This basic accretional unit characterizes the slope environments and is formed in two high-frequency relative sea-level stages: transgressive and regressive.

The transgressive pulse is represented by a unit of irregular massive and dome-shaped corals embedded in marls (Facies Association VII). The corals occur in growth position forming small patch-reefs or isolated colonies. Locally, the presence of a thin orbitoline-rich layer (Facies Association I) characterizes the basal part of these transgressive deposits. This orbitoline-bloom episode could reflect increased nutrient leaching and supply, linked to a high-frequency sea-level rise (Vilas et al. 1995; Pittet et al. 2002).

The subsequent stillstand and fall in relative sea-level increases hydraulic energy in platform settings producing resedimentation and shedding episodes. These debris-flow deposits, which consist of poorly sorted, nodular floatstones and rudstones of rudist and coral fragments (Facies Association X), crossed the slopes and accumulated in a basinal setting, forming lobe deposits. However, oversteepening of the platform margin and storm events may also have caused resedimentation and basinwards transport of platform material.

2.2.5.2 Parasequence B

The thickness of this elementary sequence, which is bounded by sharp and irregular transgressive surfaces, ranges between 4 and 8 m. This parasequence is characteristic of proximal-to-distal platform environments and is interpreted as having developed in three relative sea-level pulses: transgressive, early regressive and late regressive.

The transgressive stage is composed of nodular limestone with rudist and coral fragments and a random floatstone to rudstone texture (Facies Association III). Commonly, these deposits are clayey- and marly-influenced and may contain an orbitolina-dominated basal part. The features of the lithofacies suggest reworking in

wave- and tidal-influenced shelf settings and thus are interpreted as transgressive lag deposits. However, these reworked sediments could also correspond to storm-induced deposits.

The early regressive pulse (normal regression) records a platform construction episode characterized by floatstones of rudists and delicate branching corals in life position (Facies Association II). The absence of hydrodynamic structures and the occurrence of organisms in growth position may indicate sedimentation below wave-influence, given that protecting shoals, palaeohighs, reefs or other bioherms were not observed basinwards. Nevertheless, sporadic storm events may have lowered wave-base influence, producing reworking and debris-flow episodes.

A falling sea-level (forced regression) results in a basinwards progradation of the energetic belt. Hence, skeletal and peloidal plane-parallel stratified limestones with a packstone to grainstone fabric (Facies Association IV) were deposited above the aforementioned deposits of Facies Association II.

2.2.5.3 Parasequence C

This type of parasequence is 3- to 6-m-thick and shows the same features described for the parasequence B. However, the most regressive part of the parasequence B, which corresponds to the energetic deposits of Facies Association IV, is not present. The absence of these skeletal and peloidal plane-parallel stratified grainstones and packstones crowning the basic accretional unit could indicate that there was no sediment preservation during the relative sea-level fall (late regressive pulse) or that this forced regressive pulse did not occur or that it was not sufficiently significant to move the energetic belt basinwards.

2.2.5.4 Parasequence D

This elementary sequence is typically 4- to 6-m-thick and consist of type C parasequences capped by subaerial exposure surfaces. Locally, these subaerial unconformities correspond to erosive surfaces with a development of palaeokarst. Transgressive surfaces are superimposed on these surfaces affected by subaerial processes, and commonly mask the evidence of subaerial exposure. Hardground development associated with transgressive surfaces is common.

2.2.6 Sequence stratigraphic interpretation

In the platform-to-basin transition area of Las Mingachas (Fig. 2.2.1), the overall stratal architecture of the facies successions analyzed can be divided into five large-scale differentiated lithostratigraphic units; these reflect longer-term relative sea-level changes and can be interpreted as component systems tracts. These systems tracts occur within two large-scale T-R sequences (Sequence II and III; Fig. 2.2.2) described by Bover-Arnal et al. (under review) in an extensive study of the Aptian evolution of the western Maestrat Basin in the Iberian Chain.

Moreover, the disposition in time and space of these systems tracts seems to be consistent with the model for deposition during base-level fall of Hunt and Tucker (1992, 1993b). Hence, the sequence stratigraphic analysis presented below will be based on the works of these authors. The sedimentary succession analyzed, which embraces T-R sequences II and III, was reinterpreted using depositional sequences in the sense of Van Wagoner et al. (1988). On account of this reinterpretation, two depositional sequences can be construed from the sedimentary record studied: A and B (Fig. 2.2.2).

The upper part of Depositional Sequence A, which is of late Early Aptian age (Fig. 2.2.2), is composed of highstand systems tract (HST) deposits followed by a forced regressive wedge systems tract (FRWST). Depositional Sequence B, which is of uppermost Early Aptian and Middle Aptian age (Fig. 2.2.2), is characterized by a lowstand prograding wedge systems tract (LPWST) followed by a transgressive systems tract (TST) and the subsequent HST (Fig. 2.2.6). All these deposits analyzed show minor tilting towards the SW (Fig. 2.2.6).

The locations of the views of the outcrops displayed in the following five headings are shown in Figure 2.2.7.

2.2.6.1 Highstand System Tract (Depositional Sequence A)

The HST of Depositional Sequence A is distinguished by the development of a large prograding carbonate platform dominated by rudists and corals (facies associations II and III), and these essentially conform to the Villarroya de los Pinares Formation. Nevertheless, the presence of high-energy deposits such as sandy limestones (Facies Association V) and skeletal-peloidal packstones and grainstones (Facies Association IV) sedimented throughout this highstand stage is also noteworthy (Fig. 2.2.5).

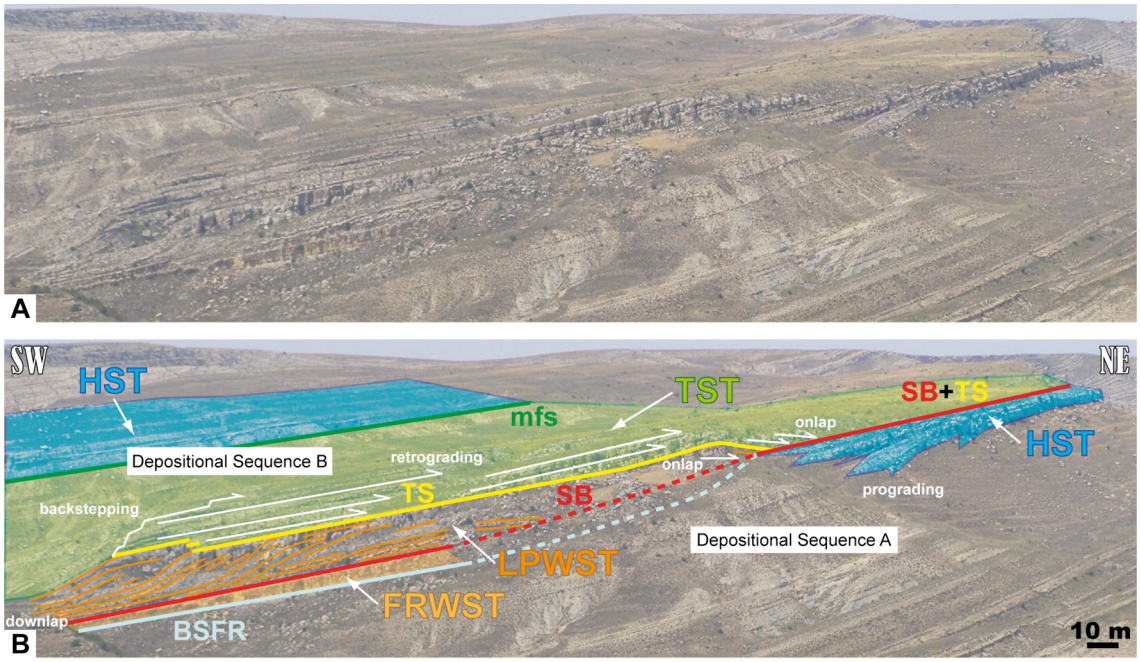

KEY

HST: Highstand Systems Tract
FRWST: Forced Regressive Wedge Systems Tract
LPWST: Lowstand Prograding Wedge Systems Tract
TST: Transgressive Systems Tract
BSFR: Basal Surface of Forced Regression
SB: Sequence Boundary
TS: Transgressive Surface
mfs: maximum flooding surface

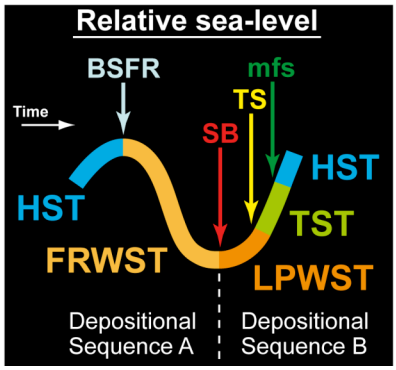

Figure 2.2.6. Photograph of platform-to-basin transition at Las Mingachas (A) (see Fig. 2.2.1 for location) with the overall sequence stratigraphic interpretation (B) and the stages of relative sea-level.

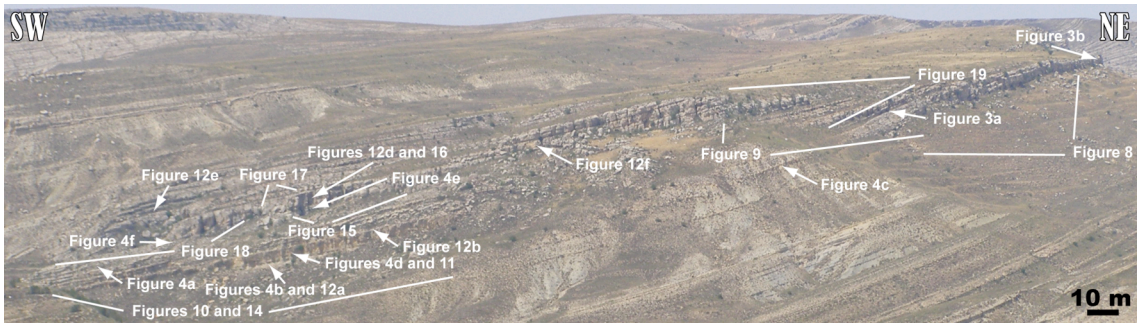

Figure 2.2.7. Photograph of Las Mingachas area (see Fig. 2.2.1 for location) displaying the situation of the outcrops and photomicrographs showed in the figures 2.2.3 (a-b), 2.2.4 (a-f), 2.2.8, 2.2.9, 2.2.10, 2.2.11, 2.2.12 (a-b, d-f), 2.2.14, 2.2.15, 2.2.16, 2.2.17, 2.2.18 and 2.2.19.

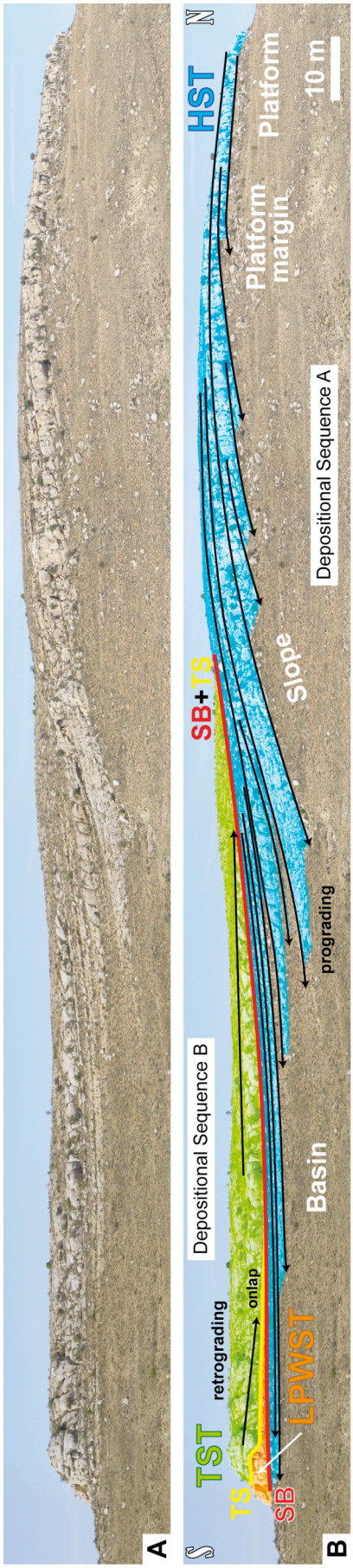

Figure 2.2.8. Photograph of an oblique cross-section from the northeastern part of Las Mingachas (A) (see Fig. 2.2.7 for location) showing the sequence stratigraphic interpretation and the shelf-margin geometries, which clearly differentiate the platform, platform-margin, slope and basin depositional settings (B). Note the flat-topped non-rimmed depositional profile that exhibits the carbonate platform. See figure 2.2.6 for legend.

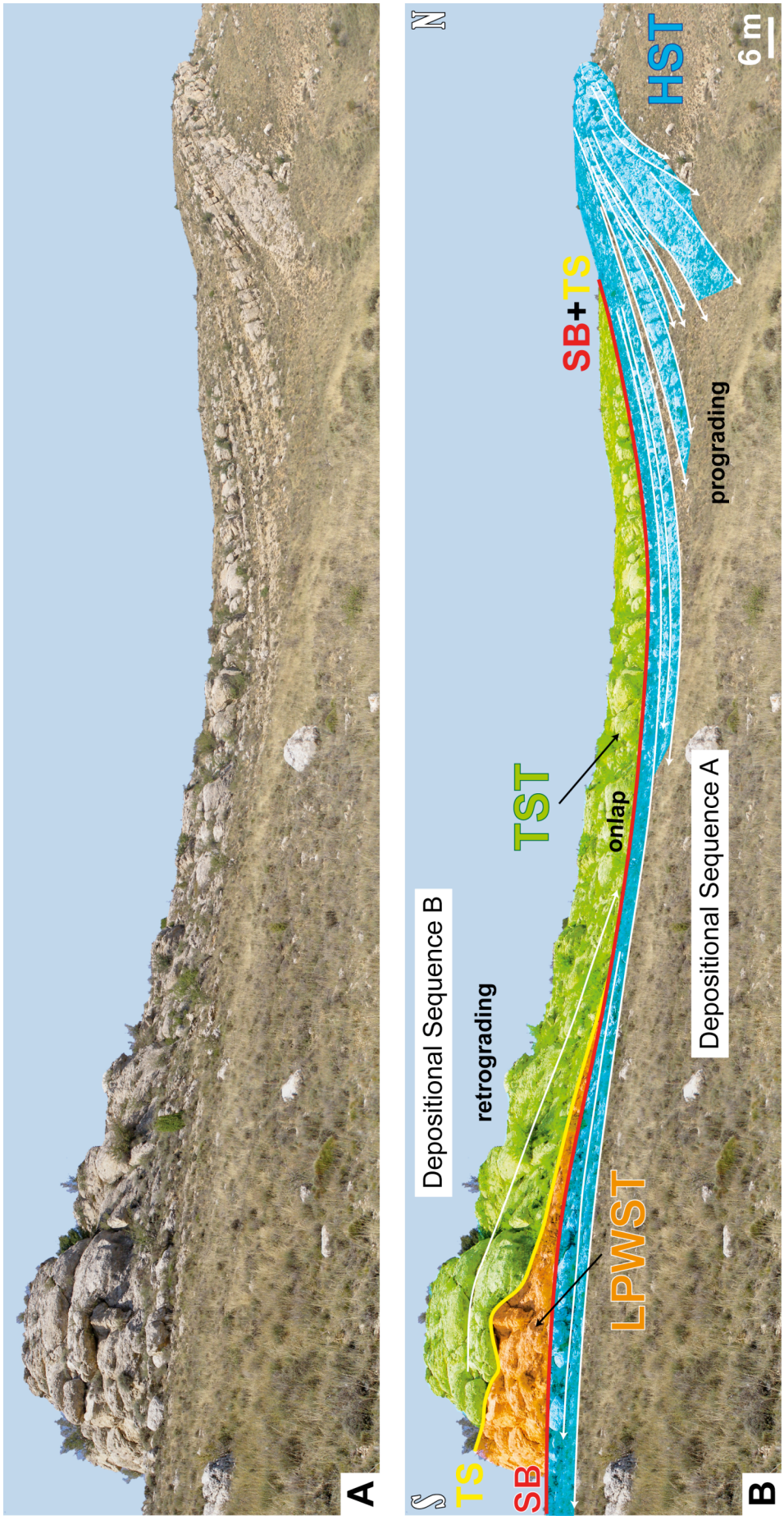

Figure 2.2.9. View from the south of the oblique cross-section located in the northeastern part of Las Mingachas (A) (see Fig. 2.2.7 for location) displaying the sequence stratigraphic interpretation (B). See figure 2.2.6 for legend.

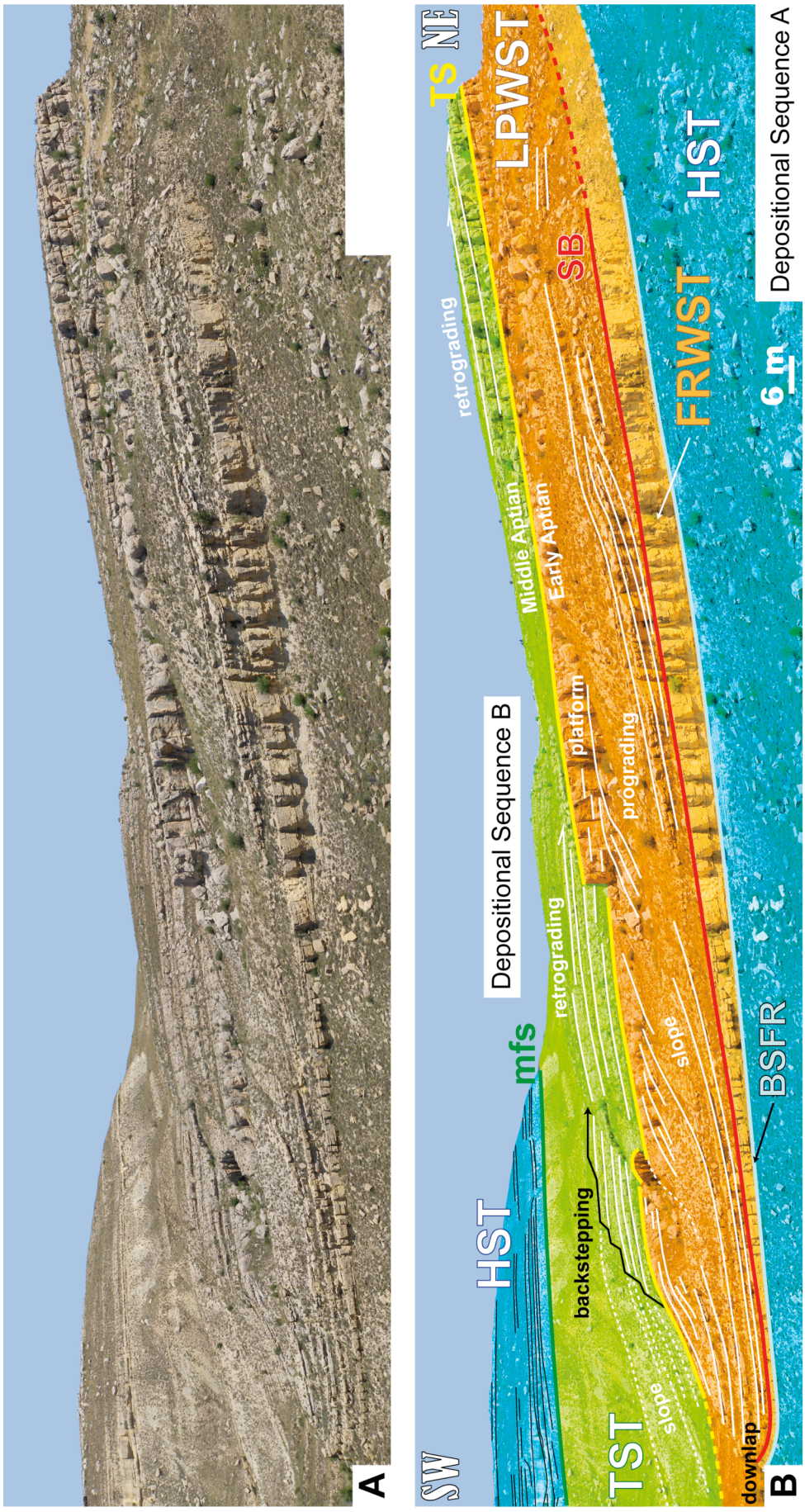

Figure 2.2.10. Photograph of the southern part of Las Mingachas (A) (see Fig. 2.2.7 for location) showing the sequence stratigraphic interpretation (B). See figure 2.2.6 for legend.

The highstand carbonate shelf extends at least from the north of the town of Camarillas to Las Mingachas (see Fig. 2.2.1 for location), where it changes laterally into slope lithofacies (facies associations I, VII and X) that pinch out into the basinal marls (Facies Association VIII) of the Forcall Formation (Figs. 2.2.5, 2.2.6 and 2.2.8). At Las Mingachas, the shelf margin exhibits facies heterogeneity and superb platform-to-basin transition geometries (Figs. 2.2.6, 2.2.8 and 2.2.9) that display a flat-topped non-rimmed depositional profile (Fig. 2.2.8).

The considerable thicknesses of the beds, the wide diversity and extensive development of facies as well as the carbonate producers observed (see Facies Association II description for species) and the large amount of lime mud, suggest that carbonate production was intense in shelf settings during the HST. The high rate of carbonate accumulation together with the slowing sea-level rise to a near standstill, which is characteristic of a highstand of sea-level, significantly reduced the available accommodation space throughout the late HST. Limited space for vertical accumulation during this late highstand phase is evidenced by type B and C parasequences (Fig. 2.2.5) that become thinner upwards in the succession, and by the development of type D parasequences in proximal parts of the carbonate platform (Fig. 2.2.5). Moreover, this is also corroborated by the overall prograding stacking pattern that exhibits the HST and the episodic downslope dumping of excess sediment (Figs. 2.2.6, 2.2.8 and 2.2.9).

2.2.6.2 Forced Regressive Wedge Systems Tract (Depositional Sequence A)

Base-level started to fall with the result that the highstand platform was subaerially exposed, essentially shutting down the carbonate factories and leaving a starved slope. During this relative sea-level drop, the sedimentation of a thick slightly cross-bedded calcarenite wedge (Facies Association IX) occurred basinwards. This calcarenitic wedge corresponds to a detached forced regressive deposit made up of allochthonous debris, which accumulated at the toe of the slope and were reworked by bottom currents. The allochthonous debris resulted from the chemical and mechanical erosion of the subaerially exposed carbonate platform, and the remains of the reduced carbonate-producing community dwelling on the slope. All these sediments deposited in this basinal position during falling relative sea-level are interpreted as the FRWST (Figs. 2.2.6 and 2.2.10).

Figure 2.2.11. Outcrop photograph of the FRWST (A) (see Fig. 2.2.7 for location) displaying the interpreted position of the BSFR and the correlative conformity of the SB (B). Note the sharp contact of these surfaces. See figure 2.2.6 for legend.

The FRWST onlaps the toe of the former highstand slope forming a basin floor component, which is bounded below by the basal surface of forced regression (BSFR) and above by the sequence boundary (SB) (Figs. 2.2.6, 2.2.10 and 2.2.11). The BSFR marks the start of base-level fall at the shoreline, and at Las Mingachas (Fig, 2.2.1) it is a sharp surface, which exhibits abundant *Planolites* bioturbation and separates the underlying highstand marls from the first forced regressive calcarenitic unit (Figs. 2.2.11 and 2.2.12a). Therefore, this surface also corresponds to a drastic change of lithofacies from basinal marls containing abundant orbitolines, ammonites and brachiopods to shallower-water calcarenitic deposits.

The SB indicates the lowest point of relative sea-level (Figs. 2.2.6 and 2.2.10), and in the area studied it is characterized by a subaerial unconformity, which becomes progressively younger seawards. Thus, it is reasonable to assume that the highstand platform margin and the uppermost slope situated at Las Mingachas (Fig. 2.2.1) were not subaerially exposed for a long time; as a result of this, only a few poorly developed palaeomicrokarst features can be observed. Furthermore, within the uppermost slope and towards the basin, the subaerial unconformity passes to its marine correlative conformity (Fig. 2.2.12b), which extends basinwards above the detached forced regressive deposits (FRWST), making its identification difficult (Figs. 2.2.6 and 2.2.10). Nonetheless, there is clear evidence of subaerial exposure in the proximal parts of the carbonate platform that was established during the HST (Fig. 2.2.5) in the vicinity of Camarillas (Fig. 2.2.1), where a long-term subaerial exposure surface was

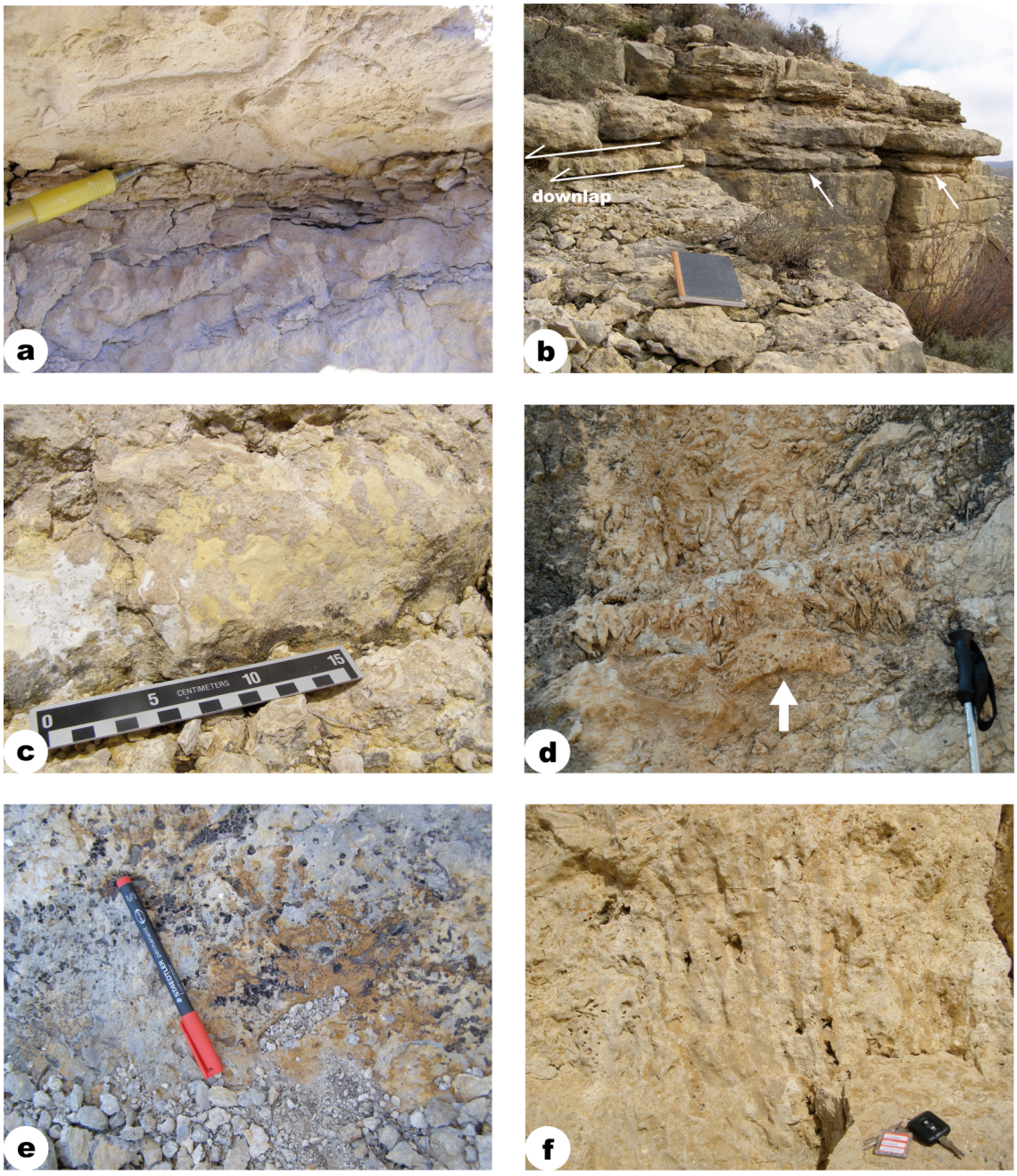

Figure 2.2.12. Sedimentary facies and key sequence stratigraphic surfaces (see Fig. 2.2.7 for exact location): a) Detail of the BSFR. Note the sharp contact between the underlying highstand marls and the forced regressive calcarenite, which displays Planolites burrows at the base. Las Mingachas. b) Close-up photograph of the correlative conformity surface (SB), which extends above the FRWST and below the LPWST. The notebook lies on this surface, while the white arrows point to it. Note the sharp contact of this surface. Las Mingachas. c) Detail of the surface boundary between the depositional sequences A and B displaying palaeokarst development. Camarillas. d) Detail of the lowstand prograding platform lithofacies. Note the Polyconites hadriani rudists (Skelton et al. 2008b; in press) grouped in bouquets. White arrow points to a platy coral. Facies Association II. Las Mingachas. e) Detail of the transgressive surface exhibiting a hardground with a ferruginous crust and borings. Las Mingachas. f) Detail of a rod-like branching coral in growth position in the backsteeping platform (TST). Facies Association II. Las Mingachas.

developed. This surface exhibits an important truncation related to subaerial processes (Fig. 2.2.13) and a broad palaeokarst development (Fig. 2.2.12c).

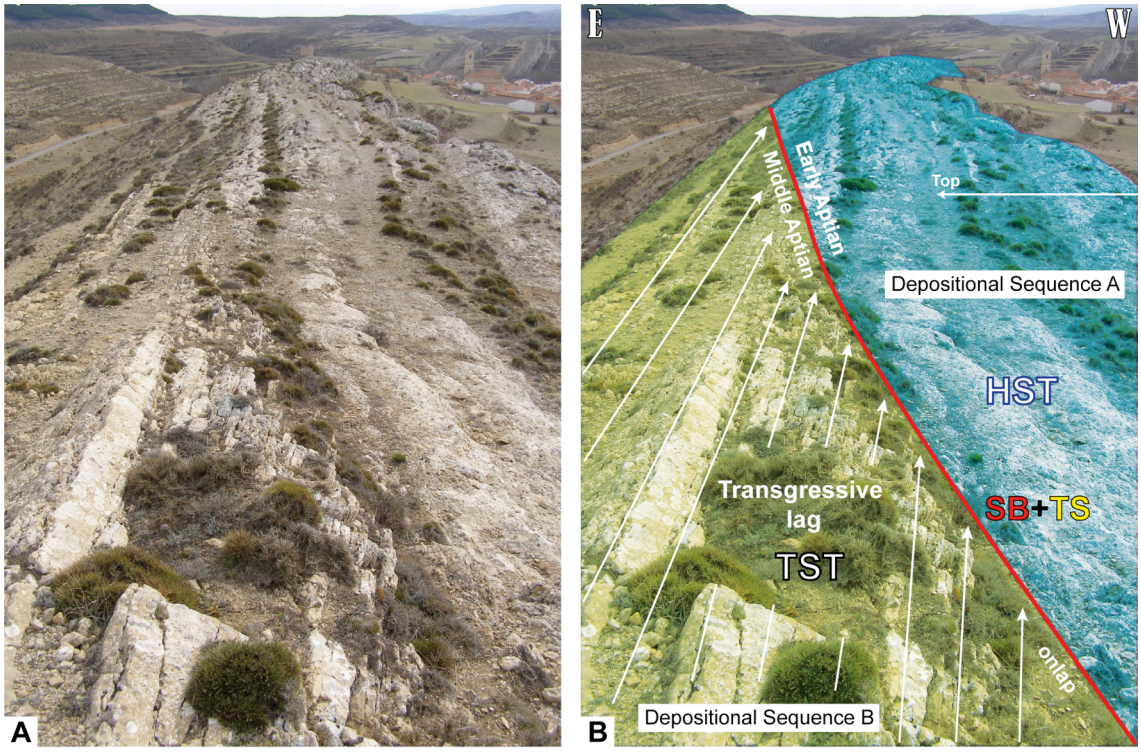

Figure 2.2.13. Photograph of the truncation surface related to subaerial exposure close to the town of Camarillas (A) (see Fig. 2.2.1 for location) displaying the sequence stratigraphic interpretation (B). Note how the transgressive lag onlaps the composite surface (SB+TS). Note that the layers are vertical. The town of Camarillas (up-right in the photo) is used for scale. See figure 2.2.6 for legend.

2.2.6.3 Lowstand Prograding Wedge Systems Tract (Depositional Sequence B)

With the stillstand and the subsequent rise of relative sea-level, a prograding small carbonate platform of rudists and corals was constructed downslope in the former basin. This platform corresponds to the basal part of Depositional Sequence B and constitutes the LPWST, which is bounded below by the correlative conformity (SB) and above by the transgressive surface (TS) (Figs. 2.2.6, 2.2.10 and 2.2.14). The dip direction of the all-embracing platform system, which developed during this lowstand phase, is around 228º towards the SW.

The lowstand platform architecture displays a flat-topped non-rimmed depositional profile, where shelf lithofacies (Facies Association II) pass into slope

deposits (facies associations VII and X), and then to basinal facies (facies associations VIII and X) (Figs. 2.2.10 and 2.2.15).

The platform facies are massive and show onlapping geometries landwards. Despite the reduced dimensions of the lowstand shelf (Figs. 2.2.10 and 2.2.15), carbonate production was significant as were shedding episodes. Proliferation of *Polyconites hadriani* (Skelton et al. 2008b; in press) grouped in bouquets characterizes the shelf margin (Fig. 2.2.12d).

The slopes are distinguished by dome-shaped corals embedded in marls (Facies Association VII) with interbedded episodes of nodular-shaped debris-flow deposits (Facies Association X) that cross the slopes and downlap over the FRWST (Figs. 2.2.6, 2.2.10, 2.2.14 and 2.2.15). Locally, these resedimented slope deposits are channelized or display intraformational smooth and erosive unconformities interpreted as slump scars (Figs. 2.2.16 and 2.2.17). In this setting, the facies succession is made up of type A parasequences (Fig. 2.2.5). The dip angles of these lowstand slopes range between 5 and 25 degrees.

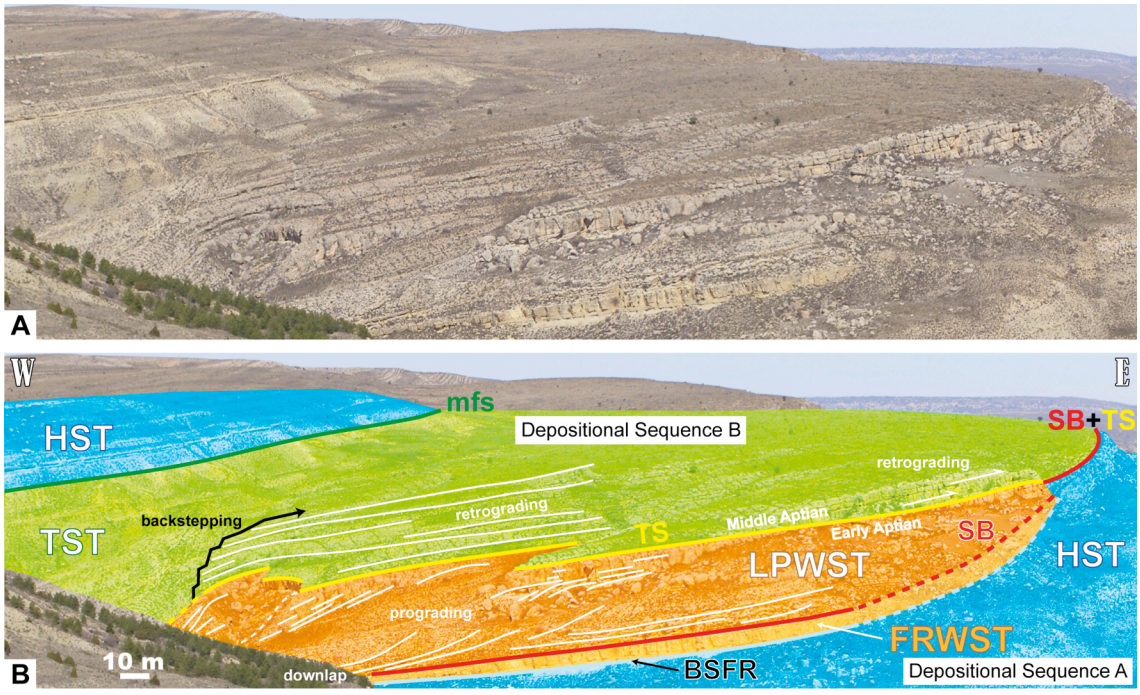

Figure 2.2.14. Panoramic view of the southern part of Las Mingachas (A) (see Fig. 2.2.7 for location) showing the sequence stratigraphic interpretation (B). See figure 2.2.6 for legend.

Figure 2.2.15. Outcrop photograph of the lowstand prograding platform (A) (see Fig. 2.2.7 for location) displaying the sequence stratigraphic interpretation (B). Note the flat-topped non-rimmed depositional profile that exhibits this carbonate platform and note how it changes laterally from shelf settings to slope environments. The massive lithofacies (above) are construed to be sedimented in situ, while the lithofacies with a nodular aspect (below) correspond to resedimented deposits. See figure 2.2.6 for legend.

Figure 2.2.16. Close-up photograph of the lowstand prograding platform (A) (see Fig. 2.2.7 for location) showing a slump scar (B). Note the nodular aspect of these debris-flow deposits. See figure 2.2.6 for legend.

Above the LPWST, the TS marks the end of this stage of normal regression (Figs. 2.2.6, 2.2.10, 2.2.14 and 2.2.15). This surface exhibits a sparsely developed hardground with borings and a ferruginous crust (Fig. 2.2.12e), and superimposes the SB landwards. Thus, the subaerial unconformity that separates depositional sequences A and B becomes a composite sequence boundary (SB+TS) (Figs. 2.2.6, 2.2.8, 2.2.9 and 2.2.14).

In addition, the TS may also correspond to the boundary between the Early and the Middle Aptian. In the lowstand carbonate platform of Las Mingachas (Fig. 2.2.15), a few specimens of caprinid rudists were identified below the TS, whereas above this surface, this rudist family disappears. According to Skelton (2003b), the disappearance of the rudist family Caprinidae coincides with the Early-Middle Aptian boundary.

2.2.6.4 Transgressive System Tract (Depositional Sequence B)

During the early TST, the highstand subaerially exposed shelf was progressively flooded towards the land. Sedimentation of a cross-bedded and plane-parallel stratified

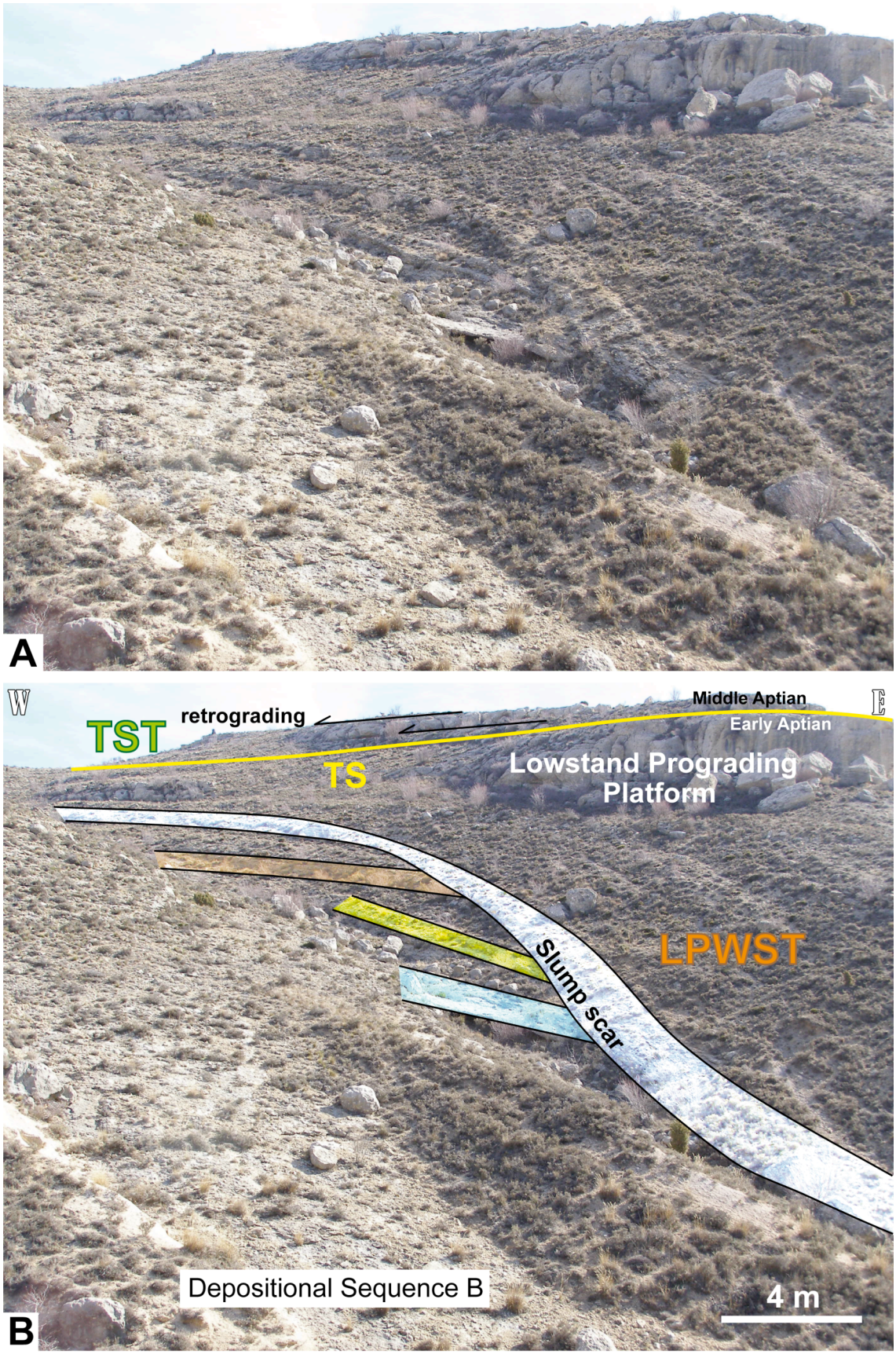
A
W
E
TST
retrograding
TS
Middle Aptian
Early Aptian
Lowstand Prograding
Platform
LPWST
Slump scar
Depositional Sequence B
4 m
B

◀ *Figure 2.2.17. Outcrop photograph of the lowstand slopes (A) (see Fig. 2.2.7 for location) displaying a discordant surface interpreted as a slump scar and the sequence stratigraphic interpretation (B). See figure 2.2.6 for legend.*

calcarenite (Facies Association VI), stacked in a retrograding pattern, took place in the Camarillas area (Fig. 2.2.1). This high energy deposit onlaps the composite sequence boundary (SB+TS) between depositional sequences A and B, and is interpreted as a transgressive lag (Fig. 2.2.13). Moreover, this transgressive calcarenite, which can be found despite discontinuities around a kilometric area and is up to 15-m-thick, could be interpreted as a relict of a transgressive migrating barrier island or strand plain.

Seawards, at Las Mingachas (Fig. 2.2.1), the transgressive phase started with backstepping of the lowstand platform (Figs. 2.2.6, 2.2.10 and 2.2.18). These platform deposits, also stacked in a retrograding pattern, onlap the composite sequence boundary (SB+TS) landwards (Figs. 2.2.6, 2.2.8, 2.2.9 and 2.2.19), and change laterally to marly deposits in a basinwards direction (Figs. 2.2.6, 2.2.10, 2.2.14 and 2.2.18).

The backstepping platform facies are essentially characterized by floatstones of rudists and corals in growth position (Fig. 2.2.12f) (Facies Association II), as observed for the previous highstand and lowstand platforms. The lithofacies succession that comprises the slope setting of this retrograding platform is basically made up of type A parasequences (Fig. 2.2.5). Furthermore, hardgrounds with ferruginous stains, borings and encrusting oysters and corals, are not uncommon in these distal environments of the transgressive platform.

During this period, the carbonate accumulation rate was outpaced by the rate of relative sea-level rise with the result that the retrograding carbonate shelf was finally drowned, evolving into marly sediment upwards in the succession (Figs. 2.2.6, 2.2.10, 2.2.14 and 2.2.18). Interbedded highly bioturbated nodular limestones, storm-induced deposits and calcareous nodules containing bivalves, echinoderms and gastropods, also constitute these marly sediments of the upper part of the TST.

The top of the TST is marked by the maximum flooding surface (mfs) of Depositional Sequence B (Figs. 2.2.6, 2.2.10, 2.2.14 and 2.2.18). This surface was placed on top of the thickest marl unit that occurs in the transgressive phase, given the absence of sedimentary or biotic features that could reflect the maximum bathymetry reached during this depositional sequence.

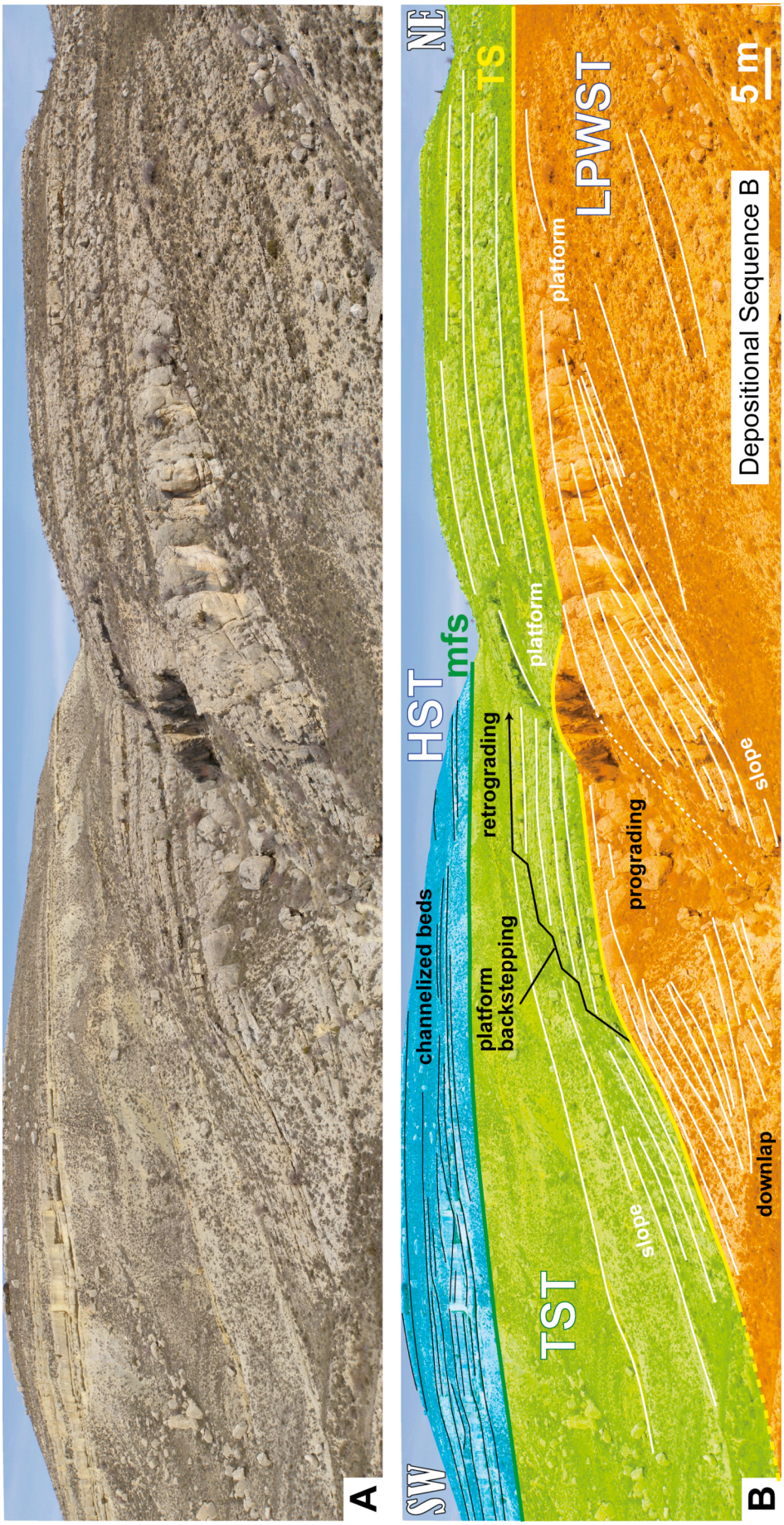

Figure 2.2.18. View of the western part of Las Mingachas (A) (see Fig. 2.2.7 for location) showing the platform backstepping geometries and the sequence stratigraphic interpretation (B). See figure 2.2.6 for legend.

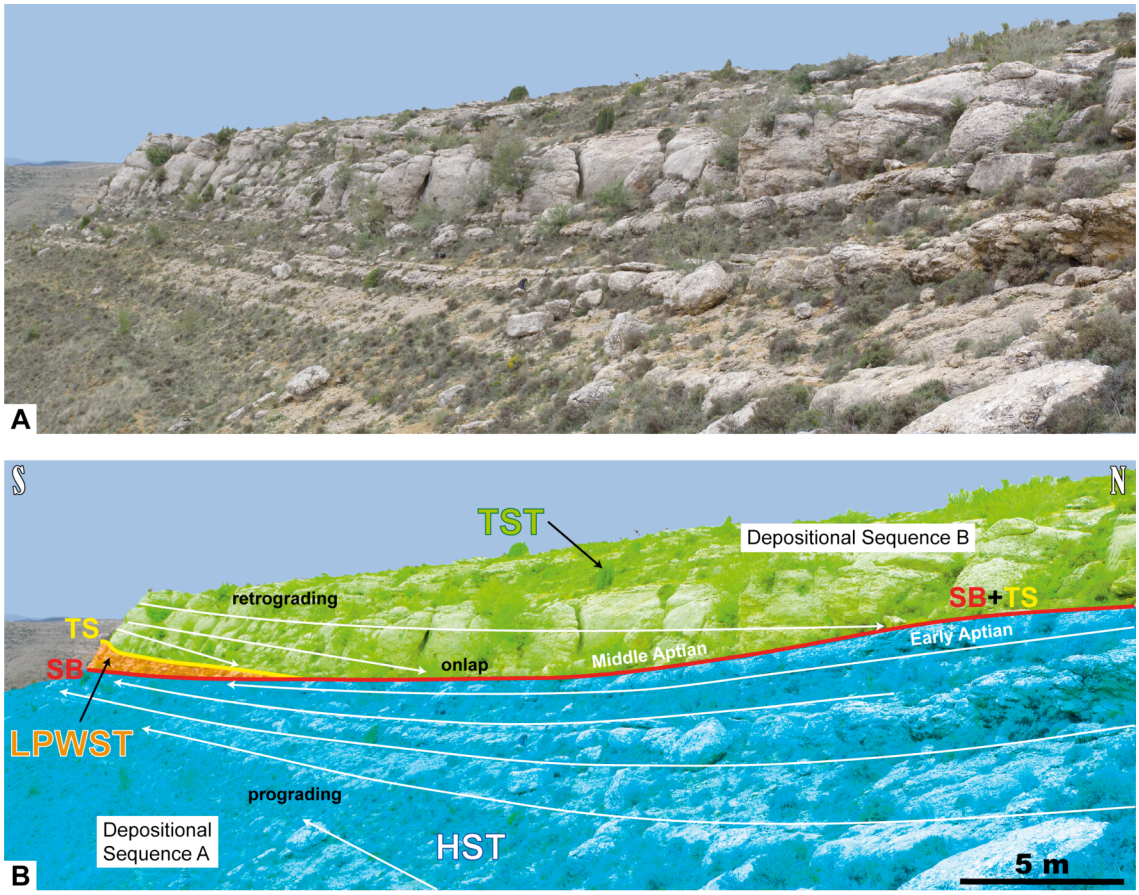

Figure 2.2.19. Outcrop photograph of the northeastern part of Las Mingachas area (A) (see Fig. 2.2.7 for location) displaying the transgressive platform onlapping the composite (SB+TS) sequence boundary and the sequence stratigraphic interpretation (B). See figure 2.2.6 for legend.

2.2.6.5 Highstand System Tract (Depositional Sequence B)

Above the mfs, the relative sea-level rise progressively slowed to a near sea-level highstand, favouring the development of a new carbonate platform of corals, large rudists and nerineid gastropods (facies associations II and III). At Las Mingachas (Fig. 2.2.1), the basal highstand marly deposits situated above the mfs rapidly evolve into slope lithofacies represented by the facies associations VII and X (Figs. 2.2.6, 2.2.10, 2.2.14 and 2.2.18), indicating the presence of carbonate shelves landwards. These slope facies, which consist of marly sediments with domal, irregular-massive and branching corals, interbedded with debris-flow deposits, display a sedimentary succession essentially composed of type A parasequences (Fig. 2.2.5). The resedimented shelf materials of Facies Association X show irregular and erosive bases, and mainly occur in the form of channels (Fig. 2.2.18).

2.2.7 Discussion

The spatial variation of facies and the sequential analysis carried out in the central part of the Galve sub-basin permitted to recognize sequence stratigraphic units of two distinct orders. These units seem to respond to two superposed orders of relative sea-level change, which significantly influenced the carbonate environments that dominated this area during the late Early-Middle Aptian.

Despite the widely held belief that the origin of sea-level fluctuations results from a combination of tectonic and eustatic processes (Vail et al. 1991), high-frequency, short-term relative sea-level variations are commonly interpreted as being essentially controlled by eustasy (Mitchum et al. 1991). These high-frequency sea-level fluctuations, which in the carbonate platform succession analyzed gave rise to deepening-shallowing small-scale cycles (parasequences), are usually interpreted as reflecting global climatic changes linked to orbital forcing within the range of Milankovitch (e.g., Vail et al. 1991; Mitchum et al. 1991; Strasser et al. 1999; Bádenas et al. 2004). Nevertheless, some authors have revealed that, during relative sea-level rise, autocyclic processes such as changes in the sedimentation and/or subsidence rates could also account for these repetitive small-scale sedimentary cycles (Kindler 1992; Drummond and Wilkinson 1993). On the other hand, the lower-frequency relative sea-level trends recognized in the area studied, which were interpreted as component systems tracts, can also be attributed, as in the case of the higher-frequency cyclicity, to variations of sea water masses related to allocyclic processes such as changes in climate (Vail et al. 1991). However, in low-frequency, long-term relative sea-level fluctuations, local and regional tectonic activity can also play a decisive role in the accommodation space available, and hence, in the stacking patterns recorded.

In the study area, the systems tracts recognized in the late Early-Middle Aptian time interval occurred during an important subsidence deceleration (Bover-Arnal et al. under review). Therefore, no signs of vertical movements were identified in the area analyzed for this time interval. Hence, the global eustatic component might have played a more significant role in controlling the HST and FRWST of Depositional Sequence A, and Depositional Sequence B (see Bover-Arnal et al. under review). In this regard, and despite minor diachronism, the major sea-level fall recorded in the central Galve sub-basin for this period, which caused a forced regression of sea-level in the uppermost late Early Aptian, close to the boundary between the Early and the Middle Aptian, could have had a widespread occurrence along the margin of the Tethys Sea (Sahagian et al.

1996; Hardenbol et al. 1998; Hillgärtner et al. 2003; Gréselle and Pittet 2005; Husinec and Jelaska 2006; Yose et al. 2006; Rameil et al. under review).

The platform margin situated at Las Mingachas (Fig. 2.2.1) is the only place in the area studied where the magnitude of this fall in sea-level can be roughly measured. Although the uppermost strata of the late HST of Depositional Sequence A was subaerially exposed and, hence eroded, the height of the top of the preserved highstand deposits with respect to the top of FRWST could be indicative of the order of this sea-level drop. However, the lithofacies of these systems tracts display distinct fossil assemblages, fabrics and sedimentary features, and were probably sedimented in different bathymetries. Therefore, a margin of error of up to several meters should be taken into account. In line with this approximation, the uppermost Early Aptian relative sea-level fall is estimated to be at least 60 meters.

The reasons for this global fall in relative sea-level are unknown. Nevertheless, in the central Galve sub-basin, this relative sea-level fall occurred within the *Dufrenoyia furcata* ammonite biozone (Fig. 2.2.2; see also Bover-Arnal et al. under review), which according to Ogg and Ogg (2006) spans 1 My. Assuming this time span for this biozone, and a probable error of hundreds of ky or even a few My, the uppermost Early Aptian relative sea-level fall in the western Maestrat Basin could have had a duration of rather less than 1 My, or at most around 1 My. Thus, one single mechanism or a combination of mechanisms triggering a sea-level fall of at least 60 m at this time would have been necessary to account for this forced regression of relative sea-level.

Immenhauser (2005) and Miller et al. (2005) concluded that probably the most plausible known mechanism that could trigger a global sea-level fall of tens-of-meters per My or less is glacio-eustasy. However, there is contradictory evidence about the feasibility of waxing and waning of ice sheets as the main mechanism governing long-term relative sea-level fluctuations during the Mesozoic (Price 1999; Immenhauser 2005; Miller et al. 2005). For this reason, the possibility that this global sea-level fall could have been controlled by a combination of several processes acting at the same time or by mechanisms that could have existed in the past, but have no actual analogues, should not be discarded (Immenhauser 2005; Miller et al. 2005).

In line with Immenhauser (2005) and Miller et al. (2005), Gréselle and Pittet (2005) in a study of a coetaneous carbonate system from Oman suggested glacio-eustasy as the most likely mechanism that could best explain this widespread forced regression of relative sea-level and other late Aptian, and Albian major sea-level

changes. Peropadre et al. (2008) in a different interpretation of the same outcrops studied here, and following Gréselle and Pittet (2005) and Steuber et al. (2005), already proposed changes in continental ice volumes as a possible explanation for the Aptian sea-level variations that they observed. Thus, given this hypothesis, this sea-level fall that occurred close to the boundary between the Early and Middle Aptian might have been linked to the late Early Aptian cooling episode proposed by Hochuli et al. (1999) and Steuber et al. (2005), which might have increased ice volumes on continents triggering the aforementioned rapid and widespread lowering sea-level.

During this major fall in sea-level, the highstand carbonate system that is basically dominated by rudists and corals of Depositional Sequence A was not able to shift downslope in response to the sea-level fall. Hence, the carbonate factories were essentially shut down throughout the FRWST. Later, with the stillstand and the subsequent rise in relative sea-level, carbonate production was able to recover in the basinal setting, at the toe of the former slope, where a small lowstand prograding platform of rudists and corals developed, downlapping onto the forced regressive deposits. This differs somewhat from the observations carried out, for the same time interval, in the carbonate systems of Oman (Hillgärtner et al. 2003) and the United Arab Emirates (Yose et al. 2006), where it seems that the carbonate producers displayed enough growth potential to shift downslope during this fall in relative sea-level. This differential response suggests that the sea-level fall was probably too rapid and linear to permit the carbonate-producing organisms to move basinwards in the central part of the Galve sub-basin. On the other hand, in Oman, the widespread sea-level fall could have had a stepped nature or been slower, allowing the carbonate system to shift downslope. Other reasons could be that, at Las Mingachas (Fig. 2.2.1) the highstand slope of Depositional Sequence A was too steep and so narrow to permit the establishment of a carbonate factory, or that the space available downslope was not sufficient to accommodate carbonate production. It is also possible that a change in the environmental conditions linked to this relative fall in sea-level could account for the closing down of the carbonate factory.

The carbonate platforms developed during the HST of Depositional Sequence A and the LPWST of Depositional Sequence B display platform-margin clinoforms. These geometries provide new insights into the nature of these Aptian carbonate systems from the Maestrat Basin. The platform-to-basin cross-sections observed show progradational clinoforms that draw a flat-topped non-rimmed depositional profile. The absence of a

rim in these carbonate platforms does not seem to have been offset by palaeohigh structures or reworked skeletal sand-banks, which could have acted as a protective barrier to these shelves at this time (see also Bover-Arnal et al. under review). The fact that the platform sediments are mainly made up of floatstones containing entire rudist specimens occurring locally grouped into bouquets, and small and large coral colonies, commonly displaying delicate branching growth types, suggests a sedimentary environment with low hydrodynamic conditions (Facies Association II). The construction of these carbonate shelves below wave-influence could account for the large amount of lime mud preserved in the facies and for the occurrence of these organisms in life position, along with their excellent preservation. Nevertheless, wave activity could have occasionally reached the shelf carbonate production zone, causing reworking and basinwards transport of sediment during times of lowered sea-level linked to episodic storm events or to high-frequency, low-amplitude short-term sea-level rhythms.

The resulting sequence-stratigraphic framework obtained from the outcrops studied (Fig. 2.2.1) reflects a carbonate depositional system conditioned by a fall and subsequent rise in relative sea-level. The sedimentary features, the types of bounding surfaces and the succession of the different stratal stacking patterns recognized, show a depositional model that is consistent with the four systems tract sequence stratigraphic scheme of Hunt and Tucker (1992, 1993b).

The key to a successful sequence stratigraphic analysis primarily depends on the identification and correlation of the stratigraphic surfaces that bound the different systems tracts. The subaerial unconformity, the correlative conformity, the transgressive surface, the maximum flooding surface and the basal surface of forced regression constitute the basis of the chronological framework, which is the essence of sequence stratigraphy. These surfaces were recognized and are widely mappable across the platform-to-basin profile that crops out at Las Mingachas (Fig. 2.2.6). However, owing to the oblique cross-section displayed by the outcrop, the BSFR and the marine correlative conformity of the SB cannot be characterized in downdip slope settings. The BSFR is only identified in basinal environments and the SB can only be delineated in shelf, shelf-margin, uppermost slope and basinal settings. Furthermore, at Las Mingachas, the BSFR was placed at the conformable sharp surface that constitutes the base of the first forced regressive calcarenitic episode. This surface, which marks the onset of forced regression (Hunt and Tucker 1992, 1993b, 1995), separates these

reworked allochthonous debris of the FRWST from the underlying marls, which are interpreted as basinal highstand deposits.

Even so, the first arrival of allochthonous debris in the basin should not necessarily mark the start of base-level fall at the shoreline, but these detached forced regressive calcarenitic deposits could represent sediments deposited once the carbonate factory was shut down after the start of base-level fall (Catuneanu 2006). Thus, the BSFR could be somewhere in the underlying marls. In this regard, Hunt and Tucker (1995) recognized the difficulty of identifying this surface because of the lack of characteristic features due to its conformable nature (see also Plint and Nummedal 2000; Catuneanu 2006). In line with the foregoing, the surface that constitutes the base of the first calcarenitic wedge developed during forced regression of the shoreline could correspond to a slope onlap surface (Embry 1995). Even so, there is no conclusive evidence that demonstrates that the surface delineated as the BSFR (Fig. 2.2.6) does not indicate the onset of relative sea-level fall. Moreover, the description of this surface by Hunt and Tucker (1995) in such a manner that it constitutes a sharp surface at the base of basinal redeposited sediments is consistent with the observations made in the field (Fig. 2.2.11). Hence, in agreement with Hunt and Tucker (1992, 1993b, 1995), the BSFR was placed at the boundary between the first detached forced regressive calcarenitic deposit and the underlying marls.

The position of the SB within the marine setting, which corresponds to the marine correlative conformity of the subaerial unconformity, has also been a subject of debate (see Kolla et al. 1995; Hunt and Tucker 1995). Hunt and Tucker (1992) placed this boundary above the basin floor component, which comprises all the deposits sedimented at the toe of the slope during falling relative sea-level. Thus, according to Hunt and Tucker (1992) this surface marks the end of base-level fall. On the other hand, Posamentier et al. (1992) placed the SB below these allochthonous debris deposited in the basinal position during forced regression of the shoreline. In this case, the marine correlative conformity marks the start of base-level fall, and would be equivalent to the BSFR of Hunt and Tucker (1992).

In this study the marine correlative conformity part of the SB was placed above the detached forced regressive unit, deposited at the toe of the slope during base-level fall following Hunt and Tucker (1992, 1995), Helland-Hansen and Gjelberg (1994), and Plint and Nummedal (2000). Therefore, the sequence boundary marks the lowest point

of relative sea-level over the platform-to-basin cross-section studied and hence the most basinwards extension of the subaerial unconformity.

2.2.8 Conclusions

In this case study, the late Early-Middle Aptian carbonate system from the western Maestrat Basin in the Iberian Chain constitutes a good example of how various orders of relative sea-level change control facies and architecture of carbonate platforms. The carbonate succession analyzed was controlled by two orders of relative sea-level change, which therefore stacked these platform carbonates in sequence stratigraphic units of two orders. Four types of parasequence were developed in relation to higher-frequency sea-level rhythms whereas the lower-frequency cyclicity reflects five differentiated systems tracts within two depositional sequences: the Highstand Systems Tract (HST) and Forced Regressive Wedge Systems Tract (FRWST) of Depositional Sequence A; and the Lowstand Prograding Wedge Systems Tract (LPWST), Transgressive Systems Tract (TST) and Highstand Systems Tract (HST) of Depositional Sequence B. It was possible to characterize these systems tracts on account of the identification of their key bounding surfaces, which are broadly identifiable and correlatable throughout the platform-to-basin transition area studied. The key surfaces with a sequence stratigraphic significance recognized are: a basal surface of forced regression, a subaerial unconformity, a marine correlative conformity, a transgressive surface and a maximum flooding surface. The sedimentary relationships of the different systems tracts within the lower-frequency relative sea-level cycle are in strong agreement with the dynamics of sedimentation during forced regression and lowstand of relative sea-level of Hunt and Tucker (1992, 1993b).

The major sea-level fall recorded during the uppermost Early Aptian in the central Galve sub-basin (western Maestrat Basin), which subaerially exposed the carbonate platform formed during the first HST and resulted in the deposition of the FRWST, is interpreted as one of global significance. This relative sea-level drop, which was of an order of tens-of-meters, and the subsequent base-level rise occurred within the *Dufrenoyia furcata* biozone. Hence, in order to explain this relative sea-level fall, a mechanism or various mechanisms that could trigger a sea-level drop of tens-of-meters in less than 1 My should be considered. Despite the existence of contradictory evidence, glacio-eustasy could be a plausible mechanism to account for this rapid and widespread forced regression of relative sea-level. In line with this hypothesis, these results are in

need of a cooling event during the late Early Aptian, and thus could corroborate the cooling episode proposed in the literature for this time slice (Hochuli et al. 1999; Steuber et al. 2005).

The late Early-Middle Aptian carbonate platforms studied display a flat-topped non-rimmed depositional profile. Palaeohigh structures or shoals, which could have acted as a protective barrier to these shelves at this time, were not observed in the platform-to-basin profile analyzed. Thus, the lithofacies association composed of platform floatstones with well-preserved rudist bivalves and corals in life position does not seem to have been formed in a lagoonal environment but may be interpreted as having been essentially built up below wave-influence. This could be of significance for other Aptian platform carbonate successions lacking platform-to-basin geometries, rimmed margins or clear protecting barriers such as reworked skeletal sand-banks or palaeohigh structures. In these cases, care should be taken to ascribe systematically the characteristic floatstone limestones dominated by rudists and corals in growth position in a lagoonal setting. This late Early-Middle Aptian case study shows that this lithofacies may also develop below wave-influence.

Lastly, the most significant implications of this paper lie in the sequence stratigraphy analysis. The resulting analysis demonstrates that the classic four systems tracts and their key bounding surfaces, even those with a conformable nature such as the basal surface of forced regression and the marine correlative conformity, can be successfully characterized not only at seismic-scale but in outcrops as well. In this regard, the late Early-Middle Aptian platform carbonates cropping out in the central Galve sub-basin might serve as a valuable example of how the theoretical model of Hunt and Tucker (1992) could be applied in outcrop-scale carbonate successions. Hence, in the light of our findings it may be concluded that the outcrops studied here would seem to display a classic example of real rocks fitting theoretical models.

2.2.9 Acknowledgements

The authors would like to express their most sincere appreciation to Maurice E. Tucker who kindly reviewed an early version of this manuscript and provided thoughtful and valuable comments during the peer-review process. We are greatly indebted to Adrian Immenhauser, whose accurate and constructive review resulted in a significant improvement of this paper. We are also especially indebted to Octavian Catuneanu who extensively helped with his useful advice. Special thanks are due to

Peter W. Skelton and Eulàlia Gili for determining the rudist species. Grateful thanks are extended to Rolf Schroeder who determined the orbitolinid species and to David García-Sellés for field assistance with the Laser Scanner. We wish to thank Luis Pomar for fruitful discussions in the field. Funding was provided by the project Bi 1074/1-2 of the Deutsche Forschungsgemeinschaft, the I+D+i research projects: CGL2005-07445-CO3-01 and CGL2008-04916, the Consolider-Ingenio 2010 programme, under CSD 2006-0004 "Topo-Iberia", the Grup Consolidat de Recerca "Geologia Sedimentària" (2005SGR-00890), and the Departament d'Universitats, Recerca i Societat de la Informació de la Generalitat de Catalunya i del Fons Social Europeu.

2.2.10 References

Aurell, M. and Bádenas, B. (2004). Facies and depositional sequence evolution controlled by high-frequency sea-level changes in a shallow-water carbonate ramp (late Kimmeridgian, NE Spain). Geological Magazine, 141, 717-733.

Bádenas, B., Salas, R. and Aurell, M. (2004). Three orders of regional sea-level changes control facies and stacking patterns of shallow platform carbonates in the Maestrat Basin (Tithonian-Berriasian, NE Spain). International Journal of Earth Sciences, 93, 144-162.

Bauer, J., Kuss, J. and Steuber, T. (2003). Sequence architecture and carbonate platform configuration (Late Cenomanian-Santonian), Sinai, Egypt. Sedimentology, 50, 387-414.

Bernaus, J.M., Arnaud-Vanneau, A. and Caus, E. (2003). Carbonate platform sequence stratigraphy in a rapidly subsiding area: the Late Barremian-Early Aptian of the Organyà basin, Spanish Pyrenees. Sedimentary Geology, 159, 177-201.

Booler, J. and Tucker, M.E. (2002). Distribution and geometry of facies and early diagenesis: the key to accommodation space variation and sequence stratigraphy: Upper Cretaceous Congost Carbonate platform, Spanish Pyrenees. Sedimentary Geology, 146, 226-247.

Borgomano, J.R.F. (2000). The Upper Cretaceous carbonates of the Gargano-Murge region, southern Italy: A model of platform-to-basin transition. The American Association of Petroleum Geologists Bulletin, 84, 1561-1588.

Bover-Arnal, T., Moreno-Bedmar, J.A., Salas, R. and Bitzer, K. (2008a). Facies architecture of the late Early-Middle Aptian carbonate platform in the western Maestrat basin (Eastern Iberian Chain). Geo-Temas, 10, 115-118.

Bover-Arnal, T., Salas, R., Moreno-Bedmar, J.A., Bitzer, K., Skelton, P.W. and Gili, E. (2008b). Two orders of sea-level changes controlled facies and architecture of late Early Aptian carbonate platform systems in the Maestrat Basin (eastern Iberian Chain, Spain). In: Kunkel, C., Hahn, S., ten Veen, J., Rameil, N. and Immenhauser, A. (eds.). SDGG, Heft 58 – Abstract Volume – 26th IAS Regional Meeting/SEPM-CES SEDIMENT 2008 - Bochum, p. 60.

Bover-Arnal, T., Moreno-Bedmar, J.A., Salas, R., Skelton, P.W., Bitzer, K. and Gili, E. (under review). Sedimentary evolution of an Aptian syn-rift carbonate system (Maestrat Basin, E Spain): effects of accommodation and environmental change. Geologica Acta.

Burla, S., Heimhofer, U., Hochuli, P.A., Weissert, H. and Skelton, P. (2008). Changes in sedimentary patterns of coastal and deep-sea successions from the North Atlantic (Portugal) linked to Early Cretaceous environmental change. Palaeogeography, Palaeoclimatology, Palaeoecology, 257, 38-57.

Canérot, J., Cugny, P., Pardo, G., Salas, R. and Villena, J. (1982). Ibérica Central-Maestrazgo. In: García, A. (ed.). El Cretácico de España. Universidad Complutense de Madrid, 273-344.

Catuneanu, O. (2006). Principles of Sequence Stratigraphy. Elsevier, New York, pp. 386.

Catuneanu, O., Abreu, V., Bhattacharya, J.P., Blum, M.D., Dalrymple, R.W., Eriksson, P.G., Fielding, C.R., Fisher, W.L., Galloway, W.E., Gibling, M.R., Giles, K.A.,

Holbrook, J.M., Jordan, R., Kendall, C.G.St.C., Macurda, B., Martinsen, O.J., Miall, A.D., Neal, J.E., Nummedal, D., Pomar, L., Posamentier, H.W., Pratt, B.R., Sarg, J.F., Shanley, K.W., Steel, R.J., Strasser, A., Tucker, M.E. and Winker, C. (2009). Towards the standardization of sequence stratigraphy. Earth-Science Reviews, 92, 1-33.

Drummond, C.N. and Wilkinson, B.H. (1993). Carbonate cycle stacking patterns and hierarchies of orbitally forced eustatic sealevel change. Journal of Sedimentary Petrology, 63, 369-377.

Drzewiecki, P.A. and (Toni) Simo, J.A. (2000). Tectonic, eustatic and environmental controls on mid-Cretaceous carbonate platform deposition, south-central Pyrenees, Spain. Sedimentology, 47, 471-495.

Embry, A.F. and Klovan, J.E. (1971). A Late Devonian reef tract on northeastern Banks Island, N.W.T. Bulletin of Canadian Petroleum Geology, 19, 730-781.

Embry, A.F. (1995). Sequence boundaries and sequence hierarchies: problems and proposals. In: Steel, R.J., Felt, V.L., Johannesson, E.P. and Mathieu, C. (eds.). Sequence Stratigraphy on the Northwest European Margin. Norwegian Petroleum Society Special Publication 5, 1-11.

Föllmi, K.B., Weissert, H., Bisping, M. and Funk, H. (1994). Phosphogenesis, carbon-isotope stratigraphy, and carbonate-platform evolution along the Lower Cretaceous northern Tethyan margin. Geological Society of America Bulletin, 106, 729-746.

Föllmi, K.B., Godet, A., Bodin, S. and Linder, P. (2006). Interactions between environmental change and shallow water carbonate buildup along the northern Tethyan margin and their impact on the Early Cretaceous carbon isotope record. Paleoceanography, 21, PA4211, doi: 10.1029/2006PA001313.

Funk, H., Föllmi, K.B. and Mohr, H. (1993). Evolution of the Tithonian-Aptian Carbonate Platform Along the Northern Tethyan Margin, Eastern Helvetic Alps.

In: Toni Simo, J.A., Scott, R.W. and Masse, J.P. (eds.). Cretaceous Carbonate Platforms. The American Association of Petroleum Geologists, Memoir 56, 387-407.

Gautier, F. (1980). Villarluengo, hoja nº 543. Mapa Geológico de España 1:50.000. 2ª Serie. 1ª Edición, Servicio de Publicaciones, Ministerio de Industria y Energía, Madrid.

Gil, J., García-Hidalgo, J.F., Segura, M., García, A. and Carenas, B. (2006). Stratigraphic architecture, palaeogeography and sea-level changes of a third order depositional sequence: The late Turonian–early Coniacian in the northern Iberian Ranges and Central System (Spain). Sedimentary Geology, 191, 191-225.

Gréselle, B. and Pittet, B. (2005). Fringing carbonate platforms at the Arabian Plate margin in northern Oman during the Late Aptian-Middle Albian: Evidence for high-amplitude sea-level changes. Sedimentary Geology, 175, 367-390.

Grötsch, J. (1996). Cycle stacking and long-term sea-level history in the Lower Cretaceous (Gavrovo platform, NW Greece). Journal of Sedimentary Research, 66, 723-736.

Hallock, P. and Schlager, W. (1986). Nutrient Excess and the Demise of Coral Reefs and Carbonate Platforms. Palaios, 1, 389-398.

Hardenbol, J., Thierry, J., Farley, M.B., Jacquin, T., de Graciansky, P.C. and Vail, P.R. (1998). Mesozoic and Cenozoic Sequence Chronostratigraphic Framework of European Basins. In: de Graciansky, P.C., Hardenbol, J., Jacquin, T. and Vail, P.R. (eds.). Mesozoic and Cenozoic Sequence Stratigraphy of European Basins, SEPM Special Publications 60, charts 1-8.

Helland-Hansen, W. and Gjelberg, J.G. (1994). Conceptual basis and variability in sequence stratigraphy: a different perspective. Sedimentary Geology, 92, 31-52.

Hillgärtner, H., Van Buchem, F.S.P., Gaumet, F., Razin, P., Pittet, B., Grötsch, J. and Droste, H. (2003). The Barremian-Aptian evolution of the eastern Arabian carbonate platform margin (northern Oman). Journal of Sedimentary Research, 73, 756-773.

Hochuli, P.A., Menegatti, A.P., Weissert, H., Riva, A., Erba, E. and Premoli Silva, I. (1999). Episodes of high productivity and cooling in the early Aptian Alpine Tethys. Geology, 27, 657-660.

Hunt, D. and Tucker, M.E. (1992). Stranded parasequences and the forced regressive wedge systems tract: deposition during base-level fall. Sedimentary Geology 81, 1-9.

Hunt, D. and Tucker, M.E. (1993a). The Middle Cretaceous Urgonian Platform of Southeastern France. In: Toni Simo, J.A., Scott, R.W. and Masse, J.P. (eds.). Cretaceous Carbonate Platforms. The American Association of Petroleum Geologists, Memoir 56, 409-453.

Hunt, D. and Tucker, M.E. (1993b). Sequence stratigraphy of carbonate shelves with an example from the mid-Cretaceous (Urgonian) of southeast France. In: Posamentier, H.W., Summerhayes, C.P., Haq, B.U. and Allen, G.P. (eds.). Sequence Stratigraphy and Facies Associations. International Association of Sedimentologists, Special Publications 18, 307-341.

Hunt, D. and Tucker, M.E. (1995). Stranded parasequences and the forced regressive wedge systems tract: deposition during base-level fall—reply. Sedimentary Geology, 95, 147-160.

Husinec, A. and Jelaska, V. (2006). Relative sea-level changes recorded on an isolated carbonate platform: Tithonian to Cenomanian succession, Southern Croatia. Journal of Sedimentary Research, 76, 1120-1136.

Immenhauser, A. (2005). High-rate sea-level change during the Mesozoic: New approaches to an old problem. Sedimentary Geology, 175, 277-296.

Kendall, C.G.St.C. and Schlager, W. (1981). Carbonates and relative changes in sea level. Marine Geology, 44, 181-212.

Kerans, C. (2002). Styles of Rudist Buildup Development along the Northern Margin of the Maverick Basin, Pecos River Canyon, Southwest Texas. Gulf Coast Association of Geological Societies Transactions, 52, 501-516.

Kindler, P. (1992). Coastal response to the Holocene transgression in the Bahamas: episodic sedimentation versus continuous sea-level rise. Sedimentary Geology, 80, 319-329.

Kolla, V., Posamentier, H.W. and Eichenseer, H. (1995). Stranded parasequences and the forced regressive wedge systems tract: deposition during base-level fall—discussion. Sedimentary Geology, 95, 139-145.

Lehmann, C., Osleger, D.A. and Montañez, I.P. (1998). Controls on cyclostratigraphy of Lower Cretaceous carbonates and evaporites, Cupido and Coahuila platforms, northeastern Mexico. Journal of Sedimentary Research, 68, 1109-1130.

Malchus, N., Pons, J.M. and Salas, R. (1996). Rudist distribution in the lower Aptian shallow platform of la Mola de Xert, Eastern Iberian Range, NE Spain. Revista Mexicana de Ciencias Geológicas, 12, 224-235.

Masse, J.P. (1993). Valanginian-Early Aptian carbonate platforms from Provence, Southeastern France. In: Toni Simo, J.A., Scott, R.W. and Masse, J.P. (eds.). Cretaceous Carbonate Platforms. The American Association of Petroleum Geologists, Memoir 56, 363-374.

Masse, J.P., Borgomano, J. and Al Maskiry, S. (1998). A platform-to-basin transition for lower Aptian carbonates (Shuaiba Formation) of the northeastern Jebel Akhdar (Sultanate of Oman). Sedimentary Geology, 119, 297-309.

Millán, M.I., Fernández-Mendiola, P.A. and García-Mondéjar, J. (2007). Pulsos de inundación marina en la terminación de una plataforma carbonatada (Aptiense inferior de Aralar, Cuenca Vasco-Cantábrica). Geogaceta, 41, 127-130.

Miller, K.G., Wright, J.D. and Browning, J.V. (2005). Visions of ice sheets in a greenhouse world. Marine Geology, 217, 215-231.

Mitchum, Jr, R.M. and Van Wagoner, J.C. (1991). High-frequency sequences and their stacking patterns: sequence-stratigraphic evidence of high-frequency eustatic cycles. Sedimentary Geology, 70, 131-160.

Moreno, J.A. and Bover, T. (2007). Precisiones sobre la edad, mediante ammonoideos, de la Fm. Margas del Forcall, Aptiense inferior, en la subcuenca de Galve (Teruel, Espanya). In: Braga, J.C., Checa, A. and Company, M. (eds.). XXIII Jornadas de la Sociedad Española de Paleontología (Caravaca de la Cruz, 3-6 de Octubre de 2007), Libro de resúmenes. Instituto Geológico y Minero de España y Universidad de Granada, Granada, 151-152.

Mutti, M. and Hallock, P. (2003). Carbonate systems along nutrient and temperature gradients: some sedimentological and geochemical constraints. International Journal of Earth Sciences, 92, 465-475.

Ogg, J.G. and Ogg, G. (2006). Updated by James G. Ogg (Purdue University) and Gabi Ogg to: GEOLOGIC TIME SCALE 2004 (Gradstein, F.M., Ogg, J.G., Smith, A.G. et al.; Cambridge University Press).

Peropadre, C., Meléndez, N. and Liesa, C.L. (2008). Variaciones del nivel del mar registradas como valles incisos en la Formación Villarroya de los Pinares en la subcuenca de Galve (Teruel, Cordillera Ibérica). Geo-Temas, 10, 167-170.

Pittet, B., Strasser, A. and Mattioli, E. (2000). Depositional sequences in deep-shelf environments: a response to sea-level changes and shallow-platform carbonate productivity (Oxfordian, Germany and Spain). Journal of Sedimentary Research, 70, 392-407.

Pittet, B., Van Buchem, F.S.P., Hillgärtner, H., Razin, P., Grötsch, J. and Droste, H. (2002). Ecological succession, palaeoenvironmental change, and depositional sequences of Barremian-Aptian shallow-water carbonates in northern Oman. Sedimentology, 49, 555-581.

Plint, A.G. and Nummedal, D. (2000). The falling stage systems tract: recognition and importance in sequence stratigraphic analysis. Geological Society, London, Special Publications, 172, 1-17.

Pomar, L. (2001). Types of carbonate platforms: a genetic approach. Basin Research, 13, 313-334.

Pomar, L., Gili, E., Obrador, A. and Ward, W.C. (2005). Facies architecture and high-resolution sequence stratigraphy of an Upper Cretaceous platform margin succession, southern central Pyrenees, Spain. Sedimentary Geology, 175, 339-365.

Pomar, L. and Kendall, C.G.St.C. (2007). Architecture of carbonate platforms: A response to hydrodynamics and evolving ecology. In: Lukasik, J. and Simo, A. (eds.). Controls on Carbonate Platform and Reef Development. SEPM Special Publication 89, 187-216.

Posamentier, H.W., Allen, G.P., James, D.P. and Tesson, M. (1992). Forced Regressions in a Sequence Stratigraphic Framework: Concepts, Examples, and Exploration Significance. The American Association of Petroleum Geologists Bulletin, 76, 1687-1709.

Price, G.D. (1999). The evidence and implications of polar ice during the Mesozoic. Earth-Science Reviews, 48, 183-210.

Rameil, N. (2005). Carbonate sedimentology, sequence stratigraphy, and cyclostratigraphy of the Tithonian in the Swiss and French Jura Mountains. A

high-resolution record of changes in sea level and climate. Ph.D. Thesis, Université de Fribourg, Suisse, GeoFocus, 13, pp. 246.

Rameil, N., Immenhauser, A., Csoma, A.É. and Warrlich, G. (under review). Surfaces with a long history: The Aptian top Shu'aiba Formation unconformity, Sultanate of Oman. Sedimentology.

Rosales, I. (1999). Controls on carbonate-platform evolution on active fault blocks: the Lower Cretaceous Castro Urdiales platform (Aptian-Albian, northern Spain). Journal of Sedimentary Research, 69, 447-465.

Sahagian, D., Pinous, O., Olferiev, A. and Zakharov, V. (1996). Eustatic Curve for the Middle Jurassic-Cretaceous Based on Russian Platform and Siberian Stratigraphy: Zonal Resolution. The American Association of Petroleum Geologists Bulletin, 80, 1433-1458.

Salas, R. and Casas, A. (1993). Mesozoic extensional tectonics, stratigraphy, and crustal evolution during the Alpine cycle of the eastern Iberian basin. Tectonophysics, 228, 33-55.

Salas, R. and Guimerà, J. (1996). Rasgos estructurales principales de la cuenca cretácica inferior del Maestrazgo (Cordillera Ibérica oriental). Geogaceta, 20, 1704-1706.

Salas, R., Guimerà, J., Mas, R., Martín-Closas, C., Meléndez, A. and Alonso, A. (2001). Evolution of the Mesozoic Central Iberian Rift System and its Cainozoic inversion (Iberian Chain). In: Ziegler, P.A., Cavazza, W., Roberston, A.H.F. and Crasquin-Soleau, S. (eds.). Peri-Tethys Memoir 6: Peri-Tethyan Rift/Wrench Basins and Passive Margins. Mémoires du Muséum National d'Histoire Naturelle 186, Paris, 145-186.

Salas, R., Martín-Closas, C., Delclòs, X., Guimerà, J., Caja, M.A. and Mas, R. (2005). Factores principales de control de la sedimentación y los cambios bióticos durante el tránsito Jurásico-Cretácico en la Cadena Ibérica. Geogaceta, 38, 15-18.

Sarg, J.F. (1988). Carbonate sequence stratigraphy. In: Wilgus, C.K., Hastings, B.S., Kendall, C.G.St.C., Posamentier, H.W., Ross, C.A. and Van Wagoner, J.C. (eds.). Sea level changes: an integrated approach. SEPM, Special Publication 42, 155-181.

Skelton, P.W. and Masse. J.-P. (2000). Synoptic guide to the Lower Cretaceous rudist bivalves of Arabia. In: Alsharhan, A.S. and Scott, R.W. (eds.). Middle East Models of Jurassic/Cretaceous Carbonate Systems. SEPM, Special Publication 69, 89-99.

Skelton, P.W. (2003a). The Cretaceous World. Cambridge University Press, Cambridge, pp. 360.

Skelton, P.W. (2003b). Rudist evolution and extinction - a north African perspective. In: Gili, E., Negra, M. and Skelton, P.W. (eds.). North African Cretaceous Carbonate Platform Systems. NATO Science Series IV, Earth and Environmental Sciences 28, Kluwer Academic Publishers, 215-227.

Skelton, P.W., Gili, E., Bover-Arnal, T., Salas, R., Moreno-Bedmar, J.A., Millán, I. and Fernández-Mendiola, K. (2008a). Taxonomic turnover and palaeoecological change among Aptian rudists: and Iberian case study. In: Kunkel, C., Hahn, S., ten Veen, J., Rameil, N. and Immenhauser, A. (eds.). SDGG, Heft 58 – Abstract Volume – 26th IAS Regional Meeting/SEPM-CES SEDIMENT 2008 - Bochum, p. 254.

Skelton, P.W., Gili, E., Bover-Arnal, T., Salas, R. and Moreno-Bedmar, J.A. (2008b). A new species of *Polyconites* from the uppermost Lower Aptian of Spain. Eighth International Congress on Rudists. Izmir, Turkey, Abstracts, p. 53.

Skelton, P.W., Gili, E., Bover-Arnal, T., Salas, R. and Moreno-Bedmar, J.A. (in press). A new species of Polyconites from the Lower Aptian of Iberia and the early evolution of polyconitid rudists. Turkish Journal of Earth Sciences.

Spence, G.H. and Tucker, M.E. (2007). A proposed integrated multi-signature model for peritidal cycles in carbonates. Journal of Sedimentary Research, 77, 797-808.

Steuber, T., Rauch, M., Masse, J.-P., Graaf, J. and Malkoc, M. (2005). Low-latitude seasonality of Cretaceous temperatures in warm and cold episodes. Nature, 437, 1341-1344.

Strasser, A., Pittet, B., Hillgärtner, H. and Pasquier, J.-B. (1999). Depositional sequences in shallow carbonate-dominated sedimentary systems: concepts for a high-resolution analysis. Sedimentary Geology, 128, 201-221.

Thrana, C. and Talbot, M.R. (2006). High-frequency carbonate-siliciclastic cycles in the Miocene of the Lorca Basin (Western Mediterranean, SE Spain). Geologica Acta, 4, 343-354.

Tomás, S. (2007). El sistema arrecifal Aptiense inferior del sector suroriental de la cuenca del Maestrat (Cadena Ibérica). Ph.D. Thesis, Universitat de Barcelona, Barcelona, pp. 192.

Tomás, S., Comas Nebot, M. and Salas, R. (2007). La plataforma carbonatada Aptiense superior de Benicàssim-Orpesa (Cuenca del Maestrat, Cadena Ibérica): modelo de depósito. Geogaceta, 41, 235-238.

Tomás, S., Löser, H. and Salas, R. (2008). Low-light and nutrient-rich coral assemblages in an Upper Aptian carbonate platform of the southern Maestrat Basin (Iberian Chain, eastern Spain). Cretaceous Research, 29, 509-534.

Vail, P.R., Audemard, F., Bowman, S.A., Eisner, P.N. and Perez-Cruz, C. (1991). The Stratigraphic Signatures of Tectonics, Eustasy and Sedimentology – an Overview. In: Einsele, G., Ricken, W. and Seilacher, A. (eds.). Cycles and Events in Stratigraphy. Springer-Verlag Berlin Heidelberg 1991, 617-659.

Van Wagoner, J.C., Posamentier, H.W., Mitchum, R.M., Vail, P.R., Sarg, J.F., Loutit, T.S. and Hardenbol, J. (1988). An overview of the fundamentals of sequence

stratigraphy and key definitions. In: Wilgus, C.K., Hastings, B.S., Kendall, C.G.St.C., Posamentier, H.W., Ross, C.A. and Van Wagoner, J.C. (eds.). Sea-level changes: an integrated approach. SEPM, Special Publication 42, 39-45.

Vennin, E. and Aurell, M. (2001). Stratigraphie séquentielle de l'Aptien du sous-bassin de Galvé (Province de Teruel, NE de l'Espagne). Bulletin de la Société Géologique de France, 172, 397-410.

Vilas, L., Masse, J.-P. and Arias, C. (1993). Aptian Mixed Terrigenous and Carbonate Platforms from Iberic and Prebetic Regions, Spain. In: Toni Simo, J.A., Scott, R.W. and Masse, J.P. (eds.). Cretaceous Carbonate Platforms. The American Association of Petroleum Geologists, Memoir 56, 243-253.

Vilas, L., Masse, J.P. and Arias, C. (1995). *Orbitolina* episodes in carbonate platform evolution: the early Aptian model from SE Spain. Palaeogeography, Palaeoclimatology, Palaeoecology, 119, 35-45.

Weissert, H., Lini, A., Föllmi, K.B. and Kuhn, O. (1998). Correlation of Early Cretaceous carbon isotope stratigraphy and platform drowning events: a possible link? Palaeogeography, Palaeoclimatology, Palaeoecology, 137, 189-203.

Weissert, H. and Erba, E. (2004). Volcanism, CO_2 and palaeoclimate: a Late Jurassic-Early Cretaceous carbon and oxygen isotope record. Journal of the Geological Society (London), 161, 695-702.

Wissler, L., Funk, H. and Weissert, H. (2003). Response of Early Cretaceous carbonate platforms to changes in atmospheric carbon dioxide levels. Palaeogeography, Palaeoclimatology, Palaeoecology, 200, 187-205.

Yose, L.A., Ruf, A.S., Strohmenger, C.J., Schuelke, J.S., Gombos, A., Al-Hosani, I., Al-Maskary, S., Bloch, G., Al-Mehairi, Y. and Johnson, I.G. (2006). Three-dimensional characterization of a heterogeneous carbonate reservoir, Lower Cretaceous, Abu Dhabi (United Arab Emirates). In: Harris, P.M. and Weber, L.J. (eds.). Giant hydrocarbon reservoirs of the world: From rocks to reservoir

characterization and modeling. AAPG Memoir 88/SEPM, Special Publication, 173-212.

Zagrarni, M.F., Negra, M.H. and Hanini, A. (2008). Cenomanian–Turonian facies and sequence stratigraphy, Bahloul Formation, Tunisia. Sedimentary Geology, 204, 18-35.

2.3 Lower Aptian coral rubble deposits from the western Maestrat Basin (Iberian Chain, Spain): records of chemical and physical disturbances

Telm Bover-Arnal[1*], Ramon Salas[2], Carles Martín-Closas[3], Felix Schlagintweit[4] and Josep A. Moreno-Bedmar[2]

[1]Abteilung Geologie, Fakultät für Biologie, Chemie und Geowissenschaften, Universität Bayreuth, Universitätsstr, 30, 95440, Bayreuth, Germany
[2]Departament de Geoquímica, Petrologia i Prospecció Geològica, Facultat de Geologia, Universitat de Barcelona, Martí i Franqués s/n, 08028, Barcelona, Spain
[3]Departament d'Estratigrafia, Paleontologia i Geociències Marines, Facultat de Geologia, Universitat de Barcelona, Martí i Franqués s/n, 08028, Barcelona, Spain
[4]Lerchenauerstr. 167, 80935, Munich, Germany

*corresponding author
E-mail address: Telm.Bover@uni-bayreuth.de

Submitted for publication to Palaios

Abstract: A singular lithofacies of Lower Aptian age mainly formed by sand- to cobble-sized coral rubble rigidly bound by *Lithocodium aggregatum* and *Bacinella irregularis* highlights the interplay of several natural disturbances with regional and global significance which were responsible for its formation. The encrusted coral rubble levels are found in the western Maestrat Basin (Iberian Chain) and are coeval with the OAE1a and with the intensified greenhouse conditions connected to this event. Therefore, severe storms, elevated seawater temperatures and ocean acidification induced by high atmospheric concentrations of CO_2 due to intensified volcanic activity in the Pacific Ocean would have had a highly recurrent catastrophic impact on the coral populations flourishing in the western Maestrat Basin, giving rise to sub-basin-wide coral rubble carpets. Feedback mechanisms of these elevated atmospheric CO_2 levels, such as increased nutrient and alkalinity fluxes and burial of carbon inventories, together with extremely low sedimentation rates, the presence of a hard substratum and

the aforementioned physico-chemical changes in seawater would have favored the mass-occurrence of *Lithocodium-Bacinella* crusts, large-sized flattened *Palorbitolina lenticularis* and bioeroders such as lithophagid bivalves and endolithic sponges. Consequently, these encrusted coral rubble deposits are here interpreted as records of chemical and physical disturbances linked to the OAE1a. However, due to the important extension and normal faulting recorded during the Lower Aptian in the western Maestrat Basin, earthquake-induced natural stresses might also have played a part in the generation and reworking of these coral rubble deposits. Due to the implications of global environmental change described in this study, the results reported here are not only applicable to the Aptian stage but could be of interest to those authors studying current global warming and other past warming events as they provide a non anthropogenic-impacted geologic example of global warming resulting from natural processes.

Keywords: Lower Aptian, Iberian Chain, Coral rubble, Natural disturbances, OAE1a, *Lithocodium-Bacinella*

2.3.1 Introduction

The presence of coral rubble deposits is extensively reported in the literature for Quaternary reef complexes from tropical latitudes (e.g., Scoffin, 1993; Hughes, 1999; Rasser and Riegl, 2002; Blanchon and Perry, 2004) as well as for older reefal records (e.g., Bosellini and Russo, 1992; Leinfelder, 1992; Bertling and Insalaco, 1998; Helm and Schülke, 2006). Their sedimentological and ecological analysis has also been the main focus of several studies, which commonly present this type of deposit as a product of hurricanes or severe tropical storms (e.g., Scoffin and Hendry, 1984; Hubbard, 1992; Blanchon and Jones, 1997; Perry, 2001).

However, to the best of our knowledge, the occurrence of widespread deposits of coral debris in the Cretaceous period, or more specifically in the Aptian time slice, resembling those formed during the Quaternary, has not been described. The reason may simply be that coral framestones are also usually absent from the Aptian and most of the Cretaceous sedimentary successions reported so far (Tomás et al., 2008 and references therein). During Aptian times, corals commonly occupied low-energy slope and muddy platform settings, probably below the fair-weather wave base, and they

mainly displayed sparsely developed unbound growth fabrics or built small patch-reefs (Tomás et al., 2008; Bover-Arnal et al., 2009, under review). All these relatively deep and calm environmental conditions, together with the loose growth features of coral communities presumably hindered the broad accumulation of coral rubble.

Therefore, Aptian deposits bearing coral pieces are often accompanied by benthic foraminifera such as miliolids and orbitolinids, and fragments of other platform and slope dwellers such as rudist and *Chondrodonta* bivalves, nerineid gastropods and echinoids, which frequently accumulated or flowed down slope suspended in a lime mud matrix, in the form of floatstones or rudstones (*sensu* Embry and Klovan, 1971; e.g., Rosales, 1999; Vennin and Aurell, 2001; Millán et al., 2007; Tomás et al., 2008; Bover-Arnal et al., 2009, under review).

The coral rubble deposits presented here differ somewhat from the aforementioned typical Aptian sediments containing fragments of corals. The resedimented levels studied were probably formed by successive episodes of accumulation of coral debris and other bioclasts in the absence of a lime mud matrix. The lack of a muddy matrix presumably permitted the subsequent binding of these deposits by microorganisms of uncertain taxonomic position, and the bioerosion of both skeletal debris and binding agents, as often occurs in the Quaternary coral rubble deposits (e.g., Blanchon and Perry, 2004).

Hence, the most noteworthy aspect of this study is the fact that these encrusted coral rubble levels represent a rare and remarkable facies of the Aptian seas, and thus, their analysis may provide new insights into this stage and the disturbance processes which affected the coral communities that thrived during this time slice.

Here we present a detailed sedimentological analysis of the facies and microfacies carried out throughout the aforementioned deposits exposed in the western Maestrat Basin (eastern Iberian Chain, Spain). Furthermore, in order to examine the mechanisms that might have led to the formation of these characteristic lithofacies and the environmental significance of their biotic content, the sedimentary interval analyzed will be put in a global context, taking into account all the major perturbations of the ocean-atmosphere system which occurred during the Early Aptian (e.g., Weissert and Lini, 1991; Erba, 1994; Scott, 1995; Weissert et al., 1998; Menegatti et al., 1998; Larson and Erba, 1999; Hochuli et al., 1999; Pittet et al., 2002; Wissler et al., 2003; Skelton, 2003; Weissert and Erba, 2004; Heimhofer et al., 2004; Föllmi et al., 2006; Burla et al., 2008).

The occurrence of this encrusted horizon in the western Maestrat Basin was previously reported by Segonzac and Marin (1972), in a study focused on the microorganisms present in this remarkable lithofacies, and by Vennin and Aurell (2001) and Embry (2005), in a general analysis of the Aptian sedimentary succession. Nevertheless, these studies merely represented a starting point for our research since we were pursuing other scientific goals and, besides, the information available on the Aptian stage and its biota has been significantly enriched during this last decade by several other publications (e.g., Pittet et al., 2002; Wissler et al., 2003; Skelton, 2003; Weissert and Erba, 2004; Heimhofer et al., 2004; Immenhauser et al., 2005; Föllmi et al., 2006; Dumitrescu et al., 2006; Burla et al., 2008; Tomás et al., 2008; Rameil et al., in press; Bover-Arnal et al., 2009, under review).

In essence, the present paper aims to document a singular Aptian case study of sedimentary records of natural disturbance events with regional and global environmental implications. Hence, the applications of the results presented here are not only restricted to the Aptian stage but could be of significance for those dealing with current or past global environmental change, since they provide a non anthropogenic-impacted geologic example resulting from changing external factors.

2.3.2 Geographical and geological setting of the study area

The encrusted coral rubble deposits analyzed here are located in the Galve sub-basin in the eastern Iberian Chain (E Spain), in the environs of the villages of Aliaga, Campos, Miravete de la Sierra, Villarroya de los Pinares, Camarillas, Jorcas and Montoro de Mezquita, in the province of Teruel (Fig. 2.3.1). During Late Jurassic-Early Cretaceous times, this region formed the marginal western side of the Maestrat Basin (Salas and Guimerà, 1996). The Maestrat Basin was one of the Iberian basins which developed as a result of the Late Oxfordian (Late Jurassic)-Middle Albian (Early Cretaceous) rifting cycle that affected the Iberian plate. Throughout this extensional process, carbonates and siliciclastics over 4000 m-thick ranging from continental to marine conditions were accumulated in the aforementioned basin. Later, owing to the Alpine contraction (Late Eocene to Early Miocene), the Maestrat Basin together with the other Iberian basins (Cameros, Columbrets and South Iberian) were tectonically inverted, thus forming the Iberian Chain (Salas and Casas, 1993; Salas et al., 2001).

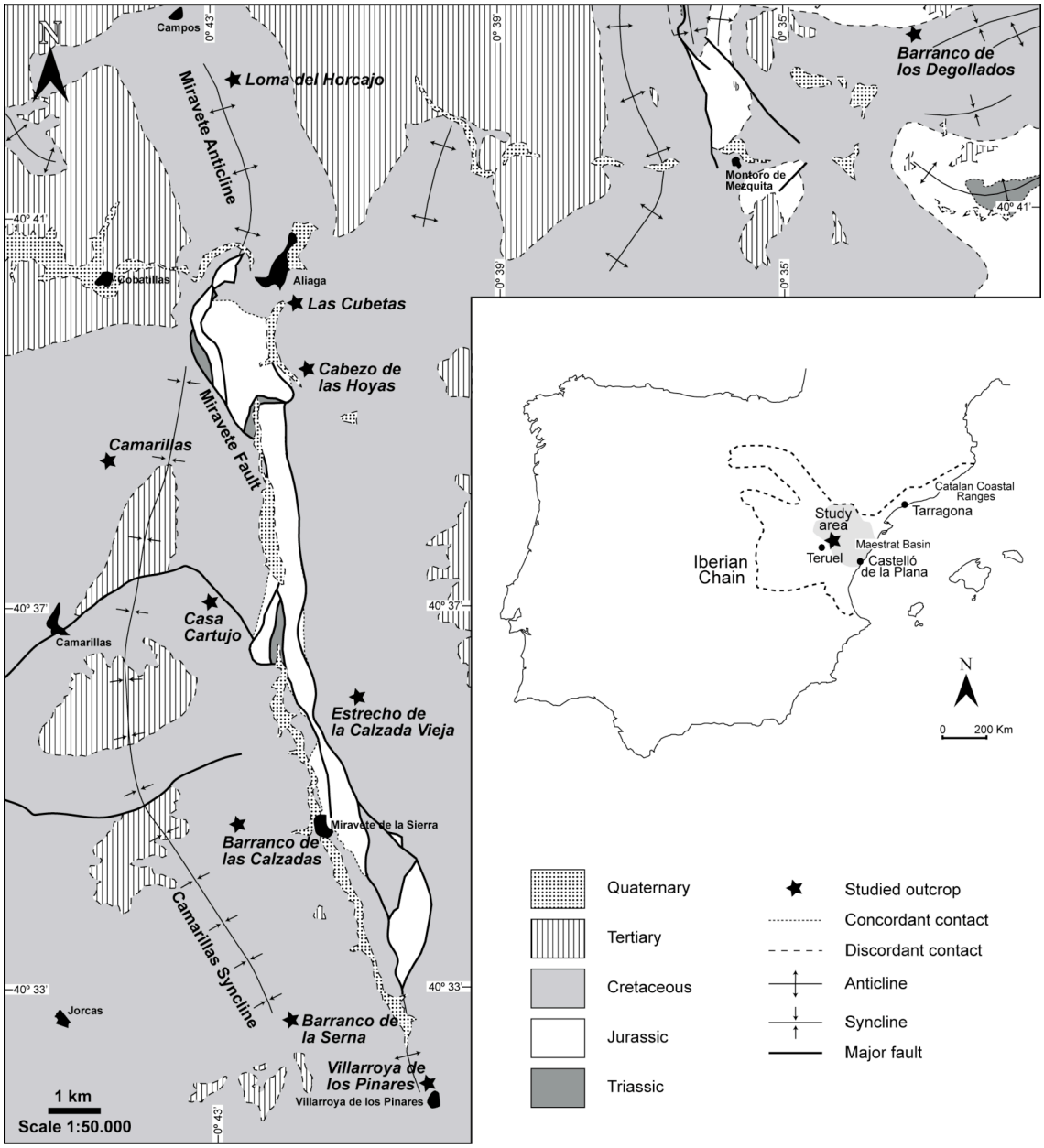

Figure 2.3.1. Geological map of the western Maestrat Basin indicating its location within the Iberian Peninsula. The areas studied are marked with a star. Modified after Canérot et al. (1979) and Gautier (1980).

The encrusted rubble facies studied in the Galve sub-basin lies inside the Lower Aptian (Early Cretaceous) epeiric marly succession belonging to the Forcall Formation (Fig. 2.3.2; Canérot et al., 1982; Salas et al., 2001; Bover-Arnal et al., under review). This marly interval, which originated in tropical latitudes, reaches a maximum thickness of 220 m and exhibits interbedded storm-induced turbidites, marly limestones and limestones with abundant *Palorbitolina lenticularis* (Blumenbach) and ammonoids, indicating relatively deep basinal conditions.

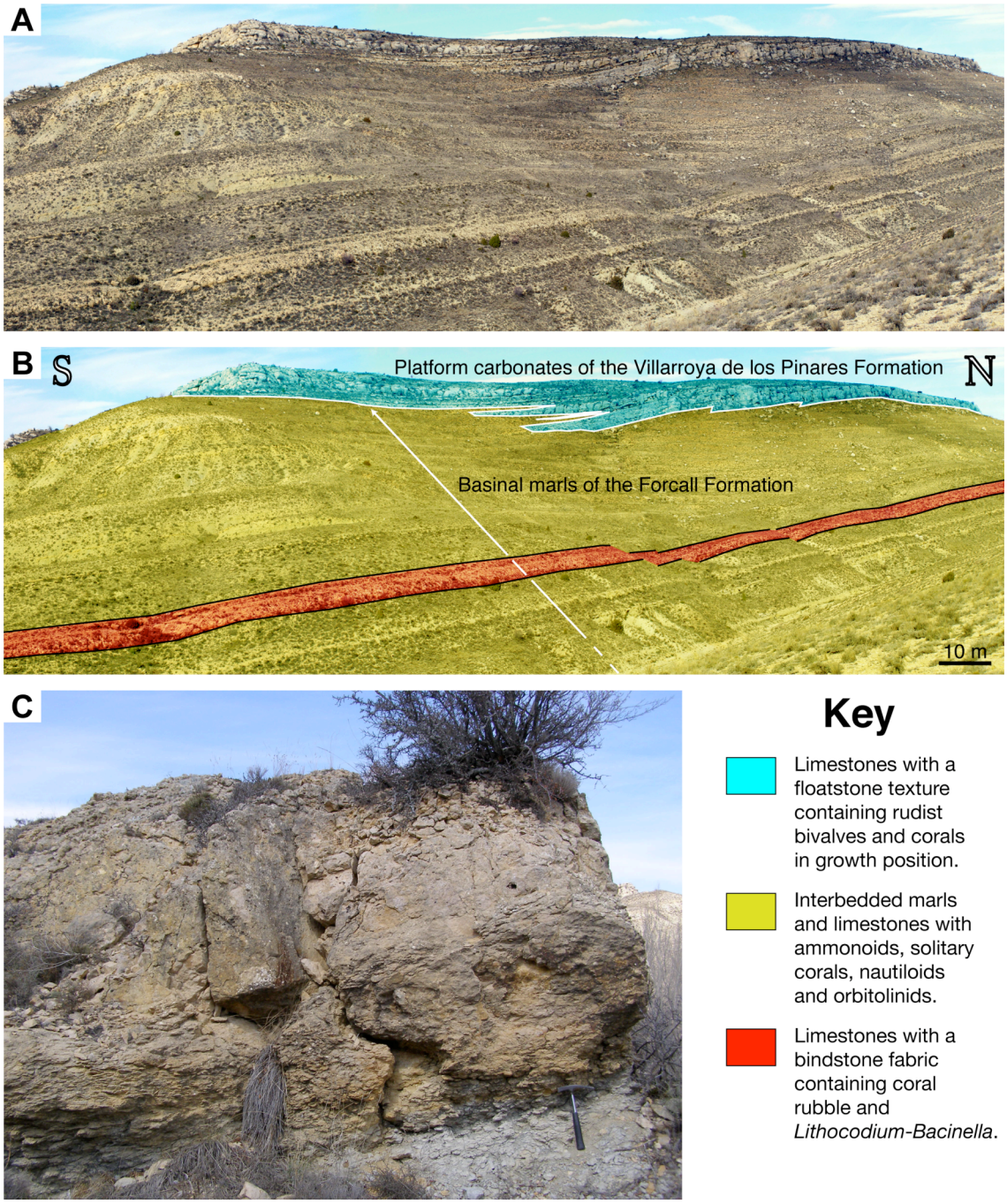

Figure 2.3.2. Field and outcrop-scale views of the studied deposits encrusted by Lithocodium aggregatum and Bacinella irregularis in the Barranco de las Calzadas locality. A) Field view of the Barranco de las Calzadas area. B) Interpretation of the Barranco de las Calzadas area with the location of the encrusted coral rubble horizon within the marls of the Forcall Formation. C) Outcrop-scale view of the encrusted coral rubble horizon in the Barranco de las Calzadas site.

The coral rubble levels constitute a sub-basin-wide continuous horizon (up to 5 m-thick), which covers an area of at least 120 Km^2. Nevertheless, the limits and extent of this lithofacies are unknown owing to erosion and to the Albian and Tertiary cover.

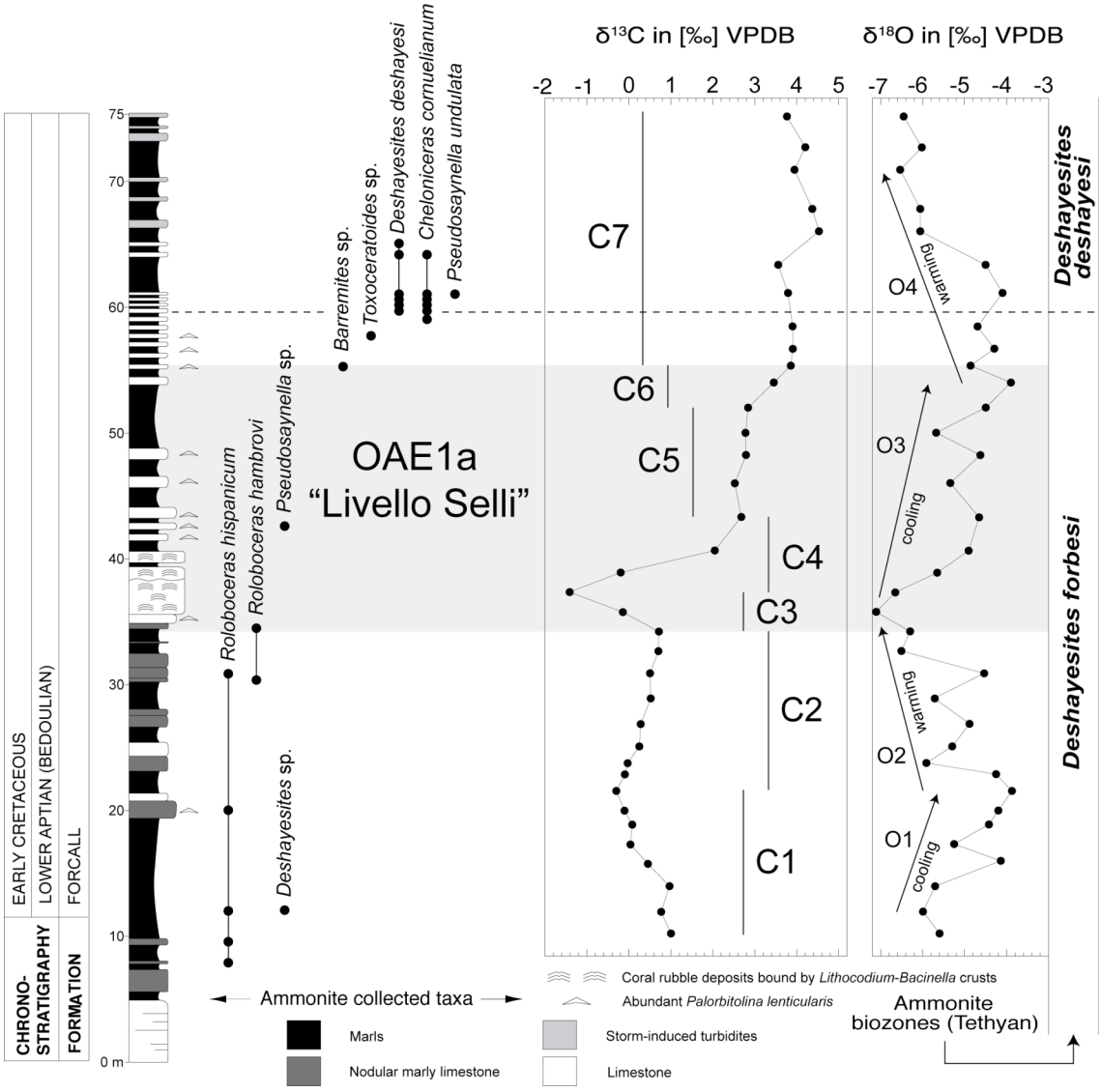

Figure 2.3.3. Schematic log of the Barranco de las Calzadas section showing the situation of the coral rubble deposits bound by Lithocodium-Bacinella crusts, the ammonite biostratigraphic framework and the C- and O-isotopic curves (modified from Bover-Arnal et al., under review). Note how these encrusted deposits are coeval with the negative C-isotopic spike (C3) marking the onset of the Early Aptian oceanic anoxic event (OAE1a) and the subsequent positive shift C4, and how they are also partly coeval with the warming trend (O2) occurring before the onset of the OAE1a and the cooling trend (O3) recorded throughout this event.

Ammonite biostratigraphy and C- and O-isotopic analyses carried out in the Galve sub-basin along the Forcall Formation by Moreno-Bedmar et al. (2009; accepted) and Bover-Arnal et al. (under review) situate the encrusted coral rubble carpets analyzed in the upper part of the *Deshayesites forbesi* ammonite biozone (Lower Aptian substage), coeval with the negative $\delta^{13}C_{carb}$ spike that marks the onset of the Early Aptian oceanic anoxic event (OAE1a) (Fig. 2.3.3). According to Bover-Arnal et al.

(under review), these levels with coral debris mark the start of the Tethyan-wide regressive context that in the Galve sub-basin ended with subaerial exposure of the platform carbonates of the Villarroya de los Pinares Formation (Fig. 2.3.2B) at the uppermost Early Aptian (Bover-Arnal et al. 2009).

2.3.3 Data collection and methods

Detailed analysis at outcrop-scale of lithofacies, sedimentary structures, fossil content, biotic community structure and bulk-rock sampling was undertaken at ten separate sites in order to obtain a sub-basin-wide representation of the facies. The localities selected are indicated in Figure 2.3.1 and comprised the following: Barranco de los Degollados, Loma del Horcajo, Camarillas, Casa Cartujo, Barranco de las Calzadas, Barranco de la Serna, Villarroya de los Pinares, Las Cubetas, Cabezo de las Hoyas and Estrecho de la Calzada Vieja. Fifty-nine centimeter-sized and eight decimeter-sized rock samples were collected at vertically spaced decimetric intervals covering the ten outcrops studied from bottom to top. The centimeter-sized samples were prepared following standard techniques as thin-sections about 5-8 μm thick with a size of 25×45, 50×90 and 75×135 mm in order to analyze the microfacies, the microfossil content and the microbiotic community structure, whereas the rock blocks were sawed and polished in order to improve the study and observation of the macrofacies carried out at foot of outcrop. The relative dominance of rubble constituents and microorganisms was visually estimated from thin sections, polished slabs and outcrop sections. The terminology used for rock fabrics is taken from the classification of Embry and Klovan (1971).

2.3.4 Results

The lower Aptian encrusted coral rubble deposits are described here in terms of their fossil content, biotic structure, sedimentary characteristics, and overall facies and microfacies features.

2.3.4.1 Biotic composition

2.3.4.1.1 Corals

The coral rubble is overwhelmingly dominated by fragments of the suborder Microsolenina with two families: Microsolenidae (Fig. 2.3.4A) and Leptophylliidae (= Latomeandridae fide auct), which constitute up to 95% of the total coral skeletal volume. The remaining 5% is composed of fragments of three suborders: Faviina (Families: Eugyridae and Placocoeniidae in Fig. 2.3.4B), Archeocaeniina (Family: Actinastraeidae) and Fungiina (Family: Haplaraeidae). Due to the small size of the coral rubble (sand- to cobble-size), it was not possible to determine the genus, species or growth forms of the corals.

2.3.4.1.2 Microencrusters

The lithofacies analyzed is characterized by a low diversity of encrusting microorganisms dominated by structureless micritic crusts of uncertain nature which exhibit internal cavities. In the literature, these dense micrite crusts have habitually been regarded as *Lithocodium aggregatum* Elliott, a well-known encrusting microproblematicum (see Immenhauser et al., 2005; Cherchi and Schroeder, 2006; Rameil et al., in press) which had a widespread occurrence along the margin of the Tethys during part of the Mesozoic. These calcified dense micrite crusts, which do not exhibit a definite internal texture, bind the coral rubble and other skeletal fragments (e.g., mollusks, tests of benthic foraminifera) together in all directions throughout the deposits studied (Figs. 2.3.4D-F, 2.3.5). The *Lithocodium*-crusts observed display different growth types and rhythms with thicknesses ranging between 0.04 and 5 mm. The crusts with thicknesses of between 0.04 and 1 mm frequently show a growth pattern characterized by densely packed ribbon-like multi-layers that indicate intermittent breaks in development (Fig. 2.3.6A). On the other hand, the thicker crusts (between 1 and 5 mm-thick) occur as a single encrustation or as a succession of few layers, giving a denser, more massive and micritic aspect to the thallus (Fig. 2.3.6B).

Frequently, the *Lithocodium aggregatum* encrustations show erosional surfaces, which are commonly spread over by other crusts (Figs. 2.3.6A, C). Moreover, between or overgrowing the *Lithocodium*-layers it is common to find microproblematica filamentous fabrics developing pseudo-cells by grain-to-grain connecting bridges and foam-like cellular structures, which have classically been regarded as *Bacinella irregularis* Radoičić (Fig. 2.3.4C), encrustations of the benthic foraminifera *Bdelloidina*? *urgonensis* Wernli and Schulte (Fig. 2.3.6D), which agglutinate abundant

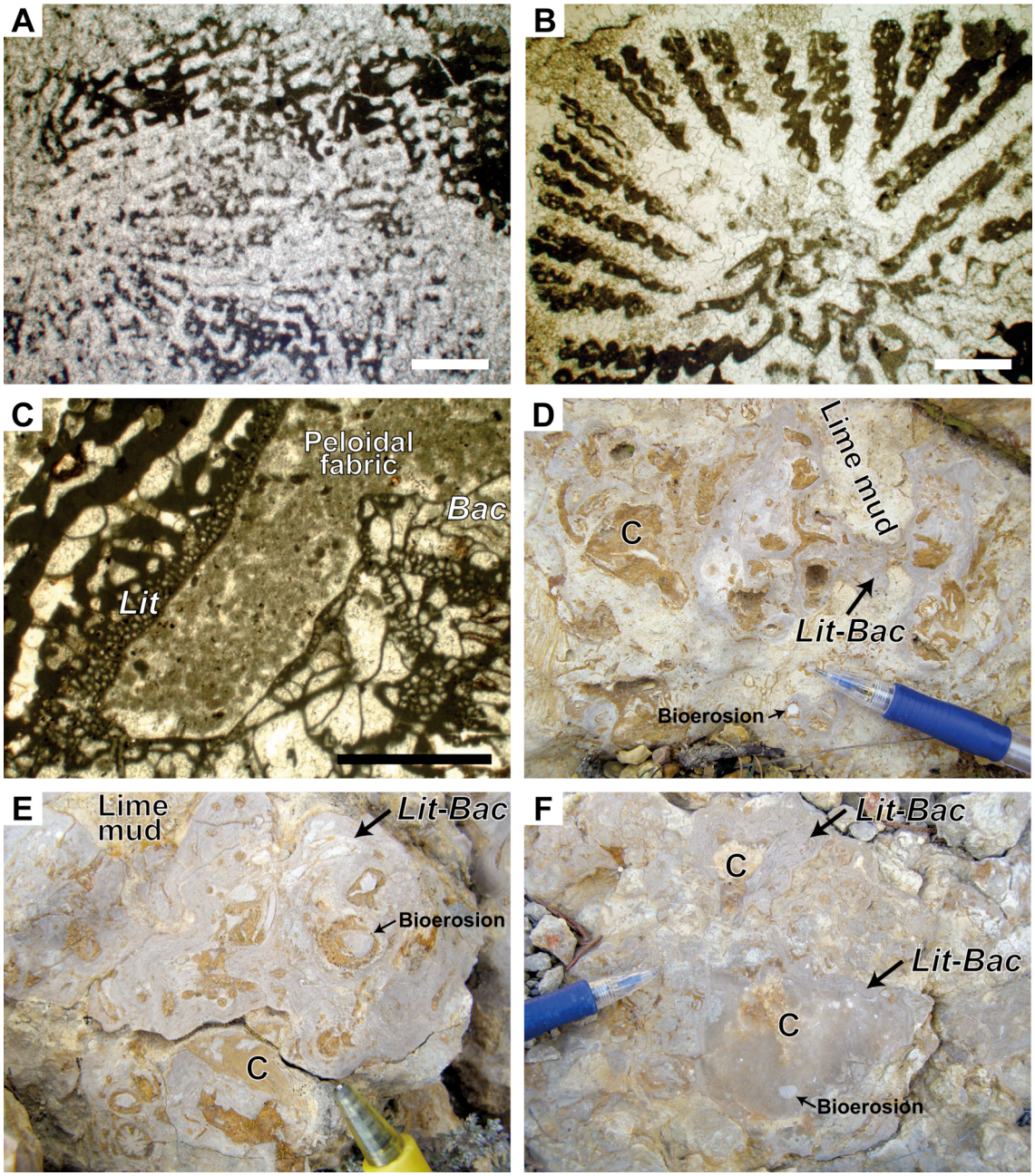

Figure 2.3.4. Thin section photomicrographs and outcrop-scale images of representative biotic composition and facies. A) Detail of coral rubble belonging to the Microsolenidae family (Microsolenina suborder). Barranco de los Degollados site. B) Detail of coral rubble belonging to the Placocoeniidae family (Faviina suborder). Barranco de los Degollados site. C) Detail of Lithocodium aggregatum (Lit) and Bacinella irregularis (Bac). Note the in-place precipitated peloidal fabric filling the void space between the microencrusters. Barranco de las Calzadas site. D-F) Details of the bindstone fabric exhibited by these encrusted deposits in the Camarillas, Barranco de las Calzadas and Cabezo de las Hoyas sites, respectively. Note how the grey colored Lithocodium-Bacinella crusts bind together and in all directions the coral rubble (C), which display an orangey color due to the presence of ferruginous saddle dolomite. Note also that the spaces between the crusts are filled with lime mud. Observe the strong bioerosion of these deposits above all in image E). Scale bars represent 1 mm.

silt-sized quartz particles, and bryozoans from the "*Berenicea*" group. Other minor encrusting microorganisms present in these deposits are serpulid worms (Fig. 2.3.6E), the peyssonneliacean red alga *Polystrata alba* (Pfender) (Fig. 2.3.6F), *Calcistella*? sp., Pseudoostracods *sensu* Samuel et al. (1972) and the incertae sedis *Koskinobullina socialis* Cherchi and Schroeder.

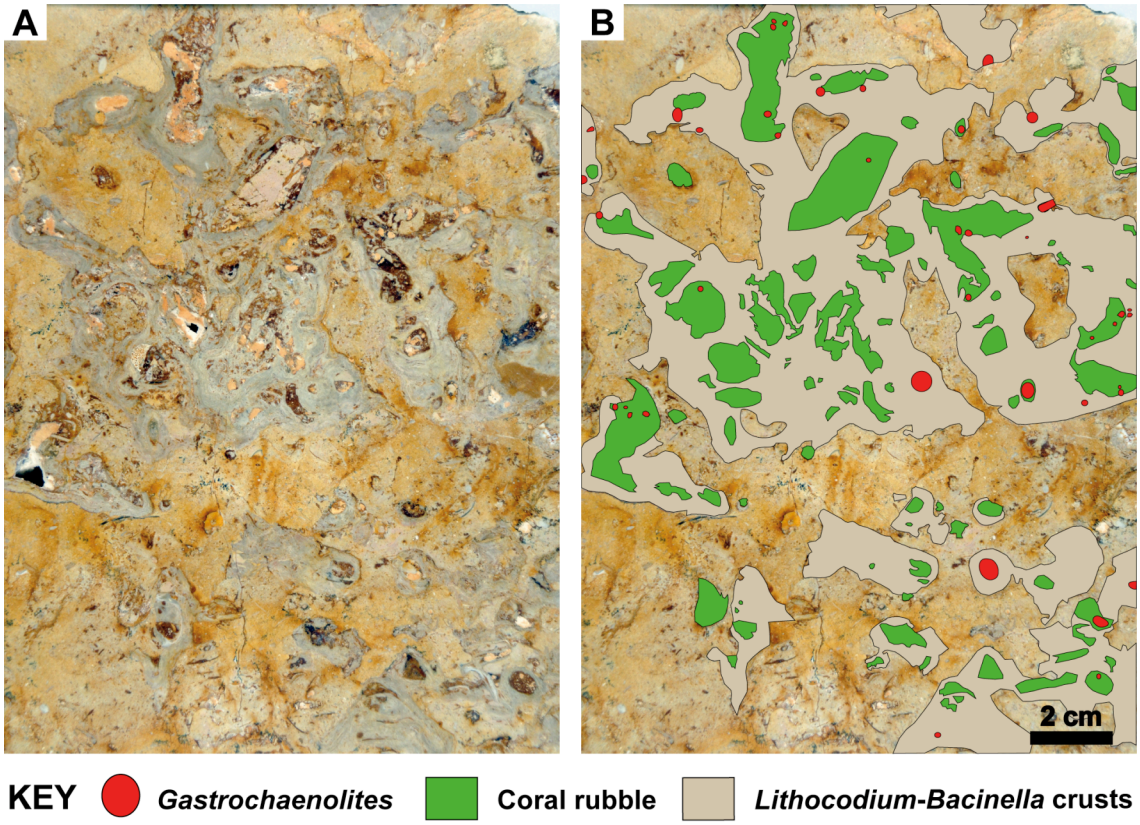

Figure 2.3.5. Close-up view of the encrusted lithofacies displaying a bindstone fabric. A) Polished slab of the encrusted coral rubble deposits. Barranco de las Calzadas site. B) Interpretation of the polished slab. Note how the Lithocodium-Bacinella crusts bind the coral rubble together in all directions, and how the interclast space is filled with lime mud. Observe the strong bioerosion present in this lithofacies.

2.3.4.1.3 Other micro and macrobiota

The catalogue of taxa identified in these encrusted coral rubble deposits is completed with the prolific occurrence of large-sized (diameter up to 1.5 cm) discoidal *Palorbitolina lenticularis* (Blumenbach) (Fig. 2.3.7A), which agglutinates abundant minute quartz grains. Other benthic foraminifera such as *Praeorbitolina* gr. *cormyi-wienandsi* Schroeder, *Neotrocholina* cf. *aptiensis* Iocheva, *Daxia minima* Laug and

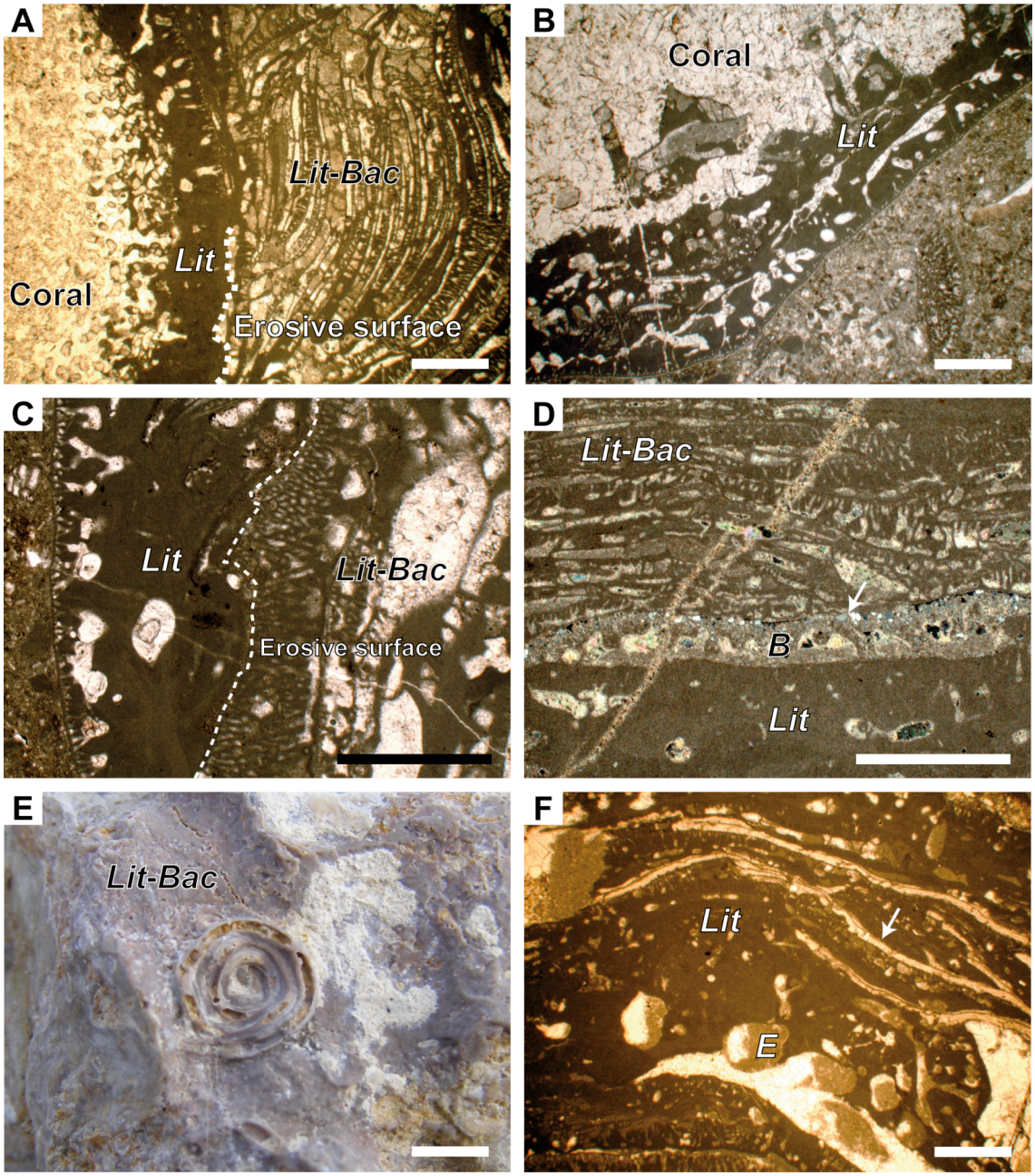

Peybernes, *Charentia cuvillieri* Neumann, *Choffatella* cf. *decipiens* Schlumberger, *Meandrospira washitensis* Loeblich and Tappan, *Everticyclammina* sp., lenticulinids and textulariids are as well common. Also present are terebratulid brachiopods (Fig. 2.3.7B), *Conulus castanea* (Brogniart), other echinoids, pharetronid sponges (Fig. 2.3.7C), decapod remains of *Carpathocancer triangulatus* (Misik et al.), solitary corals (Fig. 2.3.7D), the dasycladalean algae *Neomeris*? sp. and *Terquemella* sp., the gymnocodiascean alga *Permocalculus*? sp., the foraminifera *Troglotella incrustans* Wernli and Fookes, unidentified gastropods, lithophagid bivalves (Fig. 2.3.7E), the

rudists *Horiopleura dumortieri* (Matheron) and *Caprina douvillei* Paquier (Fig. 2.3.7F), unidentified oysters and other mollusks.

◄ *Figure 2.3.6. Thin section photomicrographs and outcrop-scale images of representative biotic composition and facies. A) Fragment of Microsolenina coral encrusted by a single massive Lithocodium aggregatum crust (Lit). Note how this single massive crust is eroded and how it is overgrown by a densely-packed succession of ribbon-like Lithocodium-Bacinella (Lit-Bac) layers. Camarillas site. B) Fragment of coral encrusted by a massive well-developed Lithocodium aggregatum crust. On the right of the figure there is a random section of orbitolinid foraminifer. Barranco de las Calzadas site. C) Detail of an erosive surface within a Lithocodium-Bacinella crust overgrown by a single massive Lithocodium-layer. Cabezo de las Hoyas site. D) Bdelloidina? urgonensis (B) agglutinating silt-sized quartz grains (white arrow) encrusting a single massive Lithocodium aggregatum crust. Note how the sessile foraminifer Bdelloidina? urgonensis is overgrown by densely-packed ribbon-like Lithocodium-Bacinella meshwork. Casa Cartujo site. E) Detail of encrusting serpulid worms at the center of the image. Villarroya de los Pinares site. F) Polystrata alba (white arrow) overgrowing Lithocodium aggregatum crusts. Note the Entobia macroborings (E) affecting the Lithocodium aggregatum encrustations. Observe that the geopetal infillings mark post-depositional tilting of the deposits. Cabezo de las Hoyas site. Scale bars represent 1 mm.*

2.3.4.2 Bioerosional structures

Micro- (width < 1 mm) and macro-borings (width > 1 mm) are abundant and widespread throughout the sedimentary interval investigated. The nomenclature used in this study for the classification of these structures produced by marine organisms with the ability to bore biogenic hard substrates follows Taylor and Wilson (2003) and Bromley et al. (2007). The bioerosion patterns identified are the following: *Gastrochaenolites*, *Trypanites*, sack-like, *Entobia* and dendriniform.

Rounded, oval and semicircular cavities of *Gastrochaenolites* borings are common and widespread throughout the resedimented levels analyzed (Figs. 2.3.4D-F, 2.3.5, 2.3.7E). They mainly occur in the coral rubble and the *Lithocodium aggregatum* crusts. The transverse sections recognized mostly preserve the *in situ* valves of the *Lithophaga* (Fig. 2.3.7E). The width of the borings observed range between 1 mm and 1 cm. Nevertheless, cavities with a diameter of 3 and 5 mm predominate.

Trypanites borings were principally identified within *Lithocodium aggregatum* layers, shell debris and coral remains. In the thin sections examined, these unbranched cylindrical borings with smooth, curved terminations commonly have a length of up to 1 mm and a width between 0.1 and 0.2 mm. However, irregular cylindrical-like macro-

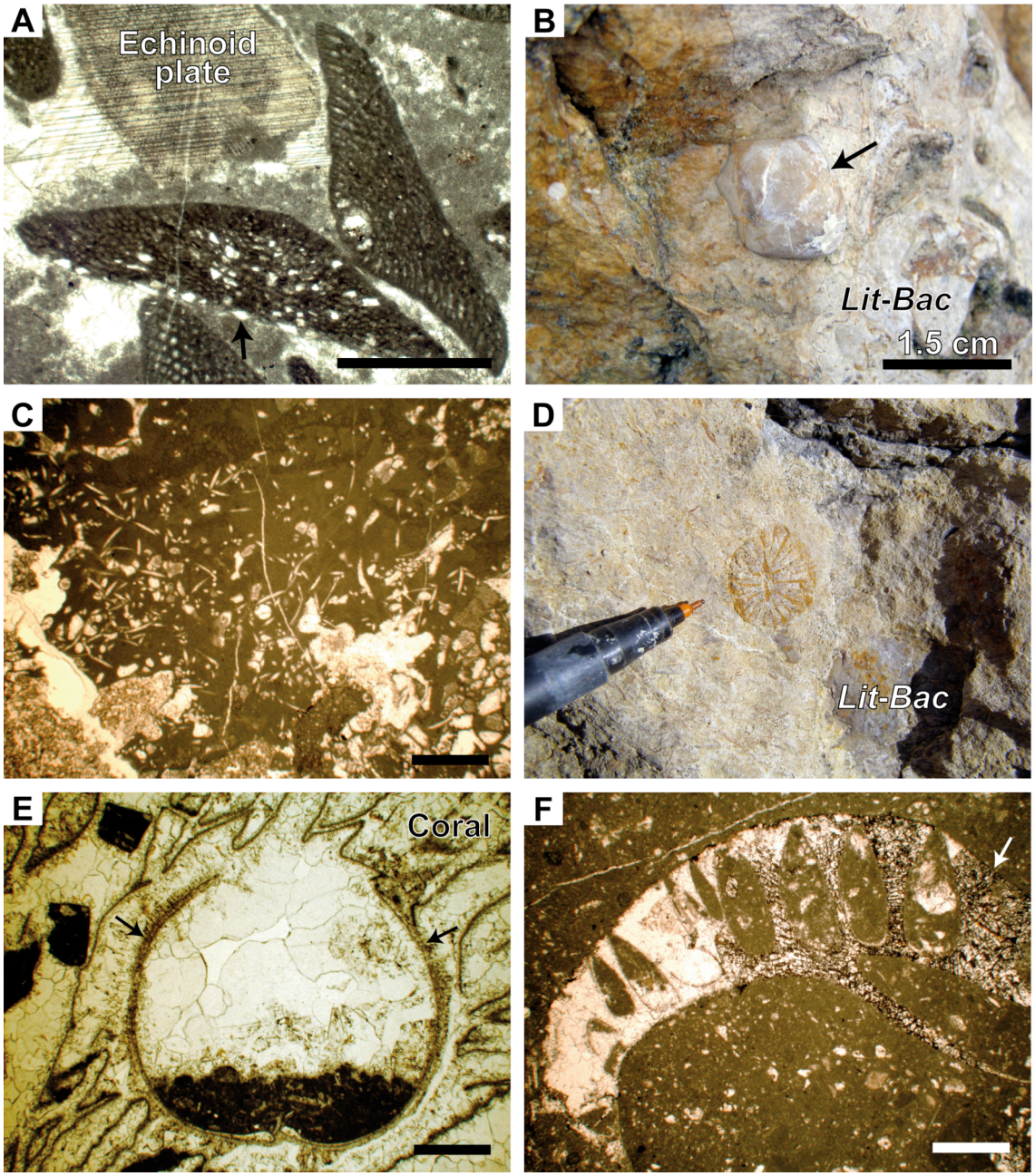

Figure 2.3.7. Thin section photomicrographs and outcrop-scale images of representative biotic composition and facies. A) Palorbitolina lenticularis agglutinating silt-sized quartz particles (black arrow). Las Cubetas site. B) Detail of a terebratulid brachiopod (black arrow). Barranco de las Calzadas site. C) Skeleton fragment of a demosponge imbued with Lithocodium aggregatum as reported in Cherchi and Schroeder (2006). Barranco de los Degollados site. D) Detail of a solitary coral. Villarroya de los Pinares site. E) Transverse section of a lithophagid bivalve boring with the in situ preserved valves (black arrows). Barranco de la Serna site. F) Section of Caprina douvillei. Note how the skeleton is partly affected by ferruginous saddle dolomite (white arrow). Barranco de la Serna site. Except in B), scale bars represent 1 mm.

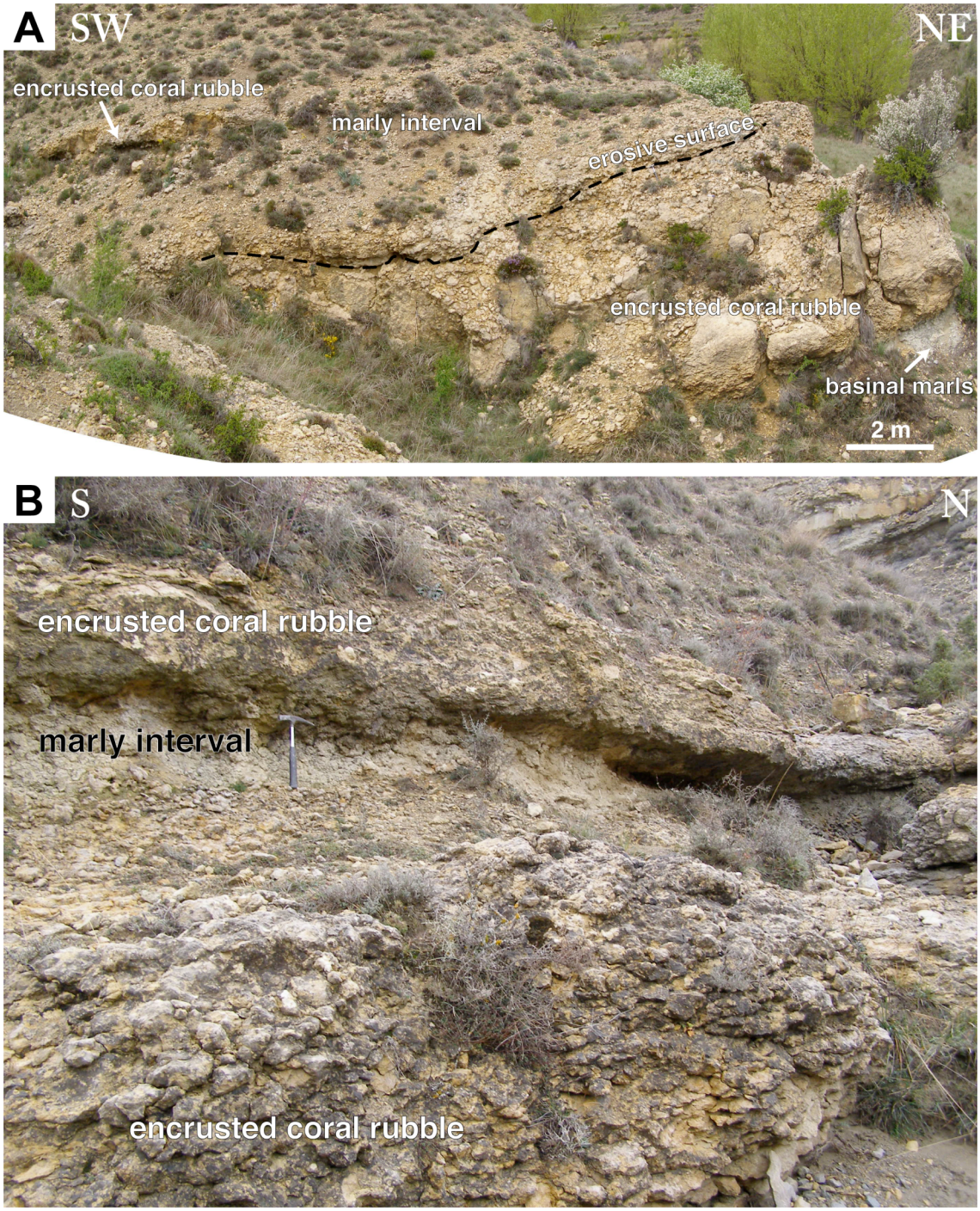

Figure 2.3.8. Outcrop-scale views of the encrusted coral rubble horizon in the Barranco de las Calzadas site. A) Note the erosive surface at the top of the first nodular layer containing coral rubble and Lithocodium aggregatum and Bacinella irregularis. Note that the second nodular level with coral debris is overlying a thin marly interval. B) Observe the decimetric marly interval between the two layers of encrusted coral rubble and the nodular aspect of the deposits.

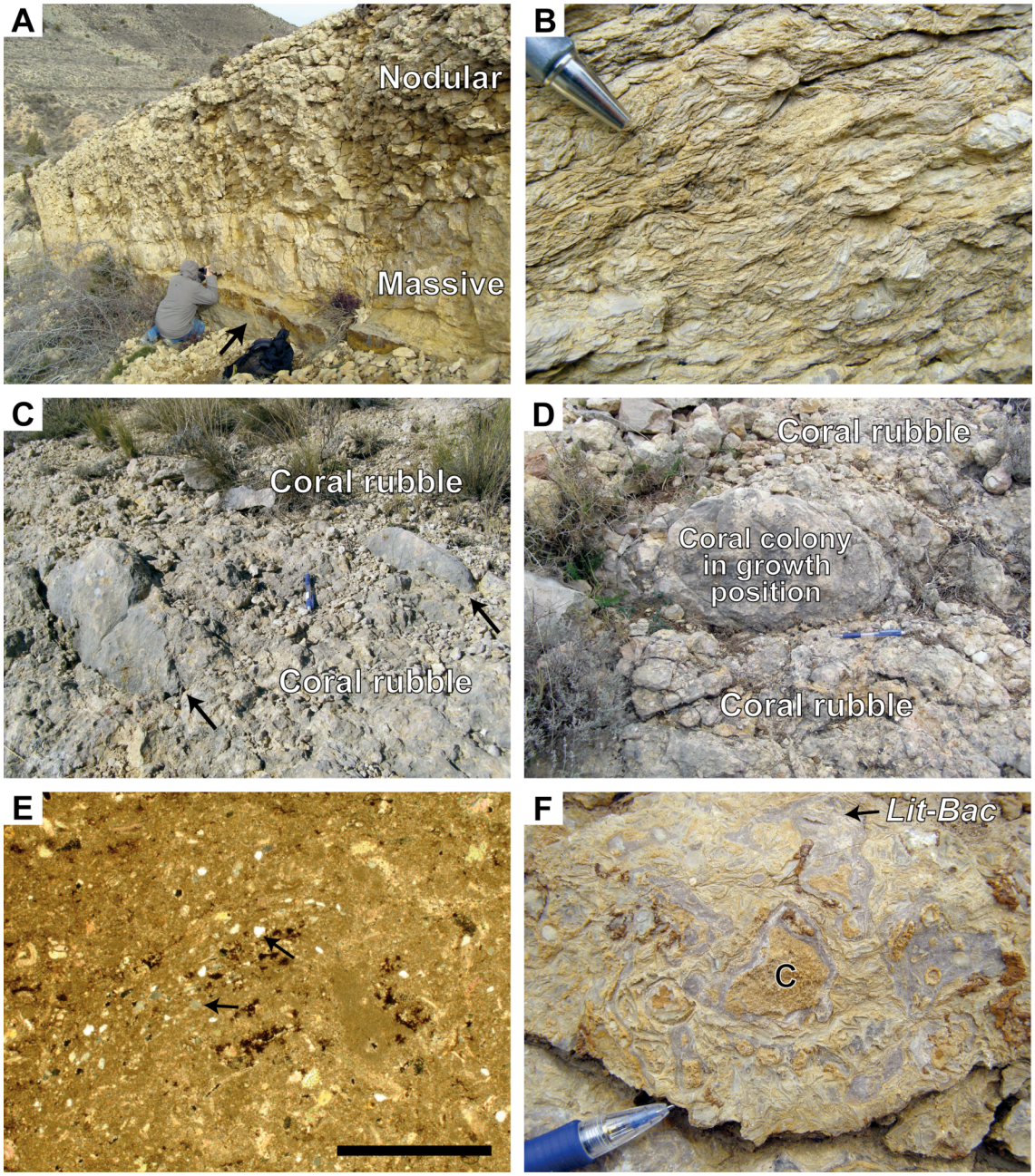

Figure 2.3.9. Thin section photomicrographs and outcrop-scale images of representative biotic composition and facies. A) Outcrop-scale view of the amalgamated encrusted coral rubble deposits in the Barranco de la Serna site. Note how the first half of the deposit is massive and how the second half adopts a nodular aspect. The black arrow points to a rock-forming Palorbitolina lenticularis grainstone, which underlies the horizon containing coral debris and microencrusters. B) Detail of the underlying grainstone shown in image A). Note that the Palorbitolina lenticularis show preferential imbrication. Barranco de la Serna site. C-D) Entirely preserved coral colonies (black arrows) in growth position embedded in encrusted coral rubble. Cabezo de las Hoyas site. E) Detail of silt-sized quartz particles (black arrows) within the lime mud matrix filling the interclast spaces. Barranco de la Serna site. F) Reworked lumps of Lithocodium-Bacinella crusts surrounding coral pieces. Note how the grey colored Lithocodium-Bacinella crusts bind together and in all directions the coral rubble (C), which display an orangey color due to the presence of ferruginous saddle dolomite. Scale bar represents 1 mm.

borings with rounded ends, and with lengths superior to 1 mm and widths between 0.15 and 0.3 mm are also present.

The sack-like borings recognized during the microfacies analysis occur within *Lithocodium*-crusts and oyster shells. They have a tiny aperture channel with a length of approximately 1 mm and a diameter of between 0.1 and 0.16 mm which ends in an ellipsoidal chamber with a width of between 1 and 1.6 mm and height of between 0.5 and 1 mm. These sack-like structures are sometimes connected.

Entobia borings consisting of rounded-to-ovoid shaped single or interconnected chambers were identified in *Lithocodium*-bearing micrite thalli (Fig. 2.3.6F) and fragments of mollusks and corals. In the thin sections studied, these chambers produced by endolithic sponges measure up to 1 mm in width and up to 0.6 mm in height. Preserved spicules within the chambers were not observed.

Dendriniform bioerosion patterns were observed in *Lithocodium aggregatum* crusts and mollusk and coral debris. These branched boring structures consist of a single channel of origin with lengths up to 2.5 mm and widths between 0.05 and 0.2 mm, which ramifies into numerous channels characterized by lengths up to more than 6 mm and diameters between 0.1 and 0.5 mm.

2.3.4.3 Deposit fabric and sedimentary features

The rocks investigated form a continuous horizon identifiable all over the Galve sub-basin that crops out embedded in basinal marls and limestones containing *Palorbitolina lenticularis*, ammonoids, nautiloids, echinoids, brachiopods and solitary corals (Fig. 2.3.2). This horizon is composed of several episodes of encrusted sand- to cobble-sized coral rubble (fragments up to 12 cm) and varies in thickness and arrangement throughout the area studied. Mostly, the coral rubble deposits encrusted by *Lithocodium aggregatum* and *Bacinella irregularis* occur in the form of amalgamated episodes (Figs. 2.3.2C, 2.3.8, 2.3.9A), which occasionally show erosive surfaces (Fig. 2.3.8A). In the Barranco de la Serna and Barranco de las Calzadas sites these amalgamated deposits reach a maximum thickness of 5 meters (Figs. 2.3.2C, 2.3.8A, 2.3.9A), while in the Villarroya de los Pinares locality they thin to 1 meter. A bindstone fabric characterizes these encrusted strata (Figs. 2.3.4D-F, 2.3.5). Nevertheless, and although the deposits are thus clast supported, there is a large amount of lime mud present in the lithofacies, which fills the spaces left between the encrustations (Figs. 2.3.4D-E, 2.3.5). It is also common to find centimeter- to meter-thick marly

intercalations between the layers forming this conspicuous horizon. These marly levels separating different episodes of formation and encrustation of coral debris were seen in the Barranco de los Degollados, Cabezo de las Hoyas, Barranco de las Calzadas (Fig. 2.3.8), Las Cubetas and Camarillas sites.

The layers with coral fragments and microorganisms have thicknesses ranging from centimeters to a few meters and are mostly nodular bedded (Figs. 2.3.8, 2.3.9A). Nevertheless, massive (Fig. 2.3.9A) or tabular stratified deposits also occur. Bioturbation is rare. Only one undiagnosed burrow with a centimetric length and a milimetric width was observed in the Barranco de las Serna locality. This finding also indicates that the fabric of the sedimentary interval studied was not mud supported. Moreover, no hydrodynamic structures were identified. At the base of these encrusted deposits it is common to find a decimetric layer of rock-forming *Palorbitolina lenticularis* with a grainstone texture (Fig. 2.3.9A). In this underlying level, the orbitolinids are preferentially imbricated (Fig. 2.3.9B). Centimeter- to decimeter-thick layers with a packstone-grainstone fabric dominated by *Palorbitolina lenticularis* are also occasionally found intercalated between encrusted coral rubble episodes. It is also noteworthy that entirely preserved centimeter- to decimeter-sized coral colonies in life position embedded in encrusted coral rubble (Figs. 2.3.9C-D) are only found in the localities of Cabezo de las Hoyas and Estrecho de la Calzada Vieja (Fig. 2.3.1). These entire corals in growth position show absence or minor presence of *Lithocodium-Bacinella* encrustations and *Lithophaga* borings, and display irregular massive, platy, sheet-like and domal morphologies.

The petrographic study revealed the presence of abundant silt-sized quartz throughout these encrusted strata. The quartz grains occur agglutinated in the tests of the orbitolinid *Palorbitolina lenticularis* (Fig. 2.3.7A) and the sessile foraminifera *Bdelloidina*? *urgonensis* (Fig. 2.3.6D), as well as within the interclast lime mud matrix (Fig. 2.3.9E). On occasions, the skeletal porosity of corals and the inherent interclast porosity are filled by in-place precipitated peloidal fabrics (Fig. 2.3.4C). Ferruginous cements of saddle dolomite within the skeletal fragments of corals and mollusks are frequent (Fig. 2.3.7F). In addition, geopetal infillings within the bioerosional structures (Figs. 2.3.6F, 2.3.7E) and other void spaces are widespread and often indicate post-depositional tilting of the deposits. Strong reworking of these deposits is also indicated by the presence in some levels of millimeter- to centimeter-sized lump-like *Lithocodium-Bacinella* crusts enclosing coral pieces. Locally, these lumps occur within

a *Palorbitolina lenticularis*-dominated matrix, which exhibits a grainstone-rudstone texture (Fig. 2.3.9F).

2.3.5 Discussion

During the Early Aptian, the western Maestrat Basin recorded, within a time period shorter than the duration of the *Deshayesites forbesi* ammonite biozone, an uncommon and remarkable facies basically constituted by coral rubble rigidly bound by *Lithocodium aggregatum* and *Bacinella irregularis* crusts. The results obtained from the study of this encrusted horizon highlight the interplay of diverse physical and chemical disturbances which were responsible for the formation of the coral rubble and the mass-occurrence of *Lithocodium aggregatum* and *Bacinella irregularis*. An understanding of these natural stresses is of importance in order to evaluate a fossil example of coral populations affected by changing environmental factors. Therefore, the discussion will focus on the recognition and examination of the different discrete events that could have disrupted the Lower Aptian coral communities flourishing in the Galve sub-basin, favoring the widespread development of *Lithocodium-Bacinella* crusts.

2.3.5.1 Origin, generation and deposition of coral rubble

The conspicuous lithofacies analyzed forms a totally continuous horizon within the Galve sub-basin and was developed as a result of countless episodes of generation and deposition of coral rubble, subsequently bound by *Lithocodium-Bacinella* crusts and bioeroded by lithophagid bivalves and sponges. Thus, during the time-slice investigated, the coral populations established in the western Maestrat Basin underwent a cyclic pattern of destruction and renewal. The multi-episodic and cyclic nature of this horizon is manifested by the presence of several levels of encrusted coral rubble, which mainly occur in the form of amalgamated deposits or separated by erosive surfaces or marly intervals. Moreover, the presence in certain sites of wholly preserved coral colonies in growth position enclosed within encrusted coral debris also lends support to the multi-episodic character of the deposits. Thus, a highly recurrent mechanism or mechanisms capable of generating large amounts of coral rubble are required.

The most plausible single mechanism known to cause periodic patterns of destruction in tropical latitudes and which could account for the creation of such large and broad piles of coral debris recorded in the Galve sub-basin would be severe storms

or hurricanes. Tropical cyclones represent the major physical disturbance process exerting recurrent catastrophic influence in Quaternary reef systems and thus, current analogues of coral damage by storm-induced waves are innumerable (e.g., Hubbard, 1992; Scoffin 1993; Blanchon and Jones, 1997). Therefore, hurricane-generated waves and storm surges might have razed extensive coral meadows developed during this time in the Galve sub-basin or nearby areas resulting in the formation of these coral rubble fields. Moreover, the influence of storms during this time-slice in the Galve sub-basin is also indicated by the occurrence, underlying the coral rubble deposits, of a centimeter- to decimeter-thick grainstone with *Palorbitolina lenticularis* in rock-forming abundance showing preferential imbrication. The presence of preferentially imbricated orbitolinids indicates that this level, which overlies basinal marly sediments, was deposited during major hydrodynamic disturbances and hence, it could be interpreted as a storm-induced turbidite.

The size of the coral stumps ranges between sand and cobble. The absence of large cobble- or boulder-sized fragments, which are common in extant coral rubble deposits (e.g., Scoffin, 1993; Blanchon et al., 1997), indicates strong reworking of these rubble carpets and/or significant transportation of the skeletal fragments. The location of the *in situ* coral communities was not found either within the Galve sub-basin or in surrounding areas. Thus, these coral populations may have completely crumbled into rubble, they may not have been preserved, or they may have been eroded. Similarly, Blanchon et al. (1997) reported a Quaternary example from the Grand Cayman's fringing-reef complex, where the reef core lacks *in situ* coral colonies and is formed exclusively by coral rubble-rudstone layers. This example could serve as a present-day analogue in order to demonstrate that in some cases the catastrophic influence of hurricanes may result in the non-preservation of coral populations in their original frames and habitats. Hence, the coral debris deposits preserved in the geological record are frequently the only source of information concerning past reefs and/or coral assemblages.

On the other hand, the entirely preserved coral colonies in growth position embedded within encrusted coral rubble in the Cabezo de las Hoyas and the Estrecho de la Calzada Vieja sites (Fig. 2.3.1) seem neither to represent nor to indicate the situation of the source *in situ* coral communities. In these sites, the presence of coral colonies in growth position is scarce and none of them shows any sign of tilting, overturning or damage. Moreover, as mentioned earlier, large cobble- or boulder-sized coral fragments

were not found close by. Thus, these coral colonies in life position overgrowing encrusted coral debris probably developed by regeneration of viable fragments. This process is common in extant reef complexes influenced by severe natural disturbances (e.g., Pearson, 1981). Furthermore, the Cabezo de las Hoyas and the Estrecho de las Calzadas sites are located on the eastern side of the Miravete normal transfer fault (see Fig. 2.3.1), which partitioned the Galve sub-basin into an eastern foot-wall side and a western hanging-wall side (see Bover-Arnal et al. under review). Therefore, these aforementioned sites represent paleohigh areas where light levels would have been favorable for the regeneration and development of coral colonies during certain time intervals free from coral debris arrivals. Nonetheless, larval settlement during propitious periods in this shallower and better-illuminated eastern side of the Miravete fault should not be discarded.

With this background, any attempt to situate the coral communities that were shattered into pieces, thus giving rise to these coral rubble deposits, in a particular setting is not straightforward. However, the coral populations in growth position identified in uppermost Lower and Upper Aptian strata in the Galve sub-basin by Bover-Arnal et al. (2009, under review) could shed light on this issue and constitute a valid analogue. These younger coral communities probably thrived on nutrient fluxes in distal marly settings such as gentle slopes, most probably below normal storm wave base, exhibiting unbound and sparse growth fabrics with irregular massive, domal and occasionally branching morphologies (Bover-Arnal et al. 2009, under review). Along the same lines, in the southeastern Maestrat Basin, Tomás et al. (2008) reported deep coral assemblages dominated by Microsolenina and Faviina suborders with sheet-like, platy and domal forms thriving in outer and middle ramp settings, below storm wave base and between fair-weather and storm wave base environments. Similarly, the coral fragments analyzed in the Galve sub-basin basically belong to the suborder Microsolenina. According to several authors, during the Jurassic and Cretaceous periods the microsolenids frequently occupied an ecological niche characterized by nutrient-rich conditions and low light levels, which could be linked to either deep and/or turbid water settings (e.g., Insalaco, 1996; Dupraz and Strasser, 2002 and references therein; Tomás et al., 2008 and further references therein). Thus, it is probable that these deep Aptian corals communities dominated by microsolenids were not adapted to high-energy conditions.

Hence, the microsolenid-dominated assemblages that were broken down into stumps forming the coral rubble carpets investigated may have flourished under nutrient-rich conditions in distal marly settings, at least below fair-weather wave base and perhaps even below normal storm wave base. In this regard, present-day reports show that the effects on coral populations of exceptionally powerful storms can be traced down to 20-37 m (e.g., Woodley et al., 1981; Kobluk and Lysenko, 1992). Therefore, the wave action generated by violent storms or hurricanes could easily have reached these relatively deep and sheltered settings causing the complete destruction of these coral colonies, which were not adapted to high-energy levels. Coral damage by the impact of suspended pebble- to cobble-sized skeletal fragments during storms would also have played a significant role in the destruction of the microsolenid-dominated meadows. Furthermore, the location of the original *in situ* coral colonies in distal marly environments could account for the absence of lime mud during the generation and deposition of these rubble carpets. Normally, when storm-induced waves impact Aptian corals thriving in proximal muddy carbonate platforms, the resulting coral debris flows downslope within a lime mud matrix exhibiting floatstone or rudstone textures (e.g., Bover-Arnal et al. 2009, under review). In this respect, floatstone and rudstone fabrics cannot be bound internally and in all directions by encrusting microorganisms and are not easy to rework by subsequent storms as occurred with the coral debris deposits reported in this study.

The submarine carpets of storm-generated rubble accumulated below fair-weather wave base at least, along a gently-sloping smooth topographic relief as suggested by the sub-basin wide continuity and gradual progressive changes in rock thickness exhibited by the encrusted horizon. For instance, in the Barranco de la Serna site this encrusted horizon is approximately 5 m-thick, thinning gradually towards the Villarroya de los Pinares site (Fig. 2.3.1), which corresponds to the most distal locality investigated (see Bover-Arnal et al. under review), where probably on account of basinal starvation it measures only 1 m. The distribution of the coral skeletal fragments generated throughout the sub-basin would have resulted from the action of the storm-induced waves and the associated powerful seaward-flowing currents (e.g., Hubbard, 1992; Blanchon and Jones, 1997). In addition, the catastrophic wave action and the strong bottom-hugging return currents triggered by the storms would also have re-mobilized the former debris episodes as suggested by the erosive surfaces present within the *Lithocodium-Bacinella* crusts and by the geopetal infillings, which reflect

post-depositional reworking of the deposits. Furthermore, reworking and sub-basin-wide dispersal of the deposits by the effects of fair-weather bottom currents should not be ruled out.

The pilling up of these coral skeletal fragments in relatively deep and basinal environments, below fair-weather wave base at least, was a key factor in their accommodation and subsequent preservation in the sedimentary record. In this respect, the geological record shows us that the coral debris deposits preserved normally accumulated in distal slope or ramp settings (e.g., Enos and Moore, 1983; Scoffin, 1993), which offer accommodation and shelter from continuous water motion.

Apart from violent storms, catastrophic wave action may also be the result of submarine landslides or earth movements originated by earthquakes, volcanic activity or bolide impacts. Due to the highly recurrent nature of the mechanism or mechanisms generating the coral rubble carpets studied, bolide impacts can be discarded. Moreover, the possibility of tsunamis induced by volcanic activity seems unlikely considering that no igneous events of Aptian age around the eastern part of the Iberian plate have been reported in the literature so far. In addition, it is not easy to establish a link between these resedimented deposits and lower Aptian igneous events recorded in areas further away. Along the same lines, no preserved vast submarine landslide deposits have been regionally recognized, thus the hypothesis of recurrent tsunamis triggered by landslide processes is difficult to test. However, the generation of coral debris and reworking of the rubble deposits by earthquakes, earthquake-induced tsunamis and their subsequent strong backwash currents must be considered. The Maestrat Basin was developed as a result of the Late Oxfordian-Middle Albian rifting stage (Salas et al., 2001). Therefore, the Aptian record of the Galve sub-basin corresponds to a syn-rift sedimentary succession. Moreover, according to Bover-Arnal et al. (under review), the coral rubble deposits analyzed here were deposited within an interval of syn-rift rapid subsidence, associated with significant extension by normal faulting. This Early Aptian episode of strong extensional tectonic activity, which recorded the highest rift subsidence rate for the Aptian in the Galve sub-basin (Bover-Arnal et al., under review), could have induced frequent fault activity with tremors at the sea bottom and tsunamis that together with powerful backwash currents, could have had a catastrophic impact on the microsolenid-dominated communities settled in this western part of the Maestrat Basin.

Nonetheless, storm and tsunami deposits preserved seaward are generally complicated to differentiate given that both types of deposit tend to exhibit similar

sedimentary patterns. Moreover, tsunami deposits are commonly reworked by storm-generated turbulences, which constitute higher recurrent disturbances, concealing their original depositional features (see Pratt and Bordonaro, 2007). Thus, due to the regional syn-rift context, part of the coral rubble generated in the Galve sub-basin as well as several of the episodes of reworking that occurred may have been caused by physical perturbations triggered by earthquakes. In this respect, the aforementioned grainstone layer containing preferentially imbricated *Palorbitolina lenticularis* which underlies the coral rubble horizon in some localities may also correspond to a tsunami deposit instead of a storm-induced turbidite.

Further mechanisms that might have given rise to the coral rubble fields recorded in the western Maestrat Basin could include uplift processes or several episodes of subaerial exposure linked to high frequency sea level rhythms. However, both mechanisms can be discarded, as no paleokarst features or marine vadose cements were observed either at outcrop-scale or in the thin sections analyzed. In addition, the O-isotopic curve measured along the Barranco de las Calzadas site by Bover-Arnal et al. (under review) does not show extremely low oxygen-isotope values or various saw-tooth-shaped negative peaks within the encrusted coral rubble horizon (Fig. 2.3.3), which would be indicative of different episodes of subaerial exposure (see Sattler et al., 2005). Similarly, and due to the absence of subaerial exposure features and diagenetic cementation acting as binding agent, neither can these coral rubble carpets be interpreted as inter-/supra-tidal rubble-cay deposits, which are typical in extant reef complexes (e.g., Blanchon and Perry, 2004).

On the other hand, harsh physico-chemical changes in the seawater, such as elevated temperatures and acidification, may have played a significant role in weakening and killing the coral communities (e.g., coral bleaching), thus favoring the generation of coral rubble. Given that these processes are currently affecting present-day reef complexes due to increasing atmospheric CO_2 despite the overall icehouse conditions (e.g., Brown et al., 1996; De'ath et al., 2009), they should not be ruled out as potential triggering factors in an earliest Lower Aptian greenhouse Earth. However, the specific results of such environmental factors and processes are difficult to detect in fossil examples or to discern from other catastrophic mechanisms such as storms or tsunamis.

2.3.5.2 Binding agents

When disturbances affect coral populations, they frequently generate new spaces for colonization by other organisms (e.g., Rogers, 1993; Perry, 2001). In this regard, the Lower Aptian coral rubble carpets created in the western Maestrat Basin provided a suitably hard substratum for the widespread development of *Lithocodium aggregatum* and *Bacinella irregularis* crusts. The *Lithocodium-Bacinella* crusts which flourished in the rubble deposits investigated show an opportunistic character given that they are clearly low diversity and correspond in all cases to the pioneer communities. These types of communities normally thrive under restrictive environmental conditions. The *Lithocodium-Bacinella* layers observed occur encrusting the skeletal debris in all directions throughout the whole of the coral rubble horizon studied, giving rise to a bindstone texture.

Therefore, and owing to the type of lithofacies displayed by the deposits, it can be inferred that after each physical disturbance event having catastrophic effects on the coral populations, the rubble generated was initially stabilized by the development of *Lithocodium aggregatum* and *Bacinella irregularis* thalli. Subsequently, with the calcification of the *Lithocodium-Bacinella* crusts, these microproblematica carbonates acted as rigid binding agents and thus played a key role in the preservation of these resedimented deposits in the geological record.

The unknown taxonomic nature of *Lithocodium aggregatum* Elliott and *Bacinella irregularis* Radoičić has classically constituted a hindrance to providing a convincing interpretation of their environmental significance. In this respect, the study by Cherchi and Schroeder (2006), which focused on the biologic affinity of *Lithocodium aggregatum*, ascribes this calcifying microorganism to cyanobacteria. In addition, the epiflourescence tests carried out by Conrad and Clavel (2008) on Hauterivian *Lithocodium aggregatum* crusts represent a significant step towards an understanding of this microproblematicum, since they suggest a probable calcimicrobial nature for these dense micritic crusts. However, the *Lithocodium aggregatum*-bearing crusts studied from the Iberian Chain do not show in the micrite itself any feature such as stromatolitic or thrombolitic fabrics or any clear palaeontological remains that could be indicative of cyanobacterial activity, but are structureless.

However, along these lines, Rasser and Riegl (2002) argued the potential of microbial mats to act as rubble binders due to their high calcification rates and capacity for overgrowing the coral skeletal fragments with continuous and widespread crusts.

Nonetheless, they failed to find a conclusive example of coral rubble bound by microbialites in the literature. Consequently, if the microbial nature of the *Lithocodium-Bacinella* crusts is confirmed, the Lower Aptian case study presented here demonstrates that benthic microbial communities can act as rigid binding agents, at least in sand- to cobble-sized coral rubble. This functional role, which in the present-day and shallower coral rubble deposits is basically performed by crustose coralline algae and vadose and freatic diagenetic cements (see Rasser and Riegl, 2002 and references therein), in this relatively deeper Lower Aptian example was carried out by these microproblematica.

Following this idea, microbial mats contain cyanobacteria communities, which are aerobic phototroph organisms, at the outermost part of the crusts close to the surface (see Riding, 1991, 2000). Nevertheless, the *Lithocodium-Bacinella* crusts studied, which developed in relatively deep settings and also bound the rubble interior in all directions, would have had the ability to thrive even in dim light. In this regard, several papers have demonstrated the highly efficient light utilization of modern microbial mats, which enables them to develop in poorly illuminated habitats (e.g., Pringault et al., 2004 and references therein). Hence, the different growth types and rhythms displayed by the *Lithocodium-Bacinella* crusts could be related to changing light irradiance conditions. The thalli showing a spasmodic type of growth with densely packed ribbon-like thin multi-layers could indicate episodic periods of harsh environmental conditions with light levels unfavorable to the development of *Lithocodium-Bacinella*. On the other hand, the thicker crusts showing a more massive and micritic aspect could reflect intervals of more suitable growth environments.

The capacity of the *Lithocodium-Bacinella* crusts to act as rigid binding agents requires high, rapid calcification rates. This rapid hardening of the crusts is suggested by the widespread occurrence of bioerosional structures and erosive surfaces within the *Lithocodium-Bacinella* thalli. In this respect, the erosive surfaces displayed by the *Lithocodium-Bacinella* crusts are commonly overgrown by other *Lithocodium-Bacinella* layers, indicating that these deposits underwent several episodes of encrustation. Moreover, the presence of erosive surfaces may be indicative of important reworking processes during the preliminary stages of stabilization of the encrusted rubble carpets. Reworking of the deposits is also indicated by the polarity shown by the geopetal infillings identified within skeletal and bored cavities. Similarly, reworking of the encrusted coral debris seems unlikely to have occurred above fair-weather wave base on account of the large amount of lime mud present in the lithofacies, indicating

important primary porosity of the deposits, and the absence of phreatic diagenetic cements and/or abundant *Lithocodium-Bacinella* lumps or oncoids, which are typical in tidal- and wave-influenced shallow water settings (e.g., Védrine et al., 2007; Rameil et al. in press). Hence, and as discussed above, all evidence points to the fact that these coral rubble fields were encrusted at least below fair-weather wave base influence. Therefore, these episodes of reworking might have been linked to storm-induced wave action, the associated seaward-deflected powerful currents and/or to earthquake-induced physical disturbances.

2.3.5.3 Associated biotic community and bioerosion

The solid coral rubble substrates generated in the western Maestrat Basin and the calcified *Lithocodium aggregatum* crusts, which acted as rigid binding agents of these rubble carpets, were broadly infested and bioeroded by lithophagid bivalves, endolithic sponges and other unknown micro-borers. Since most of the bioeroders are suspension feeder fauna (e.g., *Lithophaga*, endolithic sponges), the widespread occurrence of bioerosional structures in these encrusted coral rubble deposits may indicate nutrient-rich waters (see e.g., Hallock and Schlager, 1986).

Marine environments with high trophic levels are commonly linked to turbid seawater conditions and hence, to habitats characterized by low irradiance. These limited light conditions are also suggested by the rarity of green algae, and the presence of the peyssonneliacean red algae *Polystrata alba*, which, as a result of comparison with living analogues, is commonly regarded as growing in poorly illuminated settings. In fact, during the microfacies analysis, only scarce tiny green algae fragments, which may have been transported from more proximal areas, were recognized. Nevertheless, relatively deep waters could also account for the low light levels inferred during the formation of these coral rubble fields bound by *Lithocodium-Bacinella* crusts.

The encrusted coral rubble horizon also recorded several orbitolinid blooms that could be indicative of the environmental conditions under which these deposits were developed. In this respect, the widespread presence of large-sized *Palorbitolina lenticularis* exhibiting flattened forms is also suggestive of turbid and/or relatively deep waters (see Vilas et al., 1995; Immenhauser et al., 1999; Pittet et al., 2002). Similarly, evidence of relatively deep waters is also reflected in the occurrence of relatively deep water biota such as brachiopods and solitary corals in the Barranco de las Calzadas, Barranco de la Serna and Villarroya de los Pinares sites, which form part of the deeper

western hanging-wall side of the Miravete fault (Fig. 2.3.1; see Bover-Arnal et al., under review).

2.3.5.4 Carbonate production, sedimentation rates and environmental factors

Lithocodium-Bacinella or microbial events, if the microbial origin of the crusts is verified, such as that recorded during the Early Aptian in the western Maestrat Basin are usually linked in the literature to elevated seawater temperatures, high carbonate alkalinities, significant nutrient supplies and slow sedimentation rates (e.g., Neuweiler and Reitner, 1992; Brachert, 1999; Riding, 2000; Sprachta et al., 2001; Hillgärtner et al., 2003; Immenhauser et al., 2005; Camoin et al., 2006; Cabioch et al., 2006; Zamagni et al., 2009; Rameil et al., in press). The results obtained from this analysis of the encrusted coral rubble horizon suggest that the Early Aptian *Lithocodium-Bacinella* bloom investigated also seems to be marked by such environmental patterns.

The C- and O-isotope analysis carried out by Bover-Arnal et al. (under review) at the Barranco de las Calzadas site clearly indicates that the encrusted horizon is coeval with the negative C-isotope spike that marks the onset of the OAE1a, and that the base of these deposits coincides with the probable Early Aptian thermal maximum (Fig. 2.3.3; see Bover-Arnal et al. under review). Therefore, in the Galve sub-basin, the generation of coral rubble and its subsequent stabilization and binding by *Lithocodium aggregatum* and *Bacinella irregularis* was to a certain extent contemporaneous with the intensified greenhouse conditions that led to the OAE1a and with the $\delta^{13}C$ perturbations (segment C3) that define the start of this event (see Li et al., 2008; Méhay et al., 2009; Tejada et al., 2009; Millán et al., 2009; Bover-Arnal et al., under review). Due to the location in tropical latitudes of the Maestrat Basin during the Early Aptian, this global warming event, which is widely assumed to be linked to elevated CO_2 atmospheric concentrations due to exceptional episodes of volcanic activity in the Pacific Ocean (Larson and Erba, 1999; Weissert and Erba, 2004), probably induced frequent hurricanes and/or severe tropical storms that would have razed the relatively deep microsolenid-dominated meadows which had developed in the Galve sub-basin and/or surrounding areas, resulting in the formation of the coral rubble deposits. Furthermore, these high CO_2 atmospheric concentrations, together with the consequent intensified greenhouse conditions, would have resulted in elevated seawater temperatures and

increased ocean acidification causing a profound impact on the development of coral populations, favoring the production of coral rubble. Nevertheless, as discussed above, earthquake-induced physical disturbances might have also played a part in the origin of these coral rubble carpets.

According to Weissert et al. (1998), the intensified greenhouse conditions connected to the OAE1a led to an acceleration of the global hydrological cycle resulting in enhanced continental weathering and runoff rates. The increased terrigenous fluxes from the continents to the basins were probably accompanied by large amounts of clay, which would have brought elevated nutrient levels and turbid conditions to the epeiric seas. Such a hypothesis would seem to be corroborated by the presence of abundant silt-sized quartz throughout the sedimentary interval studied and the biotic community preserved, which is indicative of high nutrient concentrations. Nevertheless, the fossil content of the deposits indicates sufficient light levels for the development of phototrophic biota. On the other hand, the reduction of water transparency due to increased runoff and nutrient availability, together with the aforementioned physico-chemical changes of ocean-water, could also account for the low rates of carbonate production reflected in the sedimentary interval studied (see Hallock and Schlager, 1986).

In addition to the runoff caused by the high rainfall accompanying storms, and the release of nutrient inventories contained in the sediments by storm- and/or tsunami-induced reworking, additional nutrient supplies may have been brought to the Galve sub-basin by upwelling processes, which can be generated by topographic features, oceanic circulation, volcanogenic activity (Vogt, 1989) or directly caused by hurricanes, severe storms (Babin et al., 2004) and by internal waves (e.g., Sandstrom and Elliott, 1984; Wolanski and Deleersnijder, 1998). However, some of the quartz present in the lithofacies would have been transported by the storms-force winds and thus, it may not necessarily be related to the nutrification of seawater.

The rapid calcification of the prolific *Lithocodium-Bacinella* crusts investigated requires high seawater alkalinity. This increase in alkalinity could also be related to climatically enhanced weathering rates on continental subaerially exposed carbonate rocks, resulting in the transfer of large amounts of carbonate and bicarbonate anions from hinterland to the basin by runoff (e.g., Neuweiler and Reitner, 1992; Weissert et al., 1998).

Further important chemical ecofactors that could have had a significant influence on the generation of coral rubble and the broad occurrence of *Lithocodium-Bacinella* crusts are changes in the salinity and oxygenation of seawater. Nevertheless, the data obtained from the present analysis of the encrusted horizon do not lead to conclusive evidence of the oxygen and salinity levels that prevailed during the formation of these deposits. However, the presence of marine organisms such as bivalves, borers and echinoids throughout the encrusted coral rubble levels is indicative of oxygenated conditions and moreover, suggests that the salinity was euhaline.

Another key factor that favored the widespread development of *Lithocodium-Bacinella* crusts throughout the Galve sub-basin during the time span studied was the extremely low to nil sedimentation rates registered. Besides the presence of massive and laminar *Lithocodium-Bacinella* crusts, which are usually indicative of low rates of sedimentation (e.g., Rameil et al., in press), the fact that the coral rubble observed is overwhelmingly dominated by fragments of microsolenids also suggests slow sedimentation rates (see Tomás et al., 2008 and references therein). In addition, the broad occurrence of bioerosional structures within both the skeletal fragments and the microproblematica crusts and the clear evidence that these encrusted levels underwent several episodes of encrustation and reworking demonstrates that these deposits were not buried rapidly.

On the other hand, the fact that this encrusted horizon is also partly coeval with the cooling trend (O3) recorded throughout the OAE1a (Fig. 2.3.3) as a consequence of organic carbon burial (see Ando et al., 2008), should be also considered since such cooling would have resulted in additional changes to ocean-water physico-chemistry. Therefore, this trend should also be considered when evaluating the mechanisms that may have been responsible for the formation of the encrusted coral rubble levels studied. However, the resulting physico-chemical changes in ocean water induced by such mechanisms are not easy to assess in the geological record.

2.3.5.5 Regional and global significance of the Lithocodium-Bacinella event

Similar levels coeval with the OAE1a or of Lower Aptian age with widespread occurrence of *Lithocodium aggregatum* and *Bacinella irregularis* such as those studied in the Galve sub-basin have not been reported so far for other sub-basins belonging to

the Maestrat Basin. The C-isotope analyses performed by Moreno-Bedmar et al. (2009) in the eastern Morella and northern Oliete sub-basins indicate that in these other parts of the Maestrat Basin, those strata age equivalent to the encrusted coral rubble horizon studied correspond to bioclastic calcarenites and to nodular limestones and marly deposits with abundant large-sized *Palorbitolina lenticularis* exhibiting discoidal morphologies. Hence, from these results, it is clear that this *Lithocodium-Bacinella* event did not have regional implications but was only localized within a western margin of the Maestrat Basin (Galve sub-basin).

At first glance, this conclusion may appear to contradict the hypothesis put forward in the present study that several of the chemical and physical disturbances responsible for the formation of these encrusted levels investigated had a global significance. Nevertheless, the geological record constitutes clear evidence that global environmental change does not have the same expression everywhere and that the sedimentary results may vary depending on regional and local physico-chemical factors and on the biotic communities involved. In this respect, the occurrence of OAE1a coeval abundant large-sized flattened *Palorbitolina lenticularis* in other sub-basins of the Maestrat Basin can also be interpreted as records of environmental change. As mentioned previously, large-sized discoidal *Palorbitolina lenticularis* blooms have commonly been linked to elevated nutrient concentrations (e.g., Pittet et al., 2002) and therefore its presence is in accordance with the environmental hypotheses formulated above. Furthermore, the occurrence of large-sized *Palorbitolina lenticularis* displaying discoidal forms is also widespread throughout the encrusted coral rubble deposits from the Galve sub-basin. Therefore, this broad orbitolinid bloom, probably related to increased nutrient supplies, had a regional significance.

The reasons why these *Lithocodium-Bacinella* crusts only flourished in the Galve sub-basin and did not have a regional significance within the Maestrat Basin are difficult to ascertain from the sedimentary record. However, from the study of the OAE1a coeval strata in other areas of the Maestrat Basin, one thing is clear. During the time span studied, only the Galve sub-basin offered an important condition for the potential growth of these encrusting microproblematica: a hard substratum. Hence, the coral rubble carpets generated in the Galve sub-basin may have played a key role in providing a suitable habitat for the development of these two organisms of uncertain taxonomic position.

Throughout the margins of the Tethyan realm, *Lithocodium-Bacinella* events of Lower Aptian age have been reported in OAE1a coeval strata from Oman where, contrary to observations in the Galve sub-basin, the microproblematica formed by *Lithocodium aggregatum* and *Bacinella irregularis* exhibited sufficient growth potential to form buildups (Immenhauser et al., 2005; Rameil et al., in press). Although the *Lithocodium-Bacinella* buildups from Oman are coeval with the OAE1a, they are different in age to the *Lithocodium-Bacinella* event recorded in the Galve sub-basin. Immenhauser et al. (2005) reported two differentiated intervals with *Lithocodium-Bacinella* buildups correlatable with the global C-isotope cycle perturbations corresponding to the segments C5 and C6 of Menegatti et al. (1998). In the Galve sub-basin, the encrusted coral rubble horizon spans the upper part of segment C3 and the lower part of segment C4 (see Fig. 2.3.3). Consequently, the *Lithocodium-Bacinella* event recorded in the western Maestrat Basin, whilst coeval with the OAE1a, is younger than the *Lithocodium-Bacinella* buildups of Oman. Hence, and according to the data available in the literature so far, the *Lithocodium aggregatum* and *Bacinella irregularis* crusts developed in the Galve sub-basin during the Early Aptian did not have a global extent as well.

2.3.6 Conclusions

During the upper part of the *Deshayesites forbesi* ammonite biozone (Lower Aptian), the western Maestrat Basin recorded a singular horizon developed as a result of countless episodes of coral rubble generation, subsequently stabilized and rigidly bound by crusts bearing *Lithocodium aggregatum* Elliott and *Bacinella irregularis* Radoičić. The detailed study of this encrusted horizon and its sedimentological context has enabled an evaluation to be carried out of the diverse environmental factors and natural stresses of a regional and global significance that would have been responsible for giving rise to the coral rubble deposits analyzed and for the mass-occurrence of *Lithocodium-Bacinella* crusts.

The encrusted horizon investigated is coeval with the onset of the OAE1a, and its base is coincident with the acme of the Early Aptian global warming event that led to the OAE1a. Hence, owing to the location of the Maestrat Basin in tropical latitudes during the Aptian, it seems likely that highly recurrent hurricanes or severe tropical storms induced by these intensified greenhouse conditions would have razed extensive coral meadows, resulting in the formation of sub-basin-wide coral rubble carpets. In

addition, the consequent elevated seawater temperatures and ocean acidification linked to high atmospheric CO_2 levels would have also played a part in weakening and killing the coral populations, thus facilitating the formation of coral rubble.

As a consequence of the aforementioned warming event, the associated intensified rainfall enhanced weathering on the continents and increased runoff rates, resulting in significant terrigenous and carbonate and bicarbonate anion fluxes from hinterland to the sea, which in turn brought elevated nutrient concentrations and fluctuating alkalinities to the seawater (Weissert et al., 1998). These changes in the seawater chemistry, the consequent turbid conditions and elevated seawater temperatures, in combination with low sedimentation rates and the development of a sub-basin-wide hard substratum, would have favored the widespread occurrence of *Lithocodium-Bacinella* crusts, large-sized discoidal *Palorbitolina lenticularis* and bioeroders such as *Lithophaga* and endolithic sponges.

On the other hand, due to the strong extensional activity recorded in the Galve sub-basin during the Lower Aptian, these coral rubble deposits could also be the result, at least in part, of earthquake-induced disturbances. In spite of the fact that the tsunami origin of a deposit is difficult to demonstrate since tsunami-laid beds are subsequently reworked by storms and furthermore, both types of deposit usually show similar sedimentary characteristics when preserved seaward, this possibility cannot be discarded.

In essence, all these data seem to indicate a sedimentary record of the upper *Deshayesites forbesi* biozone in the western Maestrat Basin largely influenced by intensified greenhouse conditions, storm events, ocean acidification, elevated seawater temperatures, slow sedimentation rates and elevated CO_2 atmospheric concentration feedback mechanisms such as increased nutrient and alkalinity fluxes and organic carbon and carbonate burial. The latter would have induced a cooling trend throughout the OAE1a. Consequently, our observations indicate that these singular Lower Aptian encrusted coral rubble levels can be attributed to epeiric records of chemical and physical disturbances linked to the OAE1a.

Lastly, given that during the Lower Aptian, coral communities mainly flourished exhibiting loose growth fabrics in distal marly settings, together with the fact that the encrusted coral rubble horizon investigated also developed in outer environments sheltered from continuous water motion, these coral rubble deposits bound by

problematic encrusting microorganisms should not be seen in a strictly actualistic manner, although they do show some recent analogous traits.

2.3.7 Acknowledgements

The authors thank Hannes Löser, who contributed his expertise to the identification of the coral families, Peter W. Skelton and Eulàlia Gili for determining the rudist species, and Rolf Schroeder for identifying the orbitolinid species. This paper has benefited from the review provided by Klaus Bitzer. Richard Regner is warmly thanked for efficiently solving all the problems which arose during the preparation of this manuscript. Antoni Grauges is acknowledged for his enthusiastic help in the preparation of the polished slabs. Funding for this study came from the project Bi 1074/1-2 of the Deutsche Forschungsgemeinschaft, the I+D+i research projects: CGL2005-07445-CO3-01, CGL2008-04916 and CGL 2008-0809, the Consolider-Ingenio 2010 programme, under CSD 2006-0004 "Topo-Iberia", the Grup Consolidat de Recerca "Geologia Sedimentària" (2005SGR-00890), and the Departament d'Universitats, Recerca i Societat de la Informació de la Generalitat de Catalunya i del Fons Social Europeu.

2.3.8 References

Ando, A., Kaiho, K., Kawahata, H. and Kakegawa, T. (2008). Timing and magnitude of early Aptian extreme warming: Unraveling primary $\delta^{18}O$ variation in indurated pelagic carbonates at Deep Sea Drilling Project Site 463, central Pacific Ocean. Palaeogeography, Palaeoclimatology, Palaeoecology, 260, 463-476.

Babin, S.M., Carton, J.A., Dickey, T.D. and Wiggert, J.D. (2004) Satellite evidence of hurricane-induced phytoplankton blooms in an oceanic desert. Journal of Geophysical Research, 109, C03043, doi: 10.1029/2003JC001938.

Bertling, M. and Insalaco, E. (1998). Late Jurassic coral/microbial reefs from the northern Paris Basin—facies, palaeoecology and palaeobiogeography. Palaeogeography, Palaeoclimatology, Palaeoecology, 139, 139-175.

Blanchon, P. and Jones, B. (1997). Hurricane control on shelf-edge-reef architecture around Grand Cayman. Sedimentology, 44, 479-506.

Blanchon, P., Jones, B. and Kalbfleisch, W. (1997). Anatomy of a fringing reef around Gran Cayman: storm rubble, not coral framework. Journal of Sedimentary Research, 67, 1-16.

Blanchon, P. and Perry, C.T. (2004). Taphonomic differentiation of *Acropora palmata* facies in cores from Campeche Bank Reefs, Gulf of México. Sedimentology, 51, 53-76.

Bosellini, F.R. and Russo, A. (1992). Stratigraphy and Facies of an Oligocene Fringing Reef (Castro Limestone, Salento Peninsula, Southern Italy). Facies, 26, 145-166.

Bover-Arnal, T., Moreno-Bedmar, J.A., Salas, R., Skelton, P.W., Bitzer, K. and Gili, E. (under review). Sedimentary evolution of an Aptian syn-rift carbonate system (Maestrat Basin, E Spain): effects of accommodation and environmental change. Geologica Acta.

Bover-Arnal, T., Salas, R., Moreno-Bedmar, J.A. and Bitzer, K. (2009). Sequence stratigraphy and architecture of a late Early-Middle Aptian carbonate platform succession from the western Maestrat Basin (Iberian Chain, Spain). Sedimentary Geology, 219, 280-301.

Brachert, T.C. (1999). Non-skeletal Carbonate Production and Stromatolite Growth within a Pleistocene Deep Ocean (Last Glacial Maximum, Red Sea. Facies, 40, 211-228.

Bromley, R.G., Wisshak, M., Glaub, I. and Boutquelen, A. (2007). Ichnotaxonomic review of dendriniform borings attributed to foraminifera: *Semidendrina* igen. nov. In: Miller, W. (ed.). Trace Fossils: concepts, problems, prospects. Elsevier, Amsterdam, 508–520.

Brown, B.E., Dunne, R.P. and Chansang, H. (1996). Coral bleaching relative to elevated seawater temperature in the Andaman Sea (Indian Ocean) over the last 50 years. Coral Reefs, 15, 151-152.

Burla, S., Heimhofer, U., Hochuli, P.A., Weissert, H. and Skelton, P. (2008). Changes in sedimentary patterns of coastal and deep-sea successions from the North Atlantic (Portugal) linked to Early Cretaceous environmental change. Palaeogeography, Palaeoclimatology, Palaeoecology, 257, 38-57.

Camoin, G., Cabioch, G., Eisenhauer, A., Braga, J.-C., Hamelin, B. and Lericolais, G. (2006). Environmental significance of microbialites in reef environments during the last deglaciation. Sedimentary Geology, 185, 277-295.

Canérot, J., Cugny, P., Pardo, G., Salas, R. and Villena, J. (1982). Ibérica Central-Maestrazgo. In: García, A. (ed.). El Cretácico de España. Universidad Complutense de Madrid, 273-344.

Cherchi, A. and Schroeder, R. (2006). Remarks on the systematic position of *Lithocodium* Elliott, a problematic microorganism from the Mesozoic carbonate platforms of the Tethyan realm. Facies, 52, 435-440.

Conrad, M.A. and Clavel, B. (2008). A *Lithocodium* and *Bacinella* signature of a late Hauterivian, local microbial event: the Urgonian limestone in South-East France. Geologia Croatica, 61, 239-250.

De'ath, G., Lough, J.M. and Fabricius, K.E. (2009). Declining coral calcification on the Great Barrier Reef. Science, 323, 116-119.

Dumitrescu, M., Brassell, S.C., Schouten, S., Hopmans, E.C. and Sinninghe Damsté, J.S. (2006). Instability in tropical Pacific sea-surface temperatures during the early Aptian. Geology, 34, 833-836.

Dupraz, C. and Strasser, A. (2002). Nutritional Modes in Coral—Microbialite Reefs (Jurassic Oxfordian, Switzerland): Evolution of Trophic Structure as a Response to Environmental Change. Palaios, 17, 449-471.

Embry, A.F. and Klovan, J.E. (1971). A Late Devonian reef tract on northeastern Banks Island, N.W.T. Bulletin of Canadian Petroleum Geology, 19, 730-781.

Embry, J.C. (2005). Paléoécologie et architecture stratigraphique en haute résolution des platesformes carbonatées du Barrémien-Aptien de la Néo-Téthys (Espagne, Suisse, Provence, Vercors) – impact respectif des différents facteurs de contrôle. Unpublished Ph.D. thesis. Museum National d'Histoire Naturelle – Institut Français du Petrole, Paris, 299 p.

Erba, E. (1994). Nannofossils and superplumes: The early Aptian "nannofossil crisis". Paleoceanography, 9, 483-501.

Föllmi, K.B., Godet, A., Bodin, S. and Linder, P. (2006). Interactions between environmental change and shallow water carbonate buildup along the northern Tethyan margin and their impact on the Early Cretaceous carbon isotope record. Paleoceanography, 21, PA4211, doi:10.1029/2006PA001313.

Hallock, P. and Schlager, W. (1986). Nutrient Excess and the Demise of Coral reefs and Carbonate Platforms. Palaios, 1, 389-398.

Hillgärtner, H., van Buchem, F.S.P., Gaumet, F., Razin, P., Pittet, B., Grötsch, J. and Droste, H. (2003). The Barremian-Aptian evolution of the eastern Arabian carbonate platform margin (northern Oman). Journal of Sedimentary Research, 73, 756-773.

Heimhofer, U., Hochuli, P.A., Herrle, J.O., Andersen, N. and Weissert, H. (2004). Absence of major vegetation and palaeoatmospheric pCO_2 changes associated with oceanic anoxic event 1a (Early Aptian, SE France). Earth and Planetary Science Letters, 223, 303-318.

Helm, C. and Schülke, I. (2006). Patch reef development in the *florigemma*-Bank Member (Oxfordian) from the Deister Mts (NW Germany): a type example for Late Jurassic coral thrombolite thickets. Facies, 52, 441-467.

Hochuli, P.A., Menegatti, A.P., Weissert, H., Riva, A., Erba, E. and Premoli Silva, I. (1999). Episodes of high productivity and cooling in the early Aptian Alpine Tethys. Geology, 27, 657-660.

Hubbard, D.K. (1992). Hurricane-induced sediment transport in open-shelf tropical systems–An example from St. Croix, U.S. Virgin Islands. Journal of Sedimentary Petrology, 62, 946-960.

Hughes, T.P. (1999). Off-reef transport of coral fragments at Lizard Island, Australia. Marine Geology, 157, 1-6.

Immenhauser, A., Hillgärtner, H. and van Bentum, E. (2005). Microbial-foraminiferal episodes in the Early Aptian of the southern Tethyan margin, ecological significance and possible relation to oceanic anoxic event 1a. Sedimentology, 52, 77-99.

Immenhauser, A., Schlager, W., Burns, S.J., Scott, R.W., Geel, T., Lehmann, J., van der Gasst, S. and Bolder-Schrijver, L.J.A. (1999). Late Aptian to late Albian sea-level fluctuations constrained by geochemical and biological evidence (Nahr Umr Formation, Oman). Journal of Sedimentary Research, 69, 434-446.

Insalaco, E. (1996). Upper Jurassic microsolenid biostromes of northern and central Europe: Facies and depositional environment. Palaeogeography, Palaeoclimatology, Palaeoecology, 121, 169-194.

Kobluk, D.R. and Lysenko, M.A. (1992). Storm Features on a Southern Caribbean Fringing Coral Reef. Palaios, 7, 213-221.

Larson, R.L. and Erba, E. (1999). Onset of the mid-Cretaceous greenhouse in the Barremian-Aptian: Igneous events and the biological, sedimentary, and geochemical responses. Paleoceanography, 14, 663-678.

Leinfelder, R.R. (1992). A Modern-Type Kimmeridgian Reef (Ota Limestone, Portugal): Implications for Jurassic Reef Models. Facies, 26, 11-34.

Li, Y-X., Bralower, T.J., Montañez, I.P., Osleger, D.A., Arthur, M.A., Bice, D.M., Herbert, T.D., Erba, E. and Premoli Silva, I. (2008). Toward an orbital chronology for the early Aptian Oceanic Anoxic Event (OAE1a, ~120 Ma). Earth and Planetary Science Letters, 271, 88-100.

Méhay, S., Keller, C.E., Bernasconi, S.M., Weissert, H., Erba, E., Botín, C. and Hochuli, P.A. (2009). A volcanic CO_2 pulse triggered the Cretaceous Oceanic Anoxic Event 1a and a biocalcification crisis. Geology, 37, 819-822.

Menegatti, A.P., Weissert, H., Brown, R.S., Tyson, R.V., Farrimond, P., Strasser, A. and Caron, M. (1998). High-resolution $\delta^{13}C$ stratigraphy through the early Aptian "Livello Selli" of the Alpine Tethys. Paleoceanography, 13, 530-545.

Millán, M.I., Fernández-Mendiola, P.A. and García-Mondéjar, J. (2007). Pulsos de inundación marina en la terminación de una plataforma carbonatada (Aptiense inferior de Aralar, Cuenca Vasco-Cantábrica). Geogaceta, 41, 127-130.

Millán, M.I., Weissert, H.J., Fernández-Mendiola, P.A. and García-Mondéjar, J. (2009). Impact of Early Aptian carbon cycle perturbations on evolution of a marine shelf system in the Basque-Cantabrian Basin (Aralar, N Spain). Earth and Planetary Science Letters, 287, 392-401.

Moreno-Bedmar, J.A., Company, M., Bover-Arnal, T., Salas, R., Delanoy, G., Martínez, R. and Grauges, A. (2009). Biostratigraphic characterization by means of ammonoids of the lower Aptian Oceanic Anoxic Event (OAE1a) in the eastern Iberian Chain (Maestrat Basin, eastern Spain). Cretaceous Research, 30, 864-872.

Moreno-Bedmar, J.A., Company, M., Bover-Arnal, T., Salas, R., Maurrasse, F.J., Delanoy, G., Grauges, A. and Martínez, R. (accepted). Lower Aptian ammonite biostratigraphy in the Maestrat Basin (eastern Iberian chain, Spain). Geologica Acta.

Neuweiler, F. and Reitner, J. (1992). Karbonatbänke mit *Lithocodium aggregatum* ELLIOTT / *Bacinella irregularis* RADOICIC. Paläobathymetrie, Paläoökologie und stratigraphisches Äquivalent zu thrombolithischen Mud Mounds. Berliner geowiss. Abh., 3, 273–293.

Pearson, R.G. (1981). Recovery and recolonization of coral reefs. Marine Ecology Progress Series, 4, 105-122.

Perry, C.T. (2001). Storm-induced coral rubble deposition: Pleistocene records of natural reef disturbance and community response. Coral Reefs, 20, 171-183.

Pittet, B., Van Buchem, F.S.P., Hillgärtner, H., Razin, P., Grötsch, J. and Droste, H. (2002). Ecological succession, palaeoenvironmental change, and depositional sequences of Barremian-Aptian shallow-water carbonates in northern Oman. Sedimentology, 49, 555-581.

Pratt, B.R. and Bordonaro, O.L. (2007). Tsunamis in a stormy sea: Middle Cambrian inner-shelf limestones of western Argentina. Journal of Sedimentary Research, 77, 256-262.

Pringault, O., De Wit, R. and Camoin, G. (2004). Functioning of modern marine microbialites built by benthic cyanobacteria. Recent Research Development in Microbiology, 8, 1-16.

Rameil, N., Immenhauser, A., Warrlich, G., Hillgärtner, H. and Droste, H.J. (in press). Morphological patterns of Aptian *Lithocodium-Bacinella* geobodies–relation to environment and scale. Sedimentology.

Rasser, M.W. and Riegl, B. (2002). Holocene coral reef rubble and its binding agents. Coral Reefs, 21, 57-72.

Riding, R. (1991). Calcified Cyanobacteria. In: Riding, R. (ed.). Calcareous Algae and Stromatolites, Springer, Berlin, 55–87.

Riding, R. (2000). Microbial carbonates: the geological record of calcified bacterial-algal mats and biofilms. Sedimentology, 47 (Suppl. 1), 179-214.

Rogers, C.S. (1993). Hurricanes and coral reefs: the intermediate disturbance hypothesis revisited. Coral Reefs, 12, 127-137.

Salas, R. and Casas, A. (1993). Mesozoic extensional tectonics, stratigraphy, and crustal evolution during the Alpine cycle of the eastern Iberian basin. Tectonophysics, 228, 33-55.

Salas, R. and Guimerà, J. (1996). Rasgos estructurales principales de la cuenca cretácica inferior del Maestrazgo (Cordillera Ibérica oriental). Geogaceta, 20, 1704-1706.

Salas, R., Guimerà, J., Mas, R., Martín-Closas, C., Meléndez, A. and Alonso, A. (2001). Evolution of the Mesozoic Central Iberian Rift System and its Cainozoic inversion (Iberian Chain). In: Ziegler, P.A., Cavazza, W., Roberston, A.H.F. and Crasquin-Soleau, S. (eds.). Peri-Tethys Memoir 6: Peri-Tethyan Rift/Wrench Basins and Passive Margins. Mémoires du Muséum National d'Histoire Naturelle, 186, 145-186.

Samuel, O., Borza, K. and Köhler, E. (1972). Microfauna and Lithostratigraphy of the Paleogene and adjacent Cretaceous of the Middle Váh Valley (West Carpathians). Geologicky Ustav Dionyza Stura, Bratislava, 246 p.

Sandstrom, H. and Elliott, J.A. (1984). Internal tide and solitons on the Scotian Shelf: a nutrient pump at work. Journal of Geophysical Research, 89, 6415-6426.

Sattler, U., Immenhauser, A., Hillgärtner, H. and Esteban, M. (2005). Characterization, lateral variability and lateral extent of discontinuity surfaces on a Carbonate Platform (Barremian to Lower Aptian, Oman). Sedimentology, 52, 339-361.

Scoffin, T.P. and Hendry, M.D. (1984). Shallow-water sclerosponges on Jamaican reefs and a criterion for recognition of hurricane deposits. Nature, 307, 728-729.

Scoffin, T.P. (1993). The geological effects of hurricanes on coral reefs and the interpretation of storm deposits. Coral Reefs, 12, 203-221.

Scott, R.W. (1995). Global environmental controls on Cretaceous reefal ecosystems. Palaeogeography, Palaeoclimatology, Palaeoecology, 119, 187-199.

Segonzac, G. and Marin, P. (1972). *Lithocodium aggregatum* ELLIOTT et *Bacinella irregularis* RADOIČIĆ de l'Aptien de Teruel (Espagne): deux stades de croissance d'un seul et même organisme *incertae sedis*. Bulletin de la Société Géologique de France, 7/XIV, 331-336.

Skelton, P.W. (2003). The Cretaceous World. Cambridge University Press, Cambridge, 360 p.

Sprachta, S., Camoin, G., Golubic, S. and Le Campion, Th. (2001). Microbialites in a modern lagoonal environment: nature and distribution, Tikehau atoll (French Polynesia). Palaeogeography, Palaeoclimatology, Palaeoecology, 175, 103-124.

Taylor, P.D. and Wilson, M.A. (2003). Palaeoecology and evolution of marine hard substrates. Earth-Science Reviews, 62, 1-103.

Tejada, M.L.G., Suzuki, K., Kuroda, J., Coccioni, R., Mahoney, J.J., Ohkouchi, N., Sakamoto, T. and Tatsumi, Y. (2009). Ontong Java Plateau eruption as a trigger for the early Aptian oceanic anoxic event. Geology, 37, 855-858.

Tomás, S., Löser, H. and Salas, R. (2008). Low-light and nutrient-rich coral assemblages in an upper Aptian carbonate platform of the southern Maestrat Basin (Iberian Chain, eastern Spain). Cretaceous Research, 29, 509-534.

Védrine, S., Strasser, A. and Hug, W. (2007). Oncoid growth and distribution controlled by sea-level fluctuations and climate (Late Oxfordian, Swiss Jura Mountains). Facies, 53, 535-552.

Vennin, E. and Aurell, M. (2001). Stratigraphie séquentielle de l'Aptien du sous-bassin de Galvé (Province de Teruel, NE de l'Espagne). Bulletin de la Société Géologique de France, 172, 397-410.

Vogt, P.R. (1989), Volcanogenic upwelling of anoxic, nutrient-rich water: A possible factor in carbonate-bank/reef demise and benthic faunal extinctions? Geological Society of America Bulletin, 101, 1225-1245.

Weissert, H. and Lini, A. (1991). Ice Age Interludes During the Time of Cretaceous Greenhouse Climate? In: Müller, D.W., McKenzie, J.A. and Weissert, H. (eds.). Controversies in Modern Geology: Evolution of Geological Theories in Sedimentology, Earth History and Tectonics. Academic Press, London, 173-191.

Weissert, H., Lini, A., Föllmi, K.B. and Kuhn, O. (1998). Correlation of Early Cretaceous carbon isotope stratigraphy and platform drowning events: a possible link? Palaeogeography, Palaeoclimatology, Palaeoecology, 137, 189-203.

Weissert, H. and Erba, E. (2004). Volcanism, CO2 and palaeoclimate: a Late Jurassic-Early Cretaceous carbon and oxygen isotope record. Journal of the Geological Society, London, 161, 1-8.

Vilas, L., Masse, J.P. and Arias, C. (1995). *Orbitolina* episodes in carbonate platform evolution: the early Aptian model from SE Spain. Palaeogeography, Palaeoclimatology, Palaeoecology, 119, 35-45.

Wissler, L., Funk, H. and Weissert, H. (2003). Response of Early Cretaceous carbonate platforms to changes in atmospheric carbon dioxide levels. Palaeogeography, Palaeoclimatology, Palaeoecology, 200, 187-205.

Wolnaksi, E. and Deleersnijder, E. (1998). Island-generated internal waves at Scott Reef, Western Australia. Continental Shelf Research, 18, 1649-1666.

Woodley, J.D., Chornesky, E.A., Clifford, P.A., Jackson, J.B.C., Kaufman, L.S., Knowlton, N., Land, J.C., Pearson, M.P., Porter, J.W., Rooney, M.C., Rylaarsdam, K.W., Tunnicliffe, V.J., Wahle, C.M., Wulff, J.L., Curtis, A.S.G., Dallmeyer, M.D., Jupp, B.P., Koehl, M.A.R., Niegel, J. and Sides, E.M. (1981). Hurricane Allen's impact on Jamaican coral reefs. Science, 214, 749-755.

Zamagni, J., Kosir, A. and Mutti, M. (2009). The first microbialite – coral mounds in the Cenozoic (Uppermost Paleocene) from the Northern Tethys (Slovenia): Environmentally-triggered phase shifts preceding the PETM? Palaeogeography, Palaeoclimatology, Palaeoecology, 274, 1-17.

CHAPTER 3

GENERAL CONCLUSIONS

3.1 Conclusions

Through an analysis of the Aptian epicontinental sedimentary succession from the Galve sub-basin (western Maestrat Basin; Iberian Chain) it has been possible to trace the evolution and highlight the different regional and global factors that controlled the development of the mixed carbonate-siliciclastic system established during that time in this part of the northern Tethyan margin. The combination of facies analysis, sequence stratigraphy, carbon and oxygen isotopic data and quantitative subsidence analysis, together with an excellent age-calibration of the succession by means of geomagnetic polarity and ammonite and rudist biostratigraphy has been shown to be a successful procedure for providing a feasible and complete picture of the Aptian Stage and the evolution of the aforementioned depositional system which flourished in the Iberian margin of the Tethys. The main results and conclusions of this study include the following:

- The stratigraphic record of the logged sections can be subdivided into four transgressive-regressive (T-R) sequences reflecting long-term relative sea level changes: (i) Sequence I (lowermost Aptian); (ii) Sequence II (Lower Aptian); (iii) Sequence III (Middle Aptian); and (iv) Sequence IV (Middle-Upper Aptian). The transgressive systems tracts of these sequences are characterized by alternations of marls and limestones with abundant orbitolinids. The regressive systems tracts are mainly formed of wave- and tidally influenced siliciclastic and carbonate deposits, and platform carbonates with rudist bivalves, corals, orbitolinids and green algae.

- The carbonates and siliciclastics were deposited in homoclinal ramps, distally-steepened ramps and flat-topped non-rimmed platforms as follows: (i) homoclinal ramp (lowermost Aptian of the eastern and western sides of the Miravete fault); (ii) distally steepened ramp (Lower Aptian of the eastern side of the Miravete fault); and (iii) flat-

topped non-rimmed shelf (Lower Aptian of the western side of the Miravete fault). The evolution of the platform profiles was basically controlled by extensional faulting linked to the rifting and opening of the North Atlantic Ocean.

▪ Synrift subsidence was the most important mechanism providing accommodation during the Aptian evolution of this sedimentary system, although it failed to mask global eustatic trends. Consequently, the T-R sequences and relative sea level variations interpreted from the sedimentary succession analyzed are in accordance with the global sequences and inferred rises and falls of relative sea level recorded in other coeval Tethyan basins. In addition, the sedimentary record of the Galve sub-basin faithfully reflects the major environmental changes discussed in the literature for this time slice.

▪ The lower part of the Early Aptian was marked by a transgressive phase accompanied by the widespread occurrence of large-sized discoidal *Palorbitolina lenticularis*. This Early Aptian transgression is interpreted as being linked to the intensified greenhouse conditions and enhanced terrigenous influxes that may have led to the OAE1a.

▪ The expression of the OAE1a in the Galve sub-basin corresponds to a horizon of coral rubble encrusted by *Lithocodium aggregatum* and *Bacinella irregularis*, which lies within the upper part of the *Deshayesites forbesi* ammonite biozone (Lower Aptian). These encrusted coral rubble levels are regarded as records of chemical and physical disturbances connected to the OAE1a, such as high atmospheric CO_2 levels, elevated seawater temperatures, ocean acidification, severe storms, and feedback mechanisms to the aforementioned warming event such as increased nutrient fluxes, fluctuating seawater alkalinities and burial of carbon inventories.

▪ The late Early Aptian was characterized by a long-term progressive cooling episode, which was accompanied by a regressive phase distinguished by the establishment of a large carbonate platform with typical Urgonian biotic associations dominated by rudist bivalves and corals. During the latest Early Aptian a forced regression of relative sea level of glacio-eustatic magnitude exposed subaerially the carbonate platform developed during the late Early Aptian and induced the deposition of forced regressive calcarenitic wedges basinwards.

▪ The late Early-Middle Aptian stratigraphic record of the central part of the Galve sub-basin constitutes an outstanding example of the applicability of the four systems tract-based sequence stratigraphy to outcrop-scale carbonate successions. The resulting analysis demonstrates that the classic four systems tracts (Highstand Systems Tract, Forced Regressive Wedge Systems Tract, Lowstand Prograding Wedge Systems Tract and Transgressive Systems Tract) and their key bounding surfaces, even those with a conformable nature such as the basal surface of forced regression and the marine correlative conformity, can be successfully characterized not only at seismic-scale but also in outcrops.

▪ The time interval encompassed between the late Early Aptian and the Late Aptian was marked by a long-term regression of relative sea level, which ended with the installation of littoral conditions during the Late Aptian. The establishment of more proximal conditions in the Galve sub-basin was coupled with increased siliciclastic supply, which was probably linked to regional tectonics and to a progressively changing climate from a semi-arid regime during the Early Aptian, to semi-humid conditions in the Middle-Late Aptian.

In the light of these results, it may be concluded that the present study constitutes a well-documented example of a siliciclastic-influenced carbonate system of Aptian age controlled by both regional tectonic factors and global ocean-climate changes. Accordingly, this expanded and reasonably complete sedimentary succession with excellent age control provided by geomagnetic polarity and ammonoid and rudist biostratigraphic data has the potential to become a sedimentary record of reference for calibration of the Aptian Stage.

3.2 References

Allan, J.R. and Matthews, R.K. (1982). Isotope signatures associated with early meteoric diagenesis. Sedimentology, 29, 797-817.

Ando, A., Kaiho, K., Kawahata, H. and Kakegawa, T. (2008). Timing and magnitude of early Aptian extreme warming: Unraveling primary $\delta^{18}O$ variation in indurated

pelagic carbonates at Deep Sea Drilling Project Site 463, central Pacific Ocean. Palaeogeography, Palaeoclimatology, Palaeoecology, 260, 463-476.

Aurell, M. and Bádenas, B. (2004). Facies and depositional sequence evolution controlled by high-frequency sea-level changes in a shallow-water carbonate ramp (late Kimmeridgian, NE Spain). Geological Magazine, 141, 717-733.

Babin, S.M., Carton, J.A., Dickey, T.D. and Wiggert, J.D. (2004) Satellite evidence of hurricane-induced phytoplankton blooms in an oceanic desert. Journal of Geophysical Research, 109, C03043, doi: 10.1029/2003JC001938.

Bádenas, B., Salas, R. and Aurell, M. (2004). Three orders of regional sea-level changes control facies and stacking patterns of shallow platform carbonates in the Maestrat Basin (Tithonian-Berriasian, NE Spain). International Journal of Earth Sciences, 93, 144-162.

Bauer, J., Kuss, J. and Steuber, T. (2003). Sequence architecture and carbonate platform configuration (Late Cenomanian-Santonian), Sinai, Egypt. Sedimentology, 50, 387-414.

Bellanca, A., Erba, E., Neri, R., Premoli Silva, I., Sprovieri, M., Tremolada, F. and Verga, D. (2002). Palaeoceanographic significance of the Tethyan 'Livello Selli" (Early Aptian) from the Hybla Formation, northwestern Sicily: biostratigraphy and high-resolution chemostratigraphic records. Palaeogeography, Palaeoclimatology, Palaeoecology, 185, 175-196.

Bernaus, J.M., Arnaud-Vanneau, A. and Caus, E. (2003). Carbonate platform sequence stratigraphy in a rapidly subsiding area: the Late Barremian-Early Aptian of the Organyà basin, Spanish Pyrenees. Sedimentary Geology, 159, 177-201.

Bertling, M. and Insalaco, E. (1998). Late Jurassic coral/microbial reefs from the northern Paris Basin—facies, palaeoecology and palaeobiogeography. Palaeogeography, Palaeoclimatology, Palaeoecology, 139, 139-175.

Blanchon, P. and Jones, B. (1997). Hurricane control on shelf-edge-reef architecture around Grand Cayman. Sedimentology, 44, 479-506.

Blanchon, P., Jones, B. and Kalbfleisch, W. (1997). Anatomy of a fringing reef around Gran Cayman: storm rubble, not coral framework. Journal of Sedimentary Research, 67, 1-16.

Blanchon, P. and Perry, C.T. (2004). Taphonomic differentiation of *Acropora palmata* facies in cores from Campeche Bank Reefs, Gulf of México. Sedimentology, 51, 53-76.

Bogdanova, T.N. and Tovbina, S.Z. (1994). On development of the Aptian Ammonite zonal standard for the Mediterranean region. Géologie Alpine, Mémoire Hors Serie, 20, 51-59.

Bond, G.C. and Kominz, M.A. (1984). Construction of tectonic subsidence curves for the early Paleozoic miogeocline, southern Canadian Rocky Mountains: Implications for subsidence mechanisms, age of break-up, and crustal thinning. Geological Society of America Bulletin, 95, 155-173.

Booler, J. and Tucker, M.E. (2002). Distribution and geometry of facies and early diagenesis: the key to accommodation space variation and sequence stratigraphy: Upper Cretaceous Congost Carbonate platform, Spanish Pyrenees. Sedimentary Geology, 146, 226-247.

Borgomano, J.R.F. (2000). The Upper Cretaceous carbonates of the Gargano-Murge region, southern Italy: A model of platform-to-basin transition. The American Association of Petroleum Geologists Bulletin, 84, 1561-1588.

Bosellini, F.R. and Russo, A. (1992). Stratigraphy and Facies of an Oligocene Fringing Reef (Castro Limestone, Salento Peninsula, Southern Italy). Facies, 26, 145-166.

Bover-Arnal, T., Moreno-Bedmar, J.A., Salas, R. and Bitzer, K. (2008). Facies architecture of the late Early-Middle Aptian carbonate platform in the western Maestrat basin (Eastern Iberian Chain). Geo-Temas, 10, 115-118.

Bover-Arnal, T., Salas, R., Moreno-Bedmar, J.A., Bitzer, K., Skelton, P.W. and Gili, E. (2008). Two orders of sea-level changes controlled facies and architecture of late Early Aptian carbonate platform systems in the Maestrat Basin (eastern Iberian Chain, Spain). In: Kunkel, C., Hahn, S., ten Veen, J., Rameil, N. and Immenhauser, A. (eds.). SDGG, Heft 58 – Abstract Volume – 26th IAS Regional Meeting/SEPM-CES SEDIMENT 2008 - Bochum, p. 60.

Bover-Arnal, T., Salas, R., Moreno-Bedmar, J.A. and Bitzer, K. (2009). Sequence stratigraphy and architecture of a late Early-Middle Aptian carbonate platform succession from the western Maestrat Basin (Iberian Chain, Spain). Sedimentary Geology, 219, 280-301.

Bover-Arnal, T., Moreno-Bedmar, J.A., Salas, R., Skelton, P.W., Bitzer, K. and Gili, E. (under review). Sedimentary evolution of an Aptian syn-rift carbonate system (Maestrat Basin, E Spain): effects of accommodation and environmental change. Geologica Acta.

Bover-Arnal, T., Salas, R., Martín-Closas, C., Schlagintweit, F. and Moreno-Bedmar, J.A. (submitted for publication). Lower Aptian coral rubble deposits from the western Maestrat Basin (Iberian Chain, Spain): records of chemical and physical disturbances. Palaios.

Brachert, T.C. (1999). Non-skeletal Carbonate Production and Stromatolite Growth within a Pleistocene Deep Ocean (Last Glacial Maximum, Red Sea. Facies, 40, 211-228.

Bromley, R.G., Wisshak, M., Glaub, I. and Boutquelen, A. (2007). Ichnotaxonomic review of dendriniform borings attributed to foraminifera: *Semidendrina* igen. nov. In: Miller, W. (ed.). Trace Fossils: concepts, problems, prospects. Elsevier, Amsterdam, 508–520.

Brown, B.E., Dunne, R.P. and Chansang, H. (1996). Coral bleaching relative to elevated seawater temperature in the Andaman Sea (Indian Ocean) over the last 50 years. Coral Reefs, 15, 151-152.

Burla, S., Heimhofer, U., Hochuli, P.A., Weissert, H. and Skelton, P. (2008). Changes in sedimentary patterns of coastal and deep-sea successions from the North Atlantic (Portugal) linked to Early Cretaceous environmental change. Palaeogeography, Palaeoclimatology, Palaeoecology, 257, 38-57.

Camoin, G., Cabioch, G., Eisenhauer, A., Braga, J.-C., Hamelin, B. and Lericolais, G. (2006). Environmental significance of microbialites in reef environments during the last deglaciation. Sedimentary Geology, 185, 277-295.

Canérot, J., Crespo, A. and Navarro, D. (1979). Montalbán, hoja nº 518. Mapa Geológico de España 1:50.000. 2ª Serie. 1ª Edición. Servicio de Publicaciones, Ministerio de Industria y Energía, Madrid, 31 pp.

Canérot, J., Cugny, P., Pardo, G., Salas, R. and Villena, J. (1982). Ibérica Central-Maestrazgo. In: García, A. (ed.). El Cretácico de España. Universidad Complutense de Madrid, 273-344.

Catuneanu, O. (2006). Principles of Sequence Stratigraphy. Elsevier, New York, pp. 386.

Catuneanu, O., Abreu, V., Bhattacharya, J.P., Blum, M.D., Dalrymple, R.W., Eriksson, P.G., Fielding, C.R., Fisher, W.L., Galloway, W.E., Gibling, M.R., Giles, K.A., Holbrook, J.M., Jordan, R., Kendall, C.G.St.C., Macurda, B., Martinsen, O.J., Miall, A.D., Neal, J.E., Nummedal, D., Pomar, L., Posamentier, H.W., Pratt, B.R., Sarg, J.F., Shanley, K.W., Steel, R.J., Strasser, A., Tucker, M.E. and Winker, C. (2009). Towards the standardization of sequence stratigraphy. Earth-Science Reviews, 92, 1-33.

Cherchi, A. and Schroeder, R. (2006). Remarks on the systematic position of *Lithocodium* Elliott, a problematic microorganism from the Mesozoic carbonate platforms of the Tethyan realm. Facies, 52, 435-440.

Conrad, M.A. and Clavel, B. (2008). A *Lithocodium* and *Bacinella* signature of a late Hauterivian, local microbial event: the Urgonian limestone in South-East France. Geologia Croatica, 61, 239-250.

De'ath, G., Lough, J.M. and Fabricius, K.E. (2009). Declining coral calcification on the Great Barrier Reef. Science, 323, 116-119.

de Gea, G.A., Castro, J.M., Aguado, R., Ruiz-Ortiz, P.A. and Company, M. (2003). Lower Aptian carbon isotope stratigraphy from a distal carbonate shelf setting: the Cau section, Prebetic zone, SE Spain. Palaeogeography, Palaeoclimatology, Palaeoecology, 200, 207-219.

Drummond, C.N. and Wilkinson, B.H. (1993). Carbonate cycle stacking patterns and hierarchies of orbitally forced eustatic sealevel change. Journal of Sedimentary Petrology, 63, 369-377.

Drzewiecki, P.A. and (Toni) Simo, J.A. (2000). Tectonic, eustatic and environmental controls on mid-Cretaceous carbonate platform deposition, south-central Pyrenees, Spain. Sedimentology, 47, 471-495.

Dumitrescu, M., Brassell, S.C., Schouten, S., Hopmans, E.C. and Sinninghe Damsté, J.S. (2006). Instability in tropical Pacific sea-surface temperatures during the early Aptian. Geology, 34, 833-836.

Dupraz, C. and Strasser, A. (2002). Nutritional Modes in Coral—Microbialite Reefs (Jurassic Oxfordian, Switzerland): Evolution of Trophic Structure as a Response to Environmental Change. Palaios, 17, 449-471.

Embry, A.F. and Klovan, J.E. (1971). A Late Devonian reef tract on northeastern Banks Island, N.W.T. Bulletin of Canadian Petroleum Geology, 19, 730-781.

Embry, A.F. (1995). Sequence boundaries and sequence hierarchies: problems and proposals. In: Steel, R.J., Felt, V.L., Johannesson, E.P. and Mathieu, C. (eds.). Sequence Stratigraphy on the Northwest European Margin. Norwegian Petroleum Society Special Publication 5, 1-11.

Embry, J.C. (2005). Paléoécologie et architecture stratigraphique en haute résolution des platesformes carbonatées du Barrémien-Aptien de la Néo-Téthys (Espagne, Suisse, Provence, Vercors) – impact respectif des différents facteurs de contrôle. Doctoral thesis. Museum National d'Histoire Naturelle – Institut Français du Petrole, Paris, 299 pp.

Erba, E. (1994). Nannofossils and superplumes: The early Aptian "nannofossil crisis". Paleoceanography, 9, 483-501.

Föllmi, K.B., Weissert, H., Bisping, M. and Funk, H. (1994). Phosphogenesis, carbon-isotope stratigraphy, and carbonate-platform evolution along the Lower Cretaceous northern Tethyan margin. Geological Society of America Bulletin, 106, 729-746.

Föllmi, K.B., Godet, A., Bodin, S. and Linder, P. (2006). Interactions between environmental change and shallow water carbonate buildup along the northern Tethyan margin and their impact on the Early Cretaceous carbon isotope record. Paleoceanography, 21, PA4211, doi:10.1029/2006PA001313.

Frakes, L.A. and Francis, J.E. (1988). A guide to Phanerozoic cold polar climates from high-latitude ice-rafting in the Cretaceous. Nature, 333, 547-549.

Funk, H., Föllmi, K.B. and Mohr, H. (1993). Evolution of the Tithonian-Aptian Carbonate Platform Along the Northern Tethyan Margin, Eastern Helvetic Alps. In: Toni Simo, J.A., Scott, R.W. and Masse, J.P. (eds.). Cretaceous Carbonate Platforms. The American Association of Petroleum Geologists, Memoir 56, 387-407.

Gautier, F. (1980). Villarluengo, hoja nº 543. Mapa Geológico de España 1:50.000. 2ª Serie. 1ª Edición. Servicio de Publicaciones, Ministerio de Industria y Energía, Madrid, 45 pp.

Gil, J., García-Hidalgo, J.F., Segura, M., García, A. and Carenas, B. (2006). Stratigraphic architecture, palaeogeography and sea-level changes of a third order depositional sequence: The late Turonian–early Coniacian in the northern Iberian Ranges and Central System (Spain). Sedimentary Geology, 191, 191-225.

Gréselle, B. and Pittet, B. (2005). Fringing carbonate platforms at the Arabian Plate margin in northern Oman during the Late Aptian-Middle Albian: Evidence for high-amplitude sea-level changes. Sedimentary Geology, 175, 367-390.

Grötsch, J. (1996). Cycle stacking and long-term sea-level history in the Lower Cretaceous (Gavrovo platform, NW Greece). Journal of Sedimentary Research, 66, 723-736.

Grötsch, J., Billing, I. and Vahrenkamp, V. (1998). Carbon-isotope stratigraphy in shallow-water carbonates: implications for Cretaceous black-shale deposition. Sedimentology, 45, 623-634.

Hallock, P. and Schlager, W. (1986). Nutrient excess and the demise of coral reefs and carbonate platforms. Palaios, 1, 389-398.

Hardenbol, J., Thierry, J., Farley, M.B., Jacquin, T., de Graciansk, P.C. and Vail, P.R. (1998). Mesozoic and Cenozoic Sequence Chronostratigraphic Framework of European Basins. In: de Graciansk, P.C., Hardenbol, J., Jacquin, T. and Vail, P.R. (eds.). Mesozoic and Cenozoic Sequence Stratigraphy of European Basins, SEPM Special Publications 60, charts 1-8.

Heimhofer, U., Hochuli, P.A., Herrle, J.O., Andersen, N. and Weissert, H. (2004). Absence of major vegetation and palaeoatmospheric pCO_2 changes associated with oceanic anoxic event 1a (Early Aptian, SE France). Earth and Planetary Science Letters, 223, 303-318.

Helland-Hansen, W. and Gjelberg, J.G. (1994). Conceptual basis and variability in sequence stratigraphy: a different perspective. Sedimentary Geology, 92, 31-52.

Helm, C. and Schülke, I. (2006). Patch reef development in the *florigemma*-Bank Member (Oxfordian) from the Deister Mts (NW Germany): a type example for Late Jurassic coral thrombolite thickets. Facies, 52, 441-467.

Hillgärtner, H., Van Buchem, F.S.P., Gaumet, F., Razin, P., Pittet, B., Grötsch, J. and Droste, H. (2003). The Barremian-Aptian evolution of the eastern Arabian carbonate platform margin (northern Oman). Journal of Sedimentary Research, 73, 756-773.

Hochuli, P.A., Menegatti, A.P., Weissert, H., Riva, A., Erba, E. and Premoli Silva, I. (1999). Episodes of high productivity and cooling in the early Aptian Alpine Tethys. Geology, 27, 657-660.

Hubbard, D.K. (1992). Hurricane-induced sediment transport in open-shelf tropical systems–An example from St. Croix, U.S. Virgin Islands. Journal of Sedimentary Petrology, 62, 946-960.

Hughes, T.P. (1999). Off-reef transport of coral fragments at Lizard Island, Australia. Marine Geology, 157, 1-6.

Hunt, D. and Tucker, M.E. (1992). Stranded parasequences and the forced regressive wedge systems tract: deposition during base-level fall. Sedimentary Geology, 81, 1-9.

Hunt, D. and Tucker, M.E. (1993). The Middle Cretaceous Urgonian Platform of Southeastern France. In: Toni Simo, J.A., Scott, R.W. and Masse, J.P. (eds.). Cretaceous Carbonate Platforms. The American Association of Petroleum Geologists, Memoir 56, 409-453.

Hunt, D. and Tucker, M.E. (1993). Sequence stratigraphy of carbonate shelves with an example from the mid-Cretaceous (Urgonian) of southeast France. In: Posamentier, H.W., Summerhayes, C.P., Haq, B.U. and Allen, G.P. (eds.). Sequence Stratigraphy and Facies Associations. International Association of Sedimentologists, Special Publications 18, 307-341.

Hunt, D. and Tucker, M.E. (1995). Stranded parasequences and the forced regressive wedge systems tract: deposition during base-level fall—reply. Sedimentary Geology, 95, 147-160.

Husinec, A. and Jelaska, V. (2006). Relative sea-level changes recorded on an isolated carbonate platform: Tithonian to Cenomanian succession, Southern Croatia. Journal of Sedimentary Research, 76, 1120-1136.

Immenhauser, A., Schlager, W., Burns, S.J., Scott, R.W., Geel, T., Lehmann, J., van der Gasst, S. and Bolder-Schrijver, L.J.A. (1999). Late Aptian to late Albian sea-level fluctuations constrained by geochemical and biological evidence (Nahr Umr Formation, Oman). Journal of Sedimentary Research, 69, 434-446.

Immenhauser, A., Van der Kooij, B., Van Vliet, A., Schlager, W. and Scott, R.W. (2001). An ocean-facing Aptian-Albian carbonate margin, Oman. Sedimentology, 48, 1187-1207.

Immenhauser, A. (2005). High-rate sea-level change during the Mesozoic: New approaches to an old problem. Sedimentary Geology, 175, 277-296.

Immenhauser, A., Hillgärtner, H. and Van Bentum, E. (2005). Microbial-foraminiferal episodes in the Early Aptian of the southern Tethyan margin: ecological significance and possible relation to oceanic anoxic event 1a. Sedimentology, 52, 77-99.

Insalaco, E. (1996). Upper Jurassic microsolenid biostromes of northern and central Europe: Facies and depositional environment. Palaeogeography, Palaeoclimatology, Palaeoecology, 121, 169-194.

Jenkyns, H.C. (1995). Carbon-isotope stratigraphy and paleoceanographic significance of the Lower Cretaceous shallow-water carbonates of Resolution Guyot, Mid-Pacific Mountains. In: Winterer, E.L., Sager, W.W., Firth, J.V., Sinton, J.M. (eds.). Proceedings of the Ocean Drilling Program, Scientific Results, 143, 99-104.

Jenkyns, H.C. and Wilson, P.A. (1999). Stratigraphy, paleoceanography, and evolution of Cretaceous Pacific guyots: relics from a greenhouse Earth. American Journal of Science, 299, 341-392.

Kendall, C.G.St.C. and Schlager, W. (1981). Carbonates and relative changes in sea level. Marine Geology, 44, 181-212.

Kerans, C. (2002). Styles of Rudist Buildup Development along the Northern Margin of the Maverick Basin, Pecos River Canyon, Southwest Texas. Gulf Coast Association of Geological Societies Transactions, 52, 501-516.

Kindler, P. (1992). Coastal response to the Holocene transgression in the Bahamas: episodic sedimentation versus continuous sea-level rise. Sedimentary Geology, 80, 319-329.

Kobluk, D.R. and Lysenko, M.A. (1992). Storm Features on a Southern Caribbean Fringing Coral Reef. Palaios, 7, 213-221.

Kolla, V., Posamentier, H.W. and Eichenseer, H. (1995). Stranded parasequences and the forced regressive wedge systems tract: deposition during base-level fall—discussion. Sedimentary Geology, 95, 139-145.

Larson, R.L. (1991). Geological consequences of superplumes. Geology, 19, 963-966.

Larson, R.L. and Erba, E. (1999). Onset of the mid-Cretaceous greenhouse in the Barremian-Aptian: Igneous events and the biological, sedimentary, and geochemical responses. Paleoceanography, 14, 663-678.

Lehmann, C., Osleger, D.A. and Montañez, I.P. (1998). Controls on cyclostratigraphy of Lower Cretaceous carbonates and evaporites, Cupido and Coahuila platforms, northeastern Mexico. Journal of Sedimentary Research, 68, 1109-1130.

Leinfelder, R.R. (1992). A Modern-Type Kimmeridgian Reef (Ota Limestone, Portugal): Implications for Jurassic Reef Models. Facies, 26, 11-34.

Li, Y-X., Bralower, T.J., Montañez, I.P., Osleger, D.A., Arthur, M.A., Bice, D.M., Herbert, T.D., Erba, E. and Premoli Silva, I. (2008). Toward an orbital chronology for the early Aptian Oceanic Anoxic Event (OAE1a, ~120 Ma). Earth and Planetary Science Letters, 271, 88-100.

Liesa, C.L., Soria, A.R., Meléndez, N. and Meléndez, A. (2006). Extensional fault control on the sedimentation patterns in a continental rift basin: El Castellar Formation, Galve sub-basin, Spain. Journal of the Geological Society, London, 163, 487-498.

Malchus, N., Pons, J.M. and Salas, R. (1996). Rudist distribution in the lower Aptian shallow platform of la Mola de Xert, Eastern Iberian Range, NE Spain. Revista Mexicana de Ciencias Geológicas, 12, 224-235.

Marshall, J.D. (1992). Climatic and oceanographic isotopic signals from the carbonate rock record and their preservation. Geologic Magazine, 129, 143-160.

Masse, J.P. (1993). Valanginian-Early Aptian carbonate platforms from Provence, Southeastern France. In: Toni Simo, J.A., Scott, R.W. and Masse, J.P. (eds.). Cretaceous Carbonate Platforms. The American Association of Petroleum Geologists, Memoir 56, 363-374.

Masse, J.P., Borgomano, J. and Al Maskiry, S. (1998). A platform-to-basin transition for lower Aptian carbonates (Shuaiba Formation) of the northeastern Jebel Akhdar (Sultanate of Oman). Sedimentary Geology, 119, 297-309.

McKenzie, D. (1978). Some remarks on the development of sedimentary basins. Earth and Planetary Science Letters, 40, 25-32.

Méhay, S., Keller, C.E., Bernasconi, S.M., Weissert, H., Erba, E., Botín, C. and Hochuli, P.A. (2009). A volcanic CO_2 pulse triggered the Cretaceous Oceanic Anoxic Event 1a and a biocalcification crisis. Geology, 37, 819-822.

Menegatti, A.P., Weissert, H., Brown, R.S., Tyson, R.V., Farrimond, P., Strasser, A. and Caron, M. (1998). High-resolution $\delta^{13}C$ stratigraphy through the early Aptian "Livello Selli" of the Alpine Tethys. Paleoceanography, 13, 530-545.

Millán, M.I., Fernández-Mendiola, P.A. and García-Mondéjar, J. (2007). Pulsos de inundación marina en la terminación de una plataforma carbonatada (Aptiense inferior de Aralar, Cuenca Vasco-Cantábrica). Geogaceta, 41, 127-130.

Millán, M.I., Weissert, H.J., Fernández-Mendiola, P.A. and García-Mondéjar, J. (2009). Impact of Early Aptian carbon cycle perturbations on evolution of a marine shelf system in the Basque-Cantabrian Basin (Aralar, N Spain). Earth and Planetary Science Letters, 287, 392-401.

Miller, K.G., Wright, J.D. and Browning, J.V. (2005). Visions of ice sheets in a greenhouse world. Marine Geology, 217, 215-231.

Mitchum, Jr, R.M. and Van Wagoner, J.C. (1991). High-frequency sequences and their stacking patterns: sequence-stratigraphic evidence of high-frequency eustatic cycles. Sedimentary Geology, 70, 131-160.

Moullade, M., Kuhnt, W., Bergen, J.A., Masse, J.P. and Tronchetti, G. (1998). Correlation of biostratigraphic and stable isotope events in the Aptian historical stratotype of La Bédoule (Southeast France). Comptes-Rendus de l'Académie des Sciences, Paris, (II), 327, 693-698.

Moreno, J.A. and Bover, T. (2007). Precisiones sobre la edad, mediante ammonoideos, de la Fm. Margas del Forcall, Aptiense inferior, en la subcuenca de Galve (Teruel,

Espanya). In: Braga, J.C., Checa, A. and Company, M. (eds.). XXIII Jornadas de la Sociedad Española de Paleontología (Caravaca de la Cruz, 3-6 de Octubre de 2007), Libro de resúmenes. Instituto Geológico y Minero de España y Universidad de Granada, Granada, 151-152.

Moreno-Bedmar, J.A., Bulot, L., Latil, J.L., Martínez, R., Ferrer, O., Bover-Arnal, T. and Salas, R. (2008). Precisiones sobre la edad de la base de la Fm. Escucha, mediante ammonoideos, en la subcuenca de la Salzedella, Cuenca del Maestrat (E Cordillera Ibérica). Geo-Temas, 10, 1269-1272.

Moreno-Bedmar, J.A., Company, M., Bover-Arnal, T., Salas, R., Delanoy, G., Martínez, R. and Grauges, A. (2009). Biostratigraphic characterization by means of ammonoids of the lower Aptian Oceanic Anoxic Event (OAE1a) in the eastern Iberian Chain (Maestrat Basin, eastern Spain). Cretaceous Research, 30, 864-872.

Moreno-Bedmar, J.A., Company, M., Bover-Arnal, T., Salas, R., Delanoy, G., Maurrasse, F.J., Grauges, A. and Martínez, R. (accepted). Lower Aptian ammonite biostratigraphy in the Maestrat Basin (Eastern Iberian Chain, Spain). Geologica Acta.

Mutti, M. and Hallock, P. (2003). Carbonate systems along nutrient and temperature gradients: some sedimentological and geochemical constrains. International Journal of Earth Sciences, 92, 465-475.

Neuweiler, F. and Reitner, J. (1992). Karbonatbänke mit *Lithocodium aggregatum* ELLIOTT / *Bacinella irregularis* RADOICIC. Paläobathymetrie, Paläoökologie und stratigraphisches Äquivalent zu thrombolithischen Mud Mounds. Berliner geowiss. Abh., 3, 273–293.

Ogg, J.G. and Ogg, G. (2006). Updated by James G. Ogg (Purdue University) and Gabi Ogg to: GEOLOGIC TIME SCALE 2004 (Gradstein, F.M., Ogg, J.G., Smith, A.G. et al.; Cambridge University Press).

Patterson, W.P. and Walter, L.M. (1994). Depletion of ^{13}C in seawater ΣCO_2 on modern carbonate platforms: Significance for the carbon isotopic record of carbonates. Geology, 22, 885-888.

Pearson, R.G. (1981). Recovery and recolonization of coral reefs. Marine Ecology Progress Series, 4, 105-122.

Peropadre, C., Meléndez, N. and Liesa, C.L. (2008). Variaciones del nivel del mar registradas como valles incisos en la Formación Villarroya de los Pinares en la subcuenca de Galve (Teruel, Cordillera Ibérica). Geo-Temas, 10, 167-170.

Perry, C.T. (2001). Storm-induced coral rubble deposition: Pleistocene records of natural reef disturbance and community response. Coral Reefs, 20, 171-183.

Pittet, B., Strasser, A. and Mattioli, E. (2000). Depositional sequences in deep-shelf environments: a response to sea-level changes and shallow-platform carbonate productivity (Oxfordian, Germany and Spain). Journal of Sedimentary Research, 70, 392-407.

Pittet, B., Van Buchem, F.S.P., Hillgärtner, H., Razin, P., Grötsch, J. and Droste, H. (2002). Ecological succession, palaeoenvironmental change, and depositional sequences of Barremian-Aptian shallow-water carbonates in northern Oman. Sedimentology, 49, 555-581.

Plint, A.G. and Nummedal, D. (2000). The falling stage systems tract: recognition and importance in sequence stratigraphic analysis. Geological Society, London, Special Publications, 172, 1-17.

Pomar, L. (2001). Types of carbonate platforms: a genetic approach. Basin Research, 13, 313-334.

Pomar, L., Gili, E., Obrador, A. and Ward, W.C. (2005). Facies architecture and high-resolution sequence stratigraphy of an Upper Cretaceous platform margin

succession, southern central Pyrenees, Spain. Sedimentary Geology, 175, 339-365.

Pomar, L. and Kendall, C.G.St.C. (2007). Architecture of carbonate platforms: A response to hydrodynamics and evolving ecology. In: Lukasik, J., Simo, A. (eds.). Controls on Carbonate Platform and Reef Development. SEPM Special Publication, 89, 187-216.

Posamentier, H.W., Allen, G.P., James, D.P. and Tesson, M. (1992). Forced Regressions in a Sequence Stratigraphic Framework: Concepts, Examples, and Exploration Significance. The American Association of Petroleum Geologists Bulletin, 76, 1687-1709.

Pratt, B.R. and Bordonaro, O.L. (2007). Tsunamis in a stormy sea: Middle Cambrian inner-shelf limestones of western Argentina. Journal of Sedimentary Research, 77, 256-262.

Price, G.D. (1999). The evidence and implications of polar ice during the Mesozoic. Earth-Science Reviews, 48, 183-210.

Pringault, O., De Wit, R. and Camoin, G. (2004). Functioning of modern marine microbialites built by benthic cyanobacteria. Recent Research Development in Microbiology, 8, 1-16.

Rameil, N. (2005). Carbonate sedimentology, sequence stratigraphy, and cyclostratigraphy of the Tithonian in the Swiss and French Jura Mountains. A high-resolution record of changes in sea level and climate. Ph.D. Thesis, Université de Fribourg, Suisse, GeoFocus, 13, pp. 246.

Rameil, N., Immenhauser, A., Csoma, A.É. and Warrlich, G. (under review). Surfaces with a long history: The Aptian top Shu'aiba Formation unconformity, Sultanate of Oman. Sedimentology.

Rameil, N., Immenhauser, A., Warrlich, G., Hillgärtner, H. and Droste, H.J. (in press). Morphological patterns of Aptian *Lithocodium-Bacinella* geobodies–relation to environment and scale. Sedimentology.

Rasser, M.W. and Riegl, B. (2002). Holocene coral reef rubble and its binding agents. Coral Reefs, 21, 57-72.

Riding, R. (1991). Calcified Cyanobacteria. In: Riding, R. (ed.). Calcareous Algae and Stromatolites, Springer, Berlin, 55–87.

Riding, R. (2000). Microbial carbonates: the geological record of calcified bacterial-algal mats and biofilms. Sedimentology, 47 (Suppl. 1), 179-214.

Reboulet, S. and Klein, J. (reporters); Barragán, R., Company, M., González-Arreola, C., Lukeneder, A., Raisossadat, S.N., Sandoval, J., Szives, O., Tavera, J.M., Vašíček, Z. and Vermeulen, J. (in press). Report on the 3rd International Meeting of the IUGS Lower Cretaceous Ammonite Working Group, the "Kilian Group" (Vienna, Austria, 15th April 2008). Cretaceous Research, doi: 10.1016/j.cretres.2008.12.009.

Rogers, C.S. (1993). Hurricanes and coral reefs: the intermediate disturbance hypothesis revisited. Coral Reefs, 12, 127-137.

Rosales, I. (1999). Controls on carbonate-platform evolution on active fault blocks: the Lower Cretaceous Castro Urdiales platform (Aptian-Albian, northern Spain). Journal of Sedimentary Research, 69, 447-465.

Ruffell, A. and Worden, R. (2000). Palaeoclimate analysis using spectral gamma-ray data from the Aptian (Cretaceous) of southern England and southern France. Palaeogeography, Palaeoclimatology, Palaeoecology, 155, 265-283.

Sahagian, D., Pinous, O., Olferiev, A. and Zakharov, V. (1996). Eustatic curve for the Middle Jurassic-Cretaceous based on Russian Platform and Siberian stratigraphy: zonal resolution. AAPG Bulletin, 80, 1433-1458.

Salas, R. (1987). El Malm i el Cretaci inferior entre el Massís de Garraf i la Serra d'Espadà. Analisi de Conca. Doctoral thesis. Universitat de Barcelona, 345 pp.

Salas, R. and Casas, A. (1993). Mesozoic extensional tectonics, stratigraphy, and crustal evolution during the Alpine cycle of the eastern Iberian basin. Tectonophysics, 228, 33-55.

Salas, R. and Guimerà, J. (1996). Rasgos estructurales principales de la cuenca cretácica inferior del Maestrazgo (Cordillera Ibérica oriental). Geogaceta, 20, 1704-1706.

Salas, R., Guimerà, J., Mas, R., Martín-Closas, C., Meléndez, A. and Alonso, A. (2001). Evolution of the Mesozoic Central Iberian Rift System and its Cainozoic inversion (Iberian Chain). In: Ziegler, P.A., Cavazza, W., Roberston, A.H.F. and Crasquin-Soleau, S. (eds.). Peri-Tethys Memoir 6: Peri-Tethyan Rift/Wrench Basins and Passive Margins. Mémoires du Muséum National d'Histoire Naturelle, Paris, 186, 145-186.

Salas, R., Martín-Closas, C., Delclòs, X., Guimerà, J., Caja, M.A. and Mas, R. (2005). Factores principales de control de la sedimentación y los cambios bióticos durante el tránsito Jurásico-Cretácico en la Cadena Ibérica. Geogaceta, 38, 15-18.

Samuel, O., Borza, K. and Köhler, E. (1972). Microfauna and Lithostratigraphy of the Paleogene and adjacent Cretaceous of the Middle Váh Valley (West Carpathians). Geologicky Ustav Dionyza Stura, Bratislava, 246 p.

Sandstrom, H. and Elliott, J.A. (1984). Internal tide and solitons on the Scotian Shelf: a nutrient pump at work. Journal of Geophysical Research, 89, 6415-6426.

Sattler, U., Immenhauser, A., Hillgärtner, H. and Esteban, M. (2005). Characterization, lateral variability and lateral extent of discontinuity surfaces on a Carbonate Platform (Barremian to Lower Aptian, Oman). Sedimentology, 52, 339-361.

Sarg, J.F. (1988). Carbonate sequence stratigraphy. In: Wilgus, C.K., Hastings, B.S., Kendall, C.G.St.C., Posamentier, H.W., Ross, C.A. and Van Wagoner, J.C. (eds.). Sea level changes: an integrated approach. SEPM, Special Publication 42, 155-181.

Schmoker, J.W. and Halley, R.B. (1982). Carbonate porosity versus depth: a predictable relation for south Florida. AAPG Bulletin, 66, 2561-2570.

Scholle, P.A. and Arthur, M.A. (1980). Carbone isotope fluctuations in Cretaceous pelagic limestones: potential stratigraphic and petroleum exploration tool. AAPG Bulletin, 64, 67-87.

Sclater, J.G. and Christie, P.A.F. (1980). Continental stretching: an explanation of the post-mid-Cretaceous subsidence of the central North Sea Basin. Journal of Geophysical Research, 85, 3711-3739.

Scoffin, T.P. and Hendry, M.D. (1984). Shallow-water sclerosponges on Jamaican reefs and a criterion for recognition of hurricane deposits. Nature, 307, 728-729.

Scoffin, T.P. (1993). The geological effects of hurricanes on coral reefs and the interpretation of storm deposits. Coral Reefs, 12, 203-221.

Scott, R.W. (1995). Global environmental controls on Cretaceous reefal ecosystems. Palaeogeography, Palaeoclimatology, Palaeoecology, 119, 187-199.

Segonzac, G. and Marin, P. (1972). *Lithocodium aggregatum* ELLIOTT et *Bacinella irregularis* RADOIČIĆ de l'Aptien de Teruel (Espagne): deux stades de croissance d'un seul et même organisme *incertae sedis*. Bulletin de la Société Géologique de France, 7/XIV, 331-336.

Simón, J.L., Liesa, C.L. and Soria, A.R. (1998). Un sistema de fallas normales sinsedimentarias en las unidades de facies Urgon de Aliaga. Geogaceta, 24, 291-294.

Skelton, P.W. and Masse. J.-P. (2000). Synoptic guide to the Lower Cretaceous rudist bivalves of Arabia. In: Alsharhan, A.S. and Scott, R.W. (eds.). Middle East Models of Jurassic/Cretaceous Carbonate Systems. SEPM, Special Publication 69, 89-99.

Skelton, P.W. (2003). The Cretaceous World. Cambridge University Press, Cambridge, pp. 360.

Skelton, P.W. (2003). Rudist evolution and extinction - a north African perspective. In: Gili, E., Negra, M. and Skelton, P.W. (eds.). North African Cretaceous Carbonate Platform Systems. NATO Science Series IV, Earth and Environmental Sciences 28, Kluwer Academic Publishers, 215-227.

Skelton, P.W., Gili, E., Bover-Arnal, T., Salas, R., Moreno-Bedmar, J.A., Millán, I. and Fernández-Mendiola, K. (2008). Taxonomic turnover and palaeoecological change among Aptian rudists: and Iberian case study. In: Kunkel, C., Hahn, S., ten Veen, J., Rameil, N. and Immenhauser, A. (eds.). SDGG, Heft 58 – Abstract Volume – 26th IAS Regional Meeting/SEPM-CES SEDIMENT 2008 - Bochum, p. 254.

Skelton, P.W., Gili, E., Bover-Arnal, T., Salas, R. and Moreno-Bedmar, J.A. (2008). A new species of *Polyconites* from the uppermost Lower Aptian of Spain. Eighth International Congress on Rudists. Izmir, Turkey, Abstracts, p. 53.

Skelton, P.W., Gili, E., Bover-Arnal, T., Salas, R. and Moreno-Bedmar, J.A. (in press). A new species of Polyconites from the Lower Aptian of Iberia and the early evolution of polyconitid rudists. Turkish Journal of Earth Sciences.

Soria, A.R. (1997). La sedimentación en las cuencas marginales del surco Ibérico durante el Cretácico inferior y su control estructural. Doctoral thesis. Universidad de Zaragoza, 363 pp.

Spence, G.H. and Tucker, M.E. (2007). A proposed integrated multi-signature model for peritidal cycles in carbonates. Journal of Sedimentary Research, 77, 797-808.

Sprachta, S., Camoin, G., Golubic, S. and Le Campion, Th. (2001). Microbialites in a modern lagoonal environment: nature and distribution, Tikehau atoll (French Polynesia). Palaeogeography, Palaeoclimatology, Palaeoecology, 175, 103-124.

Steuber, T., Rauch, M., Masse, J.-P., Graaf, J. and Malkoc, M. (2005). Low-latitude seasonality of Cretaceous temperatures in warm and cold episodes. Nature, 437, 1341-1344.

Stoll, H.M. and Schrag, D.P. (1996). Evidence for glacial control of rapid sea level changes in the Early Cretaceous. Science, 272, 1771-1774.

Strasser, A., Pittet, B., Hillgärtner, H. and Pasquier, J-B. (1999). Depositional sequences in shallow carbonate-dominated sedimentary systems: concepts for a high-resolution analysis. Sedimentary Geology, 128, 201-221.

Taylor, P.D. and Wilson, M.A. (2003). Palaeoecology and evolution of marine hard substrates. Earth-Science Reviews, 62, 1-103.

Tejada, M.L.G., Suzuki, K., Kuroda, J., Coccioni, R., Mahoney, J.J., Ohkouchi, N., Sakamoto, T. and Tatsumi, Y. (2009). Ontong Java Plateau eruption as a trigger for the early Aptian oceanic anoxic event. Geology, 37, 855-858.

Thrana, C. and Talbot, M.R. (2006). High-frequency carbonate-siliciclastic cycles in the Miocene of the Lorca Basin (Western Mediterranean, SE Spain). Geologica Acta, 4, 343-354.

Tomás, S. (2007). El sistema arrecifal Aptiense inferior del sector suroriental de la cuenca del Maestrat (Cadena Ibérica). Ph.D. Thesis, Universitat de Barcelona, Barcelona, pp. 192.

Tomás, S., Comas Nebot, M. and Salas, R. (2007). La plataforma carbonatada Aptiense superior de Benicàssim-Orpesa (Cuenca del Maestrat, Cadena Ibérica): modelo de depósito. Geogaceta, 41, 235-238.

Tomás, S., Löser, H. and Salas, R. (2008). Low-light and nutrient-rich coral assemblages in an Upper Aptian carbonate platform of the southern Maestrat Basin (Iberian Chain, eastern Spain). Cretaceous Research, 29, 509-534.

Vahrenkamp, V.C. (1996). Carbon isotope stratigraphy of the upper Kharaib and Shuaiba Formations: implications for the Early Cretaceous evolution of the Arabian Gulf region. AAPG Bulletin, 80, 647-662.

Van Wagoner, J.C., Posamentier, H.W., Mitchum, R.M., Vail, P.R., Sarg, J.F., Loutit, T.S. and Hardenbol, J. (1988). An overview of the fundamentals of sequence stratigraphy and key definitions. In: Wilgus, C.K., Hastings, B.S., Kendall, C.G.St.C., Posamentier, H.W., Ross, C.A. and Van Wagoner, J.C. (eds.). Sea level changes: an integrated approach. SEPM, Special Publication, 42, 39-45.

Vail, P.R., Audemard, F., Bowman, S.A., Eisner, P.N. and Perez-Cruz, C., (1991). The Stratigraphic Signatures of Tectonics, Eustasy and Sedimentology – an Overview. In: Einsele, G., Ricken, W. and Seilacher, A. (eds.). Cycles and Events in Stratigraphy. Springer-Verlag Berlin Heidelberg 1991, 617-659.

Védrine, S., Strasser, A. and Hug, W. (2007). Oncoid growth and distribution controlled by sea-level fluctuations and climate (Late Oxfordian, Swiss Jura Mountains). Facies, 53, 535-552.

Vennin, E. and Aurell, M. (2001). Stratigraphie séquentielle de l'Aptien du sous-bassin de Galvé (Province de Teruel, NE de l'Espagne). Bulletin de la Société Géologique de France, 172, 397-410.

Vilas, L., Masse, J.-P. and Arias, C. (1993). Aptian Mixed Terrigenous and Carbonate Platforms from Iberic and Prebetic Regions, Spain. In: Toni Simo, J.A., Scott, R.W. and Masse, J.P. (eds.). Cretaceous Carbonate Platforms. The American Association of Petroleum Geologists, Memoir 56, 243-253.

Vilas, L., Masse, J.P. and Arias, C. (1995). *Orbitolina* episodes in carbonate platform evolution: the early Aptian model from SE Spain. Palaeogeography, Palaeoclimatology, Palaeoecology, 119, 35-45.

Vilas, L., Martín-Chivelet, J. and Arias, C. (2003). Integration of subsidence and sequence stratigraphic analyses in the Cretaceous carbonate platforms of the Prebetic (Jumilla-Yecla Region), Spain. Palaeogeography, Palaeoclimatology, Palaeoecology, 200, 107-129.

Villanueva-Amadoz, U., Pons, D., Diez, J.B., Sender, L.M. and Ferrer, J. (2008). Registro de granos de polen de angiospermas durante el Albiense-Cenomaniense en el NE de España. In: Ruiz-Omeñaca, J.I., Piñuela, L. and García-Ramos, J.C. (eds.). Libro de resúmenes. XXIV Jornadas de la Sociedad Española de Paleontología, Museo del Jurásico de Asturias (MUJA), Colunga, 15-18 de octubre de 2008, 219-220.

Vogt, P.R. (1989), Volcanogenic upwelling of anoxic, nutrient-rich water: A possible factor in carbonate-bank/reef demise and benthic faunal extinctions? Geological Society of America Bulletin, 101, 1225-1245.

Watts, A.B. (1981). The U.S. Atlantic continental margin: subsidence history, crustal structure and thermal evolution. In: Bally, A.W., Watts, A.B., Grow, J.A., Manspeizer, W., Bernoulli, D., Schreiber, C. and Hunt, J.M. (eds.). Geology of passive continental margins: history, structure and sedimentologic record (with special emphasis on the Atlantic margin). AAPG, Education Course Note Series, 19, Ch. 2, 24pp.

Weisser, D. (1959). Acerca de la estratigrafía del Urgo-Aptense en las cadenas Celtibéricas de España. Notas y comunicaciones del Instituto Geológico y Minero de España, 55, 17-32.

Weissert, H. and Lini, A. (1991). Ice age interludes during the time of Cretaceous greenhouse climate? In: Müller, D.W., McKenzie, J.A. and Weissert, H. (eds.).

Controversies in Modern Geology: Evolution of Geological Theories in Sedimentology, Earth History and Tectonics. Academic Press, 173-191.

Weissert, H., Lini, A., Föllmi, K.B. and Kuhn, O. (1998). Correlation of Early Cretaceous carbon isotope stratigraphy and platform drowning events: a possible link? Palaeogeography, Palaeoclimatology, Palaeoecology, 137, 189-203.

Weissert, H. and Erba, E. (2004). Volcanism, CO2 and palaeoclimate: a Late Jurassic-Early Cretaceous carbon and oxygen isotope record. Journal of the Geological Society, London, 161, 1-8.

Wissler, L., Funk, H. and Weissert, H. (2003). Response of Early Cretaceous carbonate platforms to changes in atmospheric carbon dioxide levels. Palaeogeography, Palaeoclimatology, Palaeoecology, 200, 187-205.

Wolnaksi, E. and Deleersnijder, E. (1998). Island-generated internal waves at Scott Reef, Western Australia. Continental Shelf Research, 18, 1649-1666.

Woodley, J.D., Chornesky, E.A., Clifford, P.A., Jackson, J.B.C., Kaufman, L.S., Knowlton, N., Land, J.C., Pearson, M.P., Porter, J.W., Rooney, M.C., Rylaarsdam, K.W., Tunnicliffe, V.J., Wahle, C.M., Wulff, J.L., Curtis, A.S.G., Dallmeyer, M.D., Jupp, B.P., Koehl, M.A.R., Niegel, J. and Sides, E.M. (1981). Hurricane Allen's impact on Jamaican coral reefs. Science, 214, 749-755.

Yose, L.A., Ruf, A.S., Strohmenger, C.J., Schuelke, J.S., Gombos, A., Al-Hosani, I., Al-Maskary, S., Bloch, G., Al-Mehairi, Y. and Johnson, I.G. (2006). Three-dimensional characterization of a heterogeneous carbonate reservoir, Lower Cretaceous, Abu Dhabi (United Arab Emirates). In: Harris, P.M. and Weber, L.J. (eds.). Giant hydrocarbon reservoirs of the world: From rocks to reservoir characterization and modeling. AAPG Memoir 88/SEPM, Special Publication, 173-212.

Zamagni, J., Kosir, A. and Mutti, M. (2009). The first microbialite – coral mounds in the Cenozoic (Uppermost Paleocene) from the Northern Tethys (Slovenia):

Environmentally-triggered phase shifts preceding the PETM? Palaeogeography, Palaeoclimatology, Palaeoecology, 274, 1-17.

Zagrarni, M.F., Negra, M.H. and Hanini, A. (2008). Cenomanian–Turonian facies and sequence stratigraphy, Bahloul Formation, Tunisia. Sedimentary Geology, 204, 18-35.

List of figures

Figure 1.1. Location and geological map of the study area. A) Geographical location of the study area in the western Maestrat Basin (eastern Iberian Chain; E Iberia). B) Map of the Maestrat Basin with the location of the Galve sub-basin, which is marked by a red star, in its western marginal part. C) Geological setting and location of the studied outcrops in the Galve sub-basin. Modified after Canérot et al. (1979) and Gautier (1980). 3

Figure 2.1.1. A) Geographical location of the study area in the eastern Iberian Chain (E-Spain). B) Geological setting and location of the studied outcrops. Modified after Canérot et al. (1979) and Gautier (1980). 20

Figure 2.1.2. Stratigraphic framework and age relationships for the Aptian in the Galve sub-basin. Identified ammonite biozones are indicated in grey (Weisser, 1959; Moreno-Bedmar et al., 2009, accepted). Discontinuous lines indicate lack of absolute dating. Absolute ages are from Ogg and Ogg (2006). Modified from Bover-Arnal et al. (2009). 21

Figure 2.1.3. Photomicrographs of representative microfacies of the different general depositional settings. Scale bars = 1 mm. A) Wackestone of miliolids (white arrows) and fragments of dasycladaceans (black arrows) (Facies Assemblage 4; Table 2.1.1). Xert Formation, Alto del Collado section. B) Floatstone of Chondrodonta with Orbitolinopsis praesimplex. The white arrow points to a fragment of Chondrodonta (Facies Assemblage 4; Table 2.1.1). Xert Formation, Las Cubetas section. C) Lithocodium aggregatum (white arrows) bioeroded by clionid sponges, encrusting coral debris (black C) (Facies Assemblage 9; Table 2.1.1). Forcall Formation, Estrecho de la Calzada Vieja section. D) Grainstone of large-sized discoidal Palorbitolina lenticularis agglutinating quartz particles in the tests (Facies Assemblage 7; Table 2.1.1). Villarroya de los Pinares Formation, Las Cubetas section. E) Peloidal-foraminiferal (mostly miliolids) grainstone (Facies Assemblage 3; Table 2.1.1). Villarroya de los Pinares Formation, Barranco de las Calzadas section. F) Debris-flow facies of coral fragments (white C) and other unidentified bioclasts encrusted by peyssonneliaceans (white arrows) (Facies Assemblage 10; Table 2.1.1). Villarroya de los Pinares Formation, Barranco de las Calzadas section. 25

Figure 2.1.4. Outcrop photographs of representative facies of the general depositional settings. A) Detail of a coarse-grained siliciclastic lag at the erosive base of a channelized sandstone (Facies Assemblage 1; Table 2.1.1). Morella Formation, Barranco de las Calzadas section. B) Dome-shaped corals embedded in marls (Facies Assemblage 6; Table 2.1.1). Villarroya de los Pinares Formation, Barranco de las Calzadas section. C) Detail of a Caprina parvula section (Facies Assemblage 4; Table 2.1.1). Villarroya de los Pinares Formation, Barranco de las Calzadas section. D) Outcrop-scale image of debris-flow deposits (Facies Assemblage 10; Table 2.1.1). Note the nodular aspect of these resedimented lithofacies. Villarroya de los Pinares Formation, Barranco de las Calzadas section. E) Detail of the boundary surface between Sequence II and Sequence III exhibiting palaeokarst development. Villarroya de los Pinares

Formation, Camarillas section. F) Detail of a herringbone cross-stratification (Facies Assemblage 2; Table 2.1.1). Benassal Formation, Barranco del Portolés section. 26

Figure 2.1.5. Eastern side sequence correlation scheme and distribution of the facies assemblages. 31

Figure 2.1.6. Western side sequence correlation scheme and distribution of the facies assemblages. Identified ammonite biozones are indicated in grey. See Fig. 2.1.5 for legend. 32

Figure 2.1.7. Sequence stratigraphic interpretation of the Aptian sedimentary succession in the Las Cubetas section (eastern side of the Miravete fault) (A) and the Villarroya de los Pinares section (western side of the Miravete fault) (B). See Fig. 2.1.5 for legend. 35

Figure 2.1.8. A) Aerial photograph of the area surrounding the Cabezo de las Hoyas section (see Fig. 2.1.1B for location), which belongs to the eastern side of the Miravete fault. B) Interpreted aerial photograph with the situation of the major ramp step located southwards of the Cabezo de las Hoyas section. C) Schematic cross-section of the eastern side distally steepened ramp of Sequence II showing the situation of the two steps located nearby to the south of the Cabezo de las Hoyas section and southwards of the Estrecho de la Calzada Vieja section. The depositional profile was reconstructed from the aerial photo. See Fig. 2.1.1B for situation. 36

Figure 2.1.9. A) Outcrop-scale view of the boundary between Sequence II (Early Aptian) and Sequence III (Middle Aptian) located southwards of the Camarillas section (western side of the Miravete fault). B) Photograph interpretation of the boundary between Sequence II (Early Aptian) and Sequence III (Middle Aptian) located southwards of the Camarillas section (western side of the Miravete fault). See Fig. 2.1.5 for legend. 42

Figure 2.1.10. Detailed section log from Barranco de las Calzadas, featuring carbon- and oxygen-isotope curves, the situation of the OAE1a interval (indicated in grey), and the collected ammonite taxa. Segments C1-C8 and O1-O7 indicate $\delta^{13}C$ *and* $\delta^{18}O$ *trends, respectively. Refer to text for detailed discussion.* 45

Figure 2.1.11. Left figure: Schematic tectonic map of the Galve sub-basin showing the situation of the different sections used in the quantitative subsidence analysis. Right figure: Decompacted total subsidence curves corrected for palaeobathymetries representing total accommodation. The average bathymetry curve is also indicated. Absolute ages are from Ogg and Ogg (2006). R/S: Stage of rapid/slow total subsidence. R: Stage of rapid total subsidence. 47

Figure 2.1.12 Photograph of the lower part of the Villarroya de los Pinares section showing an array of synsedimentary normal faults affecting Sequence I and the TST of Sequence II (Xert and Forcall formations). See Fig. 2.1.5 for legend. 48

Figure 2.1.13. Cross-plot of $\delta^{13}C$ and $\delta^{18}O$ results. The low covariance between $\delta^{13}C$ and $\delta^{18}O$ ($R^2 = 0.0789$) indicates lack of significant diagenetic overprint. 49

Figure 2.1.14. Comparison chart between the Aptian sequence chronostratigraphy according to Ogg and Ogg (2006), and the Aptian evolution of the Galve sub-basin, with the large-scale T-R sequences, stacking patterns, relative sea level curve, situation of the OAE1a, average accommodation, terrigenous inputs and biotic changes. 56

Figure 2.2.1. Geological map of the central Galve sub-basin with its location inside the Iberian Peninsula. The areas studied are marked with a star. Modified after Gautier (1980). 80

Figure 2.2.2. Aptian lithostratigraphy of the central part of the Galve sub-basin. The ammonite biozones identified are dashed in grey (Moreno and Bover 2007; Bover-Arnal et al. under review). Absolute ages are based on Ogg and Ogg (2006). 81

Figure 2.2.3. Sedimentary facies: a) Argillaceous-marly wackestone rich in orbitolines. White arrows point to specimens of Orbitolina. Facies Association I. Las Mingachas (see Fig. 2.2.7 for exact location). b) Floatstone of rudists and corals. Note the massive aspect of the lithofacies. White arrows point to delicate branching corals in growth position. Facies Association II. Las Mingachas (see Fig. 2.2.7 for exact location). c) Rudist and coral reworked floatstone-rudstone. Note the nodular aspect of the lithofacies. White arrows point to specimens of Toucasia carinata. Facies Association III. Camarillas. d) Photomicrograph of peloidal and bioclastic packstone-grainstone microfacies. Note the presence of a small nerineid gastropod at the centre of the image. Facies Association IV. El Morrón. e) Photomicrograph of sandy limestones microfacies. Note the presence of quartz (Q) particles and ooids. Facies Association V. Camarillas. f) Plane-parallel stratified calcarenite rich in oysters. Hammer encircled for scale. Facies Association VI. Camarillas. 83

Figure 2.2.4. Sedimentary facies (see Fig. 2.2.7 for exact location): a) Flattened dome-shaped coral colony embedded in marls. Facies Association VII. Las Mingachas. b) Dufrenoyia dufrenoyi ammonite specimen. Facies Association VIII. Las Mingachas. c) Large Thalassinoides bioturbation at the base of a storm-induced turbidite. Note the marly sediments at the lower part of the photograph. Facies Association VIII. Las Mingachas. d) Photomicrograph of the slightly cross-bedded calcarenite wedge microfacies. White arrows point to specimens of Orbitolinopsis simplex. Facies Association IX. Las Mingachas. e) Outcrop photograph of the debris-flow deposits. Note the nodular and chaotic aspect of the lithofacies. Facies Association X. Las Mingachas. f) Photomicrograph of debris-flow microfacies. Note the presence of rudist (r) and coral (c) fragments. Facies Association X. Las Mingachas. 84

Figure 2.2.5. Simplified scheme of the late Early Aptian platform-to-basin cross-section studied with the measured section logs (see Fig. 2.2.1 for location) and the idealized elementary sequences (parasequences) identified within each setting. 90

Figure 2.2.6. Photograph of platform-to-basin transition at Las Mingachas (A) (see Fig. 2.2.1 for location) with the overall sequence stratigraphic interpretation (B) and the stages of relative sea-level. 94

Figure 2.2.7. Photograph of Las Mingachas area (see Fig. 2.2.1 for location) displaying the situation of the outcrops and photomicrographs showed in the figures 2.2.3 (a-b), 2.2.4 (a-f), 2.2.8, 2.2.9, 2.2.10, 2.2.11, 2.2.12 (a-b, d-f), 2.2.14, 2.2.15, 2.2.16, 2.2.17, 2.2.18 and 2.2.19. 94

Figure 2.2.8. Photograph of an oblique cross-section from the northeastern part of Las Mingachas (A) (see Fig. 2.2.7 for location) showing the sequence stratigraphic interpretation and the shelf-margin geometries, which clearly differentiate the platform, platform-margin, slope and basin depositional settings (B). Note the flat-topped non-rimmed depositional profile that exhibits the carbonate platform. See figure 2.2.6 for legend. 95

Figure 2.2.9. View from the south of the oblique cross-section located in the northeastern part of Las Mingachas (A) (see Fig. 2.2.7 for location) displaying the sequence stratigraphic interpretation (B). See figure 2.2.6 for legend. 96

Figure 2.2.10. Photograph of the southern part of Las Mingachas (A) (see Fig. 2.2.7 for location) showing the sequence stratigraphic interpretation (B). See figure 2.2.6 for legend. 97

Figure 2.2.11. Outcrop photograph of the FRWST (A) (see Fig. 2.2.7 for location) displaying the interpreted position of the BSFR and the correlative conformity of the SB (B). Note the sharp contact of these surfaces. See figure 2.2.6 for legend. 99

Figure 2.2.12. Sedimentary facies and key sequence stratigraphic surfaces (see Fig. 2.2.7 for exact location): a) Detail of the BSFR. Note the sharp contact between the underlying highstand marls and the forced regressive calcarenite, which displays Planolites burrows at the base. Las Mingachas. b) Close-up photograph of the correlative conformity surface (SB), which extends above the FRWST and below the LPWST. The notebook lies on this surface, while the white arrows point to it. Note the sharp contact of this surface. Las Mingachas. c) Detail of the surface boundary between the depositional sequences A and B displaying palaeokarst development. Camarillas. d) Detail of the lowstand prograding platform lithofacies. Note the Polyconites hadriani rudists (Skelton et al. 2008b; in press) grouped in bouquets. White arrow points to a platy coral. Facies Association II. Las Mingachas. e) Detail of the transgressive surface exhibiting a hardground with a ferruginous crust and borings. Las Mingachas. f) Detail of a rod-like branching coral in growth position in the backsteeping platform (TST). Facies Association II. Las Mingachas. 100

Figure 2.2.13. Photograph of the truncation surface related to subaerial exposure close to the town of Camarillas (A) (see Fig. 2.2.1 for location) displaying the sequence stratigraphic interpretation (B). Note how the transgressive lag onlaps the composite surface (SB+TS). Note that the layers are vertical. The town of

Camarillas (up-right in the photo) is used for scale. See figure 2.2.6 for legend. 101

Figure 2.2.14. Panoramic view of the southern part of Las Mingachas (A) (see Fig. 2.2.7 for location) showing the sequence stratigraphic interpretation (B). See figure 2.2.6 for legend. 102

Figure 2.2.15. Outcrop photograph of the lowstand prograding platform (A) (see Fig. 2.2.7 for location) displaying the sequence stratigraphic interpretation (B). Note the flat-topped non-rimmed depositional profile that exhibits this carbonate platform and note how it changes laterally from shelf settings to slope environments. The massive lithofacies (above) are construed to be sedimented in situ, while the lithofacies with a nodular aspect (below) correspond to resedimented deposits. See figure 2.2.6 for legend. 103

Figure 2.2.16. Close-up photograph of the lowstand prograding platform (A) (see Fig. 2.2.7 for location) showing a slump scar (B). Note the nodular aspect of these debris-flow deposits. See figure 2.2.6 for legend. 104

Figure 2.2.17. Outcrop photograph of the lowstand slopes (A) (see Fig. 2.2.7 for location) displaying a discordant surface interpreted as a slump scar and the sequence stratigraphic interpretation (B). See figure 2.2.6 for legend. 105

Figure 2.2.18. View of the western part of Las Mingachas (A) (see Fig. 2.2.7 for location) showing the platform backstepping geometries and the sequence stratigraphic interpretation (B). See figure 2.2.6 for legend. 107

Figure 2.2.19. Outcrop photograph of the northeastern part of Las Mingachas area (A) (see Fig. 2.2.7 for location) displaying the transgressive platform onlapping the composite (SB+TS) sequence boundary and the sequence stratigraphic interpretation (B). See figure 2.2.6 for legend. 108

Figure 2.3.1. Geological map of the western Maestrat Basin indicating its location within the Iberian Peninsula. The areas studied are marked with a star. Modified after Canérot et al. (1979) and Gautier (1980). 133

Figure 2.3.2. Field and outcrop-scale views of the studied deposits encrusted by Lithocodium aggregatum and Bacinella irregularis in the Barranco de las Calzadas locality. A) Field view of the Barranco de las Calzadas area. B) Interpretation of the Barranco de las Calzadas area with the location of the encrusted coral rubble horizon within the marls of the Forcall Formation. C) Outcrop-scale view of the encrusted coral rubble horizon in the Barranco de las Calzadas site. 134

Figure 2.3.3. Schematic log of the Barranco de las Calzadas section showing the situation of the coral rubble deposits bound by Lithocodium-Bacinella crusts, the ammonite biostratigraphic framework and the C- and O-isotopic curves (modified from Bover-Arnal et al., under review). Note how these encrusted deposits are coeval with the negative C-isotopic spike (C3) marking the onset of the Early Aptian oceanic anoxic event (OAE1a) and the subsequent positive shift C4, and

how they are also partly coeval with the warming trend (O2) occurring before the onset of the OAE1a and the cooling trend (O3) recorded throughout this event. 135

Figure 2.3.4. Thin section photomicrographs and outcrop-scale images of representative biotic composition and facies. A) Detail of coral rubble belonging to the Microsolenidae family (Microsolenina suborder). Barranco de los Degollados site. B) Detail of coral rubble belonging to the Placocoeniidae family (Faviina suborder). Barranco de los Degollados site. C) Detail of Lithocodium aggregatum (Lit) and Bacinella irregularis (Bac). Note the in-place precipitated peloidal fabric filling the void space between the microencrusters. Barranco de las Calzadas site. D-F) Details of the bindstone fabric exhibited by these encrusted deposits in the Camarillas, Barranco de las Calzadas and Cabezo de las Hoyas sites, respectively. Note how the grey colored Lithocodium-Bacinella crusts bind together and in all directions the coral rubble (C), which display an orangey color due to the presence of ferruginous saddle dolomite. Note also that the spaces between the crusts are filled with lime mud. Observe the strong bioerosion of these deposits above all in image E). Scale bars represent 1 mm. 138

Figure 2.3.5. Close-up view of the encrusted lithofacies displaying a bindstone fabric. A) Polished slab of the encrusted coral rubble deposits. Barranco de las Calzadas site. B) Interpretation of the polished slab. Note how the Lithocodium-Bacinella crusts bind the coral rubble together in all directions, and how the interclast space is filled with lime mud. Observe the strong bioerosion present in this lithofacies. 139

Figure 2.3.6. Thin section photomicrographs and outcrop-scale images of representative biotic composition and facies. A) Fragment of Microsolenina coral encrusted by a single massive Lithocodium aggregatum crust (Lit). Note how this single massive crust is eroded and how it is overgrown by a densely-packed succession of ribbon-like Lithocodium-Bacinella (Lit-Bac) layers. Camarillas site. B) Fragment of coral encrusted by a massive well-developed Lithocodium aggregatum crust. On the right of the figure there is a random section of orbitolinid foraminifer. Barranco de las Calzadas site. C) Detail of an erosive surface within a Lithocodium-Bacinella crust overgrown by a single massive Lithocodium-layer. Cabezo de las Hoyas site. D) Bdelloidina? urgonensis (B) agglutinating silt-sized quartz grains (white arrow) encrusting a single massive Lithocodium aggregatum crust. Note how the sessile foraminifer Bdelloidina? urgonensis is overgrown by densely-packed ribbon-like Lithocodium-Bacinella meshwork. Casa Cartujo site. E) Detail of encrusting serpulid worms at the center of the image. Villarroya de los Pinares site. F) Polystrata alba (white arrow) overgrowing Lithocodium aggregatum crusts. Note the Entobia macroborings (E) affecting the Lithocodium aggregatum encrustations. Observe that the geopetal infillings mark post-depositional tilting of the deposits. Cabezo de las Hoyas site. Scale bars represent 1 mm. 140

Figure 2.3.7. Thin section photomicrographs and outcrop-scale images of representative biotic composition and facies. A) Palorbitolina lenticularis agglutinating silt-sized quartz particles (black arrow). Las Cubetas site. B) Detail of a terebratulid brachiopod (black arrow). Barranco de las Calzadas site. C)

Skeleton fragment of a demosponge imbued with Lithocodium aggregatum as reported in Cherchi and Schroeder (2006). Barranco de los Degollados site. D) Detail of a solitary coral. Villarroya de los Pinares site. E) Transverse section of a lithophagid bivalve boring with the in situ preserved valves (black arrows). Barranco de la Serna site. F) Section of Caprina douvillei. Note how the skeleton is partly affected by ferruginous saddle dolomite (white arrow). Barranco de la Serna site. Except in B), scale bars represent 1 mm. 142

Figure 2.3.8. Outcrop-scale views of the encrusted coral rubble horizon in the Barranco de las Calzadas site. A) Note the erosive surface at the top of the first nodular layer containing coral rubble and Lithocodium aggregatum and Bacinella irregularis. Note that the second nodular level with coral debris is overlying a thin marly interval. B) Observe the decimetric marly interval between the two layers of encrusted coral rubble and the nodular aspect of the deposits. 143

Figure 2.3.9. Thin section photomicrographs and outcrop-scale images of representative biotic composition and facies. A) Outcrop-scale view of the amalgamated encrusted coral rubble deposits in the Barranco de la Serna site. Note how the first half of the deposit is massive and how the second half adopts a nodular aspect. The black arrow points to a rock-forming Palorbitolina lenticularis grainstone, which underlies the horizon containing coral debris and microencrusters. B) Detail of the underlying grainstone shown in image A). Note that the Palorbitolina lenticularis show preferential imbrication. Barranco de la Serna site. C-D) Entirely preserved coral colonies (black arrows) in growth position embedded in encrusted coral rubble. Cabezo de las Hoyas site. E) Detail of silt-sized quartz particles (black arrows) within the lime mud matrix filling the interclast spaces. Barranco de la Serna site. F) Reworked lumps of Lithocodium-Bacinella crusts surrounding coral pieces. Note how the grey colored Lithocodium-Bacinella crusts bind together and in all directions the coral rubble (C), which display an orangey color due to the presence of ferruginous saddle dolomite. Scale bar represents 1 mm. 144

List of tables

Table 2.1.1. Facies classification and interpretation of depositional environment. 28

Appendix

List of other publications

Moreno-Bedmar, J.A., Company, M., Sandoval, J., Tavera, J.M., Bover-Arnal, T., Salas, R., Delanoy, G., Maurrasse, F.J.-M.R. and Martínez, R. (under review). Lower Aptian ammonite and carbon isotope stratigraphy in the eastern Prebetic Domain (Betic Cordillera, southeastern Spain). *Geologica Acta*.

Schlagintweit, F., Bover-Arnal, T. and Salas, R. (under review). New insights into *Lithocodium aggregatum* Elliott 1956 and *Bacinella irregularis* Radoičić 1959 (Late Jurassic-Lower Cretaceous): two ulvophycean green algae (?Order Ulotrichales) with a heteromorphic life cycle (epilithic versus euendolithic). *Facies*.

Bover-Arnal, T., Martín-Martín, J.D., Gomez-Rivas, E., Travé, A., Salas, R., Moreno-Bedmar, J.A. and Tomás, S. (under review). Insights into the Upper Aptian carbonate succession of the south-eastern Maestrat Basin (E Iberia). *Proceedings of the 27th IAS Meeting of Sedimentologists (Italy, Alghero, Spetember 20-23, 2009), Medimond International Proceedings*.

Bover-Arnal, T., Salas, R., Martín-Closas, C., Moreno-Bedmar, J.A. and Bitzer, K. (under review). *Lithocodium aggregatum* as a binding agent: a Lower Aptian case study from the western Maestrat Basin (E Iberia). *Proceedings of the 27th IAS Meeting of Sedimentologists (Italy, Alghero, Spetember 20-23, 2009), Medimond International Proceedings*.

Moreno-Bedmar, J.A., Company, M., Bover-Arnal, T., Salas, R., Delanoy, G., Maurrasse, F.J., Grauges, A. and Martínez, R. (in press). Lower Aptian ammonite biostratigraphy in the Maestrat Basin (Eastern Iberian Chain, Spain). *Geologica Acta*.

Skelton, P.W., Gili, E., Bover-Arnal, T., Salas, R. and Moreno-Bedmar, J.A. (in press). A new species of Polyconites from the Lower Aptian of Iberia and the early evolution of polyconitid rudists. *Turkish Journal of Earth Sciences*.

Moreno-Bedmar, J.A., Ramírez, L., Company, M., Delanoy, G., Bover-Arnal, T., Bulot, L-G., Latil, J-L. and Salas, R. (2009). Bioestratigrafía de los amonites de Can Casanyes. Macizo de Garraf (Barcelona, España). *Batalleria*, 14, 91-98.

Moreno-Bedmar, J.A., Company, M., Bover-Arnal, T., Salas, R., Delanoy, G., Martínez, R. and Grauges, A. (2009). Biostratigraphic characterization by means ammonoids of the Lower Aptian Oceanic Anoxic Event (OAE 1a) in the Eastern Iberian Chain (Maestrat Basin, E Spain). *Cretaceous Research*, 30, 864-872.

Moreno-Bedmar, J.A., Bover-Arnal, T., Company, M. and Salas, R. (2008). The early Aptian oceanic anoxic event in the Maestrat Basin (NE Iberian Chain). *Geo-Temas*, 10, 159-162.

Moreno-Bedmar, J.A., Bulot, L., Latil, J.L., Martínez, R., Ferrer, O., Bover-Arnal, T. and Salas, R. (2008). Precisiones sobre la edad de la base de la Fm. Escucha, mediante ammonoideos, en la subcuenca de la Salzedella, Cuenca del Maestrat (E Cordillera Ibérica). *Geo-Temas*, 10, 1262-1272.

Bover-Arnal, T., Moreno-Bedmar, J.A., Salas, R. and Bitzer, K. (2008). Facies architecture of the late Early-Middle Aptian carbonate platform in the western Maestrat basin (Eastern Iberian Chain). *Geo-Temas*, 10, 115-118.

Climent-Domènech, H., Bover, T. and Caja Rodríguez, M.A. (2007). Evolución sedimentaria y estructural del Cretácico inferior en el sector Benicàssim-Orpesa, Cadena Ibérica oriental. *Geogaceta*, 41, 47-50.

DECLARATION OF AUTHENTICITY

To the best of my knowledge and belief, this thesis contains no material previously published or written by another person, except where due reference has been made.

This thesis contains no material which has been accepted or definitely rejected for the award of any other doctoral degree in any university.

EHRENERKLÄRUNG

Hiermit erkläre ich, dass ich die Arbeit selbständig verfasst und keine anderen als die von mir angegebenen Quellen und Hilfsmittel benutzt habe.

Ferner erkläre ich, dass ich anderweitig mit oder ohne Erfolg nicht versucht habe, diese Dissertation einzureichen. Ich habe keine gleichartige Doktorprüfung an einer anderen Hochschule endgültig nicht bestanden.
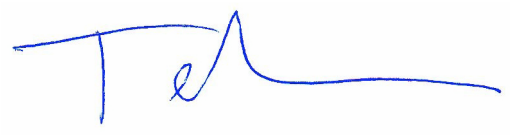
Bayreuth, den 11. Januar 2010